The Cambrian Metamorphic History of Tasmania

by
Reia M. Chmielowski,
M.Sc *(University of Alaska, Fairbanks)*,
B.Sc *(Southern Oregon University)*

Submitted in fulfilment of the
requirements for the Degree of
Doctor of Philosophy (Geology)

University of Tasmania

November 2009

STATEMENT

This thesis contains no material which has been accepted for a degree or diploma by the University or any other institution, except by way of background information and duly acknowledged in the thesis, and to the best of the candidate's knowledge and belief no material previously published or written by another person except where due acknowledgement is made in the text of the thesis, nor does the thesis contain any material that infringes copyright.

This thesis may be made available for loan and limited copying in accordance with the *Copyright Act of 1968*.

Reia M. Chmielowski

University of Tasmania

November 2009

ABSTRACT

The Tyennan Orogeny produced low to medium-grade metamorphic rocks distributed across the western third of Tasmania. Chemical U-Th-Pb monazite dating reveals that the peak episode of metamorphism took place in the Cambrian, with a weighted mean age for all units analysed of 505 ± 1 Ma. However, variations in the results by region range from ~ 511 to ~ 497 Ma. The pelitic schists of the Franklin Metamorphic Complex contain garnet porphyroblasts which record a rapid, nearly isothermal, pressure increase; the garnet cores formed at ~ 600^{o} C, 6,000 bars and the rims at ~ 700^{o} C, 14,000 bars at 511 ± 3 Ma. Likewise, the eclogite from the same region records a change from ~ 550^{o} C, 6,250 bars to ~ 650^{o} C, 19,000 bars. The whiteschist, which was obtained from the opposite side of a major local fault, formed garnet cores at ~ 545^{o} C, 19,600 bars; its garnet rims and matrix minerals formed at 506 ± 5 Ma after an increase in temperature of at least 30-90^{o} C. All of these units show evidence of very rapid isothermal exhumation. Other Franklin Metamorphic Complex fault blocks record P/T for peak conditions at ~ 570^{o} C, 8,600 bars (Mt. Mary), and ~ 700^{o} C, 11,400 bars (Raglan Range). The Forth Metamorphic Complex achieved peak metamorphism at 509 ± 7 Ma, at conditions of 670^{o} C, 16,900 bars, and the nearby Settlers Schist gives results of 513 ± 8 Ma. The garnet porphyroblasts of the Port Davey Metamorphic Complex record a single episode of metamorphism which took place at 505 ± 2 Ma at ~ 550 to 570^{o} C and ~ 6,000 bars during which a dehydration event resulted in both a change of garnet composition and texture.

The regional geology indicates metamorphism predated post-collisional extension and associated eruption of the Mount Read volcanics at 506 to 500 Ma. Most of the monazite dating is consistent with this observation. However, the Mersey River Metamorphic Complex gives very consistent results of 497 ± 3 Ma. This is problematical, as it would have been at depth undergoing metamorphism after that extension took place. This could be the result of an unknown analytical problem, but the Mersey River monazite grains are indistinguishable chemically from monazite in the other units, and this sample has undergone repeated analysis. Alternatively, this sample reflects a different metamorphic event than that recorded in all other samples studied.

TABLE OF CONTENTS

Chapter 1: Introduction 1
1.1: Geology of Tasmania 1
1.1.1: Distribution of metamorphic rocks 1
1.1.2: Metamorphic history 2
1.1.2.1: Previous work 2
1.1.2.2: Arthur Metamorphic Complex 3
1.1.2.3: North Coast 4
1.1.2.3.1 Port Sorell Formation 4
1.1.2.3.2 Settlers Schist 5
1.1.2.3.3 Forth Metamorphic Complex 6
1.1.2.3.4 Mersey River Metamorphic Complex 6
1.1.2.4: Franklin Metamorphic Complex 7
1.1.2.5: Strathgordon Metamorphic Complex 7
1.1.2.6: Port Davey Metamorphic Complex 8
1.1.2.7: Offshore Data 8
1.1.2.8: Tectonic models 9
1.2: Aims of this thesis 10
1.3: Methods of Study 10
1.3.1: Sample Collection 10
1.3.2: Analytical Methods 11
1.3.2.1: Mineral Analysis 12
1.3.2.2: Whole-Rock Analysis 13
1.3.2.3: Laser-ICPMS 14
1.3.3: Data Analysis 15
1.3.3.1: Mineral stoichiometry calculations 15
1.3.3.2: Classical Geothermobarometers 15
GB-GASP 15
GB-GBPQ 16
GBMAQ 16
1.3.3.3: Perplex 17
Whole-rock/garnet core calculations 17
PT path and automated garnet fractionation calculations 19
Manual garnet fractionation calculations 20
Display of Perple_X Results 21
1.3.3.4: Structural Analysis 21
1.4: Structure of thesis 22
Chapter 2: Collingwood River 23
2.1: Field data 23
2.1.1: Field Relations 23
2.1.2: Collingwood River Cross-Sections 24
2.1.3: Mylonite Results 25
2.1.4: Regional Cartoon 26
2.2: Description of samples 26
2.3: Whole rock compositions 29
2.4: PT from garnet rim and matrix mineral compositions and classic geothermobarometry 29
2.4.1: 67659 30
2.4.2: 160696 31
2.4.3: 160698 32

2.4.4: 160702 33
2.4.5: 160708 34
2.4.6: 160713 35
2.4.7: 160717 35
2.4.8: Summary of all Collingwood River Metapelite Peak Metamorphism Estimates 36
2.5: PT from garnet core compositions and PT paths 37
2.5.1: Sample 67662 38
2.5.1.1: 67662 Sample description 38
2.5.1.2: 67662 Composition 38
2.5.1.3: 67662 Garnet core conditions 39
2.5.1.4: 67662 Garnet rim conditions via fractionation path calculations 40
2.5.2: Sample 67665 41
2.5.2.1: 67665 Sample description 41
2.5.2.2: 67665 Composition 41
2.5.2.3: 67665 Garnet core conditions 43
2.5.2.4: 67665 Garnet rim conditions via fractionation attempts 43
2.5.3: Sample 67659 44
2.5.3.1: 67659 Garnet core conditions 44
2.5.3.2: 67659 Garnet rim conditions via fractionation path calculations 44
2.5.4: Sample 160694 45
2.5.4.1: 160694 Sample description 45
2.5.4.2: 160694 Composition 45
2.5.4.3: 160694 Garnet core conditions 47
2.5.4.4: 160694 Garnet rim conditions via fractionation path attempts 48
2.5.5: Sample 160698 49
2.5.5.1: 160698 Garnet core conditions 49
2.5.5.2: 160698 Garnet rim conditions via fractionation path calculations 49
2.5.6: Sample 160702 50
2.5.6.1: 160702 Composition 50
2.5.6.2: 160702 Garnet core 51
2.5.6.3: 160702 Garnet rim conditions via fractionation path calculations 51
2.5.7: Sample 160707 52
2.5.7.1: 160707 Sample description 52
2.5.7.2: 160707 Composition 52
2.5.7.3: 160707 Garnet core 53
2.5.7.4: 160707 Garnet rim conditions via fractionation path calculations 53
2.5.8: Sample 160708 54
2.5.8.1: 160708 Composition 54
2.5.8.2: 160708 garnet core 54
2.5.8.3: 160708 Garnet rim conditions via fractionation path calculations 55
2.5.9: Whiteschist 55
2.5.10: Summary of all Collingwood River Samples Perple_X results for garnet core 57
Chapter 3: Southwest Coast 62
3.1: Geothermobarometry 62
3.1.1: 68318 62
3.1.2: 68319 64
3.1.3: 68320 68
3.1.4: 68335 69
3.1.5: 143072 69
3.1.6: Summary of southwest coast classic geothermobarometric results 70

3.2: Whole Rock Composition 72
3.3: Perple_X results 73
3.3.1: Sample 68318 73
3.3.2: Sample 68319 74
3.3.3: Sample 143097 75
3.3.4: Summary of southwest coast Perplex results 76
3.4: Comparison of southwest Coast garnet compositions/habit 76
3.5: Southwest Coast P/T paths 77
Chapter 4: Other Locations 80
4.1: Forth 80
4.1.1: Sample 75596 80
4.1.2: Sample 75637 81
4.2: Mt. Mary 82
4.2.1: Sample 39463 82
4.2.2: Sample 39456 84
4.3: Raglan Range 85
Chapter 5: Timing Of Metamorphism 87
5.1: Introduction 87
5.2: Monazite ages 87
5.2.1: Summary of Results 87
5.2.1.1: Patterns in Age Results 87
5.2.1.2: Compositional Trends Of Monazite 91
5.2.2: Collingwood River monazite results by sample 97
5.2.2.1.1 North Block Collingwood River 100
5.2.2.1.2 Sample 67665 100
5.2.2.1.3 Sample 68788 101
5.2.2.1.4 Sample 160694 102
5.2.2.1.5 Sample 160696 103
5.2.2.1.6 Sample 160707 104
5.2.2.1.7 Sample 160708 105
5.2.2.1.8 Sample 160713 105
5.2.2.1.9 Sample 160716 106
5.2.2.1.10 Sample 160717 107
5.2.2.1.11 Sample 160736 107
5.2.2.2: South Block Collingwood River 108
5.2.2.2.1 Sample 32142 108
5.2.2.2.2 Sample 39140 109
5.2.2.2.3 Sample 160730 110
5.2.2.2.4 Sample 160734 112
5.2.3: Southwest Coast Monazite Results by Sample 113
5.2.3.1: Summary of Southwest Coast Age Results 113
5.2.3.2: Nye Bay 114
5.2.3.2.1 Sample: 68318 114
5.2.3.2.2 Sample: 68319 116
5.2.3.2.3 Sample: 68320 117
5.2.3.2.4 Sample: 68334 117
5.2.3.2.5 Sample 68335 120
5.2.3.2.6 Sample 143145 120
5.2.3.2.7 Sample 143147 121
5.2.3.3: Mulcahy Bay 122
5.2.3.3.1 Sample 143072 122
5.2.3.3.2 Sample 143106 122

5.2.3.4: Wreck Bay 123
5.2.3.4.1 Sample 143097 123
5.2.4: North Coast Monazite Results by Sample 123
5.2.4.1: Forth 123
5.2.4.1.1 Sample 75637 123
5.2.4.1.2 Sample 154322 124
5.2.4.1.3 Sample 154325 124
5.2.4.2: Settlers Hills 125
5.2.4.2.1 Sample 71334 125
5.2.4.2.2 Sample 71338 126
5.2.4.3: Mersey 126
5.2.4.3.1 Sample 7401 126
5.2.4.3.2 Sample 154328 127
5.2.5: South Central Monazite Results 128
5.3: Zircon ages 129
5.3.1: Sample 160708 130
5.3.2: Sample 160736 131
Chapter 6: Discussion & Conclusions 133
6.1: Pressure/Temperature of Metamorphism 133
6.2: Timing of Metamorphism 140
6.2.1: Devonian 140
6.2.2: Neoproterozoic 141
6.2.3: Mesoproterozoic 142
6.2.4: Cambrian 143
6.3: Conclusions 150
REFERENCES 152
Appendix 1: Full text of Berry et al. 2007
Appendix 2: Full Text of Palmeri et al. 2008
Appendix 3: Samples Collected
Appendix 4: Representative Microprobe Results
Appendix 5: Full list of microprobe results *(on CD only)*
Appendix 6: Table of XRF Whole Rock compositions
Appendix 7: Table of Laser Ablation Results *(on CD only)*
Appendix 8: Tables of geothermobarometric Results
8.1 Representative T/P by region
8.2 Thermocalc results
8.3 GB-GBPQ results
8.4 GASP results
8.5 GBMAQ results
8.6 PERPLE_X *(on CD only)*
Appendix 9: Applications of GASP and GBPQ Geobarometers to Albite and Oligoclase Bearing Pelitic Rocks.
Appendix 10: Mylonite Kinematic Indicators
Appendix 11: Lead Isotope Pilot Study

LIST OF FIGURES

Figure 1-1: Western Tasmania: Location of key metamorphic complexes. 1
Figure 1-2: Summary of previously published age data for Tasmanian metamorphic rocks..... 3
Figure 1-3: List of XRF settings and details. 13
Figure 2-1: A) Western Tasmania: location of key metamorphic complexes B) Geological Map of the north block of the Collingwood River, Franklin Metamorphic Complex, with sample collection locations. C) Cross-section—north block C. River D) Photo of Collingwood River, view upstream, between its intersections with Bills Creek and the Balaclava River. This is the location of the highest grade metamorphism in the area. E) Geological Map of the south block of the Collingwood River, Franklin Metamorphic Complex, with sample collection locations F) Cross-section—south block C. River G) Photo of whiteschist outcrop, view downstream. Note water-filled hollow around which the whiteschist is located. The whiteschist may well represent an alteration zone around the rock which has been weathered out of the hollow. 23
Figure 2-2: Location of whiteschist (39140 and 160730) and south-block Collingwood River mylonites (160734 and 160731). 24
Figure 2-3: North block Collingwood River mylonite orientations and locations. See figure 2-1 for geologic context. 25
Figure 2-4: Representative mylonite kinematic indicators. 25
Figure 2-5: Compare orientations of south block mylonite samples. See Figure 2-1 for geologic context. Note: photo of 160731 up is to the right and the view is upstream, photo 160734 view also upstream, but photo orientated such that up is up. 25
Figure 2-6: Interpretative sketch of Collingwood River region structure. Arrows show top-to-the-east displacement recorded in the mylonites. Magenta line shows the topography from the cross sections in Figure 2-1. Colours of units as in Figure 2-1. 26
Figure 2-7: Spry's (1962) interpretation of the Collingwood River region's general structure..... 26
Figure 2-8: Kyanite in Collingwood River samples. 160696: A) plane polarized light B) crossed polarized light. 160706: C) crossed polarized light D) plane polarized light. E) 160694 BSE image. F) 160730 plane polarized light. 26
Figure 2-9: Garnet compositions for representative Collingwood River pelitic samples. Note generally homogeneous cores and zoned rims. 27
Figure 2-10: Garnet composition triangle diagrams for Collingwood River samples, showing individual analyses from each sample. Cores are solid symbols, rims are hollow symbols. Symbols are the same as those used in triangle diagrams of Figure 2-9. Note general agreement between the different samples, and the marked difference in composition of cores as compared to rims. 28
Figure 2-11: AFM and ACF diagrams for Collingwood River pelitic samples whole-rock compositions. Star = average pelite of Symmes and Ferry (1992). 29
Figure 2-12: Sample 67659 A) plane and B) cross polarized light. Blue box shows location of Figure 2-13. 30
Figure 2-13: 67659 garnet graph and photo, locations of P/T calculation analysis points. 30
Figure 2-14 67659 GB-GBPQ pressure temperature results. 31
Figure 2-15: 160698 cracked and bent feldspar grain 2.7 mm long. A) crossed-polarized light B) plane polarized light. 32
Figure 2-16: 160698 garnet compositions. Garnet 2: dashed lines, closed circles. Garnet 3: dashed lines, open circles. Average composition of smallest garnet analysed: solid horizontal lines. 32
Figure 2-17: 160698 analysis points used for PT calculations 33
Figure 2-18: 160698 pressure temperature estimates 33
Figure 2-19: 160702 analysis points used for PT calculations. 33
Figure 2-20: Sample 160702 Thermocalc and GB-GBPQ pressure temperature results. 34
Figure 2-21: 160708 garnet photo and composition. 34
Figure 2-22: 160708 Thermocalc and GB-GBPQ pressure temperature results. 34
Figure 2-23: 160713 analysis points used for PT calculations. 35
Figure 2-24: 160713 GB-GBPQ and Thermocalc pressure temperature results. 35
Figure 2-25: Sample 160717 A) plane polarized light, B) crossed polarized light. 35
Figure 2-26: 160717 garnet graphs and photos. 35
Figure 2-27: 160717 large feldspar cross-polarized light images and their composition graphs. A) Feldspar 1, and its compositional graph, showing no zoning in the region analysed. B) A composite of several lesser feldspar grains showing zoned rims, and one large grain showing no zoning in the region analysed. 36
Figure 2-28: 160717 GB-GBPQ and Thermocalc pressure temperature results. 36
Figure 2-29: GB-GBPQ Collingwood River results for peak metamorphic conditions. 36

Figure 2-30: Thermocalc Collingwood River results for peak metamorphic conditions. 37
Figure 2-31: Comparison of P/T predicted by Perple_X with that predicted by GB-GBPQ for minerals of the composition Perple_X predicted at those P/T conditions. A) P (bars) comparison B) T (C) comparison. 37
Figure 2-32: 67662 garnet composition and photo. 38
Figure 2-33: Compare composition of white mica of sample 67662 with that of the other Collingwood River muscovites. 38
Figure 2-34: 67662 Perple_X standard correction garnet core results. A) the intersections at 640^{o} C, 5,900 bars. B) xAlm isopleths. C) xPrp D) xGrs E) xSps F) mineral stability fields, intersections in the TiBio(HP) Pheng(HP) feldspar IlGkPy Gt(HP) sill q field. 39
Figure 2-35: 67662 garnet core Perple_X results for the all iron = FeO run. A) the intersections at 625^{o} C, 5,500 bars. B) xAlm isopleths. C) xPrp. D) xGrs, E) xSps F) mineral stability fields, intersections in the TiBio(HP) Pheng(HP) feldspar IlGkPy Gt(HP) sill q field. 39
Figure 2-36: 67662 Perple_X standard water-saturated calculations A) Garnet Rim garnet isopleth intersections at 621^{o} C, 9,000 bars B) mineral stability fields, rim composition in the TiBio(HP) Pheng(HP) St(HP) feldspar Gt(HP) pa ru q field. 40
Figure 2-37: 67662 Perple_X standard fixed-H2O calculations. A) Garnet Rim garnet isopleth intersections at 560^{o} C, 11,400 bars B) mineral stability fields, rim intersections in the TiBio(HP) Pheng(HP) feldspar Gt(HP) ky ab ru field. 40
Figure 2-38: 67662 garnet rim Perple_X results for the all iron = FeO, water-saturated fractionation path run. A) Intersections at 554^{o} C, 11,000 bars B) mineral stability fields, rim intersections in the TiBio(HP) Pheng(HP) feldspar Gt(HP) ky ab ru q field. This one gives the best match..... 41
Figure 2-39: 67665 garnet composition diagram. A) Two profiles across full grain. B) Smaller sub grain. Yellow box in A) shows location of smaller sub-grain B). 41
Figure 2-40: 67665 compositions of matrix minerals and/or inclusions within garnet. A) Matrix & inclusion muscovite. B) & C) inclusion biotite D) inclusion rutile-ilmenite. 42
Figure 2-41: 67665 Perple_X garnet core results. A) the intersections at 618^{o} C, 8,000 bars B) xAlm isopleths C) xPrp D) xGrs E) xSps F) mineral stability fields, intersections in the TiBio(HP) Pheng(HP) St(HP) feldspar IlGkPy Gt(HP) pa q field. 43
Figure 2-42: Perple_X garnet-core results for sample 67659 (starting xH2O = 1.37) A) the intersections at 520^{o} C, 5,100 bars B) xAlm isopleths C) xPrp D) xGrs E) xSps F) mineral stability fields, intersections in the in the in the TiBio(HP) Pheng(HP) St(HP) feldspar IlGkPy Gt(HP) ky ab q field. 44
Figure 2-43: 67659 Perple_X garnet-rim results A) the intersections at 494^{o} C, 9,100 bars B) xAlm isopleths C) xPrp D) xGrs E) xSps F) mineral stability fields, intersections in the in the TiBio(HP) Pheng(HP) feldspar Gt(HP) ky ab ru q field. 44
Figure 2-44: 160694 garnet graphs and photos. A) garnet map for Mn concentration, warm colours high, cool colours low, and its relationship to the analysed points of line one, which is horizontal. B) plane-polarized light of the same grain, rotated such that line two is horizontal..... 45
Figure 2-45: 160694 muscovite composition. Most of the muscovite inclusions in garnet have a similar composition to the matrix muscovite..... 45
Figure 2-46: 160694 compare analysis lines one and two from the thinsection 160694-C with the single line from the thin section 160694-A. The distance between analysis points were normalized such that the transition between garnet core and rim occur at -1 and 1 along the x-axis. Note the difference between 160694-A and –C, particularly in the core composition. 46
Figure 2-47: 160694 muscovite inclusions within garnet. BSE image. Points 6 & 10 are lower in K and higher in Fe & Ca than the others. 47
Figure 2-48: 160694 rutile inclusions in garnet. Note difference in scale as compared to Figure 2-40D. 47
Figure 2-49: 160694 Perple_X garnet-core results A) the intersections at ~545^{o} C, 5,700 bars B) xAlm isopleths C) xPrp D) xGrs E) xSps F) mineral stability fields, intersections in the TiBio(HP) Pheng(HP) feldspar feldspar IlGkPy Gt(HP) ky olen q field. 48
Figure 2-50: 160694 Perple_X garnet-rim results A) the intersections at ~575^{o} C, 8,900 bars B) xAlm isopleths C) xPrp D) xGrs E) xSps F) mineral stability fields, intersections in the TiBio(HP) Pheng(HP) feldspar feldspar IlGkPy Gt(HP) ky q olen field. 48
Figure 2-51: 160698 Perple_X garnet-core results A) the intersections at ~600^{o} C, 6,900 bars B) xAlm isopleths C) xPrp D) xGrs E) xSps F) mineral stability fields, intersections in the TiBio(HP) Pheng(HP) St(HP) feldspar IlGkPy Gt(HP) pa q field. 49
Figure 2-52: 160698 Perple_X garnet-rim results A) the intersections at ~580^{o} C, 10,800 bars B) xAlm isopleths C) xPrp D) xGrs E) xSps F) mineral stability fields, intersections in the TiBio(HP) Pheng(HP) feldspar Gt(HP) ky ab ru q field. 49

Figure 2-53: 160698 differences in garnet composition by size of grains. A) xAlm for each. B) xPrp for each. C) xGrs for each D) xSps for each. All lines normalized to their radius to facilitate the comparison. 50
Figure 2-54: 160702 medium garnet #3 and its composition graph. 50
Figure 2-55: 160702 Perple_X garnet-core results A) the intersections at ~540^{o} C, 6100 bars B) xAlm isopleths C) xPrp D) xGrs E) xSps F) mineral stability fields, intersections in the TiBio(HP) Pheng(HP) feldspar feldspar IlGkPy Gt(HP) ky q field. 51
Figure 2-56: 160702 Perple_X garnet-core results A) the intersections at ~515^{o} C, 9,700 bars B) xAlm isopleths C) xPrp D) xGrs E) xSps F) mineral stability fields, intersections in the TiBio(HP) Pheng(HP) feldspar feldspar Gt(HP) ky ab ru q field. 51
Figure 2-57: 160707 garnet photo (plane polarized light), Mn-map, and composition. 53
Figure 2-58: 160707 Perple_X garnet-core results A) the intersections at ~650^{o} C, 6,750 bars B) xAlm isopleths C) xPrp D) xGrs E) xSps F) mineral stability fields, intersections in the TiBio(HP) Pheng(HP) St(HP) feldspar IlGkPy Gt(HP) sill q field. 53
Figure 2-59: 160707 Perple_X garnet-rim results A) the intersections at ~605^{o} C, 11,800 bars B) xAlm isopleths C) xPrp D) xGrs E) xSps F) mineral stability fields, intersections in the TiBio(HP) Pheng(HP) feldspar Gt(HP) ky ab ru q field. 54
Figure 2-60: 160708 mica and feldspar compositions. 54
Figure 2-61: 160708 Perple_X garnet-core results A) the intersections at ~580^{o} C, 5,500 bars B) xAlm isopleths C) xPrp D) xGrs E) xSps F) mineral stability fields, intersections in the TiBio(HP) Pheng(HP) St(HP) feldspar IlGkPy Gt(HP) pa q field. 54
Figure 2-62: 160708 Perple_X garnet-rim results A) the intersections at ~520^{o} C, 9,500 bars B) xAlm isopleths C) xPrp D) xGrs E) xSps F) mineral stability fields, intersections in the TiBio(HP) Pheng(HP) feldspar Gt(HP) ky ab ru q field. 55
Figure 2-63: Whiteschist A) sample 160730 plane polarized light, B) sample 39140 crossed polarized light, C) sample 39140 plane polarized light. 55
Figure 2-64: Whiteschist garnet type A: moderate cracking, no visual difference between core and rim (see Figure 2-66 for compositional profiles). 56
Figure 2-65: Whiteschist garnet type B: extensive cracking, abrupt visual difference between core and rim (see Figure 2-66 for compositional profiles). 56
Figure 2-66: Whiteschist garnet types A & B from samples 39140 and 160730. Also shown is the composition reported by Råheim and Green (1974). 56
Figure 2-67: 160730 whiteschist Perple_X garnet-core results A) the intersections at ~545^{o} C, 19,600 B) xAlm isopleths C) xPrp D) xGrs E) xSps F) mineral stability fields, intersections in the Chl(HP) Pheng(HP) Ctd(HP) Gt(HP) law pa ru q field. G) Kyanite stability field with mineral % isopleths H) Talc stability field with mineral % isopleths. 57
Figure 2-68: Differences in P/T results calculated via Perple_X for the garnet cores A) when the amount of available H_2O is changed. B) when the amount of available FeO is changed. Circle sizes are proportional to the sum of the differences between the value of each predicted end member and those measured in the sample. The smaller circles are for the fixed-H_2O results or all Fe = FeO results, and the larger for the water-saturated results or FeO = 90% measured whole-rock Fe. 58
Figure 2-69: Perple_X results for the garnet cores of the Collingwood River pelitic schists. For samples for which more than one set of calculations were undertaken the one with the "tightest" garnet-core isopleth intersections is presented. "Error" ellipses for individual samples are proportional to the tightness of the intersections (see text). The large error ellipse for the mean of the data is based upon the standard deviation from the mean, with a correlation chosen to rotate the ellipse to match the spread of the data. 58
Figure 2-70: Comparing the values of X_{Sps} measured in the garnet cores with the Perple_X pressure estimates for the cores. Note that for those samples calculated for water-saturated conditions and standard corrections there is a correlation between X_{Sps} and pressure—higher X_{Sps} yielding lower pressure estimates, while those samples for which calculations limited available H_2O or increased FeO include all iron measured in the whole rock, or both, yield consistent pressures, regardless of the differences in measured X_{Sps} . The linear trend lines were calculated automatically by Excel. 60
Figure 2-71: Perple_X results for the garnet rim of the Collingwood River pelitic schists. For samples for which more than one set of calculations were undertaken the one with the "tightest" garnet-core isopleth intersections is presented. "Error" ellipses for individual samples are proportional to the tightness of the intersections (see text). The large error ellipse for the mean of the data is based upon the standard deviation from the mean, with a correlation chosen to rotate the ellipse to match the spread of the data. 60
Figure 2-72: Collingwood River pelitic schists Perple_X results showing change in estimated conditions from core to rim. 60

Figure 3-1: Southwest coast sample locations. 62
Figure 3-2: Sample 68318 garnet composition graph and photo. 63
Figure 3-3: 68318 biotite compositions. 64
Figure 3-4: 68318 analysis points used for geothermobarometric calculations. 64
Figure 3-5: 68318 GB-GBPQ results. 64
Figure 3-6: 68319 garnets A, B, and small garnet 3 and their compositions. 65
Figure 3-7: 68319 location of PT analysis points. BSE image. 66
Figure 3-8: 68319 feldspar showing subtle zoning in the core, and abrupt change in XAn at the rims/grain boundaries. A) BSE image of feldspar grain 2, B) plane polarized light image of the same grain (2). C) BSE image of feldspar grain 1 D) plane polarized light image of same grain feldspar grain (1). 66
Figure 3-9: 68319 composition of matrix minerals and garnet inclusions and BSE image of location of some of the inclusions. 67
Figure 3-10: 68319 geothermobarometric estimates. The Thermocalc error ellipse is the reported 2σ error, and the error ellipses for GB-GBPQ and GBMAQ are drawn at ± 25° C and 1000 bars. GASP, being a pressure estimate, is drawn as horizontal lines (error ± 800 bars); however, it was calculated using the same GB temperature estimate as used for GB-GBPQ. 67
Figure 3-11: 68320 garnet graph and photo 68
Figure 3-12: 68320 biotite composition. 69
Figure 3-13: 68320 analysis points used for geothermobarometric calculations. 69
Figure 3-14: 68320 GB-GBPQ results. 69
Figure 3-15: 68335 biotite compositions. 69
Figure 3-16: 68335 garnet graph and photo 70
Figure 3-17: 68335 GBMAQ results. 70
Figure 3-18: 143072 A) garnet graph and photo. B) quartz-rich matrix. 71
Figure 3-19: 143072 other mineral compositions. 71
Figure 3-20: 143072 Geothermobarometric results. The Thermocalc error ellipse is the reported 2σ error, and the error ellipse for GBMAQ is drawn at ± 25° C and 1000 bars. 71
Figure 3-21: All southwest coast classic geothermobarometric results. The Thermocalc error ellipses are the reported 2σ error, and the error ellipses for GB-GBPQ and GBMAQ are drawn at ± 25° C and 1000 bars. GASP, being a pressure estimate, is drawn as horizontal lines (error ± 800 bars); however, it was calculated using the same GB temperature estimate as used for GB-GBPQ. 72
Figure 3-22: Southwest coast XRF whole-rock compositions. A) AFM diagram. B) ACF diagram. (For both: small triangle all Tasmanian samples analysed, large diagram just the southwest coast samples) C) Comparison of samples with the average pelite of (Shaw 1956) $Ca_{sample}/Ca_{Shaw's\ average\ pelite}$ vs $Al_{sample}/Al_{Shaw's\ average\ pelite}$. 73
Figure 3-23: 68319 Perple_X garnet core results. A) Almandine compositional contours with measured garnet core composition of 0.81 XAlm in orange, B) Pyrope (0.06 XPrp in purple) C) Grossular (0.06 XGrs in blue), D) Spessartine (0.07 XSps in green) E. The intersection of the garnet core isopleths; cross shows T/P of "best fit" intersection at ~556° C, 5600 bars. 74
Figure 3-24: Sample 143097 A) crossed polarized light B) plane polarized light. 74
Figure 3-25: Garnet composition charts for all southwest coast samples. Note trends in composition by area: Nye Bay (68318, 68319, 68320, 68334, 68335), Mulcahy Bay (143076, 143072, 143145, 143147) Wreck Bay (143097). 75
Figure 3-26: 143097 garnet graph and photo. 76
Figure 3-27: 143097 Perple_X garnet core conditions. A) Almandine compositional contours with measured garnet core composition of 0.71 XAlm in orange, B) Pyrope (0.08 XPrp in purple) C) Grossular (0.17 XGrs in blue), D) Spessartine (0.04 XSps in green) E. The intersection of the garnet core isopleths; cross shows T/P of "best fit" intersection at ~560° C, 6,500 bars. 76
Figure 3-28: Southwest coast Perple_X garnet core results. 77
Figure 3-29: All southwest coast pressure/temperature estimates. 77
Figure 3-30: Nye Bay P/T path. 77
Figure 4-1: Forth area location map. Sample 75596 (green text) was analysed for geothermobarometric work, 73637 (blue text) was analysed for both geothermobarometric calculations and monazite dating, and samples 154322 and 154325 (red text) were analysed for monazite dating. 80
Figure 4-2: Sample 75596 A) composition of chloritoid & chlorite B) composition of matrix muscovite and paragonite inclusion in garnet. 80
Figure 4-3: Sample 75596 garnet (BSE image) and composition graph. Note that core is thin bands of garnet surrounding quartz crystals, while the rim is more massive. 80
Figure 4-4: Sample 75637 A) crossed polarized light B) plane polarized light. 81
Figure 4-5: 75637 feldspar composition graph and photo (crossed polar image). 81
Figure 4-6: 75637 garnet composition graphs and photos. 81

Figure 4-7: 76537 mica compositions. 81
Figure 4-8: Location of Mt. Mary Samples, 39456 & 39463. For reference the locations of the Collingwood River highest-grade pelite (RC0601), eclogite (RC0610), and whiteschist (RC0704) are also shown. (add line between these—the captions blend together)..... 82
Figure 4-9: 39463 A) sample thin section, plane polarised light (small blue square shows location of garnet in B). B) Garnet compositional graph and photo (BSE image). Note that in the core spessartine exceeds almandine and pyrope is uniformly low throughout. 82
Figure 4-10: 39463 mica compositions. A) biotite B) muscovite C) compare this sample (filled triangles) with biotite analyses from other regions..... 83
Figure 4-11: 39456 plane and crossed polarized images. 84
Figure 4-12: 39456 feldspar grain (BSE image) and composition. 84
Figure 4-13: 39456 mica compositions A) biotite B) muscovite C) compare both Mt. Mary samples with other regions. 84
Figure 4-14: Oxides in 39456: A) Rutile core with ilmenite rim B) Hematite C) Ilmenite inclusions within garnet D) Oxide compositions. Note difference in composition between ilmenite riming large matrix grain and that included within garnet. 85
Figure 4-15: A) 39456 garnet composition and BSE image. 85
4-16: 39456 both Mt. Mary Thermocalc results. 85
Figure 4-17: Location of sample 30145, Raglan Range. 86
Figure 4-18: Sample 30145, plane and crossed polarized light. Field of view is 18 mm tall. 86
Figure 4-19: 30145 feldspar and mica composition. 86
Figure 4-20: 30145 garnet composition and photo (BSE images) A) single core grain B) double-core grain..... 86
Figure 5-1: Locations of all samples for which geochronological analysis was undertaken. See Figuress in Chapter 2 (above) and this chapter (below) for close-up maps and geologic context. Text colours match Figure 5-5 and indicate difference in the ages of the peak metamorphic event from one area to another (see text). 87
Figure 5-2: Probability diagram showing the combined monazite results for all regions. 88
Figure 5-3: Monazite age-trend diagram for all regions. Horizontal lines show the weighted mean age for the Cambrian metamorphic event (see text) and for the largest peak in the Mesoproterozoic (see text and figure 5-4). Note “gaps” in the data at ~400 Ma, 825 Ma, and 950 Ma. Note also the lesser gap associated with the sharp bend in the in slope of the data at ~600 Ma (inset—dashed line), and the gentle bends in the trend of the data at ~1,000, 1,100, 1,200, and 1,290 Ma. 88
Figure 5-4: Weighted mean ages for the Cambrian metamorphic event for all of the samples from each region, plotted as error ellipses showing the extent to which the ages overlap, and how well constrained are each region’s results. 89
Figure 5-5: Cambrian monazite results by region showing the three apparent ages for Tasmanian monazite associated with the peak metamorphic event of the Tyennan Orogeny. A) Probability diagram. Note that the youngest peak, at ~499 Ma is better constrained (narrower, taller) than the other two. B) Weighted mean ages for each of the combined regions plotted as error ellipses showing the extent to which these values overlap. 90
Figure 5-6: Probability diagram showing the combined monazite results for only those data greater than 1000 Ma for all regions. Pale blue vertical lines correspond to the “peaks” assigned by Isoplot’s “unmix ages” algorithm (see text). Yellow line shows the slope of the curve from the tallest to youngest of these peaks if the other peaks were evened out (see text). 90
Figure 5-7: Abundance of specific elements within monazite as a function of the number of spots analysed at each concentration. A) Sr B) Th C) U D) Th/U E) Y F) LREE/HREE (shape of curve is largely the same for each pair of REE chosen, though the scale changes). Note decrease in number of analyses with higher concentrations for each element and differences in the smoothness of the curves and, in particular, the change in slope for Y at the low-medium boundary. Note that the “very low” Th (< 1.0%) analyses, while shown on this Th diagram are not included in any of the other diagrams or age calculations. 91
Figure 5-8: Concentration of various elements within monazite by region A) Sr B) Th C) U D) Th/U E) Y F) LREE/HREE. Abbreviations used: SW = Southwest Coast Str = Strathgordon sbC = south block Collingwood River nbC = north block Collingwood River F = Forth M = Mersey River Set = Settlers Schist (These diagrams include the analyses of Th < 1%, although those were not considered in the weighted average mean age calculations.) 92
Figure 5-9: A) Age of monazite analyses vs. Sr B) Age of monazite analyses vs. Th (wt%) C) Age of monazite analyses vs. U (wt%) D) Th vs. U for both young (<600 Ma) and old (>600 Ma) monazite analyses E) Age of monazite analyses vs. Y F) Age of monazite analyses vs. LREE/HREE. As the analyses with Th < 1% were not included in the age calculations, they are not included in these diagrams. 93

Figure 5-10: A) U vs. Th and B) Y vs. Th for all monazite analyses used in weighted mean age calculations for this study. Blue diamonds = young (< 600 Ma). Red triangles = old (> 600 Ma). Outline of each generation's region repeated (at ¼ scale) to the right so that they can be seen without the overlap. 94
Figure 5-11: Location of north block Collingwood River samples with geochronological results. See Figure 2-1 for legend. 97
Figure 5-12: Monazite Age results for Collingwood River A) north block B) south block. 97
Figure 5-13: Location of south block Collingwood River samples in the Scarlett Creek region. Compare with Figure 2-1 for geologic context. 97
Figure 5-14: Variations in monazite composition by age. A) Sr-Age north block C. River. B) Sr-Age south block C. River. C) Y-Age north block of the Collingwood River. D) Y-Age south block of the Collingwood River. E) Th-Age north block C. River. F) Th-Age south block C. River (analyses with Th < 1 wt% are not included in the age calculations, and so not present on this figure). 97
Figure 5-15: Variations in monazite composition by age. A) U-Age north block C. River. B) U-Age south block C. River. C) Th/U-Age north block. D) Th/U-Age south block. E) LREE/HREE-Age north block. F) LREE/HREE-Age south block (analyses with Th < 1 wt% are not included in the age calculations, and so not present on this figure). 97
Figure 5-16: Sample 67665 Monazite Ages. 100
Figure 5-17: 67665 Age-monazite composition diagrams. A) Age vs. Sr B) Age vs. Y C) Age vs. LREE/HREE. 100
Figure 5-18: Sample 68788 A) plane polarized light B) crossed polarized light. 101
Figure 5-19: 68788 Monazite Ages. 101
Figure 5-20: 68788 Age-monazite composition diagrams. A) Age vs. Sr B) Age vs. Y C) Age vs. LREE/HREE. 101
Figure 5-21: 160694 Monazite ages. 102
Figure 5-22: 160694 Age-monazite composition diagrams. A) Age vs. Sr B) Age vs. Y C) Age vs. LREE/HREE. 102
Figure 5-23: BSE image of 160696 showing locations of monazite analyses in the thin section. 103
Figure 5-24: 160696 Monazite ages. 103
Figure 5-25: 160696 Age-monazite composition diagrams. A) Age vs. Sr B) Age vs. Y C) Age vs. LREE/HREE. 103
Figure 5-26: 160707 Monazite ages. 104
Figure 5-27: 160707 Age and/or monazite composition diagrams. A) Age vs. Sr B) Age vs. Y C) Ce/Dy vs. Y D) Th/U vs. Y. Note that while the analyses with young and intermediate ages are grouped based upon their Y concentrations, the analyses with old ages are grouped by their Th/U ratios, which roughly corresponds to their Y concentrations. 104
Figure 5-28: 160707 BSE images of monazite grains. 104
Figure 5-29: 160708 Monazite ages. 105
Figure 5-30: 160708 Age-monazite composition diagrams. A) Age vs. Sr B) Age vs. Y C) Age vs. LREE/HREE. 105
Figure 5-31: 160713 Monazite ages. 105
Figure 5-32: 160713 Age-monazite composition diagrams. A) Age vs. Sr B) Age vs. Y C) Age vs. LREE/HREE. 106
Figure 5-33: Sample 160716 A) plane polarized light B) crossed polarized light. 106
Figure 5-34: 160716 Monazite ages. 106
Figure 5-35: 160716 Age vs monazite composition diagrams. A) Age vs Sr B) Age vs Y C) Y vs Ce/Dy. 106
Figure 5-36: 160717 Monazite ages. 107
Figure 5-37: 160717 Age-monazite composition diagrams. A) Age vs. Sr B) Age vs. Y C) Age vs. LREE/HREE. 107
Figure 5-38: 160736 Monazite ages. 107
Figure 5-39: 160736 monazite grains showing different ages; older towards the core, younger towards the rim. Scale bars 50 μm. 107
Figure 5-40: 160736 Age-monazite composition diagrams. A) Age vs. Sr B) Age vs. Y C) Age vs. LREE/HREE. 108
Figure 5-41: Sample 32142 A) approximate sample location (McIntyre recorded the rock type and the location as “SW side of Collingwood Range”, which combination narrows the options down to this general region). Map scanned from Calver et al. (1987); compare with Figure 2-1 for units and scale. B) Sample 31242 plane polarized light. C) Sample 32142 crossed polarized light. 108
Figure 5-42: 32142 Monazite ages. 108
Figure 5-43: 32142 Age-monazite composition diagrams. A) Age vs. Sr B) Age vs. Y C) Y concentration in monazite vs. distance to the nearest garnet within the plane of the thinsection. 108

Figure 5-44: Sample 39140 photos A) plane polarized light B) crossed polarized light. Note the very cracked interiors of some garnet grains in marked contrast with the, relatively, uncracked rims of those grains, and with the, relatively, uncracked aspect of other garnet grains. 109
Figure 5-45: 39140 garnet composition A) "uncracked" garnets show distinct compositional zones B) "cracked and rimed" garnets show fairly homogeneous compositions similar to the rims of the "uncracked" grains. 109
Figure 5-46: 39140 Monazite ages. 109
Figure 5-47: 39140 Age-monazite composition diagrams. A) Age vs. Sr B) Age vs. LREE/HREE. C) Y vs. Th; red triangles: Ordovician age analyses, blue diamonds: Cambrian age analyses. 109
Figure 5-48: Cluster of monazite grains included within a single garnet in sample 160730 and locations of analysis points. The single low-Y analysis point is pink, the others are blue. Ages are given in Ma. BSE image. 110
Figure 5-49: 160730 BSE image showing circles of quartz inclusions delineating the cores of the garnet (see Figures 2-64 and 2-65 for garnet zoning associated with this grain). The large (~60 μm) monazite grain in the right hand rim is ~ 1.4 wt% Y. 110
Figure 5-50: 160730 Monazite ages. 111
Figure 5-51: 160730 Y-Age diagram showing difference in composition between monazite located within the garnet cores (very low to low Y) and those located in the garnet rims, in the matrix, and in the large cluster of monazite grains (medium to high Y). 111
Figure 5-52: Both whiteschist samples (39140 and 160730) Age-monazite composition diagrams. A) Age vs. Sr B) Age vs. Y C) Th vs. Y. 111
Figure 5-53: 160734 outcrop photo showing stretching lineation. 112
Figure 5-54: 160734 thin section photo. 112
Figure 5-55: 160734 monazite grains BSE images, scale bars 50 μm. Note corroded aspect of grains. . 112
Figure 5-56: 160734 Monazite ages. 112
Figure 5-57: 160734 Age-monazite composition diagrams. A) Age vs. Sr B) Age vs. Y C) Age vs. LREE/HREE ratio. 112
Figure 5-58: All probability diagrams for each sample analysed, sorted by region. Scale on x-axis (Age in Ma) is the same for all, and given on the bottom right. Y-axis scale varies based on the number of analyses per sample, and is given on the corresponding diagrams with the individual sample descriptions. 113
Figure 5-59: Monazite ages for all SW coast samples (including Nye Bay, Mulcahy Bay, and Wreck Bay). Inset: just the data > 600 Ma, so that the older peaks are visible. 114
Figure 5-60: Monazite Age vs. Y concentration for the southwest coast. A) Nye Bay, B) Mulcahy Bay, C) Wreck Bay. 114
Figure 5-61: Monazite Age vs. Sr concentration for the southwest coast. 114
Figure 5-62: Monazite Age vs. U concentration for the southwest coast. 114
Figure 5-63: Monazite Age vs. LREE/HREE concentration for the southwest coast. A) Nye Bay, B) Mulcahy Bay, C) Wreck Bay. 114
Figure 5-64: 68318 monazite ages. 115
Figure 5-65: 68318 Monazite included within garnet. A) Old monazite grains located well inside of a garnet and young/intermediate monazite grains at the garnet's edge (BSE image). B) The only monazite grains found included within the large (18 mm) garnet are located only within its rim. The location of a monazite grain with low totals is included in this photo only because there are only the three monazites included within this garnet at all, despite it being such a large crystal, so despite the grain not being useable in age calculations, the fact that it, and the other two grains, are within the garnet rim, is possibly significant. 115
Figure 5-66: 68318 several monazite ages in one grain; one from the "old" generation, one "intermediate-high", and the other "intermediate-low". The "intermediate" ages likely represent "mixing" of the "old" and "young" generations of monazite growth. 116
Figure 5-67: 68318 Age-composition diagrams. A) Sr vs. Age B) Y vs. Age C) LREE/HREE vs. Age. .. 116
Figure 5-68: 68319 monazite ages. 116
Figure 5-69: 68319 Age-composition diagrams. A) Sr vs. Age B) Y vs. Age C) LREE/HREE vs. Age... 116
Figure 5-70: 68319 monazite grains in BSE, sorted by age. Ages given are in Ma. 116
Figure 5-71: 68320 monazite ages. 117
Figure 5-72: 68320 Age-composition diagrams. A) Sr vs. Age B) Y vs. Age C) LREE/HREE vs. Age...117
Figure 5-73: 68334 A) photo showing location of monazite inclusions within garnet and location of microprobe analysis of the garnet and the compositional graph B) BSE image of young and old monazite included within garnet. 117
Figure 5-74: 68334 monazite ages. 118
Figure 5-75: 68334 Age-composition diagrams. A) Sr vs. Age B) Y vs. Age C) LREE/HREE vs. Age... 118
Figure 5-76: 68334 monazite grains in BSE, sorted by age. Ages given are in Ma. 119
Figure 5-77: 68335 monazite ages. 120

Figure 5-78: 68335 Age-composition diagrams. A) Sr vs. Age B) Y vs. Age C) Age vs. LREE/HREE 120
Figure 5-79: 143145 monazite ages. 120
Figure 5-80: 143145 Age-composition diagrams. A) Sr vs. Age B) Y vs. Age C) Age vs. LREE/HREE. 120
Figure 5-81: 143147 monazite ages. 121
Figure 5-82: 143147 Age-composition diagrams. A) Sr vs. Age B) Y vs. Age C) Age vs. LREE/HREE. 121
Figure 5-83: 143147 monazite grains in BSE, sorted by age. Ages given are in Ma. 121
Figure 5-84: 143072 monazite ages. 122
Figure 5-85: 143072 Age-composition diagrams. A) Sr vs. Age B) Y vs. Age C) Age vs. LREE/HREE. 122
Figure 5-86: Sample 143106 A) plane polarized light B) crossed polar image. 122
Figure 5-87: 143106 monazite ages. 122
Figure 5-88: 143106 Age-composition diagrams. A) Sr vs. Age B) Y vs. Age C) Age vs. LREE/HREE. 122
Figure 5-89: All Wreck Bay monazite results (sample 143097). 123
Figure 5-90: 143097 monazite Age-composition diagrams. A) Sr vs. Age B) Y vs. Age C) Age vs. LREE/HREE. 123
Figure 5-91: Locations of the samples from the Forth area used for monazite dating. 123
Figure 5-92: 75637 Monazite BSE images A) Badly corroded grains have no useable results B) partially corroded grains give useable results for the unaltered portion C) euhedral grains give usable results. 123
Figure 5-93: 75637 comparison of badly corroded monazite grain compositions with those which are still unaltered. 123
Figure 5-94: 75637 Monazite ages. 124
Figure 5-95: 75637 Age-monazite composition diagrams. A) Age vs. Sr B) Age vs. Y C) Age vs. LREE/HREE. 124
Figure 5-96: 154322 Monazite ages. 124
Figure 5-97: 154322 BSE images of monazite grains: (a) grain E; (b) grain I; (c) grain I with contrast adjusted to show textural environment of grain; lighter grey grains are muscovite, and darker grains are albite and quartz. Numbers are in Ma. 124
Figure 5-98: 154322 Age-monazite composition diagrams. A) Age vs. Sr B) Age vs. Y C) Age vs. U D) Age vs. Th E) Age vs. LREE/HREE. 124
Figure 5-99: 154325 monazite BSE images (d) grain E; (e) grain cluster O; (f)?rhabdophane grain. Numbers are in Ma. 124
Figure 5-100: 154325 Monazite ages. 125
Figure 5-101: 154325 Age-monazite composition diagrams. A) Age vs. Sr B) Age vs. Y C) Age vs. U D) Age vs. Th E) Age vs. LREE/HREE. 125
Figure 5-102: Location map for the two samples collected from the Settlers Schist, Beaconsfield area (geology from Brown et al. 2005). 125
Figure 5-103: Sample 71334 patch with differentiated cleavage which may have originated as a xenolith or alternatively, a rip-up clast in a metasandstone. A) plane polarized light image. B) crossed polarized light. 125
Figure 5-104: 71334 Monazite ages. 125
Figure 5-105: 71334 Age-monazite composition diagrams. A) Age vs. Sr B) Age vs. Y C) Age vs. U D) Age vs. Th E) Age vs. LREE/HREE. 125
Figure 5-106: Sample 71338 A) plane polarized light B) crossed polarized light. 126
Figure 5-107: 71338 Monazite ages. 126
Figure 5-108: 71338 Age-monazite composition diagrams. A) Age vs. Sr B) Age vs. Y C) Age vs. U D) Age vs. Th E) Age vs. LREE/HREE. 126
Figure 5-109: A) Location of Mersey Valley samples. Geology from Brown et al. (2005) B) Sample 7410 plane polarized light C) Sample 7410 crossed polarized light. 126
Figure 5-110: 7401 Monazite ages. 127
Figure 5-111: 7401 Age-monazite composition diagrams. A) Age vs. Sr B) Age vs. Y C) Age vs. U D) Age vs. Th E) Age vs. LREE/HREE. 127
Figure 5-112: 154328 Monazite ages. 127
Figure 5-113: 154328 BSE monazite images. Numbers are Age in Ma. Note that the youngest grain is inclusion poor, as is on younger section of the left hand grain. 128
Figure 5-114: 154328 Age-monazite composition diagrams. A) Age vs. Sr B) Age vs. Y C) Age vs. U D) Age vs. Th E) Age vs. LREE/HREE. 128
Figure 5-115: Location map for the sample collected from the Strathgordon Metamorphic Complex (geology from Brown et al. 2005). 128

Figure 5-116: Sample 46241 (A) plane polarized light B) crossed polarized light. 128
Figure 5-117: 46241 Monazite ages. 128
Figure 5-118: 46241 Age-monazite composition diagrams. A) Age vs. Sr B) Age vs. Y C) Age vs. U D) Age vs. Th E) Age vs. LREE/HREE. 128
Figure 5-119: Comparison of previously published Tasmanian detrital zircon ages (black filled peaks) (from figure 2 of Black et al. 2004) with the "old" monazite analyses from this study (blue lines). Note that in general the previously published zircon populations are older than the "old" monazite population, and where they do overlap there tends to be a monazite peak corresponding with a low in the zircon data. 129
Figure 5-120: Location of samples for zircon age analysis. Compare with Figure 2-1 for geologic context. 129
Figure 5-121: Zircon A14 from sample 160736 displays typical results defining isochrons on concordia. 130
Figure 5-122: A) 160708 zircon ages from upper intercepts of concordia, with the lower intercepts anchored at 510 ± 10 Ma (same as monazite metamorphic age). B) 160736 zircon ages with green line showing lower intercept for concordia (and more off graph at ~510 Ma, but x-axis was set to length appropriate to compare with figure 2 of Black et al 2004), and blue line showing upper intercept for concordia. 130
Figure 5-123: Comparison of previously published Tasmanian detrital zircon ages (black filled peaks) (from figure 2 of Black et al. 2004) with the "old" monazite analyses from this study (blue lines). Note that in general the previously published zircon populations are older than the "old" monazite population, and where they do overlap there tends to be a monazite peak corresponding with a low in the zircon data. Also shown for comparison (light blue) are the monazite "old" ages from this study—see Figure 5-6 for just the monazite. 131
Figure 6-1: Geothermobarometric and geochronological results from this study by region: [1] the north coast (including the Forth Metamorphic Complex (peak T/P/t) and the Settlers Schist (peak t)), [2] north central (Mersey River Metamorphic Complex (peak t)), [3] central (Franklin Metamorphic Complex, including the Collingwood River metapelites (P/T path and peak t), eclogites (P/T path) and, whiteschist (P/T path & peak t), the Raglan Range (peak P/T), and Mt. Mary (peak P/T) regions), [4] south central (Strathgordon Metamorphic Complex (peak t)), and [5] southwest coast (Port Davey Metamorphic Complex, including Nye (P/T path, peak t), Mulcahy (peak t), and Wreck Bays (peak t)). See figures in preceding chapters for close-up maps and geologic context. Text colours for regions with monazite results match the colours used for Figures 5-1, 5-4, and 5-5. 133
Figure 6-2: Preferred pressure/temperature estimates for all regions. Collingwood River metapelites (blue) and Nye Bay (red) have both estimates from the garnet cores and the garnet rims (max P/T conditions), with arrows showing the change in conditions between the formation of the garnet cores and final growth of the garnet rims. The Collingwood River whiteschist (muted green) is a garnet core estimate, and the Forth (purple), Mt. Mary (violet), and Raglan Range (baby blue) samples are garnet rim/matrix (max P/T) conditions. The bright green arrow shows the path interpreted for the Collingwood River eclogites (see Appendix 2). Facies boundaries after Spear (1993) and Al_2SiO_5 triple point after White et al. (2007). 134
Figure 6-3: The Port Davey Metamorphic Complex includes garnets up to ~ 5 cm in diameter. Uncollected specimen located in the vicinity of samples 68318 and 68335 (Figure 3-1). Photo courtesy of A. McNeill. 134
Figure 6-4: Comparison of garnet-zoning profiles for samples 160696 and 67662 from the Franklin Metamorphic Complex with that of garnets from the Wölz Complex, Austroalpine unit, Eastern Alps (Figure 3 of Faryad and Chakraborty 2005). Eastern Alps profiles in black, Tasmanian profiles in colour. 135
Figure 6-5: Previously published P/T results for Tasmania, by region: Arthur Metamorphic Complex: (1) blue amphibole, (Turner and Bottrill 2001). (2) blue amphibole, (Everard 1999). (3) CaD1, (Holm 2002). (4) CaD2, (Holm 2002). (5) late CaD2, (Holm 2002). Forth Metamorphic Complex: (6) kyanite-garnet-biotite schist (syn D2), (Lewis 1991). (7) early stage local calcite-altered garnet clinopyroxene zoisite interbands, (Lewis 1991). (8) peak conditions local calcite-altered garnet clinopyroxene zoisite interbands, (Lewis 1991). (9) cores in garnet-amphibole-plagioclase (Berry and Holm 2001). Port Sorell Formation: (10) medium grade metamorphism, (Reed et al. 2002). (11) greenschist precursor, (Reed et al. 2002). (12) blue amphibole (Henson 2002). (13) metapelites (Henson 2002). Franklin Metamorphic Complex: (14) eclogite peak conditions, (Kamperman 1984). (15) eclogite peak conditions, (Råheim 1976). (16) eclogite early stage conditions, (Råheim 1976). (17) eclogite peak conditions, (Goscombe 1990), (18) schist enclosing eclogite, (Goscombe 1990), (19) whiteschist, (Råheim and Green 1974). Strathgordon Metamorphic Complex: (20) schist, (Råheim 1977). Port Davey Metamorphic Complex: (21) Nye Bay, (McNeill 1985). (22) Port Davey, (Turner 1989). 138

Figure 6-6: Central Tasmania P/T results. A) Compare this study with previously published results. Grey = previously published (numbers as in Figure 6-5). Blue = metapelites & whiteschist (Chapter 2). Green = eclogite (Appendix___). B) Compare all interior Tasmania results (including Collingwood River, Raglan Range, Mt. Mary, and Strathgordon areas) with geotherms calculated in (Llana-Fúnez and Marcos 2007). 139
Figure 6-7: Forth Metamorphic Complex P/T results. A) Compare this study with previously published results. Grey = previously published (numbers as in Figure 6-5). Blue = weighted mean average results for Forth samples this study (Chapter 4). B) Compare all Forth results with geotherms calculated in (Llana-Fúnez and Marcos 2007). 139
Figure 6-8: Port Davey Metamorphic Complex P/T results. A) Grey = previously published (numbers as in Figure 6-5). Blue = results for southwest coast samples this study (Chapter 3). B) Compare all southwest coast results with geotherms calculated in (Llana-Fúnez and Marcos 2007). 139
Figure 6-9: Compare other areas previously published P/T results with geotherms calculated in (Llana-Fúnez and Marcos 2007). A) Port Sorell results B) Arthur Metamorphic Complex results. (Sources as in Figure 6-5.)..... 140
Figure 6-10: Comparison of monazite results > 600 Ma from this study (blue line) with those from the (off shore—red line) Eastern Orthogneiss, Western Tasmania terrane (Berry et al. 2008). 141
Figure 6-11: After Davies and von Blanckenburg (1995), their Figure 1: Schematic breakoff process. A) The start of continental collision. The subducting oceanic lithosphere induces flow in the surrounding asthenosphere. B) Rifting commences, with the asthenosphere rising to fill the rift. The continental crust is also shown underplating the overriding plate by slab breakup. C) The narrow rifting proceeds to slab breakoff. The impingement of hot asthenosphere at the base of the metasomatised continental lithosphere can lead to magmatism. The release of the load leads to uplift. D) As the slab sinks away the area undergoes further uplift, and a deep return flow develops, maintaining a high temperature at the base of the lithosphere. Steepening of the suture and back-propagating of the thrusts allows intrusion in rocks of both the overriding and formerly downgoing plate. 144
Figure 6-12: Schematic diagram for the sequential metamorphism model showing timing of various units' decent and initial exhumation. Not to scale. Note that diagram indicates only relative depth over time, not X-Y locations. "Group A" includes the north block of the Collingwood River, the Forth and the Strathgordon Metamorphic Complexes. Note that the Strathgordon would not have achieved the same levels of depth as obtained by the other two for this group, but it would have commenced exhumation at a similar time. 146
Figure 6-13: Compare P/T results from pelitic schist (blue line) and eclogite (green line) from the Franklin Metamorphic Complex with that of Type II (isothermal decompression) from Figure 10 of Agarad et al. (2009) 149

ACKNOWLEDGMENTS

The author is grateful to Dr. Barbara and Mr. Peter Shields for their generosity in providing a home in which to live, not only once, but twice—firstly whilst I was waiting for approval to commence studies at UTAS, and again when my scholarship expired. Their kindness has make it possible to finish the project in a timely manner, and while it will never be possible to truly repay them, it is my hope to someday "pay it forward" by opening up my home to a student in similar need. When that happens I will be certain to let the student(s) know that my inspiration in so doing was the gracious example set me by the Shields family.

This research was made possible by a scholarship from the Tasmanian State Government through the auspices of Mineral Resources Tasmania with additional financial support from the University of Tasmania and CODES.

Sample collection in the Collingwood River region of the Wild Rivers National Park was made possible by the Department of Primary Industries, Water and Environment and the National Parks and Wildlife (authority numbers ES 05278 and ES 06580).

The author is indebted to her advisor, Dr. Ron Berry, for suggesting the topic of research, guiding the research over the course of the project, and providing corrections/suggestions for improvement to chapter drafts as needed. He served as an inspiration on countless occasions—every time I felt discouraged or unable to make progress or simply stopped into his office with a quick question I'd walk away from the conversation enthused and ready to resume work with vigor, and with a plethora of information on not only the questions asked, but on diverse other topics I hadn't known I needed to ask about, but all of which proved invaluable.

Many thanks to Dr. Karsten Goemann, for his assistance with the electron microprobe and the effort he puts forth to train new users. Many thanks also to Dr. Sebastien Meffre for his assistance with the LaserICPMS, his help in interpreting the results, and for his assistance in the preparation of zircon mounts. Many thanks also to Dr. Jacqueline Halpin for providing training and assistance in zircon separation techniques.

This research would not have been possible without the many people who have collected samples from across Tasmania and stored them in the UTAS rock vault and the curators of said vault, who have kept the samples organized until needed. The individuals responsible for the collections from each area are named in the relevant sections.

The author thanks Dr. Rosaria Palmeri and her colleagues at the University in Siena for their efforts in our collaborative research leading to the publication of the eclogite results.

Much appreciation is given to Jennifer Nestojko, Krysta MacIntyre, Wendy Calabria, and Crian Shields for their assistance in proof reading portions of the text; any errors which remain are the sole responsibility of the author. Additional thanks are due Crian for having been a helpful and supportive housemate throughout my time in this project, for being there to bounce ideas off of at any hour of the day or night, and for providing parents with whom we could reside when needed. He also has my gratitude for assistance above and beyond the call of duty with late-night thesis printing.

Thank you to Dr. Andrew McNeill for sharing stories of his adventures on the southwest coast, and providing photos of the Nye Bay area for use in this thesis.

Many thanks to Crian Shields, Grant Thayer, and Eleanor Raine for providing assistance on sample-collecting trips, and to Drs. Ron Berry, Andrew McNeill, and Sandrin Feig for accompanying me on the successful quest to relocate the whiteschist.

May thanks to Dr. Jamie Connolly for his willingness to answer questions and provide assistance in the correct use of his Perple_X program suite, and to the members of the Perple_X discussion e-mail list for their helpful suggestions.

Finally, thanks are due to Dr. David Cooke for suggesting that Dr. Ron Berry had a project idea that I might find interesting. He was correct in that assessment and I have enjoyed the research from start to finish.

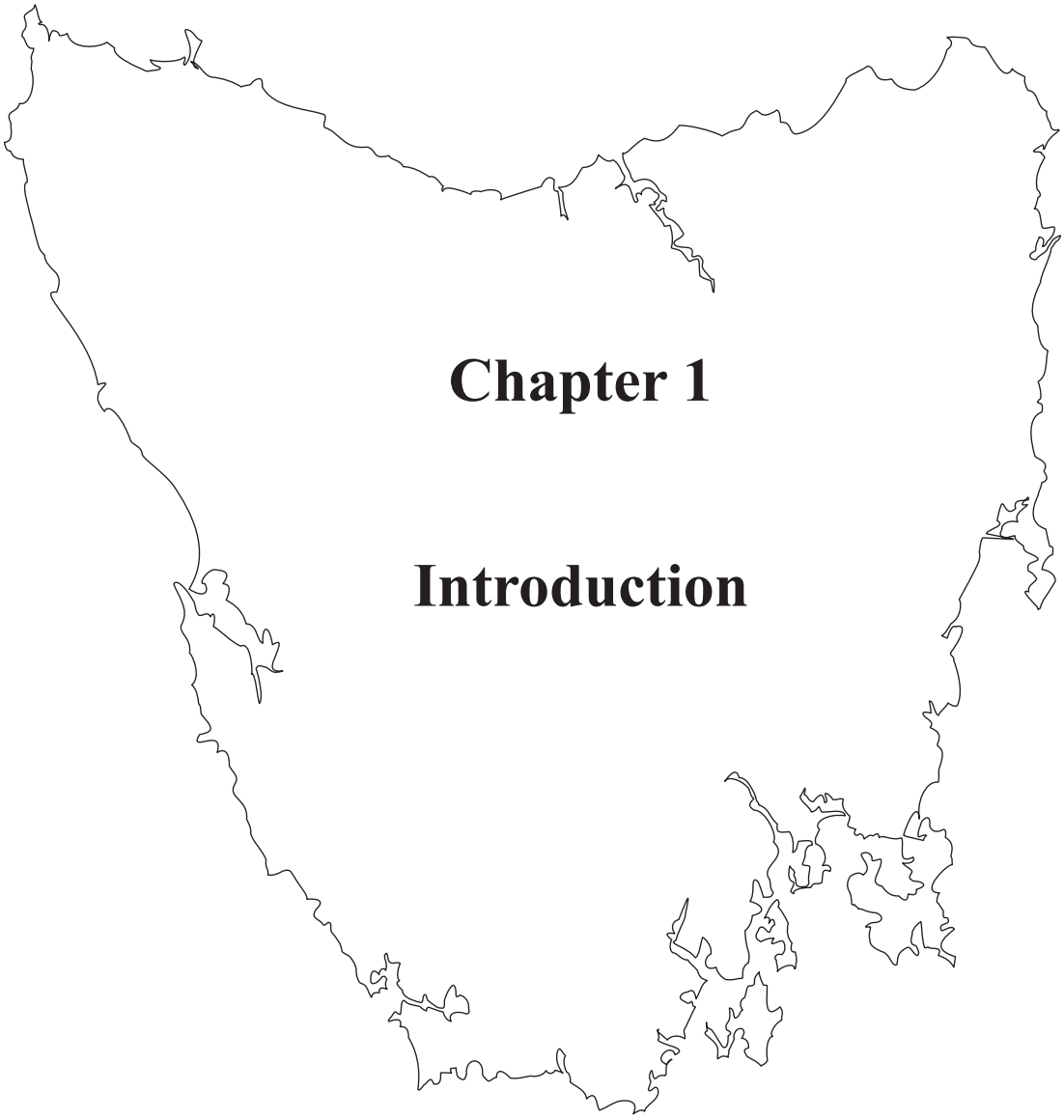

Chapter 1

Introduction

CHAPTER 1: INTRODUCTION

This study concentrates on the Cambrian regional metamorphic rocks of Tasmania that are of at least garnet zone. There is a range of regional metamorphic rock types in Tasmania; these are mainly of greenschist and amphibolite facies. There are also many examples in Tasmania of contact metamorphism but these have been excluded from this study. The regional metamorphic rocks of western King Island are excluded as these relate to Proterozoic metamorphism. In addition no attempt here is made to report on very low grade metamorphic rocks (sub-greenschist) whether the metamorphism occurred in the Devonian, as in northeast Tasmania (Patison et al. 2001), or possibly of Cambrian age, as in the Rocky Cape Group, far northwest Tasmania (Chester 2007).

1.1: GEOLOGY OF TASMANIA

1.1.1: Distribution of metamorphic rocks

The Cambrian regional metamorphic rocks of Tasmania are concentrated in the western third of the state in a series of complexes which lie in a generally mountainous belt from Ulverstone on the northwest coast to Port Davey on the southwest coast (Figure 1-1). This thesis generally follows the nomenclature for these metamorphic complexes proposed in Meffre et al. (2000). These complexes are grouped by region. The north coast includes the Arthur Metamorphic Complex, the Port Sorell Formation, the Settlers Schist, and the Forth Metamorphic Complex. The Mersey River Metamorphic Complex is in north central Tasmania, the central region contains the Franklin Metamorphic Complex, including the Collingwood River region metapelites, eclogites and whiteschist, and the Raglan Range, and Mt. Mary regions. The south central region has the Strathgordon Metamorphic Complex,

and the southwest coast has the Port Davey Metamorphic Complex, including the areas of Nye, Mulcahy, and Wreck Bays.

1.1.2: Metamorphic history

1.1.2.1: PREVIOUS WORK

The early work on Tasmanian Metamorphic rocks focused either on chemical studies (e.g. Paxton 1965; Spry 1963a) or on geologic mapping and interpreting structures in outcrop and thin section in terms of the sequence of the deformational events responsible. These studies were generally done for limited local regions, including the Northwest Coast (Spry 1964; Spry and Ford 1957), the Southwest Coast (Williams 1979), central Tasmania (Duncan 1972; Gee 1962; McIntyre 1964; Spry 1957, 1963a, b; Spry and Gee 1964; Spry and Zimmerman 1959; Turner 1971; Williams 1971), and south central Tasmania (Boulter 1972, 1978; Brown 1972; Williams 1976). However, a more regional approach was taken by Spry (1962), who focused on the petrology of all Tasmanian Precambrian Rocks. A later generation of petrological studies included geothermometry and geobarometry in addition to mapping and structural studies (see regional paragraphs below). The use of isotopic dating added a new dimension to geological research. An early application of isotopic dating on Tasmanian metamorphic rocks used whole-rock Rb-Sr dating (Råheim and Compston 1977). They correlated the strongest deformational event recorded in the rock with the results of their dating. Adams et al (1985) used K-Ar (whole-rock), Rb-Sr, and U-Pb (zircon crystals) isotopic dating. Their results fell into several age ranges. They gave a range of 630 to 690 Ma for the Burnie and Oonah Formations and the Rocky Cape Group, which they interpreted as the result of the Penguin Orogeny. They suggested a range of 540 to 610 Ma for the samples from the Tyennan Region, and 450 to 490 Ma for a number of units that were known to be Cambrian in age, for which they postulated a "significant thermal event" in the

Late Cambrian-Early Ordovician. However, the wide spread of their results was suggested by other authors (Turner et al. 1995) to be the result of the presence of "not one, but multiple generations of mica in varying proportions". Turner et al. (1995) presented a summary map of northwestern Tasmania with dates of various samples. They listed date ranges for various geologic events including uplift (486-502 Ma) and high-pressure metamorphism (502-510 Ma). A more recent study (Turner et al. 1998) questioned the assumptions in this early work and concluded that whole rock data methods were inaccurate; they concluded that Ar/Ar isotopic dating is only robust when used on mono-mineralic material. Additional dating results are summarized below and in Figure 1-2.

1.1.2.2: ARTHUR METAMORPHIC COMPLEX

The Arthur Metamorphic Complex, occupying an area called the Arthur Lineament, crosses the northwest corner of the state in a belt of fault slices more than 100 km long, but only 8 km wide (Figure 1-1). Holm (2002) recognized three different deformational events in these rocks. He interpreted CaD_1 as synchronous with blueschist facies metamorphism (~ 450 to 500^o C and 7,000 to 12,000 bars), but this metamorphism was only recognized in a few fault blocks. The blocks which reached these conditions he interpreted to be allochthonous, and other blocks, which show evidence of CaD_1 deformation, and no blueschist mineral assemblages, he interpreted to be autochthonous or para-autochthonous. CaD_2 took place in two stages. The earlier stage reached conditions near the greenschist amphibolite facies transition (just into garnet stability), but it varied in intensity, being generally stronger in the east and weaker in the west of the lineament. Again different blocks show different levels of strain and the blocks with higher metamorphic grade are para-autochthonous or allochthonous. The later stage of CaD_2 was much lower grade, only achieving greenschist conditions, lower temperatures than the early phase, and

pressures of ~ 3,000 bars. However, all blocks across the lineament experienced this phase of deformation and were apparently at the same temperature by the end of CaD_2. Holm (2002) concluded that while the various blocks came from different sources and experienced different conditions during CaD_1 and early CaD_2, they were all largely in their current configurations by the end of CaD_2. The final deformational event, CaD_3, was significantly weaker in intensity than the others, and caused no significant metamorphic recrystallisation. He recognized two different forms of albite porphyroblasts. The equigranular albite grains have a straight S_i inclusion trails, indicating growth during a non-deformational period. The elongate albite grains, on the other hand, are syn-rotational, with S_i straight in their cores, and curved towards the rims.

Another study from this complex (Turner and Bottrill 2001) focused on blue amphibole minerals within the Bowry Formation. They estimated that minimum peak metamorphic conditions at this location were ~ 350^o C, and 5,000-7,000 bars. Amphibole K-Ar ages of ~ 510 Ma have been reported for the Bowry Formation (Turner 1993).

1.1.2.3: NORTH COAST

1.1.2.3.1 Port Sorell Formation

The Port Sorell Formation contains both lower (subgreenschist facies) and higher (blueschist facies) grade rocks which were juxtaposed against one another (Henson 2002). Illite crystallinity and b_0 analysis of the pelitic units revealed medium pressure metamorphism ~ 250-300^o C, 2,000-3,000 bars while microprobe analysis of blue amphiboles in a metabasite indicated metamorphism at ~ 350^o C and 7,000 bars. The four deformational events from this area are correlated with those of the Arthur Lineament, with CaD_1 in this area corresponding to monazite U-Th-Pb age of 515 ± 14 Ma, and considered to be primarily responsible for south-directed transport

and layer-parallel shearing and fragmentation of the units. The other three local deformation events correspond to CaD_3, and two Devonian deformational events.

Additional pressure and temperature estimates from the Port Sorell area were reported by Reed et al. (2002), who combined data from blue amphibole compositions with minimum estimates from phengite geobarometry to yield estimates of 400-500^o C and 7,000-14,000 bars from blueschist facies rocks. They also recognized an earlier stage of greenschist metamorphism at ~ 3,000 bars and 350-450^o C.

1.1.2.3.2 Settlers Schist

Three small fault-bounded blocks near the Tamar River (Figure 1-1) make up the Settlers Schist as defined by Meffre et al (2000). This unit combines the Settlers metamorphosed greywackes and the Simmonds Hill metamorphics of Green (1959). The fault-bounded lenses of Settlers Schist, each less than 1 km in length, are located within Cambrian ophiolitic rocks of the Beaconsfield Ultramafic Complex, and are comprised largely of quartz-mica-plagioclase schist with minor chlorite and epidote (Gee and Legge 1979). The Settlers Schist has been the subject of some debate as to its protolith, but is most likely a metamorphosed granitic rock (Reed et al. 2001). Relict siliceous patches were interpreted as xenoliths by Berry et al. (2007—see Appendix 1 for full transcript of this companion document). Biotite K-Ar ages show that the metamorphism of the Settlers schist took place before the Early Ordovician {McDougall, 1965 #81; Turner, 1998 #30.

Reed et al. {, 2001 #112} reported an additional small body of metamorphic rocks 1 km west of Simmonds Hill which has typical amphibolite facies mineralogy and mafic composition.

1.1.2.3.3 Forth Metamorphic Complex

The Forth Metamorphic Complex, located on the north coast of Tasmania, particularly along the Forth River (Figure 1-1), contains interlayered quartzite, amphibolite and schist. The Ulverstone Metamorphics are an associated lower greenschist grade block, while the Forth Metamorphics are largely amphibolite facies (Burns 1964; Turner 1989). The Forth Metamorphics include ortho-amphibolites of tholeiitic MORB-type affinity interlayered with banded garnetiferous schist and quartzite (Lewis 1991). A garnet amphibolite from this complex has yielded zircons with an age of 514 ± 4 Ma (Black et al. 1997). A number of Ar/Ar white mica measurements form this area cluster at 508 Ma (five samples) and 522 Ma (2 samples) (Foster et al. 2005). The 508 Ma ages reflect final assembly of the low and high grade fault blocks. The significance of the 522 Ma Ar/Ar ages is less certain. Lewis (1991) estimated peak metamorphic conditions of 700 ± 50^{o} C and 13,000 ±2,000 bars for kyanite-garnet-biotite schists in the highest grade part of this complex.

1.1.2.3.4 Mersey River Metamorphic Complex

The Mersey River Metamorphic Complex is exposed in northern Tasmania (Figure 1-1) on the northern margin of the Tyennan Block. It includes the low to medium grade metamorphic rocks of the Dove Schist, Howell Group and Fisher Quartzite (Turner 1989). A few small mylonite zones from the Lake Rowallan boat ramp indicate south directed transport early in the deformational history (Berry and Bull 2004). The pelitic rocks of the Howell Group and from near Cradle Mountain contain garnet and biotite (Gee and Legge 1979) and are typical of the uppermost greenschist facies. No geothermobarometric data have been reported.

1.1.2.4: FRANKLIN METAMORPHIC COMPLEX

The Franklin Metamorphic Complex contains the highest grade of regional metamorphism in Tasmania. It is exposed along the Franklin and Collingwood Rivers, and is accessible via the Lyell Highway (Figure 1-1). The complex contains lenses of pelitic schist, quartzite, amphibolite, eclogite, and whiteschist (e.g. Goscombe 1990; Kamperman 1984; McDougall and Leggo 1965; Råheim 1976; Spry 1962; Williams 1971). The whiteschist was estimated to have formed at ≥10,000 bars at ~ 600^{o} C (Råheim and Green 1974). The eclogite has been the subject of several studies, with estimates of ~ 670^{o} C, 11,000 bars for peak conditions and ~ 520^{o} C, 7,500 bars for an earlier stage (Råheim 1976), 715-730^{o} C, 15,600-17,000 bars (Kamperman 1984), and ~ 700^{o} C, 15,200 bars (Goscombe 1990). In addition Goscombe (1990) also reported conditions for the pelitic schist surrounding the eclogite at ~ 16,400 bars at 700^{o} C.

1.1.2.5: STRATHGORDON METAMORPHIC COMPLEX

The Strathgordon Metamorphic Complex forms the core of a south plunging synform in an alternating sequence of quartzite and grey phyllite (Calver et al. 1990) exposed near the town of Strathgordon (Figure 1-1). The structure of this area was extensively studied by Boulter (1972; 1978; 1989) and the distribution of garnet was mapped. Portions of this sequence reaches garnet grade (upper greenschist?), and Boulter reported that the garnet/peak metamorphism occurred just before or during D_2. The metamorphic grade appears to be greenschist throughout the region. Detailed petrography by Råheim (1977) yielded a peak temperature estimate of 400^{o} C at 3,000 bars. Råheim and Compston (1977) reported a Rb-Sr age of ~ 780 Ma for peak metamorphism, with an isotopic disturbance (related to S_4 development) between 620 and 540 Ma.

1.1.2.6: PORT DAVEY METAMORPHIC COMPLEX

The Port Davey Metamorphic Complex is exposed on the southwest coast of Tasmania (Figure 1-1). It contains pelitic schist, with amphibolite and garnet amphibolite lenses (Meffre et al. 2000). The Nye Bay region was studied by McNeill (1985), who reported conditions of ~ 630^{o} C, 7,500 bars for the garnet-bearing schists. The garnet-rich schist of the Port Davey area was described as being below 540^{o} C (assuming pressures of ~ 4,000 bars) due to the absence of cordierite or staurolite (Williams 1982), and peak metamorphic assemblages of 450-500^{o} C for amphibolite and 400^{o} C for pelitic schist at ~ 4,000 bars was recorded by (Turner 1989), who note that the Ca and Mn zonation in the garnet crystals imply two different sets of growing conditions.

1.1.2.7: OFFSHORE DATA

Off the southern margin of Tasmania is a large area of thin continental crust (South Tasman Rise and East Tasman Plateau). Dredge samples of metamorphic rock from the area were separated into three suites by Berry et al (1997). The first suite is low to medium grade metamorphic rocks indistinguishable from those exposed in mainland Tasmania ("Slates", "Phyllites" and "Schists"). These were recovered from relatively shallow water near the present exposed areas west and south of mainland Tasmania. The other two suites are unlike Cambrian rocks from Tasmania and are excluded from this discussion. Very low to medium grade metamorphic rocks were recovered from a large number of dredge hauls. Muscovite garnet phyllites and biotite muscovite garnet schists are common. Typical P/T results were 550^{o} C and 6,000 bars. Metasedimentary rocks from the South Tasman Rise have an early Palaeozoic K/Ar biotite age and a Cambrian chemical U-Th-Pb age similar to metamorphic samples from Tasmania.

1.1.2.8: TECTONIC MODELS

Recent studies have combined all of the above categories of investigation with theories of plate tectonics. They attempt to answer questions concerning the tectonic settings/processes responsible for the deformation recorded (Foster et al. 2005; Holm 2002; Holm and Berry 2002; Meffre et al. 2000; Reed et al. 2002). There have been a variety of models proposed for the tectonic history of Tasmania. One early model proposed that Dundas Trough marks the location of a narrow rift with thinning of continental crust, followed by later compression and faulting (Brown 1986; Campana and King 1963; Varne and Foden 1987; Williams 1978). This view is in marked contrast with another which described the Dundas Trough as the location where an ocean basin closed via subduction, bringing together the Rocky Cape and Tyennan Regions during the Cambrian (Corbett and Lees 1987; Crook 1980; Green 1983; Solomon and Griffiths 1972, 1974). Both of these models were questioned by Berry and Crawford (1988), who proposed instead that various mafic/ultramafic complexes represent allochthonous sheets which were emplaced onto Tasmania, most likely from a forearc origin. Many of the recent papers (Black et al. 2005; Cayley et al. 2002; Foster et al. 2005; Meffre et al. 2000; Münker and Crawford 2000) accept that a Cambrian passive margin was overthrust during arc-continent collision by a mafic-ultramafic complex and turbidites during the early convergent stage of the Delamerian-Ross Orogeny, resulting in high-pressure metamorphism of the underlying wedge (~ 510 Ma) followed by thinning via post-collisional extension (grabens) and magmatism (505-495 Ma). An alternative view is that the metamorphic rocks discussed in this thesis are part of a core complex formed during Middle Cambrian extension (Hall 1998; Noll and Hall 2005).

1.2: AIMS OF THIS THESIS

A) Provide an overview of the pressure/temperature history of Cambrian regional metamorphic rocks in Tasmania.

B) Determine PT-t paths for selected metamorphic rocks from Tasmania with particular interest in medium grade pelitic rocks.

C) Elucidate the age of metamorphism using chemical U-Th-Pb dating of monazite.

D) Place this data in a tectonic context consistent with all of the data on the Cambrian history of Tasmania.

While this thesis concentrates on results from the pelitic rocks, the eclogites from the Collingwood River area were also studied in a cooperative project with geologists from the *Museo Nazionale dell'Antartide*, and the *Dipartimento di Scienze della Terra* at Siena University and that aspect of the project was reported in Palmeri et al. (2009—see Appendix 1). Section C) represented the continuation of an ongoing study started in 2004. The initial results of chemical U-Th-Pb monazite dating were reported after the first year of this thesis project in (Berry et al. 2007—see Appendix 2) and has continued. This thesis integrates data from all 5 years of the study.

1.3: METHODS OF STUDY

1.3.1: Sample Collection

The greatest emphasis of this study has been in the medium grade metamorphic rocks along the Collingwood River in central Tasmania. While there have been extensive structural studies in the area, the metamorphism has received less attention. This area was targeted for further field work and a new round of sampling. Forty-three samples from the Franklin Metamorphic Complex were collected over two field seasons. The exposure in this region is poor, being limited, by extensive dense

vegetation, to variably weathered road-cuts, mountain tops, and fresher outcrop within the river bed itself. The new sampling collection concentrated on the least weathered rocks along the banks of the Collingwood River. These were collected during periods of low rainfall when the river was at its lowest levels. In addition to the riverbed samples, oriented mylonitic samples were collected from both road and river outcrops for structural analysis. In addition to this sampling, this project also examined samples collected from across all metamorphic regions of Tasmania and housed in the University of Tasmania rock storage facility. Collectors include Berry (various years) Boulter (1972), Gee (1962), Holm (2002), Kamperman (1984), Lewis (1991), Meffre (2000), McIntyre (1964), McNeill (1985), Spry (1962), Turner (1971), and Williams (1971). Some additional reconnaissance mapping in the upper Mersey Valley and in the Forth Metamorphics was also conducted. However, no relevant new samples were collected from those areas. A full table of samples collected from this study, and those investigated from previous studies is available in Appendix 3.

1.3.2: Analytical Methods

Petrographic analysis of polished thin sections of the samples was carried out using a polarising microscope to determine the suite of minerals present within each sample, their textures and relationships. From several hundred samples, 170 thin sections were examined in detail and 39 were chosen from five different regions for detailed micro-analytical work. Because garnet-isopleth thermobarometery was selected as one of the primary tools for the investigation (see below), all of these samples included garnet, commonly as porphyroblasts, locally reaching 2 cm in diameter. Where possible, samples were chosen which contained the combination quartz-garnet-biotite-muscovite-plagioclase-kyanite to permit the application of more than one geothermobarometer. However, it is quite rare for any one sample in this suite to

contain all of the desirable minerals, therefore samples containing as many as possible were selected. The five regions selected for detailed analytical work are, from north to south, the Forth, Collingwood River, Mt. Mary, Mulcahy Bay, and Nye Bay areas. The Arthur Metamorphic Complex was the subject of a recent University of Tasmania PhD thesis (Holm 2002) and subsequent publications (Holm and Berry 2002; Holm et al. 2003), and as a result samples from this area were not re-examined for this project. Samples from the Mersey, Settlers, and Strathgordon areas were unsuitable for geothermobarometric analysis, generally due to the extensive alteration and/or weathering of garnet and biotite in these rocks.

1.3.2.1: MINERAL ANALYSIS

The Cameca SX100 electron probe microanalyser at the Central Science Laboratory of the University of Tasmania, equipped with five wavelength dispersive spectrometers, was used to conduct quantitative analyses of individual mineral grains within the samples. A table of representative analyses is presented in Appendix 4, and of all microprobe results is presented in Appendix 5. Two sorts of analysis were performed, standard silicate mineral analysis, and chemical U-Pb-Th dating of monazite. The microprobe was set to operate at 15keV, 10nA for the standard silicate analyses, and the monazite analyses were carried out at 20 kV and 100 nA. Prior to microprobe analysis, many samples had analysis-points pre-selected using a digitized Olympus BX40F4 light optical microscope and recorded to a file via Microbeam Services Digimax software, which was then recoordinated with software on the Microprobe, saving considerable instrument time during the set-up stage. In addition, the FEI Quanta 600 MLA Environmental Scanning Electron Microscope and associated JKTeck MLA software at the UTAS Central Science Laboratory was used to create maps detailing the locations of all monazite grains located within some of the samples selected for monazite analysis. These maps recorded the size and

location of the monazite grains, and identified the minerals surrounding the monazite grains, creating false-colour images of all monazite grains and their enclosing minerals. During this process a back-scatter electron image of the entire thin section was also created. These maps allow for very efficient selection of grains to be analysed for U-Th-Pb ages. Both manual locating and selecting of monazite grains on the microprobe, and the use of MLA maps were carried out in this project and MLA maps were vastly superior especially were the host of monazite grains needed to be identified. For example, in some sections of this study monazite grains included in garnet were targeted. Not only does the MLA mapping software save many hours of labour in terms of grain selection, but the grains thus selected have a much clearer context.

1.3.2.2: WHOLE-ROCK ANALYSIS

Whole-Rock chemical analysis was accomplished via X-Ray Fluorescence (XRF) using a PANalytical (Philips) PW1480 X-Ray Spectrometer located at the School of Earth Sciences—CODES, University of Tasmania using procedures outlined by Robinson (2003) see Figure 1-3 for settings and details. A full list of XRF results, and the corrections made thereto, is presented in Appendix 6. The XRF results underwent two standard corrections before they were used in calculations. The Fe_2O_3 reported was converted, unless otherwise specified, to FeO using the assumption that 90% of the iron present was Fe^{2+} [((Fe_2O_3 x ((2 x 71.84))/159.69) x 0.9]. The CaO in the whole rock composition was reduced to account for the phosphorous present in apatite. In most cases it was assumed that the P is primarily located in apatite, and therefore a proportional amount of calcium is also unavailable for other minerals [CaO-(P2O5/(55/42))]. However, in a few cases alternative assumptions were made and these are outlined in the relevant section.

1.3.2.3: LASER-ICPMS

Laser ablation analysis of isotopes of uranium, thorium and lead in zircon was performed on two Collingwood River samples using the Agilent HP 4500 ICP-MS in the Earth Science Department of the University of Tasmania. The zircons were separated from their samples by crushing, milling, the use of a gold pan and a strong rare earth magnet before being mounted in epoxy. They were analysed using 35 micron spot size using a 193 mm laser on the Agilent 7500 ICP-MS MS in the Earth Science Department of the University of Tasmania. The method used is similar to Meffre et al (2008). No imaging was performed on the zircons due to time constraints. This was run as a pilot study to compare the results with those obtained via monazite chemical U-Th-Pb microprobe results. In addition to the zircons the separate of one sample, RC0710, was rich in monazite. Therefore two grains of monazite from this sample were analysed with the ICP-MS in addition to the zircons. Subsequent to that analysis, this sample was also selected for microprobe monazite analysis, making it the only sample in this study to undergo EPMA of U-Th-Pb in separated grains. All other EPMA analyses were in-situ.

Laser ablation analysis of isotopes of common lead in muscovites was performed using the Agilent 7500 ICP-MS in the Earth Science Department of the University of Tasmania. For some rocks these produced useful results but in most examples the system had suffered from Pb mobility during alteration and the results were not useful. This ran as a pilot study and was not extended to a full study of the metamorphic rocks. The full table of laser ablation results is presented in Appendix 7.

1.3.3: Data Analysis

1.3.3.1: MINERAL STOICHIOMETRY CALCULATIONS

The program Ax-Activity-Composition (Holland and Powell 2000) was used to calculate mineral stoichiometry from the microprobe results. These values were used for thermodynamic calculations, except where otherwise noted.

1.3.3.2: CLASSICAL GEOTHERMOBAROMETERS

Several different approaches to geothermobarometric calculations were undertaken. A table detailing the results from each technique by sample is presented in Appendix 8.

Thermocalc

The program Thermocalc (Powell et al. 1998) was used to perform average pressure-temperature calculations for the compositions of the garnet rims and matrix minerals which were interpreted to be in equilibrium.

GB-GASP

The garnet-biotite geothermometer (Holdaway 2000) and the garnet-Al-silicate-plagioclase geobarometer (Holdaway 2001) is the combination of choice for geothermobarometry of amphibolite facies pelitic rocks. It is unfortunate that only two samples studied contained all of the requisite minerals to use these geothermobarometers in tandem with one another. The results are further complicated by the fact that best results are said to be obtained for samples containing plagioclase with at least 0.15 X_{An} and garnet with at least 0.05 X_{Grs} (Todd 1998) and the samples used in this study are mainly lower in calcium than these limits. While a number of garnet grains analysed reach that level of grossular concentration in the rim, very few of the plagioclase have the requisite X_{An}. However the error limits suggested by Todd (1998) are very pessimistic. A review of the effect of low Ca on the errors associated with these calculations is given in

Appendix 9. The errors quoted in this thesis for results using these methods have been adjusted to allow for this effect.

The calibration was applied to rim compositions for sets of the required minerals which are in close proximity to and textural equilibrium with one another. It was not used to estimate T/P for core or garnet zoning patterns.

GB-GBPQ

The formulas needed for the garnet-biotite geothermometer (Holdaway 2000) and the garnet-biotite-plagioclase-quartz geobarometer (Wu et al. 2004) are combined in a single spreadsheet available from the later set of authors. The spreadsheet takes input data in the form of the number of cations of elements for each mineral to calculate the temperature and pressure for the rim compositions for sets of the above listed minerals. As with all geothermobarometers, it is recommended that the minerals used be not only in close proximity to one another, but that they also display textural equilibrium with one another. However, the authors caution that the optimal compositional ranges for the minerals are $X_{Grs} > 3\%$ in garnet, $X_{An} > 17\%$ in plagioclase, and $X_{Al(Bt)} > 3\%$ in biotite, and suggest that caution be used for minerals outside of these ranges. While all of the biotites measured fall into the appropriate range, and many of the samples used for this study do contain garnet crystals with a sufficient X_{Grs} component at the rim, none contain plagioclase with sufficient Ca to fall within that range, the highest value measured being X_{An} 0.15. This limits the precision of pressures calculated by this technique. An assessment of the additional error has been made and this is discussed in Appendix 9. In general for most of the samples here the error is less than 1000 bars but greater than typically expected for this technique.

GBMAQ

The garnet-biotite-muscovite-aluminosilicate-quartz geobarometer (Wu and Zhao 2007) is specifically calibrated to be effective with samples, like the ones in this study, which contain Ca-poor garnet and/or plagioclase. Again the T was estimate using the garnet-biotite geothermometer of Holdaway (2000). The P and T were calculated using a spreadsheet provided by Wu (pers comm.). This assemblage was available in three samples and produce pressure estimate entirely consistent with the GASP geobarometer provided a suitable additional error was included to allow for the low Ca in plagioclase. Calculations were restricted to rim compositions in close proximity to one another and in textural equilibrium.

1.3.3.3: PERPLEX

Whole-rock/garnet core calculations

The program Perple_X07 (Connolly and Petrini 2002 – last updates downloaded on 12 Dec 2007) was used to calculate rock-specific equilibrium assemblage diagrams (also called isochemical sections (e.g. Tinkham and Ghent 2005) for samples based upon their whole-rock (XRF) compositions (Vance and Mahar 1998). Comparison of the resultant predictions of which minerals should be stable for that sample at various temperatures and pressures with the minerals actually present in the sample is a tool for determining the metamorphic history of each sample. In particular garnet compositions can be thus successfully modelled, with the program creating graphs of the change of composition with changes of temperature and pressure for each of the four garnet end-members (almandine, pyrope, grossular and spessartine). The intersection of the isopleths which correspond to the composition as measured by the microprobe for the garnet core composition gives the temperature and pressure at which this garnet would have first crystallized for that sample. In many cases there is not a precise intersection of these isopleths. However, a reasonable approximation of the garnet core formation conditions can be determined by using

the Werami application of the Perple_X07package to determine the compositions and amount of each of the minerals present for a variety of temperature and pressure combinations in the region of likely isopleth intersection, usually in increments of 5 degrees and 100 bars over the range of interest. These results were then put into an Excel spreadsheet template which calculates the activity for each of the garnet end-members and compares them with the measured values for each. The "best fit" for each sample was determined by summing the absolute values of the differences between the measured and predicted compositions for each of the garnet end members, and selecting the P/T with the smallest sum of differences, then plotting those coordinates on the graph showing the isopleth intersection to confirm that it is also a good visual fit.

In addition Perple_X07 was also used to calculate the changes in garnet assuming garnet fractionation along a PT path with the aim to explain the rim composition. There are other programs available which will accomplish these same tasks (see Hoschek 2004 for a comparison of several). Perple_X07 is relatively straightforward to use, and has been demonstrated to be an effective tool for pelitic rocks of similar composition to the ones in this study (e.g. Gaidies et al. 2006). It was used here to model the compositional zoning in selected garnet grains.

The simplified model system MnO-Na_2O-CaO-K_2O-FeO-MgO-Al_2O_3-SiO_2-H_2O-TiO2 (MnNCFMASHT) was chosen for Perple_X07 calculations because this range of oxides includes most of the common rock-forming minerals in metapelites. The program uses a gridded Gibbs free-energy minimization approach (Connolly 2005) and an internally consistent thermodynamic data set (Holland and Powell 1998 and subsequent updates). The thermodynamic data file used was hp02ver.dat (downloaded, along with the program, in December 2007), and the solution models employed in these calculations are TiBio(HP), Chl(HP), Pheng(HP), St(HP),

Ctd(HP), feldspar, TrTsPg(HP), Gt(HP), IlGkPy, and Omph(HP). For some samples where tourmaline is present, calculations were also performed using modifications to the thermodynamic data file (Van Hinsberg and Schumacher 2007) to consider the component B_2O_3 and the mineral tourmaline and a comparison of both versions (with and without B_2O_3) are presented. Other than for the tourmaline calculations, Perple_X07 calculations were initially conducted as set out by Gaidies et al. (2006), and preliminary results had been obtained using their suggested solution models and an older version of Perple_X07 (downloaded June 2006, and using solution files dating to November 2004). However, it was determined that the 2007 upgrade was a more appropriate choice, particularly as it reduced calculation times by a factor of twelve. This change required the recalculation of all results, as the new version no longer supported the feldspar model (AbPl) that had been selected for the early modelling (after Gaidies et al. 2006).

PT path and automated garnet fractionation calculations

The program Perple_X07 (Connolly and Petrini 2002) was also used for phase fractionation calculations, assuming that garnet is the only mineral in the system to fractionate, using the same solution models, system components and thermodynamic data files as were used to calculate the rock-specific equilibrium assemblage diagrams. For these calculations the conditions under which the garnet cores formed was first determined (as above), and the results input for the starting temperature, pressure and wt% of each oxide for the phase fractionation calculations. Temperature was set to change with pressure and a slope for that function was chosen and calculations performed. The results were compiled and a graph of the change in compositions of the garnet end-members with changes to pressure was created to compare the various compositions predicted for garnet rims during fractionation with the measured compositions. In general it was necessary to try

more than one slope for the fractionation path. For each slope tried, a diagram was created in P-T space which showed the slope of the path and the points upon the path at which the fractionating garnet is predicted to achieve the same composition as the measured garnet. Plotting these results for more than one path and linking the points for each end-member reveals the manner in which different fractionation paths would affect garnet composition. The path located where the lines linking each end-member target composition converge to a single temperature and pressure is regarded as that best reflecting the changes in condition which resulted in the formation of this garnet. It is worth noting that the modelled paths do not produce an exact match for all four end-members; due to the low concentration of Mn for the starting whole-rock composition, X_{Sps} is predicted to run out early in the fractionation history, requiring that the calculations be re-started from that point without Mn. (The composition for the whole-rock given at the last step before Mn runs out is used for the re-start). As a result of this circumstance, the predicted T/P for X_{Sps} matching the measured garnet rim is always substantially lower than that of the other end-members. However, once a path was found which results in the other three garnet end-members having a predicted composition close to the measured composition at a single pressure/temperature, the whole-rock composition predicted for those conditions (after garnet has been fractionated out of the system between there and the starting conditions) plus an additional 0.001 wt% was used to do a second full Perple_X07calculation, this time with the intersections of the isopleths which match the garnet rim composition being used to determine the pressure and temperature of the conditions of formation for the garnet rim.

Manual garnet fractionation calculations

The other method used with Perple_X07to attempt to determine the conditions for garnet rim formation is a manual subtraction of the quantity of garnet predicted to be

present at the temperature and pressure of garnet-core formation based rock-specific equilibrium assemblage calculations, followed by a second “rock-specific” calculation for the “whole-rock” composition thus modified.

Display of Perple_X results

Note that in addition to Perple_X generated figures within the body of the thesis, all figures are also presented in electronic format on the accompanying CD. In cases where details in the paper figures are difficult to discern the reader is advised to consult the electronic format of the figure, which will permit a greater level of magnification.

1.3.3.4: STRUCTURAL ANALYSIS

The structural analysis of the Franklin Metamorphic Complex was largely carried out during the period from 1955 to 1970. These studies pre-dated the modern application of mylonite kinematic indicators to structural problems. Berry et al. (1990) noted that mylonites occur in this area. During the regional mapping sampling program, possible and probable mylonitic rocks were widely observed. In order to contribute to a discussion of the tectonic significance of these metamorphic rocks it was considered important to carry out a reconnaissance study of the mylonitic rocks in the area. Several oriented samples were collected. Most of these samples showed typical mylonitic textures in thin section. The results of this analysis were used to constrain movement direction on faults in the Franklin Metamorphic Complex. A table of the results by sample is presented in Appendix 10. This result was combined with published structural data to develop new cross sections of the complex, orientated parallel to the direction of early ductile fault movement in the area. These results are also important in relating the metamorphic data to the tectonic history of the area.

1.4: STRUCTURE OF THESIS

The results of the thermobarometric portions of this study are presented by region. Chapter Two covers the Collingwood River area of central Tasmania, Chapter Three covers the southwest coast of Tasmania, and Chapter Four the results from other regions in the state (Figure 1-1). The timing of metamorphism for all regions is addressed in Chapter Five, which covers both the monazite age dating and the results of a pilot study on the applicability of Pb isotopic analysis to metamorphic pelitic rocks. Chapter Six contains the discussions and conclusions. The appendices includes the full text of the two papers which were published in conjunction with this project (Berry et al. 2007; Palmeri et al. 2009), as well as supplementary data on techniques used and methods applied.

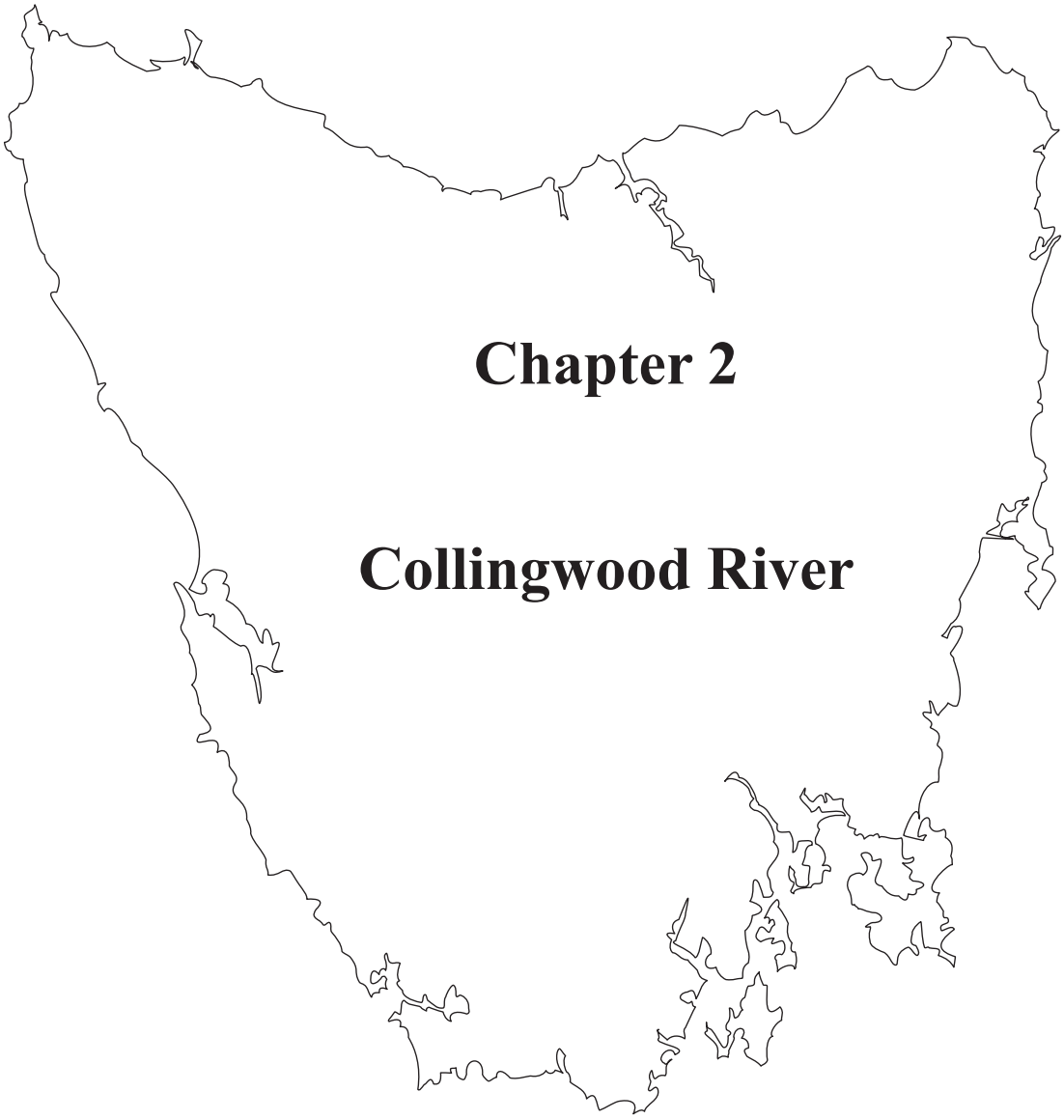

Chapter 2

Collingwood River

CHAPTER 2: COLLINGWOOD RIVER

2.1:FIELD DATA

2.1.1: Field Relations

The Collingwood River region (Figure 2-1) is intensely faulted and contains the highest-grade regional metamorphic rocks in Tasmania. It includes several different rock types, including pelitic schists, eclogite, phyllites, and whiteschist, all of which are interlayered or in blocky fault-bounded segments. This project focuses on two areas within the region—the "north block", located in the area wherein both the Collingwood River and Lyell Highway run nearly east-west (Figure 2-1B) for a roughly 3 km stretch, and the "south block", located where the river and road run generally northwest-southeast (Figure 2-1E) for five km. In general, the north block units are coarser-grained than their south block counterparts, and the south block pelitic rocks are more micaceous than are the northern block pelites. The pelitic schists, quartzites, and minor amphibolites and eclogites, of the Collingwood River area were called the Franklin Group schists by Spry (1962), and various publications based upon that research. Spry's map of the Frenchman's Cap area shows the Franklin Group throughout this region, including both "northern" and "southern" blocks as described above. The more recent nomenclature for this area is the Franklin Metamorphic Complex (e.g. Meffre et al. 2000).

The north block includes the schist with the largest crystals of garnet in the region (e.g. sample 160694 and 68788), which outcrops in the Collingwood River, between its intersections with Bill's Creek and Balaclava River (Figure 2-1D). Approximately four hundred metres downstream from the Balaclava-Collingwood River intersection is the first outcrop of eclogite (160703 & 160704) in the area; an outcrop of schist (160701) between the eclogite and the Balaclava River is richer in

quartz, has less muscovite, more albite and much smaller crystals of garnet than the schist at Bill's Creek. From the first appearance of eclogite the riverbed outcrops alternate between blocks of eclogite and various pelitic schists and quartzites for about 500 metres before the last outcrop of eclogite (for reasons of scale, that entire stretch of river is designated as "eclogite" in Figure 2-1B, despite the variety of rock types present). About two hundred metres further downstream is a quartzite, and another 500 metres downstream is a phyllite which is interpreted as the major fault zone separating the northern block from the southern block. Samples from the southern block were collected from along the Collingwood River just upstream from the intersection with Scarlett Creek (Figure 2-1E, Figure 2-2). This area contains interlayered quartzite, eclogite, fine-grained pelitic schist, mylonite, and an outcrop of whiteschist which crops out as a transitional (alteration?) zone around a ?boudin that is no longer present either due to either weathering or to some physical erosional process (Figure 2-1G). A possible interpretation of this outcrop is that this was a chlorite altered rind to a mafic boudin which was subsequently metamorphosed.

The geothermobarometric results reported below are from the northern block pelitic schists, and from the whiteschist of the southern block. In addition, there are monazite age results reported for the whiteschist and for pelitic schists from both blocks.

The eclogite of the northern block was the subject of a collaborative companion study to this project, and the manuscript (Palmeri et al. 2009) containing the details of this work is presented in Appendix 2.

2.1.2: Collingwood River Cross-Sections

Cross-sections along two lines, one in north block (Figure 2-1C), and one in the south block (Figure 2-1F) were constructed from new structural data and published field data (Brown et al. 2005; McIntyre 1964). The southern line is located

approximately five kilometres to the south east of the northern line, and its westernmost extent is eastward of the western end of the northern line (in addition to being further south). Both blocks are fault bounded, containing high-grade units surrounded by lower grade, but still strongly deformed rocks. There are minor mylonitic zones within each block, and the main boundary of at least the north block is a low temperature mylonite zone (phyllonite).

2.1.3: Mylonite Results

Five oriented samples of mylonite were collected from the Collingwood River area. Three come from the northern block from an outcrop on the Lyell Highway, near where Bill's Creek passes under the road before joining Collingwood River, and two from the southern block, from outcrops in the river bed upstream from the intersection of Scarlett Creek (Figure 2-3). The three from the northern block have a foliation that dips 32-40^{o} towards 231-258^{o}, and a stretching lineation which plunges 32-39^{o} towards 235-268^{o}. These samples are very mica-rich, and the mica fish form excellent kinematic indicators (Figure 2-4) showing a top-to-the-east displacement. The two from the southern block share very similar orientations to one another on their foliations (~ 62/205^{o}), but markedly different orientations for their lineations, which both plunge 59^{o}, but one to the south east and the other to the south west (Figure 2-5). One of these, 160731, a quartz-rich sample shares a top-to-the east sense of displacement, based on the orientation of quartz sub-grains (Figure 2-5), with the north block samples. The other, 160734, is a more mica-rich sample that has its mineral stretching lineation orientation nearly perpendicular to that of 160731, and reveals a top-to-the north sense of displacement (Figure 2-5).

2.1.4: Regional Cartoon

The cross-sections (Figure 2-1 C and F) were used in conjunction with the mylonite kinematic indicators (Figure 2-3) for the construction of schematic regional sketches showing a possible interpretation of the general structure of the Collingwood River region (Figure 2-6). A major fault zone is expressed by the outcrops of phyllonite. Lesser, related, faults bring different grades of schist to the surface, and interlayer the boudins of eclogite with schist. This interpretation is in marked contrast with that of Spry (1962) (Figure 2-7), who interpreted the section as a recumbent fold to account for the complexities inherent in the area. Early workers failed to recognize the mylonitic fabric of the area; as a result their picture of the significance of the high strain features was incomplete. The east and north directed transport inferred from the rocks is different from some of the other transport indicators for similar age rocks in Tasmania. The significance of this difference will be discussed in Chapter 6.

2.2: DESCRIPTION OF SAMPLES

The pelites from the northern block that received detailed analysis for this project contain the assemblage Qtz + Ms + Grt ± Pl ± Bt ± Tur ± Ky with rutile and monazite as accessory minerals. Quartz and muscovite are the dominant minerals, with the muscovite up to 4 mm in length. Biotite is present as a minor component in most of the Collingwood River schists, with generally much smaller grains (< 1 mm) than the muscovite, and these grains have typically been chloritised. The samples that contain tourmaline have little to no biotite. Kyanite was identified in the matrix in only two of the Collingwood River pelitic samples. It is present as large (3 x 0.6 mm long) grains in the otherwise fine-grained mylonite, 160706, and as a very small (0.1 mm diameter) grain in the coarse grained 160696 (Figure 2-8). In addition it was identified as an inclusion within garnet in sample 160694 (Figure 2-8), where it is not present in the matrix. It may also be present as small inclusions within garnet

in those other samples which did not undergo detailed inclusion analysis. Kyanite is also present in the whiteschist (160730, Figure 2-8)

The garnet grains from the Collingwood River pelites have cores that are moderately homogeneous with respect to Fe, Mg & Ca and a zoned rim (Figure 2-9). While none of the samples are very high in Mn, they generally show some change in X_{Sps} across the core, no matter how flat the graphs are for the other three end-members (Figure 2-9). This pattern of largely homogeneous cores and zoned rims holds true for various sized crystals, with garnet as small as 1 mm and as large as 1 cm displaying this feature. The garnet cores are 0.8 - 0.85 X_{Alm}, 0.08 - 0.12 X_{Prp}, 0.02-0.04 X_{Grs}, and 0.4 – 0.11 X_{Sps}. Where there is any zonation in the cores, it is dominated by spessartine zoning. The rim zoning involves a decrease of X_{Alm} down to as low as 0.70 X_{Alm}, with the most common rim composition ~ 0.78 is X_{Alm}. The rims show an increase of X_{Prp} to as high as 0.21, with most of the garnet grains analysed falling in the range 0.13 – 0.17 X_{Prp}. The X_{Grs} composition rises to as high as 0.14 on the rim, but more typically reaches 0.06 to 0.08 at the rim (and in some samples X_{Grs} is unzoned even on the rims). Finally, the X_{Sps} component decreases towards the rim (Figure 2-9). The garnet crystals of Collingwood River are remarkably similar to one another in their compositions, as shown by a comparison of the individual analyses presented in Figure 2-9. The cores and the rims of these garnet analyses plot in clearly different regions. In the Ca-Mn-Mg diagram the rims, as one would expect, are below 10% Mn and range between 40-90% Mg (10-60% Ca), while the cores are generally Mn 10-40 %, Ca 10-30%, Mg 50-90%. The compositional region defined by the cores overlaps that of the rims in the vicinity of Mn 0-10%, Ca 10-20%, and Mg 80-90%. In the Fe-Mn-Ca diagram there are again two distinct groups—primarily because the cores contain more Mn than do the rims. For this diagram there is less apparent variation in the core compositions (85-95%

Fe, 1-15% Mn, 1-10% Ca) than in the rims (75-95% Fe, 1-25% Ca, and 0-1% Mn), but again, the two regions converge on a single meeting point around 95% Fe, 2% Mn, and 5% Ca. The Fe-Mg-Ca diagram reveals that while most of the Collingwood River samples have the same sort of composition for their garnet core (the region marked by 70-80% Fe, 1-10% Ca & 10-20% Mg), there are two distinct rim populations, one of which is richer in Ca, the other richer than Mg. Of the three samples from the higher Ca-rim group one was also analysed for XRF whole-rock composition. It is much higher in whole rock Ca and lower in Mg than those from the other group with Mg rich rims. The third diagram compares X_{Alm}, $X_{Prp}+X_{Sps}$ and X_{Grs} (Figure 2-9c). It shows one cohesive group of core compositions from 75-90% X_{Alm}, 1-10% X_{Grs}, and 10-25% $X_{Prp}+X_{Sps}$, but a broader range in rim compositions, with each sample having a narrow trend in their rims, but some having rims that are noticeably different from the others. A few range from 10-20% X_{Grs} and $X_{Prp}+X_{Sps}$, and 70-80% X_{Alm}, while the others are more like 1-10% X_{Grs}, 15-25 $X_{Prp}+X_{Sps}$, and 70-80 X_{Alm}. More specific comments pertinent to the composition of garnet in each sample are included below, in conjunction with the geothermobarometric results for those samples.

Plotting the compositions of individual garnet analyses on triangle diagrams (Figure 2-9, Figure 2-10) shows marked contrast in the compositional trends of cores vs rims; the rims change their compositions along different paths than the cores. In general, all of the garnet grains analysed from Collingwood River display similar compositional trends (Figure 2-10).

2.3:WHOLE ROCK COMPOSITIONS

Whole-rock chemical analyses were measured for ten Collingwood River pelites (Figure 2-11). They are all low in calcium (0.06-0.66 wt%—see Appendix 6). The lowest of which, sample (160696), was so low in Ca that the standard correction for apatite (see section 1.3.2.2) resulted in a negative value, therefore that sample was not considered for Perple_X calculations. When compared (Figure 2-11) with the average pelite of Symmes and Ferry (1992) these samples plot considerably higher in A (both $AL_2O_3 - 3\ K_2O$ and $AL_2O_3 - K_2O - NA_2O$) and lower in F (both FeO and FeO + MgO + MnO) and M (MgO) and C (CaO). There is a much tighter grouping of these composition on the ACF diagram than on the AFM.

2.4:PT FROM GARNET RIM AND MATRIX MINERAL COMPOSITIONS AND CLASSIC GEOTHERMOBAROMETRY

The pressure and temperature for the peak metamorphism was calculated for the garnet rims and matrix minerals garnet biotite Fe-Mg exchange geothermometry. The calibration of Holdaway (2000; 2001) is used throughout. Three common geobarometers are used and in each case a very recent calibration is applied. These are GASP (Holdaway 2001), GBPQ (Wu et al. 2004) and GBMAQ (Wu and Zhao 2007). These provide an internally consistent set of calibrations.

Garnet-biotite-muscovite-kyanite-quartz (GBMAQ) is a calibration particularly designed for rocks with low Ca; there is some doubt over the accuracy and applicability of other geobarometers for such samples, as they depend on the reaction between anorthite and grossular. There was a single sample from Collingwood River in this study that contained this assemblage in apparent textural equilibrium (see section 2.4.2). The GB-GBPQ geothermobarometer has been calibrated for use in metapelites which are lacking in aluminosilicate minerals (Wu et al. 2004). Ten of the Collingwood River samples analysed contained the combination garnet-biotite-

plagioclase-quartz required for this geothermobarometer. Unfortunately, not all of these yielded useable results, due to altered biotite or plagioclase with X_{An} too low for reliable estimates (see Appendix 9); such samples are not reported here. All of these samples were also analysed for average temperature and pressure via Thermocalc. Details for the results for each sample are listed below, followed by a summary for the overall results for the region. Most of these samples have high garnet and low biotite. They are not suitable for the calculation of PT conditions for the initial growth of garnet by assuming an infinite matrix reservoir (cf. Kohn 2004). PT conditions for the garnet cores were calculated from garnet isopleth thermobarometery from the bulk rock composition.

2.4.1: 67659

Sample 67659 (Qtz-Ms-Grt-Pl-Bt schist with rutile and huttonite as accessory minerals) is more than 50% fine-grained quartz (< 1 mm), and 25% muscovite, which occurs in laths up to 2 mm long that define the foliation (Figure 2-12). This was one of the few samples analysed which did not contain accessory monazite. The grains of garnet are generally < 2 mm in diameter, and do not show a visible core-rim boundary. The rare grains of plagioclase are up to 2 mm in length. The even rarer biotite never exceeds 0.5 mm in length. However, unlike most other Collingwood River samples, most of the biotite analysed is unaltered.

The compositions for the garnet end-members of the garnet core are 0.82 X_{Alm}, 0.09 X_{Prp}, 0.025 X_{Grs}, and 0.07 X_{Sps}. The largest garnet grain analysed (0.9 mm diameter) has very different compositions on each rim (Figure 2-13). The left-hand rim (Figure 2-13), which is in contact with a grain of biotite, has values of 0.82 X_{Alm}, 0.14 X_{Prp}, 0.05 X_{Grs}, and 0.014 X_{Sps}. The right-hand rim (Figure 2-13), which is not in contact with biotite, has a composition of 0.72 X_{Alm}, 0.11 X_{Prp}, 0.15 X_{Grs}, and 0.10 X_{Sps}. Three spots on a small garnet grain (0.3 mm x 0.15 mm) were also analysed. Their

average is very similar to the right-hand rim, with values of 0.72 X_{Alm}, 0.12 X_{Prp}, 0.14 X_{Grs}, and 0.10 X_{Sps}.

A single grain of plagioclase was analysed. It is albite-rich, ranging from 0.7 to 0.10 X_{An}, which is low enough to significantly increase the error on the pressure estimate (see Appendix 9). This uncertainty in X_{An} adds an additional 900 bars error to the pressure estimates. While systematic lines across the plagioclase were not analysed, the highest X_{An} value is from the analysis point closest to the rim of the grain. Other samples, for which systematic plagioclase lines were analysed, showed an increase in X_{An} at the rims of the grain. Therefore, the highest X_{An} value for this sample is taken as the best available estimate for the equilibrium plagioclase composition. The biotite ranges from 0.41 to 0.43 Mg/Mg+Fe, the highest of these being the grain nearest the garnet rim & plagioclase used for P/T calculations (Figure 2-13). The GB-GBPQ estimate is 670^{o} C, 15,000 bars (Figure 2-14). The Thermocalc average P/T estimate for the same mineral pairs, with the addition of the nearest muscovite analysed, gives an average estimate of ~ 640^{o} C, 12,300 bars (Figure 2-14).

2.4.2: 160696

Sample 160696 was obtained from the bed of the Collingwood River, near its intersection with Balaclava River (Figure 2-1). This schist has garnet porphyroblasts up to 1 cm diameter. The muscovite reaches 0.5 mm long and define a weak foliation which wraps around the large garnet grains, the quartz is generally 0.2 mm diameter, except within alcoves of the large garnet, where individual grains within an aggregate reach 0.8 mm. The rare kyanite, felspar and biotite grains are up to 0.1 mm in their longest dimension. This sample has the lowest whole-rock calcium content of any of the Collingwood River samples (Appendix 6). It was so low in CaO that the standard correction subtracting CaO in proportion to P2O5 under the assumption that all phosphorus was locked up in apatite resulted in a negative CaO.

As a result this sample was not used in the Perplex calculations, but is included here as it is only Collingwood River sample to contain all of the requisite minerals for GBMAQ (Wu and Zhao 2007) calculations. The compositions of muscovite, biotite, and the garnet rim in close proximity to the kyanite point to conditions of approximately 700^{o} C, 9,500 bars.

2.4.3: 160698

Sample 160698 was collected from the Collingwood River, about 160 metres down stream from its intersection with the Balaclava River (Figure 2-1). It is a fine-grained schist, containing abundant quartz and plagioclase, with garnet, biotite, tourmaline and chlorite. The rock has a typical SC mylonite texture. The largest mineral present is the plagioclase, with grains up to 3.6 mm long x 1.8 wide. Some of these grains show cracking and undulose extinction (Figure 2-15). The garnet crystals are up to 2 mm diameter, and are partially cracked. They do not show a visible difference in appearance between core and rim. The larger grains of garnet are generally altered to chlorite along the edges parallel with the foliation, and remain unaltered adjacent to the primarily quartz-filled pressure shadows. The composition of the garnet grains, measured from unaltered to unaltered edge, shows a homogeneous core and zoned rim, with $X_{Sps} > X_{Grs}$ in the core and reversed in the rim. The composition of the rims is similar to that of the tiniest garnet grains (Figure 2-16). The muscovite laths, which define a foliation, are up to 3 mm long, and mica fish geometries are common. The dark reddish-brown biotite laths are up to 0.4 mm long, and are parallel with the muscovite foliation. The tourmaline is up to 0.3 mm wide, and has rims that are a paler brown than the biotite, and greenish cores. The chlorite is a greenish grey in aggregate bundles of laths up to 1 mm long, and occurs both along garnet edges and within muscovite grains. Both the biotite and chlorite contain pleochroic “haloes” around inclusions, which are interpreted to be monazite.

However, this sample was not one of the many selected for monazite analysis, as a result the composition of those grains is inferred by comparison with the other samples in the area. The large grains of plagioclase were analysed only in random interior spots, not in lines across the grains, so it is unknown if they exhibit zoning as do other Collingwood River plagioclase grains. These random analyses range from 0.05 to 0.07 X_{An}, which is lower than recommended for geothermobarometric analysis (see Appendix 9) and thus increases the errors associated with the pressure estimates obtained. The set of analyses which are in closest proximity to one another and are unaltered (Figure 2-17) yield a GB-GBPQ estimate of ~ 760^{o} C, 17,300 bars and a Thermocalc estimate of ~ 770^{o} C, 14,600 bars Figure 2-18. The Thermocalc result is the preferred pressure estimate; the low X_{An} of the plagioclase increases the error on the GB-GBPQ result.

2.4.4: 160702

Sample 160702, collected from the Collingwood River bed immediately next to the first outcrop of eclogite east of Bill's Creek (Figure 2-1), has abundant muscovite and quartz, plagioclase, lesser garnet, and only a small amount of biotite. Rutile is present as an accessory mineral up to 0.1 mm wide. This sample does not have a pronounced foliation. There are two differently sized populations of garnet. The larger is generally between 1-2 mm in diameter; the largest found is 2.4 x 1.3 mm. The smaller population generally ranges from 0.1-0.2 mm, and are more likely to be equidimensional. The muscovite laths range up to 1.5 mm long, and the plagioclase grains are up to 1.5 mm wide. As with some of the other Collingwood River samples, the plagioclase was analysed in random spots, most of which were in the 0.05-0.07 X_{An} range, below the recommended X_{An} content for accurate pressure estimates (see Appendix 9). The rare biotite laths are less than 0.3 mm in length, and are commonly chloritised. The set of minerals shown in Figure 2-19 were chosen for

P/T calculations. The average composition of the three analysis points on the small garnet was chosen as the best representative of the garnet rim composition after comparison with the rim measurements from the larger grains. The estimate from GB-GBPQ is ~ 750^{o} C, 16,900 bars, and from Thermocalc ~ 700^{o} C, 13,200 bars (Figure 2-20).

2.4.5: 160708

Sample 160708 was collected from an outcrop on the Lyell Highway roughly half of the distance between Bill's Creek and the first river eclogite outcrop thereafter (Figure 2-1). It contains primarily quartz, muscovite, plagioclase, with minor garnet and biotite as well as rutile, chlorite, and monazite as accessory minerals. The plagioclase occurs as subhedral porphyroblasts up to 1.5 mm in length. The white mica laths are up to 2 mm long and 0.3 mm wide and define a foliation. The biotite laths are up to 0.9 mm long and parallel with the foliation. Most garnet occurs as small (~ 0.5 mm) subhedral grains (Figure 2-21), but rare porphyroblasts up to 4 mm across were found. The garnet rim chosen for geothermobarometric calculations is the one nearest the matrix grains analysed, and with the lowest (0.010) X_{Sps} value. Three grains of plagioclase were analysed in this area of the thin section, ranging in composition from 0.06 to 0.08 X_{An}. As with most Collingwood River plagioclase analyses, this is lower than recommended for geothermobarometric calculations (see Appendix 9), and pressures thus obtained must be considered a maximum. Much of the biotite has been partially altered. GB-GBPQ yields an estimate of ~ 700^{o} C, 18,000 bars using an unaltered biotite analysis in conjunction with nearby other grains and Thermocalc yields an estimate of ~ 730^{o} C, 15,200 bars (Figure 2-22). The Thermocalc result is preferred as the maximum pressure.

2.4.6: 160713

Sample 160713 was collected from ~ 60 metres downstream from 160711, and approximately 90 metres upstream from the next outcrop of eclogite (Figure 2-1). It is a quartz-rich schist (most quartz grains < 0.1 mm). There are occasional flakes of muscovite which can reach 1 mm in length. The garnet reaches a diameter of 1.8 mm, and the plagioclase is up to 0.6 mm wide. The biotite laths, which are much less common than the muscovite, reach 0.5 mm in length. This sample has a weak foliation. While systematic lines across the plagioclase were not analysed, one grain was analysed in two interior points ~ 0.08 X_{An}, and one point at the rim edge 0.14 X_{An}. The rim composition is one of the rare examples of Collingwood River plagioclase with a high enough X_{An} component to yield reasonable results via GB-GBPQ (see Appendix 9). Five analysis points on three different grains of biotite have unaltered compositions and are usable for geothermobarometric calculations. One of these grains is not in contact with a garnet, and so was less likely than the other two to have suffered diffusion exchange during cooling. This grain was used in conjunction with the nearest (Figure 2-23) muscovite, plagioclase rim (0.14 X_{An}), and garnet rim (0.75 X_{Alm}, 0.18 X_{Prp}, 0.05 X_{Grs}, 0.014 X_{Sps}), for GB-GBPQ and Thermocalc P/T estimates. GB-GBPQ yields an average of 680^{o} C, 9,800 bars, and Thermocalc yields 880^{o} C, 13,600 bars (Figure 2-24). Thermocalc is the preferred pressure estimate, but 680^{o} C is a more reasonable temperature for this rock.

2.4.7: 160717

Sample 160717 (Figure 2-25) was collected from the Collingwood River, just downstream from the main eclogite outcrop (Figure 2-1). This quartz schist also has a (?S2) crenulation cleavage. The garnet grains are up to 1.5 mm in diameter, and they have a pronounced visual difference between the cores and the rims (Figure 2-26). Like many other Collingwood River garnet crystals, the cores are quite

homogeneous, and the rims are zoned. However, unlike most others, there is a reversal in the zoning direction at the rim edge for some of the end members (Figure 2-26). The muscovite laths are up to 1 mm long, and the biotite laths are up to 0.5 mm long. The plagioclase is typically fine-grained, but large grains up to 6 mm occur (Figure 2-27). Both biotite grains analysed in this sample were sufficiently unaltered as to be useable for geothermobarometric calculations. One of them (b4) ranges from 0.39-0.49 Mg/Mg+Fe and is located near (~ 0.3 mm away) a small (0.35 mm) grain of garnet and large grain of plagioclase (Figure 2-27), the near-by rim of which ranges from 0.14-0.15 X_{An}. The three points analysed on this small garnet are similar in composition to that of the rims of the larger garnet grains, with the interior of the small grain having a composition which matches that of the transition point on the rims, and the edge matching that at the rims edge of the larger grains (Figure 2-26). Due to the slight reversal at the garnet rims, the interior of the small grain of garnet was selected as more likely to be representative of conditions approximating peak metamorphism, and so this is the analysis selected for use in the geothermobarometric calculations. GB-GBPQ yields an estimate of ~ 700^{o} C, 14,100 bars and Thermocalc ~ 740^{o} C, 13,100 bars (Figure 2-28) for the small garnet interior and the other grains all within 0.3 mm of one another. This represents the best match between the two techniques obtained for the Collingwood River samples.

2.4.8: Summary of all Collingwood River Metapelite Peak Metamorphism Estimates

The GB-GBPQ results for all of the Collingwood River samples are centred on ~ 720^{o} C, 17,000 bars for most of the samples (Figure 2-29). The error ellipses of Figure 2-29 were created via Isoplot by setting the error to 25^{o} C and 1000 bars as a minimum estimate of error for this technique.

The Thermocalc results are centred on ~ 750^{o} C, 14,000 bars (Figure 2-30). The error ellipses of Figure 2-30 were created via Isoplot from the errors reported by Thermocalc, which tend to be conservative compared to those suggested for the other geothermobarometers. Despite the larger ellipses on the Thermocalc graph as compared to the GB-GBPQ graph, this technique actually yields a more robust pressure estimate, and the value of ~ 750^{o} C, 14,000 bars is the preferred estimate for the peak metamorphic conditions for the Collingwood River region of the Franklin Metamorphic Complex.

2.5:PT FROM GARNET CORE COMPOSITIONS AND PT PATHS

As described in the introduction (section 1.3.3.3), the program suite Perple_X was used to calculate the conditions for the formation of the garnet cores in the Collingwood River samples and to calculate pressure/temperature paths which would account for the changes in composition of the garnet from core to rim. The results for each sample will be presented first, followed by a summary of the patterns observed for all.

To test for systematic differences between Perple_X predictions and P/T estimates via other techniques the predicted mineral assemblages from each of the Perple_X runs (including those which were not successful in matching garnet core conditions) were entered into GB-GBPQ and the P/T predicted by each plotted against one another (Figure 2-31). The pressures predicted by Perple_X tend to be higher than those obtained via GB-GBPQ for the same mineral compositions, and the higher the pressure, the greater the difference, with all data > 6,400 showing higher estimates for Perple_X than GB-GBPQ (Figure 2-31A). The temperatures are generally estimated slightly higher by GB-GBPQ than Perple_X had predicted for the lower temperatures (Figure 2-31). Note that some of the rim results differ by as much as ~ 1,500 bars lower for GB-GBPQ than for the Perple_X. However, above ~ 560^{o} C the

Perple_X estimated temperatures are higher than the GB-GBPQ estimates for the same assemblage for more than half of the data garnet rims (> 6400 bars) , and generally lower for that predicted to be in equilibrium with the garnet cores than that originally estimated by Perple_X (Figure 2-31B).

2.5.1: Sample 67662

2.5.1.1: 67662 SAMPLE DESCRIPTION

Sample 67662, collected by Kamperman (1984) from the hill above the Lyell Highway near where it crosses Bill's Creek (Figure 2-1), is a coarse-grained schist containing quartz, muscovite, plagioclase, and garnet, with a few rare, small (up to 0.2 mm) grains of biotite. It is quartz-rich, the fine-grained quartz rarely exceeding 0.1 mm in diameter. The plagioclase is up to 0.6 in length. The muscovite occurs in laths up to 3 mm long, but does not have a strong preferred orientation. It contains two populations of garnet; the larger garnet crystals are 2-5 mm in diameter, and the smaller, more numerous garnet grains range up to 0.3 mm. The garnet crystals of this sample do not show any sort of change in appearance between core and rim, but exhibit a uniformly cracked and inclusion-poor aspect throughout (Figure 2-32).

2.5.1.2: 67662 COMPOSITION

The garnet cores are as high as 0.82 X_{Alm} and 0.06 X_{Sps}, and as low as 0.09 X_{Prp} and 0.03 X_{Grs} (Figure 2-32). The rim composition is zoned, with the composition dropping to 0.72 X_{Alm} and 0.003 X_{Sps} and rising to 0.10 X_{Grs} and 0.18 X_{Prp}. The increase in Ca and Mg on the rims suggests a path to high P and T. The smallest garnet crystals have compositions the average of which matches the rim composition of the large garnet. The muscovite ranges from 0.17-0.26 Na/Na+K; this is higher in Na than the other Collingwood River muscovites analysed, and this composition may represent fine intergrowths of paragonite and phengite similar to that reported by Shau (1991) (Figure 2-33). All of the biotite analysed in this sample has been

chloritised. The plagioclase, which exhibits albite twinning, was not analysed; all of the other Collingwood River samples have plagioclase with 0.15 X_{An} or less. The whole rock composition for this sample falls in the middle of the range for Collingwood River samples, with low values of TiO_2, CaO, P_2O_5, and MnO, moderate values of MgO, K_2O, and FeO, and high values of Al_2O_3 and SiO_2 (Figure 2-11). However, it does have the second-highest FeO concentration of the Collingwood River samples

2.5.1.3: 67662 GARNET CORE CONDITIONS

Two different approaches to calculations were attempted for this sample, one using the standard correction (section 1.3.2.2) and one using the assumption that all of the iron measured in the XRF analysis is present in the form FeO. Using the standard corrections to the whole-rock composition and calculating isochemical sections for this sample provides a match to the garnet core compositions at 640^o C and 5,900 bars (Figure 2-34). At this condition, X_{Grs} is predicted to be 0.002 lower than the measured value, X_{Sps} and X_{Alm} are both predicted to be 0.006 higher than measured, and X_{Prp} 0.014 higher than measured. At these conditions a rock of this composition is predicted to contain approximately 41 wt% quartz, 20 wt% biotite, 18 wt% phengite, 10 wt% sillimanite, 9 wt% plagioclase, 1.22 wt% garnet, and 0.96 wt% ilmenite. The present matrix mineralogy is very different from this. The results using all Fe as FeO has a very good intersection with the measured value of all four garnet end members within 0.003 of their predicted values at ~ 630^o C, 5,500 bars (Figure 2-35). At these conditions the minerals predicted to be present are ~ 41 wt% quartz, ~ 22 wt% biotite, ~ 16 wt% phengite, ~ 11 wt% sillimanite, ~ 9 wt% plagioclase, and ~ 1 wt% each garnet, and ilmenite. The list of minerals predicted is comparable to that predicted via the standard run, with compositions similar for each, but the match for the garnet core composition is better for this run.

2.5.1.4: 67662 GARNET RIM CONDITIONS VIA FRACTIONATION PATH CALCULATIONS

Having two different sets of core calculations, each was used as a starting point for garnet fractionation path calculations, first for the standard correction core results, with an assumption of water-saturated conditions, where the best match with measured rim compositions for this sample was found with a path which decreases ½ of a degree for every 100 bar increase in pressure [c(0) = 942.5, c(1) = -0.005]. Perple_X calculations based upon the bulk rock composition predicted from that garnet fractionation path were done, and yielded an estimate of ~ 620^{o} C, 9,100 bars (Figure 2-36). However, at these conditions paragonite is predicted to be present. Therefore further paths were attempted from the same starting point but with a fixed-H_2O to seek a set of predicted conditions wherein both the garnet composition and the matrix mineralogy were predicted. Extensive modelling identified a path of decreasing temperature by 1.75^{o} C for every 100 bar increase in pressure [c(0)=1016.25, c(1)= -0.0175] producing a reasonable match to the garnet rim composition at ~ 11,000 bars. Therefore the effective bulk composition reported for that step in the path was used for a new Perple_X calculation, with the addition of 0.001 MnO, as is standard practice for these Perple_X garnet rim calculations. This results in the isopleths which correspond to the measured garnet rim compositions having tight intersection at ~ 560^{o} C, 11,400 bars and a paragonite-free assemblage (Figure 2-37).

A second set of garnet-fractionation path calculations were undertaken using the conditions calculated for the garnet core formation if all iron is FeO (~ 630^{o} C, 5,500 bars) as the starting point for Perple_X. Several paths were attempted; the one providing the best match to the garnet composition of the sample decreases temperature by 0.16 degrees for every 100 bar increase in pressure [c(0) = 909.8 c(1) = -0.0016]. Accordingly, Perple_X was re-run for this sample using the composition predicted to be remaining after garnet fractionation. While tight intersections (at ~

620^{o} C, 9,000) bars are achieved from this starting point for both water saturated and only slightly limited H_2O, paragonite is predicted to be present. However, limiting the starting H_2O to the range 3.0-3.55 results in predicted paragonite free assemblages with rim compositions achieved at ~ 555^{o} C, 11,000 bars. The all Fe = FeO run selected as having the best results was that with H_2O set to 3.25. For this run at ~ 555^{o} C, 11,000 bars (Figure 2-38) the minerals predicted to be present are ~ 41 wt% phengite, ~ 33 wt% quartz, ~ 9 wt% albite, ~ 7 wt% kyanite, ~ 3 wt% newest layer of garnet formed, and ~ 1 wt% rutile. These results are a much better match for the matrix minerals than those predicted via other methods above.

2.5.2: Sample 67665

2.5.2.1: 67665 SAMPLE DESCRIPTION

Sample 67665 is a muscovite-quartz-garnet-plagioclase schist, without matrix biotite, from the hill above the Lyell Highway near where it crosses Bill's Creek (Figure 2-1). There are numerous small garnet grains (up to 0.5 in diameter) and a few skeletal garnet porphyroblasts (largest found: 9.8 x 4.3 mm). The porphyroblasts appear, in at least one instance, to be composed of more than one smaller grain which grew together to form a cluster of garnet grains. This feature was revealed during inclusion studies of the largest grain (see below), which has an inclusion-rich domain (~ 1 mm diameter) that has an outline that appears to be a single grain, though it is contiguous with other parts of the porphyroblast on two sides. The muscovite, occurring in laths up to 2 mm long, defines a foliation which wraps around the garnet porphyroblast. The plagioclase occurs as rare grains, up to 0.6 mm in length.

2.5.2.2: 67665 COMPOSITION

This sample had an initial microprobe session which included a line analysis spots across the centre region of the large (9.7 x 4.6) garnet, with a spacing of 9.6 to 1.5 mm between analysed points (Figure 2-39A, red marked analysis points). There was

an additional session, primarily for inclusion work, which also analysed lines along the garnet in the vicinity of the inclusion rich areas (Figure 2-39A, blue marked analysis points, and Figure 2-39B). One of lines from the second session bisects the small, inclusion-rich, sub-grain with a spacing of 0.1-0.2 mm, and the other, with a spacing of ~ 0.3 mm between spots, runs parallel to the line from the first session, but closer to the rim of the garnet cluster (Figure 2-39B). The composition ranges from 0.73 to 0.81 X_{Alm}, 0.13 to 0.19 X_{Prp}, 0.03 to 0.09 X_{Grs}, and 0.003 to 0.020 X_{Sps}. A comparison of the composition of the three lines (Figure 2-39) reveals that the garnet does not exhibit systematic zoning, though it does show some variation in composition. The line across the inclusion-rich sub-grain is, generally, the lowest in X_{Alm} and X_{Sps}, and highest in X_{Grs}, and is generally higher in X_{Prp}. This grain has a zoning in Ca which may reflect distance from the matrix. For the cluster as a whole, X_{Sps} decreases towards the edge, but the pattern is very scattered.

The matrix muscovite ranges from 0.07 to 0.16 Na/Na+K, and the muscovite inclusions in the garnet ranges from 0.09 to 0.20 Na/Na+K. The graph of Si vs Na/Na+K shows that the inclusions and the matrix muscovite overlap in composition, and show a trend with Na/Na+K decreasing as Si increases (Figure 2-40). There was no biotite observed within the matrix, but it was present as inclusions within the garnet, where it ranged from 0.43 to 0.55 Mg/Fe+Mg. Three out of the four points analysed plot within the siderophyllite field of the Al(IV) vs Fe/Fe+Mg diagram (Figure 2-40). One other grain is comprised of alternating light/dark patches in the BSE image, the light patches are chlorite, and the dark patch is Al-rich compared to the other micas. The plagioclase, which is present in the matrix, but was not observed as inclusions in the garnet, ranges in composition from 0.95 to 0.97 X_{Ab}. Other inclusions include rutile-ilmenite (Figure 2-40D), and monazite.

This samples falls in the middle of the range with respect to the Al_2O_3, SiO_2, FeO, CaO, MnO portions of the whole-rock composition, but has the second-highest MgO content and the lowest Na_2O and second lowest TiO2 concentration of any of the Collingwood River samples (Figure 2-11).

2.5.2.3: 67665 GARNET CORE CONDITIONS

The analysis with the highest X_{Sps} value was selected as representative of the garnet core; this analysis has the lowest X_{Alm} (0.78) and X_{Sps} (0.020), and the highest in X_{Prp} (0.15) and X_{Grs} (0.05) of any identified early garnet compositions for the Collingwood River samples. It is also the sample with the best-fit intersections for the isopleths which correspond to the garnet core composition, with all four end-members predicted to be within 0.001 of the measured composition at ~ 620^o C, 8,000 bars (Figure 2-41). At those conditions, this sample is predicted to have 45 wt% quartz, 33 wt% phengite, 10 wt% biotite, 4 wt% staurolite, 3 wt% garnet, 2 wt% paragonite, and less than 1 wt% each of plagioclase and ilmenite. The compositions of the predicted micas are a reasonable match to those included within garnet. The biotite inclusions range from 0.43-0.55 Mg/Fe+Mg, and the predicted biotite is 0.53 Mg/Fe+Mg. The predicted phengite is 0.13 Na/Na+K, and the average of the muscovite inclusions is also 0.13. Plagioclase was not observed included within the garnet, and it is predicted to be only a minor component at garnet core-forming conditions. This sample predicted paragonite to be present during garnet core conditions, but only as a minor (< 2.5 wt%) component. Since the quality of the intersections for the garnet-core isopleths was excellent no further variations on Perple_X calculations were attempted.

2.5.2.4: 67665 GARNET RIM CONDITIONS VIA FRACTIONATION ATTEMPTS

Attempts at running garnet-fractionation paths with Perple_X for this sample were unsuccessful. Three attempts each were made for water-saturated and fixed-H_2O

(using the amount of water predicted to be present at core conditions) paths (one near-vertical, one with a positive, and one negative slope). The rim composition was not reproduced along any simple path.

2.5.3: Sample 67659

Sample 67659 is fully described above (see section 2.4.1) and illustrated in Figure 2-12 and Figure 2-13.

2.5.3.1: 67659 GARNET CORE CONDITIONS

Perple_X garnet core calculations were run twice for this sample, with the best result obtained with a fixed H_2O setting. A P-xH_2O diagram revealed that paragonite disappears at H_2O = 1.37, which value was used for the garnet-core calculations. Unlike the water-saturated version, this model allows the predicted X_{Alm} to reach values as high as those measured in the garnet core. The intersections for this model (Figure 2-42) have all four end-members compositions within 0.005 of their measured values at 520^o C and 5,100 bars.

2.5.3.2: 67659 GARNET RIM CONDITIONS VIA FRACTIONATION PATH CALCULATIONS

Extensive modelling for garnet fractionation paths gave the best result for a path starting with the composition predicted from the above fixed-H_2O core calculations and decreasing 0.45^o C for every 100 bar increase in pressure [c(0) = 815.95, c(1) = -0.0045]. Using the new bulk composition predicted by this path and continuing to limit H_2O Perple_X was run again, yielding tight intersections for the garnet end-members at ~ 500^o C, 9,100 bars, with all four end-members predicted to fall within 0.003 of their measured values (Figure 2-43). This gives reasonable match for the quantity of each mineral present, save for kyanite, which was not observed in this sample. The garnet and plagioclase compositions are modelled quite closely, and the micas are well predicted.

2.5.4: Sample 160694

2.5.4.1: 160694 SAMPLE DESCRIPTION

Sample 160694 comes from just upstream from the intersection of Bill's Creek and the Collingwood River, the location of the largest garnet crystals in the region (Figure 2-1). It is a quartz-muscovite-garnet-tourmaline schist with minor rutile, monazite, apatite, and kyanite. The garnet is subhedral and ranges from small grains of 100 microns to large crystals over two centimetres long. The larger garnet grains are patchy and skeletal (Figure 2-44) with large quartz inclusion. In addition there are also small inclusions of apatite, kyanite, rutile, zircon, and muscovite. The included muscovite is generally richer in Na than those in the matrix (Figure 2-45); average Na/Na+K for the inclusion muscovite is 0.15, with a range from 0.12 to 0.20, while in the matrix the average is 0.12 with a range from 0.07 to 0.16. While kyanite was found as inclusions in the garnet of this sample, it was not observed in the matrix. The matrix muscovite, with elongate grains as large as 3 mm in length, but more commonly 0.5 to 1 mm in length, defines a foliation, which curves gently around the large grains of garnet. Some of the muscovite laths have undulatory extinction. The tourmaline is mostly equigranular (generally 0.1 to 0.3 mm diameter) as viewed in thin section, with weak alignment of elongate (~ 0.1 x 0.4 mm) tourmaline crystals with the mica foliation. The matrix quartz is fine-grained (~ 0.1 mm) and anhedral, and uniformly distributed among the mica, but the quartz in the strain shadow of the large garnet grain is much coarser grained (up to 1.6 mm long).

2.5.4.2: 160694 COMPOSITION

This sample had several different probe sessions. An initial, low resolution traverse (160694-A) across a garnet (11.6 mm across) was followed by a higher resolution traverse (160694-C) in a second, larger, garnet (18.6 mm long). The larger garnet

was cut in serial-thin sections, spaced ~ 2 mm apart, and the largest three were mapped (Figure 2-44) to determine which had the highest Mn concentration, and where within the grain it was located. Two lines were then analysed across that garnet roughly perpendicular to one another, at a spacing of ~ 0.3 mm between spots, crossing the region of high Mn (Figure 2-44). The feldspar is albite, with 0.96-0.97 Na/(Na+Ca+K). The white mica ranges from 0.12-0.15 Na/Na+K (Figure 2-45). Biotite was not observed in this sample, but tourmaline is common.

There are noticeable differences (Figure 2-46) between the initial probe session (160694-A) and the subsequent session (160694-C). The larger, mapped, grain is lower in X_{Sps} and X_{Grs} than the core of 160694-A. The closest match between the two garnet grains is in X_{Prp}, where the core of 160694-A is slightly higher than that of 160694-C, and finally the X_{Alm} is noticeably higher in for the second session than the first. It is possible that diffusion in the older, larger grains (Gaidies et al. 2008) is responsible for these differences. Alternatively, the locations on sample from which the two thin sections were cut could be a factor due to local inhomogeneities in the rock composition.

Both of the large crystals of garnet analysed for sample 160694-A and 160694-C have generally homogeneous cores, and gently zoned rims (Figure 2-44, Figure 2-46). The greatest component of zoning within the core is exhibited by X_{Sps}, which ranges from 0.028 to 0.040 for 160694-A, and from 0.11 to 0.29 for 160694-C. X_{Grs} ranges from 0.027 to 0.030 for 160694-A, and 0.18 to 0.03 for 160694-C. X_{Prp} is nearly homogeneous ranging from 0.09 to 0.10 for 160694-A, and from 0.08 to 0.11 for 160694-C, and X_{Alm} for the core shows little variation, ranging from 0.840 to 0.842 for 160694-A, and from 0.858 to 0.874 for 160694-C.

The rim, which is up to 1.6 mm wide on the 18 x 10 mm 160694-C grain, shows little zoning in Ca and Mn, both of which are very low in the whole rock composition,

ranging from 0.005 to 0.011 X_{Sps} for 160694-A and from 0.003 to 0.008 X_{Sps} for 160694-C. The rim ranges from 0.15 to 0.17 X_{Grs} for 160694-A, and 0.020 to 0.027 X_{Grs} for 160694-C. It has more pronounced zoning in Fe and Mg, ranging from 0.15 to 0.17 X_{Prp} for 160694-A and 0.09 to 0.15 X_{Prp} for 160694-C and 0.782 to 0.800 X_{Alm} for 160694-A and 0.829 to 0.869 X_{Alm} for 160694-C (Figure 2-46).

Many workers opt to use the analysis spot with the highest Mn value as the core for all calculations wherein one needs a core value for the garnet end members. However, this sample has a sufficiently homogeneous core that the average core values yield a better representation of composition with which to calculate core conditions.

The inclusions within the large garnet in 160694 include muscovite, apatite, rutile, kyanite, and monazite. The muscovite inclusions in the garnet are found 0.9 mm from the edge of the grain (Figure 2-47). It ranges from 0.12-0.20 Na/Na+K, and is generally very similar to the matrix muscovite (Figure 2-45). However two small grains are noticeably higher in Fe and Ca and lower in K than the others. Rutile occurs throughout the garnet. There are two variations in compositions of rutile with one ranging from 0.40-0.75 wt% FeO, the other 0.85-1.50 wt% FeO (Figure 2-48). The spatial distribution of the two sorts of rutile does not conform to any recognisable pattern.

2.5.4.3: 160694 GARNET CORE CONDITIONS

A variety of different options were attempted in Perple_X modelling for sample 160694 changing the assumptions for the starting amounts of Fe, Ca and H_2O, with and without the expanded thermodynamic dataset of Van Hinsberg and Schumacher (Van Hinsberg and Schumacher 2007), which adds boron and the mineral tourmaline to the solution set. Most of the attempts were unsatisfactory, with no or poor intersections for the isopleths corresponding to the measured average core

composition, and for most calculations attempted almandine was not predicted to achieve values as high as those measured in the garnet core. However, the calculations which combined the assumptions of all Fe = FeO, water is unsaturated, tourmaline included in the solution set, and 95% of the Ca measured in the whole-rock composition is available for reactions (i.e. not locked up in apatite) resulted in the successful modelling of the almandine end member, and good intersections for all four end-members at ~ 545^{o} C, 5,700 bars, with each end member predicted to be within 0.002 of its measured value (Figure 2-49). At these conditions, the minerals predicted to be present are ~ 39 wt% quartz, 17 wt% feldspar (in two forms) 14 wt% kyanite, 6 wt% phengite, 3 wt% garnet, 2 wt% tourmaline, and ~ 1 wt% ilmenite. This is not a close match of the composition of the current matrix. However, changes in conditions between core and rim may account for the differences.

2.5.4.4: 160694 GARNET RIM CONDITIONS VIA FRACTIONATION PATH ATTEMPTS

The conditions predicted for the garnet core above were used to calculate the results for a variety of possible "paths", assuming the fractionation of garnet, over which temperature and pressure may have changed. The path which best predicts the rim composition is the one which increases temperature by 0.8 degrees for every 100 bar increase in pressure [c(0) = 772.4, c(1) = 0.008]. The modified bulk composition reported from that path was used for a new Perple_X calculation, with the addition of 0.001 MnO (which is otherwise predicted to run out before rim conditions are attained). This results in a very good intersection for all four garnet end-members at ~ 575^{o} C, 8,900 bars, with all four end-members within 0.003 of their measured rim values (Figure 2-50). At these conditions, the sample is predicted to contain ~ 35 wt% quartz, 20 wt% plagioclase, 15 wt% phengite, 14 wt% kyanite, 13 wt% biotite, 2 wt% tourmaline, ~ 1 wt% ilmenite, and less than 1 wt% newest layer of garnet formed. However, while kyanite was found as inclusions within the garnet, it was

not observed in the matrix, nor was biotite or plagioclase. Therefore, while a set of conditions was found at which the garnet composition can be modelled for this sample, the matrix minerals are not correctly predicted.

2.5.5: Sample 160698

Sample 160698 (for a complete sample description see section 2.4.3) contains garnet that, like most of those from the Collingwood River, has a fairly homogeneous core and a zoned rim (Figure 2-16).

2.5.5.1: 160698 GARNET CORE CONDITIONS

Perple_X was used to calculate the garnet core conditions for this sample, plotting the isopleths for the highest X_{Sps} composition measured in the sample. The core composition is reasonably well matched at 600^{o} C, 6,900 bars (Figure 2-51). However, the highest possible X_{Alm} predicted is not quite as high as that measured in the garnet core. Therefore, the fit might be improved if the calculations were to be redone using the assumption that all the Fe in this rock was FeO, as was necessary for some of the other samples that did not achieve this level of match on the standard corrections attempt. At these conditions the minerals predicted to be present are 42 wt% quartz, 25 wt% phengite, 12 wt% biotite, 11 wt% paragonite, 5 wt % plagioclase, 4 wt% garnet, 1 wt% ilmenite, and trace staurolite. While most of these are present in the sample, paragonite and staurolite are not.

2.5.5.2: 160698 GARNET RIM CONDITIONS VIA FRACTIONATION PATH CALCULATIONS

Extensive Perple_X garnet fractionation modelling gave the best results in terms of both predicting the garnet rim composition and reasonably matching the matrix minerals in a path which fixed the starting H_2O to 3.0 wt%, which gives an estimate for rim formation at ~ 580^{o} C, 10,800 bars (Figure 2-52).

2.5.6: Sample 160702

2.5.6.1: 160702 COMPOSITION

Five different crystals of garnet, in three size ranges, were analysed in sample 160702 (for sample description see section 2.4.4). The sizes have been designated large (2.1-2.5 mm in length and elongate in shape), medium (1.9-2.0 mm in diameter and equidimensional), and small (0.7 mm diameter). Figure 2-53 displays the difference in composition for each type. The two large grains are located ~ 37 mm from the other grains. The smallest garnet grain analysed has the lowest X_{Sps} values (0.005-0.006) and is otherwise similar to rim compositions on the large grains. It is generally high in X_{Grs} (0.10-0.15), lowest in X_{Alm} (0.72-0.75) and intermediate in X_{Prp} (0.13-0.14). The large grains are nearly homogeneous in X_{Sps}, and while they contain more Mn than the smallest garnet, they are notably lower (0.08-0.09) in X_{Sps} than the medium grains (0.01-0.03 X_{Sps}). The large grains contain, generally, more X_{Grs} (0.04-0.07) and X_{Prp} (0.11-0.16) than the medium grains (0.02-0.03 X_{Grs} and 0.10-0.16 X_{Prp}). The difference in composition between the medium grains and the smallest garnet grains, all four of which are in close proximity to one another, is consistent with patterns expected due to garnet fractionation, with the small grains similar to the rim composition, and the medium grains showing some zoning from core to rim. The large grains, on the other end of the thin section, are generally more homogeneous, and have compositions that are intermediate between the medium and small grains (Figure 2-53).

This sample has the highest TiO_2 content in whole-rock composition of the Collingwood River samples, and it is the second highest in SiO_2, CaO, and Na_2O. It also has the lowest K_2O of the Collingwood River samples analysed (Figure 2-11).

2.5.6.2: 160702 GARNET CORE

The analysis point chosen for the garnet core composition for Perple_X calculations was the highest X_{Sps} point, from the middle of medium garnet #3 (Figure 2-54). Extensive modelling gave the best results by setting the starting H_2O = 1.0, which results in intersections at ~ 540^o C, 6100 bars, with all four end members within 0.005 of their measured values (Figure 2-55). At these conditions the minerals predicted to be present are 36 wt% quartz, 26 wt% feldspar (two types), 13 wt% biotite, 10 wt% phengite, 8 wt% kyanite, 4 wt% garnet, and 1 wt% ilmenite. Kyanite was not observed in this sample, and the matrix currently contains considerably more phengite, and noticeably less biotite than those predicted to coexist with the garnet core.

2.5.6.3: 160702 GARNET RIM CONDITIONS VIA FRACTIONATION PATH CALCULATIONS

The conditions calculated for the garnet core above were used for garnet fractionation path calculations. A number of paths were attempted and the one which provided the best match for the rim composition (taken as an average of the three spots analysed on the smallest garnet grain) was the one which decreases 0.6^o C for ever 100 bar increase in pressure [c(0) = 848.6, c(1) = -0.006]. The after-garnet fractionation bulk rock composition from that path was used for a second Perple_X calculation to determine rim conditions. This resulted in a reasonable intersection for the garnet end-members at ~ 515^o C, 9,700 bars (Figure 2-56). At these conditions the sample is predicted to contain 32 wt% quartz, 20 wt% phengite, 25 wt% plagioclase, and 7 wt% K-feldspar, 8 wt% biotite, 7 wt% kyanite, 1 wt% rutile, and less than 1 wt% newest layer of garnet formed. Neither kyanite nor K-feldspar were observed in this sample, but the others are a reasonable match to the proportion of minerals present.

2.5.7: Sample 160707

2.5.7.1: 160707 SAMPLE DESCRIPTION

Sample 160707 was collected from an outcrop on the Lyell Highway, just south of where Bills Creek intersects Collingwood River (Figure 2-1). Its location is less than 20 metres south-westward along the road from 160706, but whereas the latter is mylonitic, this sample is more massive. It contains quartz, white-mica, plagioclase, garnet, and minor biotite, rutile and monazite. The mica exhibits a preferred orientation and the rock has a gneissic texture. The garnet is commonly in small grains ranging from 0.5 mm to 2 mm, but there are also garnet porphyroblasts up to 2 cm in diameter. While the small garnet grains are mainly euhedral, the large grains are skeletal and full of inclusions, particularly of quartz. The muscovite occurs in laths up to 5 mm long, which are usually straight, but occasionally (esp. near the large garnet) are bent. The plagioclase is up to 3 mm across, and the quartz grains rarely exceed 2 mm, except where they are inclusions within the garnet. This sample also contains accessory rutile and monazite. As with many of the other Collingwood River samples, most of the biotite analysed has been chloritised. However, one grain was found which was unaltered, with an Mg/Mg+Fe of 0.45. The plagioclase is reasonably uniform in composition at ~ 0.05 $X_{An.}$ There is a subtle difference between the muscovite analysed in the first thin section as compared to the second. The first ranged from 0.14 to 0.18 Na/Na+K, and the second from 0.12 to 0.16 Na/Na+K.

2.5.7.2: 160707 COMPOSITION

Element maps of the largest garnet (9 mm long) found in this sample have been produced, and two lines, at nearly right angles, were then analysed at a spacing of ~ 0.18 mm. The zoning is off centre, with the highest concentration of Mn mostly along one edge forming an elongate core region of reasonably uniform composition

(Figure 2-57) with an abrupt transition to the rim, which is also largely homogeneous. Line 1 crosses both the narrow portion of the core and the widest extent of the rim, and line 2 transverses the widest extent of the core and the narrow rims on either side of it in that region.

The core is higher in X_{Sps} (core average: 0.05, rim average 0.02 X_{Sps}) and X_{Alm} (core average: 0.81, rim average 0.77 X_{Alm}), and lower in X_{Prp} (core average: 0.11, rim average 0.18 X_{Prp}) than the rim. X_{Grs} is variable in composition across most of the grain. It has an average core of 0.025 and rim of 0.034 X_{Grs} if calculated for the same points as used for the other end members, but it lacks the abrupt change in composition between core or rim that the other three end members display.

2.5.7.3: 160707 GARNET CORE

The large garnet described above, for which element compositional maps were prepared, is lower in X_{Sps} than is the core of a smaller (~ 4 mm) grain which was analysed in a single line across the grain. This may be due to the largely homogenized nature of these garnet grains, diffusive re-equilibration of the larger grains could account for the lower concentration of X_{Sps} in the core than is present in smaller, potentially younger, grains. The compositions of both garnet grains were used for Perple_X modelling; the best results were obtained from the smaller grain, with all four predicted end members intersecting within 0.003 of their measured values (Figure 2-58) at 650^{o} C, 6,750 bars. The minerals predicted to be present during these conditions include 39 wt% quartz, 24 wt% phengite, 16 wt% biotite, 8 wt% plagioclase, 8 wt% staurolite, just under 2 wt% each sillimanite and garnet, and less than 1 wt% ilmenite.

2.5.7.4: 160707 GARNET RIM CONDITIONS VIA FRACTIONATION PATH CALCULATIONS

Extensive modelling of garnet fractionation paths yielded the best results for the one which increases the temperature by 0.1^{o} C for every 100 bar increase in pressure

[c(0)=916.25, c(1)=0.001], wherein X_{Alm}, X_{Sps}, and X_{Grs} are all predicted to achieve their measured rim composition at just over, 10,000 bars and fixing H_2O for the final calculations to 3.61, which results in a paragonite-free assemblage, with good intersections of the garnet end-members at ~ 600^o C, 11,800 bars (Figure 2-59). At these conditions, this sample is predicted to contain ~ 42 wt% phengite, 33 wt% quartz, ~ 7 wt% biotite, ~ 7 wt% kyanite, ~ 9 wt% plagioclase, ~ 1 wt% newest layer of garnet formed, and ~ 1 wt% rutile.

2.5.8: Sample 160708

2.5.8.1: 160708 COMPOSITION

Sample 160708 (for sample description see section 2.4.5) is the one with the highest SiO_2 and lowest Al_2O_3, FeO & MgO whole-rock analysis from Collingwood River (Figure 2-11). The garnet has a fairly homogeneous core and a zoned rim (Figure 2-21). It reaches a high of 0.11 X_{Sps} in the core decreasing to 0.02 at the rim. XPrp is flat at ~ 0.09 across the core, increasing after the core-rim boundary to 0.13, and dropping at the very rim to 0.10, XGrs is flat and low (0.01 to 0.05) , save for the very rim, which increases to 0.13), and XAlm is relatively constant (0.77 to 0.79, but drops to 0.75 at the very rim. Most of the biotite analysed is chloritised, but one grain analysed has an Mg/Mg+Fe of 0.41 (Figure 2-60). The plagioclase ranges from 0.91-0.94 X_{Ab}, and the muscovite ranges from 0.09-0.12 Na/Na+K (Figure 2-60).

2.5.8.2: 160708 GARNET CORE

Perple_X was used to calculate PT conditions for the garnet core composition for sample 160708. Reasonable intersections are obtained for 580^o C, 5,500 bars (Figure 2-61), where both X_{Prp} & X_{Sps} are predicted to fall within 0.005 of their measured values, and X_{Grs} and X_{Alm} are within 0.014 of their measured values. At those conditions, the minerals predicted to be present are: 43 wt% quartz, 23 wt%

phengite, 14 wt% plagioclase, 12 wt% biotite, 6 wt% paragonite, 1 wt% ilmenite, and less than 1 wt% garnet and staurolite.

2.5.8.3: 160708 GARNET RIM CONDITIONS VIA FRACTIONATION PATH CALCULATIONS

Extensive Perple_X garnet fractionation modelling obtained the best match to garnet rim compositions for the path which increases temperature by 0.7^{o} C for each 100 bar increase [c(0)=814.5, c(1)=0.007]. The new bulk composition predicted from that path with fixed-H_2O conditions yields good intersections ~ 520^{o} C, 9,500 bars (Figure 2-62). The minerals predicted to be present at these conditions is a reasonable match for both the matrix minerals and the garnet rim compositions, with 33 wt% phengite of 0.5 Na/Na+K (measured at 0.9-0.12 Na/Na+K), 32 wt% quartz 25 wt% plagioclase, 6 wt% biotite of 0.62 Mg/Mg+Fe (measured at 0.41 Mg/Mg+Fe), 2 % kyanite (not observed in the sample), 2 % rim garnet, and 1% rutile.

2.5.9: Whiteschist

The Collingwood River whiteschist is from a small outcrop in the southern block, located on a bend in the river just east of its intersection with Scarlett Creek (Figure 2-2). The outcrop itself is a narrow (<1 m) band which wraps around a hollow which may have once contained something with sufficient Mg to provide a source for the whiteschist as an alteration zone (Figure 2-1). The minerals present include talc, kyanite, garnet, and quartz. Two samples were analysed; sample 39140, collected by Boulter in 1978, is richer in quartz than 160730, collected from the same outcrop for this study (Figure 2-63). The garnet crystals are up to 4 mm wide and have two different habits/compositions. Type A exhibits only moderate cracking, shows little to no visible difference between core and rim, few inclusions, and tends to have very distinct compositional difference from core to rim (Figure 2-64). Type B shows very distinct visual difference between the cores, which tend to be very cracked and have

a lower relief and abundant inclusions, and the rims, which are higher in relief, have few inclusions and less extensive cracking (Figure 2-65). While type A has an appearance which is unchanged from core to rim, its composition from core to rim is quite different; Type B, which has rims which look very different from the cores shows little compositional change across that core-rim boundary (Figure 2-66). The cores of type A are richer in X_{Grs} (~ 0.25) than X_{Prp} (~ 0.15) and the rims are very low in X_{Grs} (near detection limits) and high in X_{Prp} (~ 0.45). X_{Alm} shows little change from core to rim, remaining ~ 0.60 throughout, and X_{Sps} is low, reaching 0.05 in the cores and decreasing on the rims. Type B, on the other hand tends to have a uniform composition throughout that is similar to the rims of Type A, with ~ 0.60 X_{Alm}, ~ 0.40 X_{Prp}, up to 0.10 X_{Grs} and 0.02 X_{Sps}. Both types occur in both samples, though the extent of the interior cracking and the visual contrast with the rims of Type B is much more pronounced in 39140 (Figure 2-65).

The Perple_X results for 160730 show the garnet core isopleths intersecting within 0.005 for X_{Sps} and X_{Grs}, 0.007 for X_{Prp} and 0.014 for X_{Alm} of their measured values at 545^{o} C, 19,600 bars (Figure 2-67). However, that puts it in the field 45^{o} C below stability of kyanite (Figure 2-67G) and 50^{o} C below the stability field of talc (Figure 2-67H) at this pressure (kyanite is not predicted at this temperature; talc is only predicted to be stable at this temperature at higher P). Attempts at using the Perple_X path modelling to find a path predicting the rim composition for all four isopleths were unsuccessful. This is due to the low availability of Ca in the bulk rock composition. The Type A garnet grains from both whiteschists have cores which have up to 0.29 X_{Grs}, while the rims, and the centres of other grains have less than detection limits of X_{Grs}. There is a very abrupt change in the garnet composition of the Type A garnet from cores to rims, with the biggest difference being the abrupt drop of X_{Grs}. All of the paths modelled predict that Ca will run out during the course

of garnet fractionation, with a corresponding abrupt drop in X_{Grs}. Likewise X_{Sps} also is predicted to run out over the course of garnet fractionation. While it was not possible to find a garnet fractionation model which predicts a unique pressure and temperature for all four end members to achieve the values as measured in the garnet rims for this sample, it is clear from the mineral stability fields that temperature has increased during the garnet growth, which then permitted the growth of kyanite and talc.

2.5.10: Summary of all Collingwood River Samples Perple_X results for garnet core

The above pressure/temperature estimates were obtained by graphing the isopleths which correspond to the measured garnet core values and inspecting the graph for the point at which they are nearest to intersecting. Since it is rare for the four end members to actually intersect at a single point in P/T space, the "best fit" intersection of the garnet core isopleths was evaluated by using the Werami program of the Perple_X suite to calculate the compositions of the garnet end members for a variety of pressure/temperature combinations in the vicinity of the region of intersection and selecting as the "best fit" the one with the smallest sum of the absolute value of the differences between the predicted composition and the composition measured for the sample. For those samples wherein the sum of the absolute value of the differences was less than 0.10 the pressure/temperature was reported. For those samples for which using the "standard" corrections (see section 1.3.2.2) failed to yield such a result additional runs were made changing one or more of the following variables: limiting the amount of H_2O available to the system, increasing the FeO content to have all of the iron reported for the whole-rock composition in the form of FeO, changing the amount of Ca assumed to be unavailable for reactions by being locked up in apatite, and/or the addition of boron/tourmaline to the solution set.

Each of the above changes to the standard corrections has a result on the T/P predicted, as well as the "tightness" of the resultant intersections. Limiting the H_2O results in a decrease in temperature and pressure at which the best match for garnet core compositions is obtained while improving the "best fit" of the intersection (Figure 2-68A). Likewise, increasing the amount of FeO available to the system also improves the fit whilst decreasing the pressure and, usually, the temperature (Figure 2-68B). Note that the "error" ellipses in Figure 2-68 were obtained by first taking the sum of the absolute value of the differences between each garnet end-members' measured value and Perple_X predicted values at the intersection T/P and then multiplying it by a constant (n) large enough to plot the ellipses in a scale appropriate to the graph (n = 100 for temperature and 1500 for pressure). This results in ellipses which are roughly circular and are proportional to the "tightness" of the isopleth intersections.

It is difficult to place an error on the P/T estimates obtained via Perple_X garnet core isopleth thermobarometery. Since these samples all come from the same location it may be considered that the population variance can be used to estimate the error. Therefore the standard deviation was determined using all of Perple_X P/T of garnet core estimates and the mean plotted (Figure 2-69) via Isoplot with the standard deviation inserted as the error and a correlation coefficient chosen to rotate the ellipse to match the spread of the data (note that the correlation coefficient chosen, 0.7, is approximately the same as that which was assigned by Thermocalc for errors associated with the peak metamorphic conditions above).

The conditions of garnet core formation for the Collingwood River samples as calculated by Perple_X ranges in temperature from 520-650^o C, with an average of 580^o C and ranges in pressure from 5,100-8,000 bars with an average of 6,000 bars for the eight samples (Figure 2-69). The significance of the cores of the garnet

requires consideration. Most of the cores are nearly homogeneous, at least with respect to X_{Alm}, X_{Prp}, and X_{Grs}. For low amphibolite grade rocks, garnet usually retains the complete growth profile while for upper amphibolite zone garnet the cores are commonly homogenised and only the cooling path is recorded in the rims (Spear 1993). The level of homogenisation of the cores in the garnet from the Collingwood River is similar in habit and intensity to that reported by Faryad and Chakraborty (2005) (see also comparison of garnet profiles in Chapter 6, Figure 6-4). They calculate that T > 540^{o} C is sufficient to permit diffusion on these scales. This temperature is compatible with these P/T estimates, but noticeably lower than that reported by Tracy (1982). If the assumptions used in Tracy (1982) are closer to correct, then the temperature quoted here is not high enough to homogenise garnet cores in a realistic time, and the key temperature for the core should be closer to 650^{o} C to explain the level of homogenisation seen.

This would be even more significant if the Collingwood River garnet were not largely homogeneous in their cores as a steep zoning profile would mean that a garnet with its core positioned off the surface of the thin section would give a pressure which is higher than could have been obtained if the plane of the thin section aligned with its core/highest X_{Sps} value. However, these samples have cores that are homogeneous with respect to X_{Alm} and X_{Prp}, and largely homogeneous with respect to X_{Grs} and X_{Sps}. Therefore the values chosen to represent the garnet core for each sample are likely to be similar to the highest value of X_{Sps} obtainable for any slice through the central region of that garnet (see Figure 2-44, Figure 2-57 for garnet compositional maps showing the uniformity of Mn distribution across the core). The correlation between pressure and X_{Sps}, however, is only present for those samples which were calculated using standard corrections and water-saturated assumptions. Limiting H_2O or assuming very reduced conditions ($FeO/(FeO+Fe_2O_3)=1$) causes the

pressures estimated to be nearly uniform for each sample, regardless of the value of X_{Sps} measured in the garnet core (Figure 2-70).

The conditions of garnet rim formation for the Collingwood River samples as calculated by Perple_X ranges in temperature from 494-605^{o} C, with an average of ~ 550^{o} C and ranges in pressure from 8,900-11,800 bars with an average of ~ 10,100 bars with for the eight samples (Figure 2-71). This represents an increase in pressure of ~ 4,000 bars with garnet growth from core to rim (Figure 2-72). For most samples, this method shows is a slight decrease in temperature (16 to 70^{o} C cooler) with garnet growth from core to rim. Only sample 160694 displays an increase in temperature (~ 30^{o} C) with garnet growth. This is also the only sample to make use of the expanded solution set of Van Hinsberg and Schumacher (2007) which includes boron and the mineral tourmaline. Unlike with the core calculations, spessartine is not a major factor in these pressure estimates, both because the values measured for X_{Sps} for the garnet rims is low enough as to be approaching the detection limits of the microprobe, and because for each of these samples the garnet fractionation path calculations predicted that MnO would run out after only a few fractionation steps and the paths were continued in an MnO-free system. Some small fraction of MnO was available for the real system; this could be due to a very resistant Mn phase not included in the model or indicate that the early formed garnet was not completely closed to MnO.

The results obtained via Thermocalc and GB-GBPQ indicate that the temperature and pressure for rim formation is ~ 700^{o} C, or ~ 150 degrees higher than that predicted by Perple_X. The pressure estimate for the rim condition is 3,000-5,000 bars higher than the Perple_X result. These differences must reflect problems with the assumptions used and it is assumed here that the direct measurement of rim and matrix is more reliable. It is likely that the assumption that garnet is completely

preserved during growth is not accurate. Both techniques indicate that a substantial increase in pressure was required to move the mineral assemblages from that in equilibrium with the garnet core to that in equilibrium with the garnet rims. This increase was nearly isothermal. The garnet zoning profiles for this region record evidence of prograde growth with little to no diffusional modification or retrograde rim reactions. There is no evidence for resorption of garnet, such as high Mn rims. The garnet-biotite geothermometer preserves high temperatures and has not been noticeably reset during exhumation. In order to preserve the zoning of the rims it requires that while there was sufficient time elapsed for the garnet core growth and subsequent partial homogenisation by diffusion, the rims would have grown very quickly under rapidly changing pressure conditions, followed by an equally rapid return to surface temperatures such that there was very little in the way of retrograde re-equilibration between biotite and garnet.

Chapter 3

Southwest Coast

CHAPTER 3: SOUTHWEST COAST

Eleven different samples from the southwest coast of Tasmania, from Nye Bay to Wreck Bay were selected for detailed analysis for this project. Five of these had the correct mineral assemblage present in unaltered conditions to permit classical geothermobarometric modelling, four had suffered sufficient late stage alteration as to be unsuitable for such calculations, and two were analysed only for dating purposes (see Chapter five).

3.1: GEOTHERMOBAROMETRY

Classic geothermobarometric calculations to determine the conditions of formation for the matrix/garnet rim assemblage has been applied to three of samples from Nye Bay, and one from Mulcahy Bay (Figure 3-1). The techniques used are GB-GBPQ (Wu et al. 2004), GBMAQ (Wu and Zhao 2007), GASP (Holdaway 2001), and Thermocalc (Powell et al. 1998). For further details on these methods, see the introduction (section 1.3.3.2).

3.1.1: 68318

Sample 68318, collected (McNeill 1985) from the north side of Nye Bay (Figure 3-1), is a biotite-rich schist which contains garnet porphyroblasts up to 18 mm wide. Unlike the Collingwood River garnet porphyroblasts, these have well developed crystal faces with inclusions as a minor component of the grains, completely surrounded by garnet rather than being two (or more) minerals inter-grown into a composite crystal. There is a distinct visual difference between the dusty-inclusion rich rim, and the inclusion-poor core, with a very sharp core-rim boundary (Figure 3-2). The biotite grains are up to 1.4 mm long, and define a pronounced foliation, which wraps around the large garnet crystals and their accompanying quartz-rich pressure shadows. The plagioclase is fine grained (0.2 mm) and does not display

albite twinning in crossed-polarized light. Monazite is present as an accessory mineral Muscovite was not observed in this sample.

The garnet of sample 68318, as mentioned above, has visually distinct core and rim regions (Figure 3-2). The core is largely homogeneous with respect to pyrope and grossular (~ 0.07 or 0.08 X_{Prp} and ~ 0.02 or 0.03 XGrs), but zoned with respect to spessartine, with the highest X_{Sps} (0.56) occurring near the centre of the grain, and decreasing to a low of 0.2 X_{Sps} just before the core-rim boundary on both sides of the crystal. There is a subtle zoning of almandine in the core, with the values ranging from a low of 0.85 X_{Alm} in the centre of the grain, and rising to 0.88 just before the core-rim boundary on each side of the crystal. Crossing the core-rim boundary into the inclusion-rich rim zone there is a marked compositional change, with grossular increasing abruptly to 0.11, and the other end members decreasing to 0.83 X_{Alm}, 0.04 X_{Prp}, and 0.01 X_{Sps}. The rim zoning can be divided into two regions with a "transition point" between them occurring at approximately half way between the core-rim boundary and the outer most rim of the garnet. There is no visual difference between in the garnet on either side of that transition point. The composition of almandine in the rim first increases, to a high of 0.91 at the transition point, then decreases to a low of 0.85 X_{Alm} at the outer edge of the crystal. Pyrope increases continuously across the rim to a high of 0.13 X_{Prp}, with a slight change in slope at the transition point (steeper on the outermost portion). Grossular decreases steeply and steadily to the transition point, where its composition is once again as low as it was in the garnet core. From that point its composition holds generally steady, with only slight variation up or down, finally dropping to a low of 0.01 at the edge of the grain. Spessartine, having dropped abruptly after crossing the core-rim boundary, continues to decrease, at a slower rate, until the transition point (where it

is almost non-existent as a component) and then shows a slight increase, rising to a high of 0.008 at the edge of the crystal (Figure 3-2).

The biotite of sample 68318 ranges in composition from 0.36 to 0.40 Mg/(Mg+Fe) and plots within the siderophyllite field of the Al(IV)-Fe/(Fe+Mg) diagram (Figure 3-3). The plagioclase ranges from 0.06 to 0.11 X_{An}. The higher X_{An} may be associated with the rim of the plagioclase, as it is in sample 68319 below. However, no systematic lines across plagioclase grains were analysed for this sample to confirm this possibility. If the plagioclase with the higher X_{An} is taken as the rim composition which would have been in equilibrium with the garnet rim and matrix biotite (Figure 3-4) then the GB-GBPQ estimate is ~ 660^{o} C, 4,100 bars (Figure 3-5). If it had been the lower X_{An} plagioclase in the same grain which is in equilibrium with the other minerals the pressure estimate increases by just over 1,000 bars. However, at this low X_{An} large positive errors in the pressure estimate are expected (see Appendix 9). Unfortunately, Thermocalc was unable to find sufficient reactions available for mineral compositions analysed for this sample to calculate an average pressure/temperature.

3.1.2: 68319

Sample 68319 was collected from the same location as samples 68318 and 68320 (McNeill 1985), on the north side of Nye Bay (Figure 3-1). It is a quartz-garnet-biotite schist. This sample contains abundant biotite, up to 1 mm in length, and rare muscovite, up to 0.2 mm in length, generally inter-grown with the smaller biotite flakes. The plagioclase is up to 6.3 mm long, but is more typically 1 to 2 mm. It contains monazite, the largest grain of which is long enough (0.3 mm) to easily see in thin section, and the biotite regularly displays pleochroic haloes around the monazite. The rare kyanite in this sample consists of small, straight grains up to 0.3 mm long.

The garnet porphyroblasts display two very different aspects in thin section (Figure 3-6). Garnet A is elongate, measuring 11.8 x 7.7 mm, with few inclusions, most of which are quite small (< 80 μm). Garnet B is much rounder, measuring 5.3 x 4.7 mm. It has abundant large quartz inclusions (100-200 μm) scattered randomly within the core. Both show a visible core-rim boundary marked by a concentration of quartz inclusions on the rim side of the core-rim boundary, and both lack a rim on one edge of the crystal. The core of garnet B is euhedral, while outer rim is somewhat rounded. The compositions of these two porphyroblasts are quite distinct (Figure 3-6). Garnet A is zoned, particularly with respect to spessartine, which reaches a high of 0.071 X_{Sps} at the core, and falls to 0.014 before rising again to 0.041 at the core-rim boundary, and then falling again to 0.019. It is very low in pyrope, which, at the core, is lower than the spessartine at 0.06 X_{Prp}. It then rises gradually to 0.09 just before the core-rim boundary and then jumps abruptly to a high of 0.13 beyond the core-rim boundary. Grossular is also lower than spessartine in the core, but it is fairly homogeneous, approximately 0.06 across the core and then rising up to a high of 0.07 just after the core-rim boundary, and then dropping to 0.04 at the rim edge. Almandine is also zoned, with a low of 0.81 in the core, rising to a high of 0.85 before the core-rim boundary, and then dropping abruptly to a low of 0.79 X_{Alm} before rising up to 0.81 X_{Alm} at the rim edge.

Garnet B, on the other hand, shows a very different profile (Figure 3-6). It is very low and largely homogeneous in spessartine, holding between 0.007 and 0.011 $X_{Sps.}$ It shows only subtle zoning for the other three end members in the core, with grossular showing the greatest tendency for zoning, as it generally increases from a central region of (usually between 0.013-0.021) to a high of 0.033 just before the core-rim boundary (which is very pronounced visually), and then drops abruptly to a low of 0.013 just outside the core rim boundary, and showing little variation from

there to the rim edge. Almandine shows oscillations across the core, with a slight tendency to decrease from core towards the core-rim boundary, but generally staying within 0.82-0.83 X_{Alm}. Just after the core-rim boundary it jumps to a high of 0.84 X_{Alm}, drops back to a low of 0.83, and then increases again to a high at the rim edge to 0.86 X_{Alm}. Pyrope is generally constant at 0.14-0.15 X_{Prp} across the grain, with a slight dip just before and just after the core-rim boundary, and a definite drop to 0.12 at the rim edge. Comparing the two side-by-side (Figure 3-6) shows that garnet B composition is lower in grossular than even the rim (lowest) portion of garnet A, and it is higher in pyrope than even the rim (highest) portion of garnet A. It is also lower in spessartine than the lowest point in garnet A. Only in almandine do the two porphyroblasts overlap their compositional range, with the range of garnet A reaching lower (0.79 X_{Alm}) than the lowest X_{Alm} in garnet B, and B reaching higher (0.86 X_{Alm}) than the highest X_{Alm} in A. A small (1.3 x 0.6 mm) garnet also analysed has average compositions of 0.84 X_{Alm}, 0.13 X_{Prp}, 0.017 X_{Grs}, and 0.011 X_{Sps}, which is similar to garnet B in composition. It is possible that type B represents a slice through a portion of grain which is elongate and zoned like garnet A, but is cut far enough from the core of the grain as to miss most of the zoning. However, as mentioned above, there is not a single point in the zoning in garnet A which exactly corresponds to the composition of garnet B.

The garnet rim chosen for geothermobarometric work is from a much smaller grain (1.3 mm long), which is in close proximity to the analysed matrix minerals (Figure 3-7). This grain shows a composition which is lower in pyrope than the rim of Garnet A or the “core” of garnet B, intermediate in almandine as compared to A or B, and similar in spessartine and grossular to garnet B (Figure 3-6).

The plagioclase, which ranges from 0.05 to 0.11 X_{An}, shows only subtle zoning in the core, but it displays an increase in X_{An} at grain boundaries (Figure 3-8). The biotite

ranges from 0.36-0.48 Mg/(Mg+Fe), and the muscovite ranges from 0.2-0.3 Na/(Na+K) (Figure 3-9).

The inclusions analysed within garnet in this sample are quartz (by far the largest and most common of them) monazite, biotite (~ 0.47 Mg/(Mg+Fe)), muscovite (0.02 Na/(Na+K)), chlorite (~ 0.34 Mg/(Mg+Fe)), Mn-rich chlorite (~ 0.22 Mg/(Mg+Fe)), ilmenite, and zircon(?) (Figure 3-9). Unfortunately, the garnet immediately adjacent to the inclusions was not analysed, so geothermobarometric calculations including the inclusion compositions was not undertaken.

Since it is necessary to choose sets of minerals which display equilibrium textures for classical geothermobarometry, it was not possible to use the rim compositions of either garnet porphyroblast, for no biotite or plagioclase was analysed in proximity to the rims. However, the small garnet analysed is in close proximity (0.3 mm) to a biotite grain and a plagioclase porphyroblast (plagioclase 2 of Figure 3-8). Using the rim composition of both the small garnet and the plagioclase porphyroblast with the biotite yields estimates of (Figure 3-10) ~ 630^{o} C, 5,800 bars for GB-GBPQ, GASP gives an estimate of ~ 6,200 bars, and GBMAQ results for the same small garnet and biotite, plus muscovite inter-grown with the biotite gives an estimate of ~ 640^{o} 6,900 bars. The Thermocalc average pressure temperature estimate for these grains is ~ 700^{o} C, 8,100 bars. As shown in Figure 3-10, these values all overlap within error; the change in pressure from one technique to another is dependent upon the temperature estimate—note that the highest pressures are obtained for techniques which yield higher temperature estimates. Changes to the temperature estimates would result in changes to the pressure estimates; running Thermocalc average pressure calculations gives pressures of 7,100 to 7,700 bars for the range 550 to 650^{o} C, which, while still higher than the P estimate from other techniques, is more in keeping with them. Likewise, using the higher T obtained via Thermocalc in GB-

GBPQ would yield a higher pressure estimate for that technique of 6,300 bars. Using the numbers as reported for each of the four techniques results in a weighted mean average temperature of 640 ± 17^{o} C with a MSWD of 0.94 for the three temperature estimates. The low MSWD confirms the visual estimate that the temperatures are all approximately the same, within error. The weighted mean average pressure for this sample is 6,500 ± 1,400 bars with a MSWD of 3.0 for the four pressure estimates. The higher MSWD for the pressure highlights the difference between the Thermocalc result and the other three (without the Thermocalc results the weighted mean average is 6,300 ± 1,500 bars with a MSWD of 1.7 for the remaining three pressure estimates.

3.1.3: 68320

Sample 68320, like 68318 & 68319 was collected (McNeill 1985) from the north side of Nye Bay (Figure 3-1). It is a quartz-biotite schist, with garnet porphyroblasts up to 6 mm long. The garnet contains abundant quartz inclusions, which are larger and more numerous in the rims, resulting in a very distinct visual contrast between the cores and rims of the garnet (Figure 3-11). The biotite, in laths up to 1 mm long, defines a foliation, which wraps around the garnet. It contains monazite inclusions which cause pleochroic haloes in the biotite. There are plagioclase grains up to 1 mm wide. Neither muscovite nor kyanite were observed in this sample.

The garnet analysed in this sample, while displaying very clear visual differences between the core and rim, shows only subtle compositional zoning (Figure 3-11), with the core ranging between 0.018-0.013 X_{Sps}, 0.025-0.016 X_{Grs}, 0.14-0.15 X_{Prp}, and 0.80-8.82 X_{Alm}, and the rim ranging from 0.008-0.011 X_{Sps}, 0.13-0.24 X_{Grs}, 0.13-0.14 X_{Prp}, and 0.83-0.85 X_{Alm}. Of the end members, grossular and spessartine are nearly uniform in value. Almandine and pyrope display more of a pattern, with pyrope generally dropping from the centre of the core to the core-rim boundary,

increasing slightly in the early-formed rim, then dropping to the outer rim, and almandine increasing from core to rim, but with a change in slope at the core-rim boundary (Figure 3-11). The biotite ranges from 0.37 to 0.40 Mg/(Mg+Fe) and plots in the siderophyllite field of the Al(IV)-Fe/(Fe+Mg) diagram (Figure 3-12). The plagioclase ranges from 0.09 to 0.12 X_{An}. As with 68318, lines across the plagioclase were not analysed to check for zoning. However, it is likely that this plagioclase conforms to the pattern displayed by neighbouring sample 68319, with X_{An} increasing at the rims of the grains. If this is the case, using the higher X_{An} compositions in conjunction with the nearby (0.7 mm) biotite, and the closest garnet rim analysed (2.3 mm past the biotite—Figure 3-13) gives a GB-GBPQ estimate of ~ 640^{o} C, 4,700 bars (Figure 3-14). However, if one of the other plagioclase analyses represents the composition which was in equilibrium with the garnet rim and matrix biotite the calculated GB-GBPQ pressure is higher than that reported above, with a maximum result of 6,200 bars (for 0.09 X_{An}).

3.1.4: 68335

Sample 68335, from the coast on north side of Nye Bay (Figure 3-1) contains quartz, garnet up to 5.7 mm wide, kyanite up to 1.5 mm long, biotite flakes up to 0.3 mm wide, and muscovite which is normally very fine-grained, but flakes up to 0.2 mm long can be found. Unlike many of the other Tasmanian samples, the biotite is unaltered, ranging in composition from 0.30 to 0.36 Mg/Mg/Fe and plotting well in the siderophyllite field of the Fe/(Fe+Mg) vs. Al(VI) diagram (Figure 3-15). The single grain of muscovite analysed is 0.03 Na/(Na+K). The garnet appears to have fairly homogeneous core with a narrow rim. It is higher in X_{Sps} (0.019) and X_{Alm} (0.76) at the rim than in the core (lows of 0.006 X_{Sps} and 0.64 X_{Alm}) and lower in the rim in X_{Grs} (0.11) and X_{Prp} (0.11) than in the core (highs of 0.23 X_{Prp} and 0.13 X_{Grs}) (Figure 3-16). Using the garnet rim and biotite grain nearest the analysed muscovite

gives a GBMAQ estimate of ~ 700^{o} C, 6,100 bars (Figure 3-17). The other grain of biotite has a larger range of composition, which, if used for GBMAQ calculations, results in the average for all possible combination of muscovite-biotite-garnet shifting only one degree and 200 bars higher than considering only the nearer grain. The Thermocalc average pressure temperature estimate using the nearer biotite grain is ~ 700^{o} C, 7,000 bars.

3.1.5: 143072

Sample 143072 was collected by Meffre in 2000 from the point 2 km south of Mulcahy Bay (Figure 3-1). It is a quartz rich schist (Figure 3-18), with poikiloblastic garnet porphyroblasts up to 7.4 mm in diameter, the inclusions of which are primarily quartz. The outermost rim of the garnet is, relatively, inclusion-free. The matrix foliation is formed both by the alignment of mica, and by elongate quartz aggregates. Muscovite occurs in sheets up to 1.4 x 3 mm, and biotite grains are up to 0.06 x 0.8 mm. Rare grains of calcite up to 1.1 mm long are present. Monazite is also present.

The garnet is zoned, with a change in compositional trends at the core-rim boundary, and a minor reversal at the very rim (Figure 3-18). Spessartine reaches a high of 0.15 in the core, and decreases slowly through the core to 0.12 X_{Sps}, then drops more steeply to a low of 0.008 at the rim. Unlike some of the other components, spessartine does not increase at the outer rim. Grossular has a high of 0.11 in the core and generally decreases to 0.08 at the core-rim boundary, then increases abruptly to 0.14 X_{Grs} before decreasing to a low of 0.02 and then increasing again to 0.05 at the outer rim. Pyrope is about 0.08 through much of the core, but drops (on the left side of the grain) to a low of 0.05 X_{Prp} just after the core-rim boundary, and then increases to 0.22 X_{Prp} at the outer rim. Almandine is at a low of 0.66 in the core, and increases to 0.70 X_{Alm} at the core-rim boundary, then rises to a high of 0.76 X_{Alm}

before dropping to 0.73 at the rim edge. Most of the biotite analysed was too chloritised to use for thermobarometric calculations, but two acceptable analyses, which plot in the siderophyllite field of the Al(IV)-Fe/(Fe+Mg) diagram and has a Mg/(Mg+Fe) of ~ 0.41 (Figure 3-19). The muscovite ranges from 0.8-0.10 Na/(Na+K) (Figure 3-19). This sample also contains rare small (1 x 0.5 mm) calcite grain(s). Using either of the unaltered biotite analyses with their nearest garnet rim analysis in conjunction with any of the muscovite analysed in this sample results in a GBMAQ estimate of 820^{o} C, 12,300 bars (Figure 3-20). The results obtained via Thermocalc average pressure/temperature estimates for the garnet rim/matrix formation conditions is 880^{o} C, 12,200 bars. This temperature is unrealistically high, as that is above the quartz-muscovite breakdown reaction. The X_{Prp} of the garnet rim is higher than typical for the region. One possibility is that as the garnet grew the biotite reservoir was depleted and the equilibrium biotite was pushed to very Mg-rich compositions, followed by reactions bringing the biotite back to the present composition later. Some of the grains of garnet display evidence of breakdown and alteration to chlorite. That garnet breakdown could be responsible for the growth of a relatively Fe-rich biotite that is not in equilibrium with the garnet rim analysed.

3.1.6: Summary of southwest coast classic geothermobarometric results

There is very good agreement in the results for the four samples from Nye Bay, with the results for each overlapping some of the other samples at roughly 650^{o} C, 6000 bars (Figure 3-21). The only southwest coast sample for which it was possible to use all four classic geothermobarometric techniques applied in this study is 68319 from Nye Bay (Figure 3-1). For this sample the various techniques yielded results which are essentially the same within error. However, there was a difference in specific pressures and temperatures reported for each technique such that Thermocalc gives slightly higher P/T than does GBMAQ, which gives slightly higher P than does

GASP, which is slightly higher than GB-GBPQ. If this pattern would have held true for the other southwest coast samples (had they contained the requisite minerals present/analysed to apply more than one geothermobarometer), the agreement between the four Nye Bay samples would be even more evident, as the two lowest P/T estimates were obtained via GB-GBPQ; if they had not been lacking in muscovite the other techniques may well have resulted in higher-P estimates for these two, which would have closed the gap between the highest and lowest Nye Bay pressure estimates. The preferred PT conditions for the rims of garnet in the Nye Bay rocks is 640^{o} C, 6,000 bars.

A single sample (143072) from south of Mulcahy Bay (Figure 3-1) had the requisite minerals to undertake geothermobarometric calculations but resulted in an unreasonable temperature estimate, as discussed above. However, using a T of 640^{o} C (the T from Nye Bay) in the GBMAQ calculations the pressure estimate for this sample is lowered to ~ 8,200 bars, which is still higher than the Nye Bay results. While it is possible that the higher grade conditions implied by these calculations arise solely from complications arising from the compositions of the minerals in this sample, the collection area is from a separate fault block to the Nye Bay samples and this leaves open the possibility that this sample had a different metamorphic history.

3.2: WHOLE ROCK COMPOSITION

In preparation for Perple_X modelling XRF whole-rock analyses were obtained for a number of southwest coast samples. They are compositionally distinct from the Collingwood River samples (Figure 3-22), being lower in aluminium and higher in iron/magnesium/manganese than the Collingwood River samples. The three north Nye Bay samples plot closely together on the AFM diagram (Figure 3-22A), while the two from the south side of Nye Bay are slightly different from the north Nye Bay group, plotting to either side, one lower and the other higher in aluminium. The two

samples from Mulcahy Bay and the one from just north of Wreck Bay are generally higher in aluminium than the north Nye Bay samples. The ACF diagram (Figure 3-22B) emphasizes the very low calcium nature of all of these samples, which plot along the A-F edge. In general, the more southern locations plot closer to A, while the northern locations plot closer to F (Figure 3-22B). Taking the ratio of the amount of aluminium and calcium in Tasmanian pelites versus that of the average pelite (Shaw 1956) emphasises that the samples from different regions plot in groups (Figure 3-22C). The samples from the south of Nye Bay have the lowest values for both $Al_{sample}/Al_{Shaw's\ average\ pelite}$ and $Ca_{sample}/Ca_{Shaw's\ average\ pelite}$, the north Nye Bay samples are higher in both, and the Mulcahy Bay samples a little higher in Al, but similar in Ca to the Nye Bay samples. Note that the whiteschist from the Collingwood River plots near the Mulcahy Bay and north Nye Bay samples on this diagram (Figure 3-22C) and the sample from Wreck Bay, which is higher in Al than Shaw's average pelite, plots with the Collingwood River samples. All samples analysed for this project fall well below the line (Figure 3-22C) which separates monazite and allanite stability (Wing et al. 2003) and monazite was found to be present in all of these samples in which minor components were analysed.

3.3: PERPLE_X RESULTS

3.3.1: Sample 68318

Perple_X modelling for sample 68318, fully described in section 3.1.1: above, was undertaken using several different starting parameters. A) using the XRF whole-rock composition, B) using that composition modified to contain additional MnO, and C) using a bulk-rock composition calculated from modal abundance and composition of the minerals for this sample. Both the XRF and the modified XRF whole rock composition calculations resulted in loosely constrained intersections for the garnet

core isopleths at ~ 570^{o} C, 5,100 bars. However, a variety of calculations using various estimates of mineral mode/composition failed to give intersections for all four isopleths of garnet core composition, though three of the four do converge at ~ 550^{o} C, 4,400 bars for some of the attempts. Several attempts were made to model the garnet fractionation path for this sample using the XRF-based Perple_X results. However, possibly due to the complexity in the zoning for this sample, no straight path was obtained which models the observed compositional changes to the garnet rim. The garnet zoning pattern for this sample (Figure 3-2) indicates the growth of an inclusion-free uniform core at ~ 570^{o} C, 5,100 bars. The abrupt change at the core-rim boundary is marked both by a compositional change (X_{Grs} up, X_{Alm}, X_{Prp} down) and the appearance of numerous fine-grained inclusions. While such a compositional change could have been produced by a complex PT path, the balance of evidence is that the change in inclusion density is produced by dehydration, resulting in a transient increase of available Ca, possibly due to the breakdown of calcite and the consumption of biotite in the matrix. Finally, a small increase in temperature to 660^{o} C, 4,000 bars is recorded by the garnet rim & matrix mineral compositions.

3.3.2: Sample 68319

Sample 68319 is fully described in section 3.1.2: above. Perple_X modelling using the XRF whole-rock composition in conjunction with the microprobe analysis with the highest Mn concentration (from garnet A) for Perple_X calculations gives a region of garnet-core isopleths intersecting with a “best fit”, with all four predicted garnet end-members matching their measured compositions within 0.003 of the measured value, and X_{Grs} and X_{Sps} within 0.001 of their measured values at ~ 550^{o} C and 5,600 bars (Figure 3-23). At these conditions the sample is predicted to contain ~ 51 wt% quartz, 14 wt% biotite, 13 wt% chlorite, 12 wt% phengite, 4 wt%

plagioclase, 4 wt% paragonite, 1 wt% ilmenite, and 1 wt% garnet. Chlorite was found as inclusions within the garnet, although with a lower Mg/(Mg+Fe) value than predicted. However, as with the other Tasmanian samples, paragonite was not detected in the sample, indicating that the water saturated assumption of the calculations may not be appropriate, or the paragonite may have reacted out during the subsequent history of the rock.

3.3.3: Sample 143097

Sample 143097 (Figure 3-24) is the southern most of the southwest cost samples analysed for this project, coming from the coast north of Wreck Bay (Figure 3-1). It is a fine-grained quartz-muscovite-garnet-biotite schist. The mica defines a foliation, with muscovite flakes up to 3 mm long, and the less common biotite grains up to 0.9 mm. The garnet is reasonably uniform in size, reaching up to 1 mm in diameter. It has cores which are rich in inclusions (chiefly quartz) compared to the rims. The garnet crystals have generally homogeneous cores and zoned rims. The garnet cores are higher in calcium than those of any other Tasmanian sample (Figure 3-25). Spessartine reaches a high of 0.041 in the core, and decreases slowly across the core to 0.20 X_{Sps}, before dropping more steeply to 0.006 at the rim edge, grossular ranges from 0.16 to 0.20 X_{Grs} across the core, with the lower values in the centre, then drops to 0.03 at the rim edge, pyrope fluctuates between 0.07 and 0.09 X_{Prp} in the core, and then raises to 0.18 at the rim edge, and almandine hovers between 0.70 and 0.73 in the core, rising to 0.79 at the rim edge (Figure 3-26). The muscovite ranges from 0.11 to 0.16 Na/(Na+K). Unfortunately, all of the biotite analysed in this sample were too chloritised for use in geothermobarometric calculations. Perple_X modelling using the XRF whole-rock composition results in the isopleths corresponding to the composition measured in the garnet core intersecting at 560^{o} C and 6,500 bars (Figure 3-27). At those conditions the minerals predicted to be

present are 42 wt% quartz, 37 wt% phengite, 11 wt% chlorite, 6 wt% biotite, 3 wt% garnet, and 1 wt% plagioclase.

3.3.4: Summary of southwest coast Perplex results

The three southwest coast samples for which garnet core isopleth thermobarometery led to a pressure/temperature estimate all yield similar results, which average to ~ 560^{o} C, 5,700 bars (Figure 3-28). The four other southwest coast samples for which Perple_X analysis was attempted all failed to yield useable results, with several of them resulting in isopleths which are parallel to one another and nearly completely temperature dependent. None of the southwest coast samples analysed yielded working Perple_X "path" results.

3.4: COMPARISON OF SOUTHWEST COAST GARNET COMPOSITIONS/HABIT

In general, the garnet crystals in schists from the southwest coast of Tasmania are larger in size in the northern area of the coastal outcrops of schist. The garnet in the Nye Bay schists (Figure 3-1) reaches 17 mm (sample 68318) in diameter in thin section (larger crystals of garnet were observed in the field, but not collected (A. McNeill, personal communication)). The smallest grains of garnet (samples 143076 & 143097) from southwest coast schists analysed for this project were from south of Mulcahy Bay (Figure 3-1). The two samples just south of Mulcahy Bay, 143072 & 143076, have the highest spessartine component of any Tasmanian samples, as well as having much lower almandine components (Figure 3-25). Their pyrope component in the garnet cores is lower than any of the other three end members, and their grossular is lower than spessartine in the cores.

The southern-most sample, 143097, from the coast 3 km north of Wreck Bay (Figure 3-1) has the highest grossular component for the core compositions, with nearly twice as much grossular than pyrope (Figure 3-25).

The two samples from the south side of Nye Bay have cores which are quite high in almandine, fairly low in pyrope, and lower still in grossular and spessartine (Figure 3-27).

The five samples from the north side of Nye Bay have three types of garnet. Type A (samples 68318 & 68319) has more spessartine in the core than grossular, and nearly as much as pyrope, type B (samples 68319B & 68320) has virtually no spessartine or grossular and more pyrope than does Type A (Figure 3-25). These two types are from a single location, and have been observed in a single thin section (Figure 3-6)—it is possible that the type B version merely represents a slice through the garnet at a point well removed from the true core, but still far enough in from the edge so as to show the visible core-rim boundary, or these grains nucleated after most of the Mn in the rock had been consumed by other garnet grains. Type C (samples 68334 & 68335), which comes from 225 meters northwest along the coast from samples containing types A & B, have cores which is quite high in pyrope and rims which are low in almandine. Unlike all of the other Tasmanian garnet types analysed, this type has a decrease in pyrope towards the rims probably reflecting garnet growth during cooling (Figure 3-25).

The garnet zoning patterns (Figure 3-25) from the south west coast show that there was no notable increase in pressure during garnet growth, as none of the garnet analysed show an increase of X_{Grs} to the rims. Indeed, most of the garnet analysed show fairly flat and low X_{Grs} across the profile, a few decrease in X_{Grs} from core to rim, and one sample shows a minor reversal with X_{Grs} increasing again at the rim. They do, however show an increase in temperature, with fully half of the samples showing an increase in X_{Prp} from core to rim. However, the others show either a fairly homogeneous core with decrease in X_{Prp} at the rims or an increase in X_{Prp} from core towards rim, and a decrease at the rim. Likewise, fully half of the samples show

a slight increase in X_{Sps} again at the rims indicating some resorption of garnet. Oddly enough, none of the samples show a reversal in all three end members—usually only one changes its trend at the rim, with the result that nearly all samples from the southwest coast show a minor reversal in compositional trend at the rim for one of the end members.

3.5:SOUTHWEST COAST P/T PATHS

In the absence of working Perplex path calculations for the southwest coast samples we must rely upon the classic geothermobarometric estimates in conjunction with the Perple_X results for the garnet core formation conditions (Figure 3-29, Figure 3-30). These show only a slight increase (~ 80^{o} C) in temperature, combined with a slight increase in pressure (~ 100 bars) for the Nye Bay samples.

The garnet zoning patterns can be used to add some additional detail to this interpretation. Most samples show increasing pyrope towards the rims. This could be due to increasing T or due to the elimination of the biotite reservoir as the garnet grew. Many of the rocks have relatively low biotite contents, which leaves open the latter interpretation. The classic textural pattern of larger garnet grains with highly included rims suggests that the rate of garnet growth was greatly increased towards the rim. This is a recurring theme. Typically this would be expected if the pressure increased rapidly but there is very little support for that interpretation. Most rims have lower Ca than the cores. Only in sample 68318 (Figure 3-2) is there a pulse of higher Ca, and this is only for a very small interval before the Ca returns to the original value. An alternative interpretation that may fit these patterns is that the change in garnet growth habit reflects the loss of a water-rich phase. On dehydration, biotite would be reduced in stability and any chlorite and paragonite would disappear. In such conditions garnet is favoured. As the garnet grows, biotite is pushed to more Mg rich compositions, leading to an increase in X_{Prp} in the garnet

rims. Loss of paragonite would push the An content of plagioclase down and the drop in Can in garnet without much drop in pressure may fit this model. Finally, the short pulse in Ca in the rims of garnet in 68318 (Figure 3-2) is consistent with the discrete disappearance of a high Ca phase, such as calcite, which at 640^{o} C and 5,000 bars would occur at an X_{CO_2} of about 0.05 (Spear 1993).

In summary, the PT path recognized on the southwest coast is from a core composition at 560^{o} C, 5,700 bars to a rim composition at 640^{o} C, 6,000 bars. The early growth is in the kyanite field, and there is late fibrolitic sillimanite in some of these rocks consistent with this path. The strong garnet zonation probably reflects the exhaustion of matrix elements as the garnet grows, probably including the loss of a fluid phase.

Chapter 4

Other Regions

CHAPTER 4: OTHER LOCATIONS

In addition to the Collingwood River samples from the Franklin Metamorphic Complex and the Nye and Mulcahy Bay samples from the Port Davey Metamorphic Complex discussed in Chapters 2 and 3, a few samples which achieved garnet-grade metamorphism were selected for analysis from other areas in Tasmania, specifically from the Forth Metamorphic Complex, on the north coast, and the Mt. Mary and Raglan Range areas from central Tasmania. The latter two areas are near Collingwood River, but represent a lower metamorphic grade and separate fault bound block.

4.1:FORTH

Two samples from the Forth area (Figure 4-1) were analysed for geothermobarometric work.

4.1.1: Sample 75596

Sample 75596, collected by Lewis (1991) from the hills to the west of the River Forth (Figure 4-1), contains chloritoid, in blades up to 3 mm long, skeletal garnet grains up to 2 mm long and chlorite flakes up to 0.5 mm long; finer grained chlorite with a slightly different composition is present in cracks in the garnet (Figure 4-2A). There are muscovite (0.16 to 0.21 Na/NA+K) grains (up to 2 mm) in the matrix, and paragonite (0.82 to 0.85 Na/Na+K) is present as an inclusion within the garnet (Figure 4-2B); this is the only example of a discrete grain of paragonite observed in this study. The garnet core has a sieve texture comprised of a network of thin (10-30 μm) garnet bands surrounding abundant quartz grains (up to 0.4 mm long) while the rim is massive and inclusion poor (Figure 4-3). There are abundant late-stage cracks in the garnet which have been filled by retrograde chlorite with a different (0.42 to 0.43 Mg/Mg+Fe) composition to that of the matrix chlorite (0.52 to 0.58

Mg/Mg+Fe). Thermocalc average pressure/temperature estimate for the garnet rim and matrix minerals for this sample is ~ 670^{o} C, 17,700 bars.

4.1.2: Sample 75637

Sample 75637 (Figure 4-4) collected by Lewis (1991) from the Forth River valley (Figure 4-1), is a quartz-mica schist with garnet and albite porphyroblasts. The garnet crystals reach up to 1.3 mm diameter, and plagioclase up to 2.25 mm wide. The plagioclase is nearly pure albite, but does exhibit zoning at the rims, which are higher in X_{An} than the central portion (Figure 4-5) However, even the rims are considerably lower in calcium (0.02 X_{An}) than recommended for use in GB-GBPQ (see Appendix 9). The garnet zoning is asymmetrical, generally decreasing in spessartine and grossular and increases in pyrope and almandine from the cores to the rims (Figure 4-6). Muscovite is the most common mica present, usually as narrow laths up to 0.5 mm. Occasional grains which are split biotite on one side and muscovite on the other are present. Unlike the biotite from the other regions, this sample plots entirely within the eastonite field of the Al(VI)-Fe/Fe+Mg diagram (Figure 4-7) and has ~ 0.55 Mg/Mg+Fe. The muscovite is ~ 0.19 Na/Na+K (Figure 4-7). The requisite minerals were present to use both GB-GBPQ and Thermocalc geothermobarometry for this sample. However, as discussed in Appendix 9, the GB-GBPQ estimate of ~ 670^{o} C, 20,300 bars can only be regarded as an upper limit on the pressure, due to the very low X_{An} in the plagioclase, which substantially increases the errors on pressure. The Thermocalc average pressure/temperature estimate of ~ 670^{o} C, 16,100 bars is the more reliable of the two, as it draws upon the muscovite as well as plagioclase to estimate the metamorphic pressure.

Two other samples from the Forth area, 154324 and 154325 were analysed but proved unsuitable for geothermobarometric calculations. Sample 154324 has abundant muscovite, and garnet, and contains kyanite and tourmaline, but it lacks

biotite and plagioclase. Sample 154325 contains garnet, plagioclase, and muscovite, and biotite. The biotite is largely replaced by chlorite, and is unsuitable for geothermobarometric calculations. There are insufficient reactions among the relict minerals to calculate an average P/T for this assemblage.

4.2:MT. MARY

Two samples from Mt. Mary (Figure 4-8) were analysed for this project.

4.2.1: Sample 39463

Sample 39463, collected by Turner (1971) from along Mary Creek (Figure 4-8), is a fine grained quartz-mica-garnet schist (Figure 4-9A). The crystals of garnet are up to 0.7 mm diameter and show a central core containing curved inclusion (quartz) trails, with a more massive rim (Figure 4-9B). The garnet composition is quite different from that of the Collingwood River or the southwest coast samples. The garnet crystals of the other regions are primarily almandine, their second highest component is generally pyrope, and spessartine is generally the lowest component. However, the garnet crystals of sample 39463, while almandine-rich in the rims, have very spessartine rich cores (Figure 4-9B). The cores show a gentle decrease in X_{Sps}, from 0.55 to 0.38, followed by a change in slope at the transition from the inclusion-rich core to the more massive rim, where it decreases to 0.11 before rising again to 0.15 on the left-hand rim (Figure 4-9B). Note that on the left side the compositional difference between the core and the rim is much more abrupt than on the right-hand side, as is the visual transition between core and rim. Almandine increases from a low of 0.51 in the core to a high of 0.77 just in from the left-hand rim. Grossular ranges in the core from ~ 0.19-0.24 X_{Grs}, and decreases at in the rim to a low of 0.17 X_{Grs}. Pyrope is very low across the core (~ 0.01 X_{Prp}), and rises to 0.04 X_{Prp} at the rim. The muscovite ranges from 0.06 to 0.11 Na/Na+K, plotting generally lower

than the Collingwood River and higher than the Nye Bay muscovites on the Si-Na/Na+K diagram (Figure 4-10). Much of the biotite is too chloritised to use for geothermobarometric calculations, but three analyses were acceptable (Figure 4-10). These three have a Mg/Mg+Fe of ~ 0.30, and plot lower on the Si-Mg/Mg+Fe diagram than do the biotites from the other regions of Tasmania. They plot well within the siderophyllite field of the Fe/Fe+Mg-Al(IV) diagram and are more Fe rich than biotites from the other Tasmanian regions (Figure 4-10C). The plagioclase ranges from 0.01 to 0.06 X_{An}, which, as with most of the other samples from other regions, is lower than recommended for use with GB-GBPQ (see Appendix 9). Therefore, while the GB estimate of ~ 560^{o} C gives a GBPQ pressure of 16,500 bars this can only be regarded as a maximum pressure. Thermocalc gives an average pressure/temperature result of ~ 430^{o} C, 9,000 bars for the garnet in Figure 4-9, using the right-hand rim (side without the increase in X_{Sps}) and nearby matrix minerals. There was one plagioclase analysed which has a higher X_{An} on its rim. Using that grain, in conjunction with the closest garnet and muscovite, and the unaltered biotite (~ 10 mm away) gives an estimate of ~ 540^{o} C, 11,000 bars, which is a more reasonable temperature estimate, despite relying upon grains which are distant from one another. Samples from these other regions were not selected for whole-rock analysis and Perple_X modelling, so no estimate of conditions for garnet core formation is available. However the garnet growth pattern permits some inferences to be made. The central portions of the garnet grains in this sample are characterized by curved inclusion trails. Whether one accepts the hypothesis that such trails are the result of garnet rotation during growth or strain partitioning and overprinting, both models agree that they are indicative of deformation during garnet growth, by either hypothesis the inclusion-poor rim is likely to have formed under different (non-directional?) stress conditions than did the core with its curved inclusion trails. The

X_{Grs} pattern changes from the core-rim boundary to the rim (pink-lines, Figure 4-9), first decreasing slightly, then rising, then dropping down to the lowest levels at the rims. There are additional inclusions of quarts associated with the transition from peak rim X_{Grs} to the lower outer rim composition.

4.2.2: Sample 39456

Sample 39456, also collected by Turner (1971) from along Mary Creek (Figure 4-8), is a quartz-mica-garnet schist with albite porphyroblasts (Figure 4-11). The plagioclase is up to 0.8 x 0.6 mm, the garnet occurs in frequent very small (~ 0.15 mm) grains, but occasional larger grains (up to 1 mm—e.g. upper left corner of Figure 4-11) are present. The mica is fine-grained with muscovite (the dominate mica) up to 0.3 mm, and biotite up to 0.17 mm. The foliation is formed both by alignment of mica and by elongated quartz grains. The long axis of the plagioclase is not concordant with the foliation (e.g. lower right corner of Figure 4-11). The plagioclase ranges from 0.01 to 0.28 X_{An}. The lower X_{An} values are in the interior of the grain, and the high X_{An} analysis is on the rim (Figure 4-12). Most of the biotite is altered; a single analysis was obtained which was unaltered (Figure 4-13A). During the second microprobe session care was taken to select only points for analysis on biotite grains which showed higher K peaks during pre-analysis screening than the other grains. However, despite being higher in K than was available in other pre-screened grains, all biotite analysed on the second session was chloritised, with K_2O < 7 wt%. The single biotite analysis has a Mg/Mg+Fe value of 0.30. Like the other Mt. Mary sample, it plots lower on the Si-Mg/Mg+Fe diagram than the biotites from other locations, and is well within the siderophyllite field of the Fe/Fe+Mg-Al(IV) diagram (Figure 4 13). The muscovite ranges from 0.06 to 0.17 Na/Na+K (Figure 4-13B), and like the other Mt. Mary sample, plots generally below the Collingwood River and above the Nye Bay muscovites on the Si-Na/Na+K diagram (Figure

4-13C). This sample contains rutile, hematite, and ilmenite. The rutile is preserved as a core in a large (0.5 mm) matrix grain with a rim (25-50 μm) of ilmenite (Figure 4-14A), the hematite appears as narrow embayed matrix grains up to 0.2 mm long (Figure 4-14B), and there are small (0.1 x 0.01 mm) inclusions of ilmenite within garnet (Figure 4-14C). The small ilmenite inclusions have a slightly different composition than the rim of the large ilmenite-covered grain, with the inclusion being slightly higher in SiO_2 and lower in TiO_2 than the rim of the large grain (Figure 4-14D). The garnet shows zoning with a reversal at some rims, but, usually, only on one side of the grain (Figure 4-15). The GB-GBPQ gives an estimate of ~ 500^o C, 9,000 bars using the plagioclase rim, the non-reversed rim of the nearest garnet (Figure 4-15), and the only usable biotite analysis. Thermocalc average pressure/temperature calculations using these same points and a nearby muscovite grain gives an estimate of ~ 570^o C, 8,600 bars (Figure 4-16).

The two Mt. Mary samples have overlapping P/T results, and the result of ~ 570^o C, 8,600 bars is the preferred result for this region.

4.3: RAGLAN RANGE

One sample from the Raglan Range region was analysed for geothermobarometric work. Sample 30145, collected by Gee (1962) from the south side of the range along the banks of the Joyce River (Figure 4-17), is a crenulated schist (Figure 4-18). The foliation is defined by muscovite laths up to 1 mm long, with smaller (up to 0.25 mm) biotite grains. The garnet crystals are up to 0.2 mm long, the plagioclase is up to 1.25 mm, and the chlorite mats are up to 1 mm wide. The plagioclase, unlike that from samples from other regions analysed for this project ranges from 0.33-0.34 X_{An} (Figure 4-19). The muscovite ranges between 0.10-0.21 Na/Na+K, the biotite ranges from 0.58-0.61 Mg/Mg+Fe, and the chlorite ranges from 0.41-0.44 Mg/Mg+Fe (Figure 4-19). Plagioclase being rare in this sample, only one grain was analysed.

The garnet is zoned (Figure 4-20), with one of the two grains analysed showing a core which is largely homogeneous with respect to almandine (~ 0.60 X_{Alm}) and pyrope (~ 0.16 X_{Prp}), but increases slightly in grossular (0.16 to 0.20 X_{Grs}) and decreases in spessartine (0.075 to 0.57 X_{Sps}), and a rim in which spessartine continues to decrease (to 0.038 X_{Sps}) while the other three end-members reverse their trends (to 0.68 X_{Alm}, 0.22 X_{Prp}, and 0.06 X_{Grs} (Figure 4-20A). The other garnet analysed shows subtle zoning which appears to consist of two grains (Figure 4-20B), each of which shows a slight decrease from core to rim of grossular (0.27 to 0.21 and 0.23 to 0.19 X_{Grs}) and spessartine (0.048 to 0.016 and 0.021 to 0.014 X_{Sps}) and a slight increase in almandine (0.56 to 0.57 and 0.59 to 0.60 X_{Alm}) and pyrope (0.13 to 0.19 and 0.15 to 0.19 X_{Prp}). This double-grain is considerable richer in grossular and poorer in spessartine than the other. Since the highest level of spessartine in the double-cored grain is just less than that in the single-cored grain at its core-rim boundary and that level of spessartine is achieved in the same analysis point as the highest level of grossular in that grain, and the single-cored garnet achieved its highest level of grossular at the core-rim boundary, the double-cored grain is interpreted to represent an off-centre slice through the pair of grains along the core-rim boundary of those grains. Therefore, I have chosen to use the rim of the single cored garnet for geothermobarometric calculations, even though it is higher in spessartine than is the rim of the double cored grain, because its rim grossular composition is more likely to be compatible with the conditions during which the garnet rims formed. GB-GBPQ yields an estimate for this sample of ~ 700^{o} C, 11,400 bars. Thermocalc was unsuccessful.

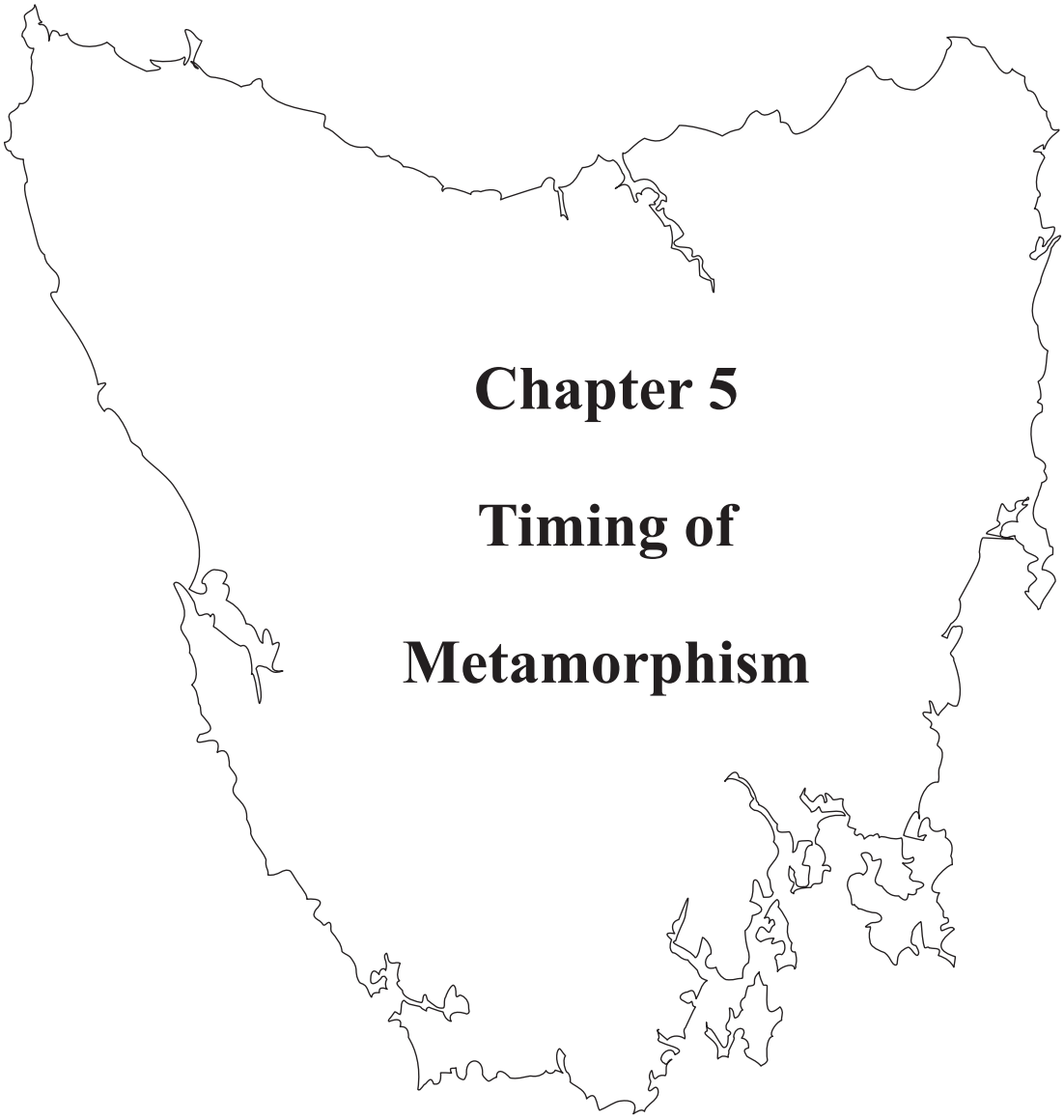

Chapter 5

Timing of

Metamorphism

CHAPTER 5: TIMING OF METAMORPHISM

5.1:INTRODUCTION

The timing of Tasmanian metamorphism has been constrained primarily via chemical U-Th-Pb dating of in-situ monazite grains (see section 1.3.2.1 for methods details). In addition, two pilot studies were conducted; one to determine detrital zircon ages (see section 5.3) and another investigating the lead isotopes in micas (see Appendix 11). The locations of the thirty-three samples for which geochronological analyses have been undertaken are shown in Figure 5-1. This figure includes the fourteen samples reported in Berry et al (2007—see Appendix 1), some of which have had subsequent supplementary analyses, and nineteen additional samples analysed after that publication. Detail maps showing each region and the locations of the samples therein are available in the sections relating to each sample. For those samples wherein geothermobarometric work was also undertaken, the maps are with their sample descriptions in the earlier chapters; this chapter contains maps and sample descriptions for those samples for which only geochronological results have been reported.

5.2:MONAZITE AGES

5.2.1: Summary of Results

The overall trends in the monazite results will be presented first, followed by detailed results for each sample, sorted by region, showing how the individual samples relate to the overall trends.

5.2.1.1: PATTERNS IN AGE RESULTS

The combined monazite data probability diagram for all Tasmanian regions included in this study shows that the primary metamorphic episode occurred in the Cambrian, with additional data in the Mesoproterozoic, a range of ages between those two

peaks, and a few, rare Devonian age analyses (Figure 5-2). Figure 5-3, which displays these results sorted by age and plotted sequentially (without their error bars), shows trends in the data that are useful when considering how much of the data to include in the weighted mean age calculations for each peak. The primary pattern within the data falls in the Cambrian, where the curve segment approaches horizontal (Figure 5-3). This portion of the curve is centred at ~ 505 Ma with "tails" bending off approaching right angles at each end in a symmetrical pattern; this portion of the pattern ends at gaps in the data at ~ 400 and 600 Ma (Figure 5-3 inset). Therefore, those two end ages were selected as the arbitrary cut-off points for calculating the weighted mean age of the main, Cambrian, Tasmanian metamorphic event recorded by this episode of monazite growth. This age comes to 505 ± 1 Ma with a MSWD of 1.02 after Isoplot rejected 31 of the 643 points that fall between 400 and 600 Ma (the main peak of Figure 5-2 represents 67% of the monazite analyses considered in this study). However, there are variations in this age if one considers the results by region. The region which best agrees with the above mean age for all Cambrian monazite results is the southwest coast; the 11 samples from Mulcahy, Nye, and Wreck bays combine to give a weighted mean age of 505 ± 2 Ma with a MSWD of 1.12 for 196 out of 205 analyses (small green ellipse, Figure 5-4). The two non-whiteschist samples from the southern block of the Collingwood River have a combined age that plots with a similar centre, but larger error ellipse, at 506 ± 6 Ma with a MSWD of 3.4 for 37 out of 39 analyses (larger green ellipse, Figure 5-4). One of the regions plots at a lower age than the above reported mean for all results (red ellipse, Figure 5-4); the oft-analysed sample from Mersey River gives weighted mean age of 497 ± 3 with a MSWD of 1.12 for 166 of the 171 points analysed on sample 7401). The other regions all plot (varying shades of blue and teal, Figure 5-4) with ages higher than the above total combined mean, with the best of these

results obtained for the north block of the Collingwood River, which has a weighted mean age of 511 ± 3 Ma with a MSWD of 1.2 for 87 of 90 analyses from eight samples. The north coast samples have a weighted mean age of 511 ± 5 Ma with a MSWD of 1.09 for 73 of 76 analyses. The single sample from Strathgordon has a weighted mean of 510 ± 11 Ma with a MSWD of 1.4 for 19 points analysed, and finally the whiteschist from the south block of the Collingwood River has a weighted mean age of 508 ± 9 Ma with a MSWD 1.2 for 19 of 21 analyses on two thin sections obtained from this outcrop.

Further combining the regions (grouping them by their ages), results in three distinct sets: 511 ± 3 Ma (for the north coast, the north block of the Collingwood River, and Strathgordon Region—blue ellipse and peak, Figure 5-5), 504 ± 2 Ma (for the southwest coast and the south block of the Collingwood River—purple ellipse and peak, Figure 5-5), and 497 ± 3 Ma for the Mersey River region (red ellipse and peak, Figure 5-5). These numbers are similar enough that they may be regarded as being a single population, with random distribution of the data accounting for the apparent differences by region. Alternatively, they could reflect the onset of a single episode of metamorphism at different times within the Tyennan Orogeny at different locations. However, if these three ages are to be considered representative of such differences in timing within this metamorphic event by region an explanation as to their current spatial distribution would be required, since the three sub-ages within the Cambrian event do not have a sequential map distribution (see Figure 5-1 for locations of each region—note that the text colours of Figure 5-1 match those of Figure 5-5 to assist with seeing the age variations by region). This question will be addressed in Chapter Six.

In addition to the above peak metamorphic event in the Cambrian, there are also a few (< 1% of the total analyses) Devonian aged grains, which come from two of the

samples analysed; one is a mylonite in the south block of the Collingwood River, the other is from the Mersey Valley (see discussion below). These are not considered be part of the main metamorphic event and they were not considered in the Cambrian weighted mean age calculations; their weighted mean age is 347 ± 23 Ma with a MSWD of 1.4 for 7 analyses.

The remaining data show some variation in its trends (Figure 5-3). The region between ~ 600 and 950 Ma is very linear and approaches vertical, due, in part, to the sparseness of the data in that age range (4% of the total data). Arranged in this type of diagram, the more horizontal segments of the curve are due to multiple analyses which share ages which are the same, within error, while the steeper segments of the curve occur when the adjacent ages have markedly different ages and are thus widely scattered, and do not form a discrete age population. It is interpreted that the analyses which fall into the ~ 600-1000 Ma age range are "mixed" ages with no specific significance. Above ~ 950 Ma there are four subtle bends in the data (centred, one each, in the teal, green, olive, burgundy, and purple portions of the curve—Figure 5-3) before it settles into a smooth symmetrical curve (upper blue segment) again above ~ 1300 Ma. Given these patterns, Figure 5-6 was prepared showing only those data from all regions with ages greater than 950 Ma (29% of the analyses) so that the patterns in this portion of the data would be more clearly visible. This diagram illustrates the spread in the older data, which has a main, broad peak, and some lesser bumps (which account for the above mentioned "subtle bends" in trend on Figure 5-3). Isoplot's "unmix ages" algorithm is a useful tool in determining which data can reasonably be included in assigning an age to such a broad peak as the largest shown in Figure 5-6. However, that algorithm is limited to breaking the data down into six categories; therefore it is not useful applied to the entire range of data from all analyses (~ 300-1550 Ma), which, clearly (Figure 5-2, Figure 5-6), contains more

than six “groups” of ages. The above observations in the trend suggested that the “unmix ages” be applied only to those data with ages greater than 1000 Ma, which results in the assignment, with a total “relative misfit” of 0.223, of ages to the “peaks” at 1027 ± 9 Ma (10%), 1107 ± 11 Ma (11%), 1202 ± 7 Ma (15%), 1291 ± 8 Ma (18%), 1367 ± 7 Ma (32%), and 1430 ± 10 Ma (14%). These values visually line up with the minor peaks on the graph (Figure 5-6). However, it is very unlikely that each number thus obtained represents a discrete metamorphic event. Certainly, the largest peak, at 1367 ± 7, which comprises 32% of the data considered by Isoplot (or 86 of the analyses) is the most reliable event recorded by monazite growth. The other “peaks”, with their height gradually diminishing towards the younger ages may be a result of mixed ages (as is almost certainly the case for those data between 600 and 1000 Ma) or a series of less significant events. The pale yellow line in Figure 5-6 is the (offset for visibility of the underlying probability curve) smooth curve that connects the highest peak (~ 1366 Ma) with the lowest (~ 1030 Ma), and evens out the lesser peak and accompanying troughs. A two stage Mesoproterozoic history would explain the gross shape of the combined monazite age probability diagram. The peaks at 1107, 1202 and 1291 Ma must be considered as low reliability, but possible, events based on this data.

5.2.1.2: Compositional Trends Of Monazite

Figure 5-7 shows the range in abundance of the elements Sr, Th, U, and Y within the Tasmanian monazite grains analysed for this study. The changes in slope for each of the plots were used to delineate concentrations of each of these elements within monazite in this study, with boundaries set for each segment of the curve with a unique trend; the designations “very low”, “low”, “medium”, and “high” were assigned such that consistent terminology could be used throughout the following discussion, particularly when linking differences in concentration of individual

elements in monazite to specific monazite generations. In addition, comparisons of concentration of each element by region are presented to illustrate changes in monazite composition across the state (Figure 5-8).

The element with the smoothest curve for its graph showing the number of analyses at each concentration (Figure 5-7A) is Sr. This is due, in part, to the very low concentrations of Sr in the monazite, with the highest level of Sr in monazite analysed for this project being 0.99 wt% Sr. Fully 67% of the monazite analyses used for the weighted mean age calculations for this study fall into the "very low" category (< 0.026 wt% Sr). Unlike the other elements addressed in this section, the boundary "very low" for Sr is set at the detection limit for the microprobe analysis. An additional 23% of these analyses are "low" (0.03-0.14 wt% Sr), 9% are "medium" (0.14-0.40 wt% Sr), and the final 1% of these analyses are "high" (> 0.40 wt% Sr). The few monazite analyses with high Sr come primarily from the Southwest coast, with a couple from the south block of the Collingwood River (Figure 5-8A). The medium Sr monazite analyses are from the above two regions and also the north block of the Collingwood River (Figure 5-8). The low Sr monazite results are from the above regions plus the Forth, Mersey River, and Strathgordon areas. The Settlers Schist monazite analyses are all very low in Sr, as are some analyses from each of the other regions (Figure 5-8). The presence of Sr in monazite has been linked to growth in an environment of elevated pressure, which breaks down plagioclase, thus liberating Sr for other minerals (Finger and Krenn 2007) therefore Sr-Age monazite diagrams have been prepared for these samples (Figure 5-9A; see also individual sample results below). In general, the older monazite analyses are very low to low (often below detection limits) in Sr, but those from the main, Cambrian, metamorphic event range from below detection limits to

high Sr, which could be indicative of a higher pressure regime for that episode of monazite growth than for the earlier one(s).

The divisions for Th concentration (Figure 5-7B) have been set several levels, the lowest of which is “very low” < 1 wt% Th. This category contains 5% of the all of the monazite analysed for this study, but 0% of those used for weighted mean age calculations as the assumption of zero common Pb becomes increasingly inappropriate in low Th monazite as the proportion of radiogenic Pb drops. The primary source of radiogenic Pb is Th; below 1% Th, and there is ample evidence in this data that the ages have serious systematic errors that can be attributed to common Pb or to errors in estimating the background value on Pb. The other categories are low 1 to 5 wt% Th (72% of the monazites analysed which were used for weighted mean age calculations), 5-10 wt% Th (24%) and high > 10 wt% Th (3% of the monazite analysed for this study). By region (Figure 5-8B) most of those analyses which are high in Th come from the southwest coast and the south block of the Collingwood River, with a couple of isolated analyses from the north block of the Collingwood River and the Mersey River. The medium Th analyses come from those areas plus some from Forth, two analyses from Strathgordon, and one analysis from the Settlers Schist. All regions have low Th monazite analyses, but only the southwest coast and both blocks of the Collingwood River display an appreciable number of very low Th monazite analyses, with only one each from Mersey and Settlers Schist, and none from Strathgordon or Forth. A comparison of Th in monazite by age (Figure 5-9B) shows that the high Th analyses are most likely to be from the young generation, but that there is no pattern to the age vs. Th for the other concentrations of Th, and the young generation also contains abundant analyses with very low, low, and medium levels of Th.

The divisions for U concentration (Figure 5-7C) in monazite have been set at < 0.1 wt% U for very low (3% of the monazite analyses used for weighted mean age calculations for this study), 0.1 to 0.9 wt% U for low (80%), 0.9 to 2 wt% U for medium (17%) and > 2 wt% U for high (only 1% of the monazite analyses used for weighted mean age calculations). Comparing U concentration by region (Figure 5-8C) shows that the high U analyses are primarily from the southwest coast, with three individual analyses from the south block of the Collingwood River, and one individual analysis from Strathgordon. The medium U analyses are primarily from the south west coast and from the south block of the Collingwood River, with additional analyses from the north block of the Collingwood River, Strathgordon, and two analyses each from Forth and Mersey River. However, most of the latter medium U analyses are from the low end of the medium range (Figure 5-8C). All regions have low U monazite analyses, and only Forth and Strathgordon are without very low U monazite analyses. The high U monazite analyses are all from the young (~ 505 Ma) monazite generation (Figure 5-9C). The medium U analyses reach their higher levels in the young generation, but all ages fall into the lower range of medium, and there is no correlation between age and the low and very low levels of U in monazite analysed for this study. Finger and Krenn (2007) reported distinct differences in U and Th contents of their different monazite generations. A comparison of U vs. Th concentration in monazite by age of analysis location (Figure 5-10) reinforces the above observations that only the analyses with young ages show high levels of U or Th, though by far most of the analyses of either generation fall into the overlapped region of very low to medium U and Th levels.

Divisions for the ratio of Th/U (Figure 5-7D) fall at very low < 3 (4% of the monazite analyses used for weighted mean age calculations for this study), low 3 to 10 (62% of the monazite analysed), medium 10 to 48 (32%), and high > 48 (2% of

the monazite analysed for this study). By region (Figure 5-8) Forth is mostly low with some (lower end of the range) medium Th/U, Mersey River is low to medium with a couple of high Th/U, Settlers has a few analyses on the very low/low boundary, then a gap with the remainder in medium save for two high Th/U, both the north and south blocks of the Collingwood River range across the spectrum from very low to high, though with the south block there are only two high, and considerably fewer medium than there are low. Strathgordon is only very low to low, and the southwest coast monazite analyses range from very low to the low end of high, but few of those analyse fall above the middle of the medium range Th/U.

As shown in Figure 5-7E, analyses with Y > 2 wt% (3% of monazite analyses used for weighted mean ages for this study) are designated “high” in Y, “medium” ranges from 0.8 to 2 wt% Y (60%), “low” ranges from 0.09 to 0.83 wt% Y (30%), and “very low” are < 0.09 wt % Y (6%). The monazite analyses that are high in Y are from the southwest coast, the south block of the Collingwood River, and the Settlers Schist (Figure 5-8E). All regions save Strathgordon have medium-Y monazite analyses, though neither Forth nor Mersey, nor, to a lesser extent, the north block of the Collingwood River reach as high as the top of the medium range. While low-Y monazite analyses do appear in all regions, they are rare in the Settlers Schist. There are no very-low Y monazite analyses from the Mersey River, Strathgordon or Settlers Schist.

The high Y analyses are only seen in the Cambrian monazite generation, while the older generation are most likely to be in the middle Y range (though there are a few older low Y analyses; Figure 5-9E). As with figure 5 of (Krenn et al. 2008) the high Y samples are also in the lower Th range (Figure 5 4B). Yttrium is an element which is very compatible with garnet (e.g. Pyle and Spear 2003), and monazite has been shown to be richer in Y + HREE when it grows in a pre-garnet environment or

during a time of garnet breakdown (Zhu and O'Nions 1999) and changes in concentration of Y across individual grains have been linked to individual age domains (e.g. Gibson et al. 2004). Therefore graphs plotting age vs. Y and age vs. LREE/HREE ratios in monazite were made for each these samples to show the relationships between the different generations of monazite with the timing of the garnet growth (see individual sample results below). There is a distinct change in the slope of concentration of Y in monazite (Figure 5-7E) that was used to differentiate the low and medium levels of Y. This change in slope has been interpreted to reflect a distinct difference in composition of monazite based upon the changing availability of Y during different monazite growth periods and/or changes during a single growth event. These changes in Y availability are likely linked to changes in garnet growth or breakdown as discussed above.

Ratios of LREE/HREE elements in monazite show patterns much like the other elements, with the bulk of the analyses of all generations falling into the low category, with only a few of the older generations falling just across the border into very low or medium categories (Figure 5-7F), but the young monazites spanning the range from very low through to high (Figure 5-9F). As with the other elements, the southwest coast shows the largest range in LREE/HREE ratio, and Strathgordon the narrowest (Figure 5-8F).

Of note from this analysis is that the Cambrian monazite analyses are skewed to lower Y and higher Sm/Gd, both of which support more garnet in the rocks during the Cambrian event than had been available during earlier growth episodes. Similarly the Sr is skewed to higher values in the Cambrian monazite suggesting less plagioclase in these samples during the Cambrian than in the Mesoproterozoic.

5.2.2: Collingwood River monazite results by sample

The Collingwood River area is separated by faults into different packages; the two "blocks" are considered separately here due to their differences in age results. The samples from the north block, near Bill's Creek (Figure 5-11) show two distinct age populations. The north block younger monazite population is tightly constrained with a weighted mean age of 512 ± 4 Ma with a MSWD of 1.2 for 88 analyses. The older generation shows considerable variation in ages (Figure 5-12A), with a pattern that is very similar to that obtained from all Tasmanian data (Figure 5-6) as the north block of the Collingwood River is the source of 189 of the 270 analyses with ages greater than 1000 Ma. There are also an additional 22 analyses ranging from ~ 600 to 1000 Ma which probably represent "mixed" ages, representing new monazite growth from the ~ 500 Ma episode on pre-existing grains with the analysis location comprising both zones. The southern block of Collingwood River, near Scarlett Creek (Figure 5-13) has the greater majority of its analyses from the Cambrian generation of monazite (Figure 5-12B), with only five analyses (from three samples) greater than 600 Ma and an additional five analyses from the Devonian which have a weighted mean age of 342 ± 30 Ma with a MSWD of 1.5 (from one sample). All of the southern block of the Collingwood River monazite results taken together yield a weighted mean age of 504 ± 5 Ma (Figure 5-12) with a MSWD of 3, with 9 of the 95 analyses rejected by Isoplot, which agrees quite well with the results obtained when considering only those 76 data points whose ages fall within the range 400-600 Ma.

There are some variations in the composition of monazite with the age of the grains (Figure 5-14, Figure 5-15). Both blocks of the Collingwood River have older monazite grains which are very low in Sr, whilst the intermediate age grains range from very low to low, and the young grains range from very low to medium (Figure 5-14A, B). The skew to higher Sr in the Cambrian analyses should correlate with the

destruction of plagioclase and therefore could indicate that the younger generation of monazite grew during increasing pressure conditions whilst the older generation of monazite grew under lower pressure conditions where plagioclase was stable (Finger and Krenn 2007). That the grains with "intermediate ages" tend to have Sr concentrations which lie between the levels seen in the old and young grains supports the hypothesis that the intermediate ages do not reflect a separate period of crystallization, but rather result from a mixing at that point in the monazite grain of compositions from both the older and younger periods of metamorphism.

The north block of the Collingwood River has intermediate and old monazites with Y concentrations which primarily fall into the medium category (0.8 to 2.0 wt% Y), while the young grains tend to be low Y, with only 18% of the young monazites reaching medium Y levels, and then not more than 1.3 wt% (Figure 5-14C). The south block, on the other hand, has young monazites spanning the full range from very low to high Y (> 2 wt%), with a gap in the data at the low-medium Y boundary (Figure 5-14D). The high-Y monazites come from two samples, 160730 (one of the two whiteschists), where it is associated with the garnet rims, and 32142, a garnet-poor schist. There is a correlation in the latter sample between the concentration of Y in monazite and the distance to the nearest garnet visible within the plane of the thin section (see below), which is interpreted to indicate that the garnet and the monazite were growing in unison, with the garnet taking up available Y in its immediate vicinity, causing near-by monazite grains to be depleted in Y with respect to those further away from garnet. While there may well be garnet just off the plane of the thin section, the overall garnet-poor nature of this sample, and the concentration of garnet into patches, nonetheless permitted the recognition of this correlation. The correlation of the high and medium Y monazite with the garnet rims in sample 160730 while the very low-low Y monazite is included within the garnet

cores is interpreted to indicate that the low Y grains grew during a period of garnet growth and the high Y monazite grew during a lull in garnet formation, or, perhaps, even during a period of garnet break-down. The fact that both the high and the low Y monazite grains in this sample are from a single generation of growth indicates that the transition from garnet growth to no garnet growth may have taken place during the same episode of metamorphism which created the monazites. The growth of the garnet rims, which encloses some of the high-Y grains, may well have occurred during a later stage of the same event, however a t-test comparing the ages of the low-Y with the high-Y grains for this sample does not show a statistical difference in age between the two compositional types.

The north block of the Collingwood River contains monazite with a tight range of Th values clustered at low-medium Th boundary, while south block young generation monazites range from very low to quite high Th (Figure 5-14E, F) for the young generation (~ 510 Ma) when compared to the older generation (~ 0-11 wt% Th). The old monazites from the north block range from very low to (just) high Th, though the bulk of them fall at the same level as do the young ones (Figure 5 49 E). The south block older grains fall only into the low Th category (Figure 5-14F), however, they are so few in number no reliable conclusion can be drawn.

The north block monazites are consistently low in U. However, the old grains range across the entire low field, whilst the young ones are concentrated in the upper levels of the low category (Figure 5-15A). The south block, on the other hand, has young monazites which range from very low to high U, though the other generations are only low U (Figure 5-15B). As a result of the above, the Th/U ratio is consistently low for the young and intermediate north block monazite grains, but ranges from very low through to high in the old grains; the south block monazite grains have a

few young/intermediate grains reaching medium, while the old grains, which are the majority of the grains sampled, are very low to low (Figure 5-15C, D).

The LREE/HREE ratios for the north block monazite grains are consistently low for the old and intermediate grains, but range from low into medium for the young grains; the south block young grains range all the way from the very low/low boundary up to high, while the intermediate grains (and most of the very young grains) are low, and the few old grains have very low LREE/HREE ratios (Figure 5-15E, F). The expectation is that garnet growth drives the Sm/Gd higher because of the strong fractionation of HREE into garnet. The results from Collingwood River support a general trend of garnet growth during monazite crystallisation.

5.2.2.1.1 North Block Collingwood River

5.2.2.1.2 Sample 67665

Sample 67665 (for sample description see section 2.5.2.1) contains at least two generations of monazite, with a few analysis spots of intermediate age (Figure 5-16). The bulk of the analyses are for the younger, mostly Cambrian, age. However, the sample gives a weighted mean age of 535 ± 24 with a MSWD of 6.8 for ten analyses on three grains (two of which have analyses with old ages in their cores). Comparing this sample with the results from the other samples shows that there is a minor "peak" at 590 Ma (Figure 5-16). Excluding grains more than 2 standard deviations older than the weighted mean age, the weighted mean age becomes 529 ± 10 Ma with a MSWD of 1.06 after Isoplot rejected one of the remaining eight analyses. This age is anomalously older than is typical for the other samples.

The remaining ten analyses range in age from 587 to 1510 Ma, but no discrete age populations can be identified. There is a clear correlation between age of the analysis and the amount of Sr present (Figure 5-17), with the oldest grains incorporating little to no Sr (less than detection limits), and the young generation

containing up to 0.24 wt% Sr. There is more Y in the older monazites than in the younger generation (Figure 5-17). There are no high or very low Y monazite analyses for this sample. Ratios of LREE/HREE are highest for the young generation of monazite and lowest for the older generation (Figure 5-17). The older monazite generation is interpreted from these results to have grown in a garnet-free system, while the young generation grew in tandem with garnet. These compositional differences hold true for this sample, even when the younger analyses are overgrowths on older cores.

5.2.2.1.3 Sample 68788

Sample 68788 was collected from the intersection of Collingwood and Balaclava Rivers (Figure 5-11). This location contains the largest crystals of garnet from the Collingwood River area. This sample includes patchy grains of garnet ~ 2 cm in length intergrown with quartz (Figure 5-18). The matrix is fine grained and primarily muscovite (usually ~ 0.09 x 0.30 mm), which displays a crenulation cleavage, with a mylonitic foliation which wraps around the garnet porphyroblasts. There are larger grains (~ 0.9 x 0.5 mm) of undeformed muscovite in the garnet pressure shadow. No biotite was observed, but fine-grained tourmaline (~ 0.2 mm) is present. There is a large spread in the age of the monazite results for this sample (Figure 5-19). There are only a few analyses with young ages, all of which are located within the matrix, which have a weighted mean age of 521 ± 11 with a MSWD of 0.69 for only six analysis points on two grains. There are two analysis points of intermediate age and the remaining 25 analyses range in age from ~ 1150-1481 Ma (Figure 5-19). The youngest analysis point was ~ 1170 Ma for the monazite included within the large grain of garnet. Sr for the oldest grains is at or below detection limits, but it is present in the younger grains, with some intermediate grains showing intermediate amounts of Sr (Figure 5-20). The ~ 521 Ma monazite

grains are generally very low in Y, and the older grains fall into the medium Y range (Figure 5 10). However, the older grains which are highest in Th/U ratios are lower in Y than the other old grains, falling just at the boundary between "low" and "medium" Y concentrations as used in this study. The young grains have higher LREE/HREE ratios than do the intermediate and old grains (Figure 5-20). These features indicate that garnet was much less abundant during the growth of the older grains.

5.2.2.1.4 Sample 160694

Sample 160694 (for sample description see section 2.5.4.1) also contains a range of ages, with the young generation consisting of only 4 analysis points (each on different monazite grains), all of which are included within in the rims of various grains of garnet. The largest of these garnet crystals contains two young monazite grains, both of which are located within the compositional rim of the garnet, as determined by analysing the garnet on either side of the monazite grains and comparing with the garnet profile; the core of this garnet is very homogeneous (see garnet composition Figure 2-44), which facilitates assigning the designation of "core" or "rim" to isolated analysis points. Those four grains range in age from 496 Ma ± 13 to 541 ± 14 Ma. They combine to a weighted mean age of 519 ± 33 with a MSWD of 2.2. This high MSWD results from the fact that there are few analyses with a spread in the results which is larger than the errors for the data. The remaining 17 monazite grains range in age from 611-1399 Ma, with almost half of them greater than 1300 Ma (Figure 5-21) and are located within the garnet core, the garnet rim, and in the matrix. There is a correlation between age and amount of Sr present (Figure 5-22), with the older grains having Sr at or below detection limits, the young grains having up to 0.27 wt % Sr, and the intermediate aged grains (which may well reflect mixed ages of younger growth on an older core) showing intermediate Sr

values. The young monazite grains analysed are low to medium Y (Figure 5-22B). The older grains generally fall into the medium Y range. However, the older grains which are highest in Th/U ratios are lower in Y than the other old grains, falling just above the boundary between “low” and “medium” Y concentrations as used in this study. The youngest generation has the largest range in LREE/HREE ratios (Figure 5-22C). As a result of these compositional differences, the younger monazite is interpreted to have grown in tandem with garnet and in a higher pressure environment than the older, which had less garnet.

5.2.2.1.5 Sample 160696

A MLA map of monazite locations was created for sample 160696 (for sample description see section 5.2.2.1.5), permitting the selection for analysis of only monazite grains included within garnet, with 33 monazite grains included within six different grains of garnet analysed (Figure 5-23). All of monazite grains analysed from this sample belong to the older generation (Figure 5-24), with the highest peak ~ 1370 Ma. Sr is generally below detection limits in these monazites (Figure 5-25A). There being only one generation of monazite present, the Y concentrations nearly all fall in the “medium” level, save for the few with the highest Th/U ratios, which fall right on the low-medium boundary (Figure 5-25B). The LREE/HREE ratios plot in a tight cluster, with values in keeping with those of other Collingwood River Mesoproterozoic monazites (Figure 5-25C). It is not known if any of the monazite grains located in the matrix of this sample belong to the young generation, but given the patterns associated with the other samples, it is possible. The old grains, however, are included within both the cores and the rims of the garnet, and are very common.

5.2.2.1.6 Sample 160707

Sample 160707 (for sample description see section 2.5.7.1) contains multiple generations of monazite. The younger generation has a weighted mean age of 509 ± 6 Ma with a MSWD of 0.65 for 22 analyses on 19 different grains, all of which were either located in the matrix or at the very edge of a garnet grain. The older analyses range in age from 610-1443 Ma (Figure 5-26), and are located within the garnet cores, rims and in the matrix. The younger grains have Sr ranging from low to medium (0.05-0.20 wt%), and the older analyses are very low Sr (generally at or below detection limit), with some intermediate analyses having Sr values plotting between the two groups (Figure 5-27A). This sample, containing a large number of analyses from both generations of monazite, displays low Y concentrations for most of the Cambrian monazite and medium Y concentration in the older monazite analyses (Figure 5-27B). As is typical for the Collingwood River samples, the analyses which have low Th/U ratios also have lower Y concentrations (Figure 5-27B). There is a gap in the range of Y values for the younger analyses separating the low and medium concentrations, which corresponds with LREE/HREE ratios. An example of this is provided in Figure 5-27D, which plots Y vs. Ce/Dy (here Ce/Dy was chosen for its broad range, making patterns easier to see). This graph shows that for those analyses with young ages with medium Y concentrations Cd/Dy is markedly lower than for the low-Y analyses with young ages. In general, as the analyses decrease in Y, they increase in Sr. The low-Y analyses are found only in matrix monazite, while those with medium Y are usually located within garnet, though two large (~ 100 μm) matrix grains show both old (med-Y) and young (low-Y) analyses in a single grain. The range of Y in the younger grains overlapping that of the older could be attributed to the older generation growing in a relatively garnet-free environment, and the younger generation commencing growth before there was much garnet present (higher Y monazite analyses), but as the monazite growth

continued, garnet growth resulted in a (initially local) decrease of availability of Y for the monazite (which zones would increase in volume with time). The change in Sr could indicate an increase in pressure taking place during this episode of monazite growth. The old grains tend to show zoning in the BSE images (Figure 5-28), while the young ones are uniformly bright. There does not appear to be a difference in appearance between the grains of varying compositions, though the largest monazite grains in this sample are all located in the matrix, rather than included within garnet.

5.2.2.1.7 Sample 160708

Sample 160708 (for sample description see section 2.5.8) contains only young monazites (Figure 5-29), with a weighted mean age of 505 ± 7 and a MSWD of 0.96 for 24 analyses on eleven grains which were located either within the matrix or in contact with the rim of garnet grain. There being only one generation on monazite analysed for this sample, there is no change with age for Sr or Y (Figure 5-30). Most of the analyses fall between 0.13-0.26 wt% Y (straddling the border between "very low and low Y as used in this study), which values are comparable with other Collingwood River analyses with young ages. There are two analyses that fall into the medium Y category, which also show much lower LREE/HREE ratios than do the others (Figure 5-30). The Sr levels, on the other hand, are very low to low, which is more typical of the older generation of monazite in other Collingwood River samples.

5.2.2.1.8 Sample 160713

Sample 160713 (for sample description see section 2.4.6) contains monazite from both generations, but only three analyses on two grains from the young generation of monazite, ranging in age from 503 ± 16 to 539 ± 17 Ma. The weighted mean comes to 525 ± 49 with a MSWD of 1.5 for the three points. The other 12 analyses (12 grains) range in age from 1196-1511 Ma (Figure 5-31). The two young grains

analysed are located within wide (~ 30-50 μm) mica-filled cracks in garnet, the older grains are located within garnet grains, both in uncracked (in the plane of the thin section) regions, along unfilled cracks, and one grain within one of the mica-filled cracks in a garnet. The three analyses with young ages are markedly higher in Sr than the older analyses, which are near or below detection limits (Figure 5-32A), and may have grown in a higher-pressure environment than the older grains. Likewise, those three analyses fall in the very low Y category whilst the older grains are generally in the medium Y category (Figure 5-32B), and so it is likely that more garnet was present during their growth than for the older grains. They are also higher in LREE/HREE ratios than the older analyses (Figure 5-32C).

5.2.2.1.9 Sample 160716

Sample 160716 was collected for this study from the bed of the Collingwood River, about 35 meters downstream from the last outcrop of eclogite (Figure 5-11). It is fine grained with ample quartz and muscovite (~ 1 mm long) that define a weak foliation, rare altered biotite (~ 0.05 mm) grains, and garnet porphyroblasts up to 3 mm diameter (Figure 5-33). As with the other Collingwood River samples, the garnet crystals have cores which are generally homogeneous and zoned rims, with no visual difference between the cores and the rims. This sample contains a young generation of monazite, an old generation, and some intermediate grains (Figure 5-34). The younger generation has a weighted mean age of 509 ± 8 with a MSWD of 0.88 for eighteen analyses on sixteen grains. The older grains range in age from 1149 ± 21 to 1431 ± 55 Ma, with 12 of those 17 analyses greater than 1330 Ma. A separate compositional and age population occurs at ~ 1200 Ma. The analyses with young ages range between 0.02-0.10 wt% Sr and the intermediate and older ones fall around or below detection limit (Figure 5-35). For this sample, there is a gap in the range of Sr values that generally corresponds to changes in Y concentration (Figure

5-35A) and with LREE/HREE ratios. An example of this is provided in Figure 5-35C, which plots Y vs. Ce/Dy, demonstrating that for those analyses young ages with medium Y Cd/Dy is markedly lower than for the low-Y analyses with young ages.

5.2.2.1.10 Sample 160717

Sample 160717 (for sample description see section 2.4.7) is unusually low in monazite when compared to the other Collingwood River sample, with very few grains found. Of the fifteen grains analysed, six were very low Th (<0.1). The remaining eight grains include both generations of monazite (Figure 5-36) with Sr, Y and LREE/HREE age correlations that match the other Collingwood River samples (Figure 5-37). The three analyses with young ages have a weighted mean age of 498 ± 19 Ma with a MSWD of 1.1; they range from a low of 444 ± 51 to a high of 509 ± 13 Ma. The analyses with older ages range from 702 ± 18 to 1361 ± 18 (Figure 5-38).

5.2.2.1.11 Sample 160736

Sample 160736 is a mylonite showing top-to-the-east displacement (see section 2.1.3) collected for this study from an outcrop along the Lyell Highway just east of where it crosses Bills Creek (Figure 5-11). It contains abundant mica fish, quartz, and small grains of garnet. It was selected for detrital zircon analysis (see section 5.3 below) and the mineral separate was found to contain abundant monazite as well, therefore monazite analysis of the mounted grains was undertaken. Unlike most of the other Collingwood River samples, this sample had no young (Cambrian) monazites analysed (the only other sample for which this was true is 160696, where only grains included within garnet were analysed). However, the mineral separation does not recover small grains, so it is possible that there is also an unanalysed young monazite population is this sample. The ages of the analysed grains range from ~

728 to ~ 1425 Ma (Figure 5 27). Multiple analysis points were chosen for every monazite grain analysed, and whilst some have all analysed points giving the same age (within error), seven of them show distinctly younger rims than cores (Figure 5-39). Three show older ages ranging from 1,300 to 1,400 Ma with rims ~ 1,200 Ma, and the other four have rims between 700 and 900 Ma. These younger rims may represent a metamorphic overgrowth during the time period(s) calculated for these points. More likely, they are the result of a partial resetting of the rims of, and along cracks within, these grains during the ~ 510 Ma event which affected the other samples from this region. The composition of those younger analysis points is higher in Sr than the older points, but narrower in range for Y and LREE/HREE (Figure 5-40). The Mesoproterozoic monazite analyses fall into two groups in terms of the Y content. The lower group is consistently near the major peak at 1375 Ma. The higher Y group includes most of the younger Mesoproterozoic analysis.

The monazite in this study show a rounded morphology (Figure 5-41) that is consistent with a detrital origin for these grains. They are mostly 50-100 μm across. The age distribution is compared with detrital zircon ages in the section below.

5.2.2.2: SOUTH BLOCK COLLINGWOOD RIVER

5.2.2.2.1 Sample 32142

Sample 32142 (Figure 5-41), collected by McIntyre (1964) from the "southwest side of Collingwood Range" is a schist with a folded foliation defined by coarse muscovite (up to 2 mm), fine biotite (up to 0.25 mm), and occasional late-stage chlorite. There are rare garnet grains up to 0.25 mm, and plagioclase crystals up to 1.5 mm. It contains two generations of monazite. The bulk of the grains analysed are from the younger generation (Figure 5-42), with a weighted mean age of 505 ± 9 and a MSWD of 0.38 for 15 of the 16 points. The point rejected by Isoplot as not appropriate to the data set is the youngest analysis for this sample at 455 ± 12 Ma,

and is the second spot from a single grain, the first of which has an age of 505 ± 18. This grain (M) is higher in Y and lower in all of the LREE/HREE ratios than the other monazite grains in this sample (Figure 5-43). The three older grains analysed range in age from 1094 ± 47 to 1237 ±18 Ma. As with the north block Collingwood River samples, the younger analyses show a much broader range in their compositions than do the older analyses. However, in this case the older grains fall into the middle of the range, rather than being significantly lower or higher in Y than the younger samples (Figure 5-43). There is a very clear correlation between distance of monazite grain from the nearest garnet (in the plane of the thin section) and the amount of Y in the monazite, with those grains at a distance to the garnet having higher concentrations of Y than those in close proximity to garnet (Figure 5-43C). This relationship demonstrates that trends in composition of monazite have both a spatial and temporal component. It may not be easy to separate these two effects. This may also explain why most samples have monazite with large range of y contents, since each monazite grain will be located at a different distance to the nearest grains of garnet than the others.

5.2.2.2.2 Sample 39140

Sample 39140 (Figure 5-44) is a whiteschist, collected by Boulter in 1978 from the Collingwood River, just upstream from its intersection with Scarlett Creek (Figure 5-13). Note that there had been some question as to the precise location of this outcrop. Therefore this study included an expedition to re-sample the whiteschist, and the location reported here for both this sample and 160730 below is deemed to be the correct location, it being unlikely that there is more than one outcrop of whiteschist in this region. This sample contains garnet up to 3 mm wide with two very different aspects. One of the garnet forms (Type B, see discussion in Chapter 2) consists of very cracked interiors and relatively intact, narrow rims, but these grains

are compositionally homogeneous. The other (Type A) features a relatively uncracked aspect, with no visual difference between rims and cores, but distinct compositional differences between the two zones, with the interior showing one fairly uniform composition and the rims showing another. Type B, with its fairly uniform composition, is similar to the rims of the Type A (Figure 5-45). The heavily cracked interiors of Type B, with their relatively uncracked rims, could relate to a period of garnet breakdown due to an abrupt change of pressure followed by subsequent garnet growth; however, such a scenario does not account for the similarity between the composition of the cracked grains with the rims of the uncracked garnet. The whiteschist also contains talc, quartz, and kyanite. This sample contains only young monazite grains, with the results clustered in a Cambrian peak centred ~ 510 Ma, with smaller bumps in the Ordovician (Figure 5-46). Compositionally, there is a notable difference in Y concentration, with the higher Y grains tending to have Ordovician ages (with a weighted mean age of 461 ± 28 Ma with a MSWD of 1.8 for 4 analyses with Y > 0.2), and the lower Y grains scattering across the width of the peak, from 486 ± 6 to 531 ± 7 Ma (with a Cambrian weighted mean age of 508 ± 9.3 and a MSWD of 3.4 for eleven analyses) (Figure 5-47). The young population potentially records a period of garnet breakdown that is not recorded in the other samples, including the other whiteschist thinsection (see below).

5.2.2.2.3 Sample 160730

Sample 160730 is the whiteschist collected for this study, and is fully described in section 5.2.2.2.3. This sample is noteworthy for the large cluster of more than 70 monazite grains included in a 1.2 x 1.0 mm region within the core a single garnet grain that measures 2.9 x 2.4 mm (Figure 5-48). This sample had two different monazite microprobe analysis sessions. The first session analysed 18 points on 13

grains which are not part of the above mentioned cluster. These grains were located within the matrix (five analyses on two grains), within the garnet cores or along the core-rim boundary zone (six grains) as determined by the location of a ring of quartz inclusions within the garnet (the garnet cores containing monazite were not analysed—however, analyses on other garnet grains in this sample show that the visible core-rim boundary corresponds with the compositional transition—e.g. Figure 5-49), and within the garnet rims (seven analyses on six grains), again as determined by the rings of quartz inclusions. The second session analysed 29 spots on 25 grains within the above mentioned cluster of monazite grains. All of the monazite analysed for this sample group fall into a single, broad based peak (Figure 5 40), with the individual analyses ranging from 469 ± 32 Ma to 667 ± 21 Ma. The weighted mean for all analyses (over 1% Th) is 506 ± 8 Ma with a MSWD of 3.3 for 24 of the 25 analysis points (Figure 5-50). There is a notable range in the amount of Y in the monazite. The isolated grains which are present as inclusions within the rim of the garnet (as determined by their position relative to circles of quartz inclusions within the garnet e.g. Figure 5-49) are all medium Y while those that are present in the garnet cores are low Y (Figure 5-51). In addition, the analyses from the matrix monazite and the large cluster of monazite (Figure 5-48) are medium to high Y. A comparison of this sample with the other whiteschist, 39140, reveals those analyses wherein Y is greater than 1 wt% are present only in this sample, and they show a much broader range of ages than do the low Y analyses from both samples (Figure 5-52). The high Y grains are also notably lower in Sr (< 0.05) than the low Y grains (Sr > 0.05) from both whiteschist samples (Figure 5-52A). The high Y grains range from 1 to 19 wt% Th, (analyses less than 1% Th have not been included in these diagrams, as discussed above), but are generally less than 4% Th (Figure 5-52C). While there is a clear difference in age of the analyses for 39140, with the Y > 0.2

analyses being younger than those < 0.2, such a correlation could not be demonstrated for 160730, which has medium to high Y analyses both younger and older than the low Y analyses. A t-test was not able to detect a difference in the ages between the two types of monazite for this sample.

5.2.2.2.4 Sample 160734

Sample 160734 is a mylonite with top-to-the-north displacement (see section 2.1.3) collected from the south block of the Collingwood River, approximately 130 meters downstream from the whiteschist (Figure 5-13). It has a pronounced stretching lineation (Figure 5-53) and it is dominated by coarse grained muscovite (up to 1 mm) and occasional grains of plagioclase defining the foliation and segregated from the finer grained quartz (0.2 mm). In addition there are small (up to 1 mm) grains of garnet which occur in both the mica rich and quartz rich regions (Figure 5-54). The monazite grains in this sample are rare and corroded in appearance (Figure 5-55). They range in age from 306 ± 17 to 742 ± 25 Ma. The weighted mean age for all eleven analyses for this sample is 470 ± 70 with a MSWD of 40 for eleven analyses (Figure 5-56). However, the late Paleozoic results (< 400 Ma) may be considered to be a separate population (only one other sample analysed for this project also has results < 400 Ma), in which case they have a weighted mean age of 342 ± 30 with a MSWD of 1.5 for five analyses. These grains could represent reactivation of this mylonite zone during the Carboniferous, which might account for the difference in the sense of displacement recorded in this mylonite than in the others from the region (see Appendix 10). The remaining six analyses range in age from 477 ± 15 to 742 ± 25 Ma. Discarding the oldest and considering only those between 400 and 600 Ma gives a weighted mean age of 523 ± 41 with a MSWD of 5.3 for five analyses. While one of these analyses is compositionally different from the others, being notably higher in Y and Sr and lower in Th, U, and LREE/HREE ratio (Figure 5-57),

it falls into the middle of the age range, and its removal does not improve the MSWD.

The monazite in this sample is generally very low to low in Y, low to medium in LREE/HREE ratio, and ranges from low to high in Sr (Figure 5-57).

Unlike some of the other samples, there does not appear to be a pattern correlating the location of the monazite (quartz-rich vs. mica-rich layers or distance to nearest garnet grain in the plane of the thin section) and the composition of the monazite. None of the monazite in this sample is located within garnet grains. The interpretation is that the monazite in this sample has been disturbed by a hydrothermal event related to shear zone reactivation during the Late Devonian or Carboniferous.

5.2.3: Southwest Coast Monazite Results by Sample

5.2.3.1: Summary of Southwest Coast Age Results

The samples from the south west coast come from three locations. The northernmost costal samples analysed are from Nye Bay (Figure 5-1), where there are two monazite generations, with a variety of intermediate ages as well (Figure 5-58). The Mulcahy Bay samples are primarily Cambrian, but do contain a few analyses which show intermediate ages. The southernmost sample is from Wreck Bay and only young monazite grains were analysed in this sample. Taking all of the southwest coast monazite results together (Figure 5-59) gives a weighted mean age of 505 ± 2 with a MSWD of 1.12 for 196 out of 205 analyses for the younger generation (all < 600 Ma). The older generation, when taken together for all SW coast samples, comprises two major peaks, the larger at ~ 1090 Ma, and the other at ~ 1340 Ma (Figure 5-59 inset). This is in contrast with the combined results for all of Tasmania (Figure 5-6), where the largest Proterozoic monazite population is at ~ 1370, and the other peaks on the probability diagram decreasing in height with decreasing age.

The composition of the monazite from the Port Davey Metamorphic Complex also changes southward along the coast. Nye Bay shows a pattern for Y similar to the south block of the Collingwood River, with the analyses with young ages spanning the full range from low to high, and the analyses with old ages falling into a tighter cluster in the medium Y range (Figure 5-60A). The Mulcahy Bay monazites have a much smaller range of Y, reaching only to the middle of the medium range (Figure 5-60B), and the Wreck Bay monazite analyses are even narrower yet, with all but one falling in the very low to low range (Figure 5-60C). This pattern is repeated for Sr (Figure 5-61), with the Nye Bay samples showing very low Sr for the old monazite, while the young range from very low to high, Mulcahy Bay monazite analyses range up to low Sr (and there is a correlation between age and Sr level for a discrete population of grains with higher Sr levels). At Wreck Bay the single sample shows a smaller range in Sr. The Nye Bay monazites are primarily low in U with some medium (and one high) analyses, while the Mulcahy Bay range from very low to high in U, and Wreck Bay from low to just into medium U (Figure 5-62). Note that the Proterozoic analyses are low in U. The range in the ratio of LREE/HREE in the Southwest Coast samples shows that the Nye Bay analyses with young ages have the broadest range, from very low through to high; Wreck Bay shows the next broadest range from low fully across medium; and Mulcahy Bay has the tightest range, spreading only from low to part way into medium (Figure 5-63).

5.2.3.2: NYE BAY

5.2.3.2.1 Sample: 68318

Sample 68318 (for sample location and description see section 3.1.1) contains two distinct monazite age populations, and two minor intermediate age peaks (Figure 5-64). The young grains have a weighted mean age of 504 ± 17 Ma with a MSWD of 0.75 for six out of seven points analysed on six grains, all of which were either

within the matrix, or at the boundary between a garnet grain and the matrix. The older 21 analyses on fifteen grains range from 590 ± 24 to 1142 ± 129 Ma (Figure 5 51). Four are in the matrix; the other nine are included within garnet grains (Figure 5-65). The only monazites found included within the large (18 mm) garnet are located within its rim (Figure 5-65). Three of the four analyses with intermediate ages are in matrix monazites, the fourth is at the edge of a garnet (Figure 5-65) adjacent to a monazite grain with a Cambrian age, and likely represents a "mixed" age of both young and older generation present in the same grain. Two of the other intermediate spots are from the same grain, which also has an old spot analysis (Figure 5-66), and again possibly represents a "mixed" age. The monazite in this sample range from small (~ 10 microns) to large (< 100 microns). The large grains are either old or contain mixed ages, but the small and intermediate sized grains are of all ages. The age spectra for this rock provides clear evidence for a 1030 Ma ?detrital event. This is different from the typical pattern at Collingwood River. All of the "old" monazite analyses in this sample (ages ~ 1000 Ma) fall into the very low Sr category, as do more than half of the young and intermediate age analyses. In addition there are several young/intermediate age analyses in the low, and one each in the medium and high Sr categories (Figure 5-67A). These analyses with higher amounts of Sr are also higher in Y; most of the monazites analysed for this sample fall into the medium Y category (with three in the low Y category). In general, within the medium Y category, the older grains are lower in Y than the younger ones (Figure 5-67). There is no change in LREE/HREE ratios with age in this sample. The fact that the younger analyses have a broad range in Y, ranging from higher than the older analyses to considerably lower, could indicate that the older grains grew in a garnet-poor environment, then there was a period of garnet break-down (freeing up Y) prior to, or in conjunction with, the first growth of the younger monazite

immediately followed by new garnet growth (taking up excess Y once again) before the monazite completed its growth phase. The garnet in this sample does record a period of garnet consumption with an increase in XSps at the rims (see Figure 3-2).

5.2.3.2.2 Sample: 68319

Sample 68319 (for sample description see section 3.1.2) also contains two distinct age populations and an intermediate (possibly "mixed") age (Figure 5-68). The young population has a weighted mean age of 503 ± 12 Ma with a MSWD of 1.03 for 14 analyses on 12 grains, all of which are located in the matrix. The old population has a weighted mean age of 1047 ± 17 Ma with a MSWD of 1.2 for 12 analyses on 11 grains, half of which are in matrix monazite, the other half are included within garnet. Alternatively, the unmix ages algorithm of Isoplot, when applied to all 15 analyses greater than 600 Ma, gives two generations with a relative misfit of 0.667, one at 795 ± 49 Ma for 20% of the analyses, and 1047 ± 14 Ma for 80%. The three intermediate age grains are all in the matrix (one is at the boundary between a small garnet and the matrix), and each was the only point analysed on their grains. They may represent mixing of the old and young ages in a single grain.

For this sample both the old and the young population are primarily very low in Sr, but the intermediate age samples tend to be higher in Sr (Figure 5-69A). Both of the generations tend to fall into the medium Y category, with a few analyses with young ages in the low to very low Y category. However, of the ones in the medium Y category, the younger ones tend to be higher in Y than the older ones (Figure 5-69B). The two monazite age populations are very similar in size (20 to 150 μm) and habit (Figure 5-70), with grains of all ages displaying rounded corners. As with 68318, the larger range of Y concentration in the younger monazite grains could reflect a period of garnet growth followed by garnet destruction and then further growth that is implied from the garnet zoning profile, which shows a bell-shaped spessartine profile

in the core, an increase in XSps starting about 1 mm from the grain edge, and a subsequent decrease in XSps starting about 0.5 mm from the grain edge (see Figure 3-6).

5.2.3.2.3 Sample: 68320

Sample 68320 (for sample description see section 3.1.3) contains mostly grains from the younger monazite generation (Figure 5-71). The young grains have a weighted mean age of 507 ± 8 Ma with a MSWD of 0.80 for 23 points on five grains. The older grains range from 1012 ± 14 to 1137 ± 18 Ma. All of the older analyses and roughly half of the younger ones for this sample have little to no Sr. However, some of the younger range to medium or high Sr (Figure 5-72). Those grains which are in contact with plagioclase, or which are included within biotite near grains of plagioclase, have the highest Sr levels for this sample, while those which are included in garnet or fully surrounded by quartz are very low in Sr. The young monazite analyses range from very low to high Y, whilst the old grains cluster tightly at medium Y (Figure 5-72). The analyses with young ages range from very low to medium LREE/HREE ratios, whilst the older analyses cluster at low values (Figure 5-72). The increased Sr for some of the younger analyses could indicate elevated pressure and breakdown of plagioclase, while the elevated Y for some of the younger grains could indicate a short-lived period of garnet breakdown before new garnet growth once again out-competed monazite for the available Y, or they may reflect spatial distribution. The garnet in this sample does show an increase in XSps at the rim (see Figure 3-11), but the analysis points were not closely spaced enough to determine if it decreased again thereafter as in sample 68319.

5.2.3.2.4 Sample: 68334

Sample 68334 (Figure 5-73) is coarse grained, containing garnet up to 6 mm, kyanite, with undulatory extension, up to 1.5 mm long, patches of chloritised biotite

up to 1 mm long, sericite, quartz and ilmenite. While it does contain monazite from the young generation, it primarily has older grains (Figure 5-74). The young generation for this sample has a weighted mean age of 511 ± 53 with a MSWD of 8.8 for only five spots analysed on three grains. This sample, like that of 160694, shows a distinct extra small peak between the main Cambrian peak and 600 Ma, which may well account for the high MSWD. The composition of those five analyses with young ages are very similar in most elements, save for iron content. Both the eldest and youngest are higher in Fe (> 1.2 wt%) than the other three (< 0.2 wt% Fe). Excluding those two high Fe analyses results in a weighted mean age of 504 ± 52 with an MSWD of 2.2 for the remaining three analyses, or using the unmix age algorithm on the six analyses under 900 Ma gives a relative misfit of 0.553 for two generations at 495 ± 14 (67%) and 611 ± 25 (33%). In reality, there are simply not enough analyses with young ages with similar ages from this sample to achieve a reasonable estimate of the age of that generation of monazite growth for this sample. By comparison, the older grains in this sample are easier to unravel—the Isoplot "unmix ages" algorithm finds that 23% of the grains > 1000 Ma fall at 1359 ± 13 Ma, which is in the same, within error, as the 1376 ± 7 calculated for all of the samples across Tasmania. This sample shows a very clear difference in composition between the generations. The older grains are very low Sr, and the younger grains are mostly medium Sr (up to 0.17 wt%; Figure 5-75). The old monazites are all medium in Y, the analyses with intermediate ages are mostly low, and the young all very low in Y, and the LREE/HREE ratios are higher for the analyses with young ages than for these with old ages (Figure 5-75). This pattern is similar to that of samples from the Collingwood River; the older monazites grew in a low-garnet period, while the younger ones grew in equilibrium with garnet, in a higher pressure environment. It is markedly different from some of the other Nye Bay samples collected nearby

(68318, 68319, 68320), which show a large range in Y for the analyses with young ages that extend both higher and lower than the analyses with old ages. This sample was mapped with the MLA prior to monazite dating. As a result, all monazites analysed were included within garnet, which could explain why they do not show the record of increased Y seen in the young generation of the other samples, as the young grains included within the garnet are located well inboard of the reversal of the XSps trend. This supports the argument that distance form garnet is more important than timing in controlling the Y content. Higher Y contents are expected in matrix monazite crystallized in this rock during the Cambrian.

The grains of monazite in this sample are generally small (< 50 μ) with most grains in the 20-40 μm range. Because there was abundant monazite available for analysis and the usually small grain size, most grains had only one analysis point each. Monazite was found in eight different grains of garnet with more grains of monazite present in the larger grains. The young monazites were located in only two of the garnet grains, and were intersected by obvious cracks in the garnet (Figure 5-73). Some of the old monazites were not intersected by garnet cracks within the plane of the thin section.

The monazites in sample 68334 range in size from too small to be analysed (not pictured) to 80 μm long and have three different appearances in BSE image (Figure 5-76). The first, most common type, are uniform in their brightness, with all of the above age-groupings represented. The next most common are those with patchy zones of different brightness—these are limited to grains with ages of 1077 Ma and greater, and two grains are “variegated”, with one portion quite dark, zoning gradually to a bright portion. These latter two are both more rounded than many other grains in this sample, and belong to the oldest generation (1323 Ma, 24 μm long and 1343 Ma, 30 μm long).

5.2.3.2.5 Sample 68335

Sample 68335 (for sample description see section 3.1.4) contains both young and old generation monazites (Figure 5-77). The young grains have a weighted mean age of 507 ± 10 Ma with a MSWD of 1.00 for 12 points analysed. Comparing this sample with the other sample collected at the same location, 68334, (Figure 5-74) shows that this sample has fewer old grains and less overall spread in the data. Just as with sample 68334, Sr is present in detectable quantities only in the younger generation monazite grains, which are also very low in Y and notably higher in LREE/HREE ratio than the older analyses (Figure 5-78). This sample was mapped with the MLA prior to monazite analysis, and as a result, many of the grains analysed are inclusions within garnet. The four largest (80-170 μm) monazite matrix grains were also analysed. Most of the young monazite grains are from the matrix or on the interface between a garnet rim and the matrix. However, four young monazite grains are included within the cores of garnet (as determined by analysing the garnet composition on either side of the monazite locations), each located within a major crack in the grain. The old grains were included within both core and rim of the garnet. The monazite included in garnet is lower in Sr than that located in the matrix or within the garnet rims. The old grains are all low in their LREE/HREE ratios, and the young grains range from medium to high (Figure 5-78).

5.2.3.2.6 Sample 143145

Sample 143145 contains only young monazite grains, with a weighted mean age of 510 ± 12 with a MSWD of 0.92 for 20 analyses on 10 monazite grains (Figure 5-79). These monazites have a much higher range of Sr and Y than was present in the samples from the north side of Nye Bay, with a high of 0.99 wt% Sr and 3.7 wt% Y, and a tighter range for the LREE/HREE ratios (Figure 5-80). Most of the monazite for this sample was found in the matrix, with only one grain included within garnet.

The very low Sr analyses are all from one of the grains included within biotite, but the other grains included within biotite show the full range of Sr compositions, as do the monazites surrounded by quartz.

5.2.3.2.7 Sample 143147

Sample 143147 mainly contains Cambrian monazites, which have a weighted mean age of 494 ± 7 Ma with a MSWD of 1.5 for 18 of 19 analysis points (Figure 5-81). There are also four older grains with a weighted mean age of 1013 ± 16 (MSWD = 0.29). Most of the monazite in this sample is located within the matrix. Two young grains are included within one of the large (~ 7 mm) garnet crystals, within the potion which is visibly garnet core (this sample, as mentioned above, having a core which is very rich in (quartz) inclusions, and a rim which is inclusion-poor. As with some of the other samples, monazite grains with detectable Sr are all young grains, the older ones being below the detection limit (about 0.02 wt% Sr in these analyses) (Figure 5-82). The largest monazite grains are generally the older grains, with one exceeding 300 μm, and the smallest grains are generally young. However, the oldest grain is only ~ 40 μm, and the largest of the young grains is 83 μm across. Some of the grains have crisp, smooth edges, while others are very irregular, but there is no correlation with age. Likewise, both generations show some grains with uniform brightness in the BSE image, and some which are visibly zoned (Figure 5-83). As is typical for the Nye Bay samples, the analyses with old ages show no detectable Sr, while the analyses with young ages range from very low/no to medium Sr. Y ranges from very low to high for the analyses with young ages, and the few analyses with old ages cluster tightly in medium, and the LREE/HREE ratios range from very low to medium for the analyses with young ages, while the analyses with old ages are all very low (Figure 5-82). This sample has anomalously low chemical U-Th-Pb age compared to most other samples. The age of 494 ± 7 hardly overlaps with the

weighted mean age of other samples and is lower than expected based on the geological constraints. There are no obvious chemical or textural indicators that suggest this sample has been substantially disturbed although many of the very low ages come from very small grains (Figure 5-83).

5.2.3.3: MULCAHY BAY

5.2.3.3.1 Sample 143072

Sample 143072 (for sample description see section 3.1.5) contains young monazite (Figure 5-84), with a weighted mean age of 505 ± 3 with a MSWD of 1.3 for 49 of 52 analyses on ten grains from two different analysis sessions. The only analyses with apparently older ages were also very low in Th, and have been discarded. This sample is very low to medium in Sr and Y, and low to medium in LREE/HREE ratios (Figure 5-85). This sample gives one of the most precise ages from any of the samples in this study. It shows a coherent simple age structure with no evidence of inheritance or disturbance.

5.2.3.3.2 Sample 143106

Sample 143106 (Figure 5-86) is a quartz-biotite-muscovite schist with both monazite and xenotime as accessory minerals, collected from a 100m wide mylonite zone. This is the only sample in this study in which xenotime was analysed. It is well foliated with the quartz mostly in microlithons between the mica rich cleavage domains. It contains only monazite from the young generation (Figure 5-87) with weighted mean age of 511 ± 5 Ma with a MSWD of 1.02 for 24 analyses on 5 grains. This sample ranges only from very low to low Sr, very low to medium Y, and low to medium LREE/HREE ratios (Figure 5-88), which pattern is in keeping with other young samples from the area. The exception is for Sr in 68334 and 68335, as discussed above.

5.2.3.4: WRECK BAY

5.2.3.4.1 Sample 143097

Sample 143097 (for sample description and location see section 3.3.3) contains monazite only from the young generation (Figure 5-89), with a weighted mean age of 504 ± 6 Ma and a MSWD of 1.17 for 23 points analysed on 19 grains. Some of these are matrix grains, but the majority are inclusions within garnet, usually in the garnet rims (which lack quartz inclusions), and rarely in the garnet cores (which are very rich in quartz inclusions). Most of the grains analysed are low to very low in Y, low to medium in Sr, and LREE/HREE ratios (Figure 5-90), and likely grew in equilibrium with garnet. This is a good quality result in a rock with no evidence for complications.

5.2.4: North Coast Monazite Results by Sample

5.2.4.1: FORTH

Three samples from the Forth Metamorphic Complex (Figure 5-91) were analysed. These display a single generation of monazite, which has a combined weighted mean age of 509 ± 7 Ma with a MSWD of 1.17 for 35 of the 37 analyses for all data from the three samples. The compositions of these grains is fairly consistent (see below), reflecting similar growing conditions for the monazites in each sample.

5.2.4.1.1 Sample 75637

Sample 75637 (for sample description see section 4.1.2) contains monazite with three different aspects. The badly corroded grains (Figure 5-92A) yielded no useable results, and their compositions are noticeably different from the other monazite analyses from this sample. The deviations from the normal Y, Sr, and Th are sometimes considerably higher, and others notably lower than normal monazite composition for this sample (Figure 5-93). The undamaged interiors of grains that showed corroded margins (Figure 5-92B), and the, smaller, largely euhedral, grains

(Figure 5-92C) both yielded useable age results. These combine to give a weighted mean age of 503 ± 10 Ma with a MSWD of 0.97 for 13 analyses on ten grains (Figure 5-94). There being a single generation present, the analyses have a fairly consistent composition, with only subtle differences between the undamaged interiors of the partially corroded grains and those which still appear unaltered (Figure 5-95).

5.2.4.1.2 Sample 154322

Sample 154322 is a garnet – muscovite – chlorite schist, with a foliation defined by micaceous cleavage grains alternating with quartz-dominated domains. There is only one generation of monazite (Figure 5-96), with a weighted mean age of 518+13 Ma with an MSWD of 2.0 for 18 analyses on nine grains. This high MSWD reflects the scatter in the data, which ranges from a low of 479 ± 17 Ma to a high of 569 ± 21 Ma, however, the composition of the analyses is fairly uniform, and no basis was found for setting aside some analyses as clearly belonging to a separate population. Monazite occurs as 10 – 50 μm grains and grain clusters with very irregular margins. Larger elongate grains are aligned in the foliation and show evidence of micro-boudinage (Figure 5-97). Sr levels in the monazite range from very low to low, and Y, Th and U from low to medium, and LREE/HREE ratios tend to fall in the low category (Figure 5-98).

5.2.4.1.3 Sample 154325

Sample 154325 is a garnet–muscovite–quartz schist. The dominant texture is a crenulation cleavage (S2). The sample contains two populations of REE-rich phosphates. About 20% of the grains are monazite and the remainder have low totals, high Ca and high Fe, and were tentatively identified as rhabdophane (Berry et al. 2007). The monazite grains are small (5 – 10 mm) and in clusters (Figure 5-99). The rhabdophane is in larger sieve textured grains 20 – 70 mm long (Figure 5-99) and has

crystallised with high common Pb, since calculated U– Th– Pb ages scatter up to 3000 Ma. In contrast, the monazite yielded a weighted mean age of 510 ± 11 Ma with an MSWD of 0.64 for six analyses on four grains (Figure 5-100). The composition is consistent with very low to low Y and Sr, low U, med Th, and medium to high LREE/HREE ratios (Figure 5-101).

5.2.4.2: SETTLERS HILLS

Two samples from the Settlers Schist were collected 150 m apart (Berry et al. 2007), (Figure 5-102). They both contain only one generation of monazite, with a combined weighted mean age of 513 ± 8 with a MSWD of 1.15 for all 39 points analysed. The monazite from this region ranges in Y content from high to very low, but the bulk of the analyses are in the medium to high Y range. They are low to very low in Sr, and tend to be low in LREE/HREE ratios (see figures below).

5.2.4.2.1 Sample 71334

Sample 71334 is a biotite–white mica–quartz schist. The white mica mainly occurs as sericitic patches, where it replaced some of the plagioclase, whereas the biotite occurs in larger flakes. Part of the sample has a random crystal orientation. A discrete patch (Figure 5-103) is foliated with a differentiated cleavage, which is interpreted as a xenolith (Berry et al. 2007). This interpretation is dependent on the conclusion of Reed et al. (2001) that the Settlers Schist is a metagranite. This sample contains anhedral 10 – 20 mm monazites with very irregular margins that are Cambrian in age (Figure 5-104). The weighted mean age of 504 ± 22 Ma has a mean squared weighted deviate (MSWD) of 2.0 for eleven analyses on six grains. The high MSWD suggests that a mixed age is included, but no specific evidence of disequilibrium or disturbance was detected. The compositions for each of the analyses plot in tight clusters (Figure 5-105). The Settlers Schist is exposed in a

zone of strong Devonian faulting so the large MSWD may reflect some Pb loss, but this could not be demonstrated from the analyses or the texture.

5.2.4.2.2 Sample 71338

Sample 71338 is biotite schist with a similar primary texture to 71334, and a weak alignment of the biotite grains (Figure 5-106). The plagioclase has been extensively altered to sericite. The monazite grains are 10 – 30 mm and subhedral with irregular inclusions. There is a single generation of monazite (Figure 5-107), with a weighted mean age of 517 ± 9 Ma with an MSWD of 0.79 for 28 analyses on eleven grains. As with 71334 its composition is reasonably uniform, with very low Sr, very low to medium U, low Th, medium to high Y, and low to medium LREE/HREE ratios (Figure 5-108).

5.2.4.3: MERSEY

Two samples from the Mersey Valley were analysed for monazite dating, one contains only Cambrian analyses, the other has a few, isolated older grains, and two from the Devonian. Because one of these was used as an in-house standard and has had many repeat analysis sessions and the other had a single session, it is not appropriate to combine them for a weighted mean age, since the data from the one would eclipse the other, and the above reported Cambrian age for this region is based only upon the data from 7401. Their compositional patterns are notably different, even when considering only the Cambrian analyses (see figures below).

5.2.4.3.1 Sample 7401

Sample 7401 is a quartz – muscovite – albite – garnet schist which was collected by Spry (1962) from the Howell Group on the west side of Mersey Valley, south of Walters Marsh (Figure 5-109). The dominant foliation, S2, is a differentiated crenulation cleavage (Spry 1962). S1 is defined by gently curved lines of quartz inclusions preserved in albite porphyroblasts. The monazite grains are very abundant,

5–15 mm across and irregular in shape. This sample has a single generation of monazite (Figure 5-110) with a weighted mean age of 497 ± 3 Ma with an MSWD of 1.12 after Isoplot rejected 5 of 171 analyses. As discussed in section 5.2.1 above, this age is younger than those from the other regions. This sample, having an abundance of consistent composition monazite, has been used as one of the in-house standards run during each monazite session, and results from all seven sessions to date have been combined for the above age, giving a result indistinguishable (within error) from that published (Berry et al. 2007) before this sample commenced use as a standard. Note that if the rejection option is turned off, Isoplot calculates a weighted mean age of 498 ± 4 with a MSWD of 1.5 for all 174 analyses, the close match between these two results underlies the suitability of this sample as a standard. As would be expected from a single generation of monazite which gives consistent age results, the composition is fairly uniform, with medium levels of Y, very low levels of Sr, and low levels of U (Figure 5-111). Th shows significant variation from 1-10% (Figure 5-111) and it is this aspect of the composition that makes it attractive as a standard. This sample has been used regularly to test the background corrections on Pb by calculating the initial Pb using an isochron approach.

5.2.4.3.2 Sample 154328

Sample 154328 is a pelitic schist collected (Berry et al. 2007) from a quarry below the Rowallan Dam on the Mersey River (Figure 5-109) consisting primarily of fine grained quartz with lesser muscovite, occasional rounded grains of plagioclase (~ 1 mm), rare biotite, and some late stage chlorite. The dominant foliation is S2. The monazite grains are common and are typically 10 – 20 mm across. This sample has two generations of monazite (Figure 5-112). The monazites with Cambrian analyses have a weighted mean age of 502+10 Ma with an MSWD of 1.2 for 22 of 24 analyses on 13 grains (2 analyses were rejected by Isoplot). The six older analyses

range in age from 1110 ± 45 to 1456 ± 12 and are from three grains, two of which are larger (~ 20 mm) and more equal-dimensional than typical monazite grains from this sample but do not form a distinct recognisable population from morphology alone (Figure 5-113). Sr levels in monazite for this sample range from very low to low, with the highest levels associated with the analyses with the youngest ages from the older generation (Figure 5-114A). The analyses with younger ages tend to have more Y than do the older ones (Figure 5-114B). There is a much larger range of U in the younger generation of monazite analyses, which range from very low just into medium, while the older generation is generally very low (Figure 5-114C). Th, on the other hand, has a broader range in the older generation, which gets into high levels, while the younger generation is low to medium in Th (Figure 5-114D). The LREE/HREE ratios are slightly higher for the older generation than for the younger. There is no evidence in this rock of an earlier high-grade metamorphic event, so these ages are interpreted to indicate the presence of detrital monazite, which is consistent with the more equal-dimensional shape of the grains which include old domains. The two lowest ages are distinct from the main peak (Figure 5-112) and are interpreted here as the result of partial resetting possibly during the Devonian Tabberabberan deformation.

5.2.5: South Central Monazite Results

A single sample from the Strathgordon area, collected (Boulter 1972) from 5 km west of Strathgordon (Figure 5-115), was selected for monazite analysis. Sample 46241 is a fine grained garnet–muscovite schist with distinct layers of quartz and muscovite and more than 5% opaque (Figure 5-116). The Strathgordon Metamorphic Complex has a maximum metamorphic grade of upper greenschist facies, and garnet-bearing rocks are relatively rare, with a garnet content of ~ 1% in this sample. The monazite grains here are mostly very small (5 – 10 μm) with rare

grains to 20 μm. Grain L was included in garnet. The chemical U– Th– Pb measurements yielded an age of 510 ± 11 Ma with an MSWD of 1.4 for nineteen analyses on twelve grains (Figure 5-117). The monazite grains have low Y and Sm/Gd 41.5 consistent with growth in equilibrium with garnet (Figure 5-118).

5.3: ZIRCON AGES

A small study of zircon ages was initiated in an attempt to shed further understanding upon the above monazite results. The widespread presence of old monazite grains is problematic in these samples. It is not clear from the analyses alone if these are metamorphic or detrital in origin. The wide range in ages is perhaps more typical of a detrital monazite pattern. However, the age range is different from the detrital zircon age spectra in the Proterozoic sandstones of Tasmania (Black et al. 2004), which typically show older populations than found from the monazite analysed for this study (Figure 5-119). Only the Wings Sandstone, the Jacob Quartzite, and the Port Sorell Formation sandstones show age-range spreads young enough to match the range of "old" monazites from the metapelites, but even these units tend to have lows which correspond to the main peak for the old monazites (Figure 5-119). The other regions have zircon which is predominantly older than the monazites from this study, but some areas do have a minor peak at 1400-1450 Ma

Two samples from the north block of the Collingwood River (Figure 5-120) were selected for zircon isotopic analysis (see 1.3.2.3 for methods used for this study) to determine if the zircons from this region match the patters of Black et al. (2004), or the monazite results obtained in this study for this region. Two quartz-rich samples from the Collingwood River were selected. The samples were both selected from the northern block because the ones from the southern block of the Collingwood River were deemed unsuitable candidates for detrital zircon analysis, being much higher in their mica component.

The zircons in these samples are primarily strongly zoned in terms of age, so that each analysis is a mixture of Cambrian and Proterozoic domains. Many of the single analyses define isochrons on concordia (e.g. Figure 5-121). In order to plot these isochrons the analyses were divided into ten equal splits based on time of laser ablation and plotted using Isoplot to determine upper and lower intercepts.

5.3.1: Sample 160708

Sample 160708 (see section 2.4.5 for sample description) has a heavy mineral separate which is dominated by zircons, but monazites and rutile are also present. The zircons in this sample are ~ 100—200 μm in size and mainly euhedral to subhedral. The analyses of zircons from 160708 which have intercepts plotting close to 510 Ma were then recalculated by anchoring the lower intercept at 510 ± 10 Ma (approximately the age of the metamorphism for this region based on above chemical U-Th-Pb monazite data) in order to improve the age of the upper intercept (detrital core) of the zircon. The metamorphic portions of the zircon are low in Th/U as expected for grains growing in the presence of metamorphic monazite of the same age (Harley et al. 2007). The detrital component has a high in Th/U, largely in the range 1400-2000 (Figure 5-122A). They have a peak at 1450 ma and are dominated by 1600-1800 Ma grains. This pattern is similar to Proterozoic sandstone such as the sample from Oonah Formation (Figure 5-123). Quite a few of the zircons in 160708 have evidence of common Pb and Pb loss. In these cases, the data from each of 10 splits from individual analyses plot on impossible isochrons heading towards the upper right of the reverse concordia diagram, and these analyses were not used for further geochronology.

5.3.2: Sample 160736

160736 is a fine-grained mylonite with discrete bands of quartz and mica and scatterings of small garnet grains (~ 0.15 mm) concentrated in the mica-rich layers. It has a heavy mineral separate which is dominated by monazite with a lesser component of zircon and rutile. The zircons plot mostly on concordia between an interpreted detrital age and 1200 Ma (Figure 5-122B). A few of the zircon crystals also show some resetting toward 510 Ma. The oldest age analyses contain both high and low Th/U, while the late Mesoproterozoic grains have low Th/U, indicating growth contemporaneous with monazite (Harley et al. 2007). Unlike sample 160708, most of the metamorphic overgrowths plot between 1100-1300 Ma (Grenvillian--Rivers 1997). Two of the monazite grains in this mount were also analysed during the zircon analysis session, and they are also Grenvillian in age. Without further information as to the exact age of this Grenvillian metamorphic overgrowth it was not possible to anchor the data to a lower intercept. Therefore the intercepts were calculated automatically via Isoplot (Ludwig 2003) to determine the age of both the upper and lower intercepts based on the trends in the data. A few of the zircon crystals exhibited Pb loss and common Pb. In those cases a 204 Pb (common) Pb corrected 207Pb/206Pb age which, in theory, takes into account both common Pb and Pb loss was utilized. Sample 160736 is interpreted to have been a similar sandstone to 160708, with a detrital zircon pattern resembling that from other Tasmanian regions (Black et al. 2004) with a variety of peaks between 1400-1900 Ma (Figure 5-123). However it was strongly metamorphosed at 1220 ± 36 Ma, growing new monazite and zircon overgrowths on the detrital crystals (green line of Figure 5-123). It then experienced an additional metamorphic episode at 510+/-10 Ma, growing more zircons and monazite. An alternative interpretation is that the

sandstones were deposited after 1,220 Ma, receiving abundant sedimentary material from a 1,220 Ma metamorphic complex.

The monazite data indicates an early population at 1,350 Ma reset to 1,190 Ma. The monazite does not record the Palaeoproterozoic detrital history seen in the zircon data. However in other aspects the two data sets give the same result of an early detrital history reset at about 1,200 Ma. There is no textural evidence in these rocks of this high grade reset event. It is more likely that it records events in the source terrane for this metasedimentary rock.

Detrital zircons at 1,200 Ma are relatively restricted in Tasmania with about 25% of Proterozoic sandstones including a detrital population at this age. The strong association with monazite of the same age in this rock supports the existence of a major metamorphic event. Berry et al (2008) reviewed the evidence for Mesoprotrozoic events in Tasmania. The event recorded on King Island at 1,290 Ma may correlate with this event. However, the age and intensity of metamorphism implied by the resetting of zircon is more compatible with a source in the Grenville province of Laurentia which in some continental reconstructions was close to Tasmania in the Neoproterozoic. 1,200 Ma fits neatly with the Elzevirian Orogeny which was an early stage of deformation in the Grenville Province.

Chapter 6

Discussion & Conclusions

CHAPTER 6: DISCUSSION & CONCLUSIONS

This study has investigated the pressure/temperature, and/or timing of metamorphism for five regions (Figure 6-1) within Tasmania: 1) north coast (including the Forth Metamorphic Complex and the Settlers Schist), 2) north central (Mersey River Metamorphic Complex), 3) central (Franklin Metamorphic Complex, including the Collingwood River metapelites and eclogites in the north block, the whiteschist of the south block, and the Raglan Range, and Mt. Mary regions), 4) south central (Strathgordon Metamorphic Complex), and 5) southwest coast (Port Davey Metamorphic Complex, including the areas of Nye, Mulcahy, and Wreck Bays). The pressure/temperature results from each region are summarized and compared with previously published Tasmanian results, followed by the timing results for each region, in conjunction with their tectonic implications. The highest grade metamorphic units of Tasmania include both medium and high pressure rocks and occur in metamorphic complexes across the western third of the state (see Figure 1-1). However, the high pressure examples are volumetrically minor and have been reported only from the north coast and central regions. All examples of high P/T units reported from Tasmania are restricted to fault-bounded slivers adjacent to medium P/T schists.

6.1: PRESSURE/TEMPERATURE OF METAMORPHISM

Two different approaches were used to investigate the pressure and temperature of metamorphism. Garnet-core isopleth thermobarometery was used to reveal the conditions of formation during the first growth of the garnet grains, while Thermocalc, GB-GBPQ, GB-GBMAQ, and GASP were used to determine the conditions of metamorphism during which the garnet rims and matrix minerals formed.

The garnet-core isopleth thermobarometery for both the Franklin and Port Davey Metamorphic Complexes yielded very similar results (~ 600^{o} C, 6,000 bars) for the formation of the garnet cores in the pelitic schists from these two regions (Figure 6-2). However, their metamorphic history subsequent to their early stage of garnet growth is very different.

The southwest coast garnet rims and matrix minerals record a temperature (~ 650^{o} C at 6,000 bars) for their formation which is only slightly higher temperature than was obtained for the formation of the garnet cores (Figure 6-2). This isobaric increase in temperature predicts a shift from the kyanite stability field just over the line into the sillimanite field. This prediction is verified by the presence of fine blades of sillimanite in some samples from this region, particularly mantling deformed grains of kyanite (McNeill 1985). Garnet porphyroblasts (up to 5 cm across; Figure 6-3), which typically display euhedral shape, are found in this region; these generally display distinctive changes in their inclusion density inboard from their rims indicative of an abrupt shift in growing conditions (e.g. Figure 3-2). Given the subtle difference in calculated P/T between the garnet cores and rims for this region, this change in inclusion density is probably associated with dehydration during a single growth episode, rather than to a cessation of growth followed by mantling during a subsequent metamorphic episode. The presence of a fluid phase may act as a flux assisting in the exclusion of extraneous matrix minerals during the growth of a porphyroblast; in such cases continued growth under dry conditions may lead to the incorporation of numerous fine-grained inclusions in addition to causing an abrupt change in mineral composition as observed in these samples (see Chapter 3).

The samples from the Collingwood River area, on the other hand, appear to have maintained nearly isothermal conditions whilst undergoing a rapid increase in pressure. The eclogites (Appendix 2) and metapelites (Chapter 2) record garnet core

conditions (~ 600^{o} C, 6,000 bars) which are approximately the same as those for the southwest coast (Figure 6-2), but both show much higher pressure conditions of formation for the garnet rims and matrix minerals. The garnet rims and matrix minerals in the eclogite were estimated to have formed at ~ 650^{o} C, 19,000 bars, and the metapelites record conditions of ~ 700^{o} C, 14,000 bars (Figure 6-2). The difference in estimates for rocks in close proximity probably reflects error in one or both of calibrations used rather than a true difference in pressure.

The metapelites have zoning patterns which are reminiscent of those of the Wölz Complex, Austroalpine unit, Eastern Alps (Faryad and Chakraborty 2005). The cores of the large garnet crystals from the metapelites tend to show bell-shaped profiles for X_{Sps}, a subtle increase in X_{Alm} from centre to edge of the core, and very flat profiles across the for X_{Prp} and X_{Grs}, which is comparable (Figure 6-4) to the Pre-Alpine (Garnet I) cores observed by Faryad and Chakraborty (2005). However, the Collingwood River garnet grains tend to be notably lower in X_{Grs} than those from the Alps (see below). Faryad and Chakraborty indicate temperatures of 560-580^{o} C obtained via garnet-core isopleth thermobarometery for the Pre-Alpine metamorphism responsible for their (Garnet I) cores before focusing their discussion upon the later episodes of metamorphism. That temperature is very compatible with those obtained via the same technique for the Franklin Metamorphic Complex (see Chapter 2). The Wölz Complex garnet crystals show an abrupt change in composition at the boundary between Garnet I and II which is similar to that observed in the samples from this study (Figure 6-4). However, due to the fact that all of the samples from the Franklin Metamorphic Complex studied are low in whole-rock Ca, these samples are considerably lower in X_{Grs} than that from the Wölz complex, though the shape of the pattern is similar. There are two different patterns in the transition of X_{Grs} from core to rim in the garnet zoning from the Franklin

Metamorphic Complex samples. For those samples which are very low in Ca, such as sample 160696 (Figure 6-4A), there is only the smallest rise in X_{Grs} at the boundary from core to rim garnet compositions, and it is the other three end members which truly exhibit the reversal in zoning that marks the boundary, while those with a slightly higher whole-rock Ca components show a more substantial rise in X_{Grs} (Figure 6-4B). However, even these do not achieve the same levels of X_{Grs} as obtained for those in the Wölz Complex. Faryad and Chakraborty (2005) estimated that their Garnet II crystallized over the range from 540^{o} C, 7,500 bars to 600^{o} C, 10,000 bars, which range is very compatible with the results obtained from the Franklin Metamorphic Complex (see above and Chapter 2). An additional similarity between these two regions is the fluctuations in composition of their Garnet II, which is similar in pattern, though differing in intensity, to that observed in some of the garnet from this study (Figure 6-4A). Not all of the garnet analysed in this study show such fluctuations during the garnet rim growth, and those that do generally do so on only one side of the grain. However, detailed garnet mapping and analysis in other areas (e.g. Zeh and Millar 2001) reveals that syntectonic garnet mantle growth over pretectonic garnet cores often occurs preferentially in response to directed pressure, with the growth in the regions of pressure shadow being limited with respect to the other crystal faces. The Franklin Metamorphic Complex has experienced directional stress resulting in foliations, crenulations, and folds, and as such it is reasonable for the garnet rim growth to be limited to the crystal faces in the correct orientation with respect to the directional stress. Many of the analysed lines across the garnet grains begin and end at faces with very different orientations with respect to the foliation, so it is not surprising that the left and right ends of the zoning profiles are not always symmetrical. It is clear from the above that while the garnet rims in the pelitic schists of the southwest coast grew under very similar P/T

conditions to their garnet cores, the pelitic schists and eclogites of the Franklin Metamorphic Complex saw a substantial increase in pressure after the formation of the garnet cores, during which there was new garnet growth mantling the previously existing cores.

The third rock type analysed from the Collingwood River is the whiteschist which, unlike the eclogite and the pelitic schist, does not record a low-pressure episode; the garnet-core isopleth thermobarometery for the whiteschist indicates that the garnet did not begin to grow until high pressures (~ 545^{o} C, 19,600 bars) were achieved (Figure 6-2). Note that an increase of at least 30-90^{o} C is required to shift from the assemblage predicted to be stable during garnet core growth into the talc/kyanite stability field, which is the field compatible with the garnet rims and matrix minerals of the whiteschist (see section 2.5.9). Such an increase (at the upper end of the range) brings the whiteschist temperature at peak metamorphic conditions into line with the eclogite peak temperature and approaches the peak temperature calculated for the pelitic schists. However, given that the eclogite and pelitic schist were collected from north of a major fault boundary and the whiteschist from south of it (see Chapter 2), it is not required that the conditions recorded in the whiteschist be the same as the other rocks studies in this area. Other samples collected from the whiteschist locality lacked the key mineral assemblages required for detailed P/T estimates.

The results from the other regions studied have all been obtained via classic geothermobarometry. The samples from Mt. Mary, collected ~ 10 km from the Collingwood River samples, give results slightly higher pressure than the Collingwood River garnet core conditions, at ~ 570^{o} C, 8,600 bars and the Raglan Range sample, collected from ~ 5 km from the Collingwood River samples, yielded a

P/T estimate only slightly lower (~ 700^{o} C, 11,400 bars) than the Collingwood River metapelite rim results (Figure 6-2).

The Forth Metamorphic Complex, on the north coast, yields a maximum P/T estimate of ~ 670^{o} C, 16,900 bars, which is comparable with those obtained for the high pressure results from Collingwood River (Figure 6-2).

Prior to this study there have been a number of other published pressure/temperature estimates for various Tasmanian metamorphic complexes. The graph of these estimates (Figure 6-5), shows two broad trends in the data, both starting in the greenschist facies region for the low-pressure results, but with temperatures diverging with increasing pressure. The lower temperature suite includes greenschist and blueschist facies results from Port Sorell, Arthur and Port Davey Metamorphic Complexes, with a trend from 350^{o} C at 5,000 bars to 400^{o} C at 10,000 bars. The higher temperature sequence ranges from upper greenschist through epidote-amphibolite and amphibolite facies and into the eclogite field and includes results from the Port Davey, Strathgordon, Franklin, and Forth Metamorphic complexes. Comparison of the previously published data with the results from this study shows a reasonable correlation with the Franklin Metamorphic complex (Figure 6-6A), with the eclogite results from this study (Appendix 2) giving similar, if slightly higher temperature/lower pressure early stage results to those obtained by Råheim (1976), and similar pressures (though cooler temperatures) to those obtained by Kamperman (1984) and Goscombe (1990). The whiteschist results from this study, on the other hand, are notably higher in pressure and lower in temperature than previously published results from this outcrop (Råheim and Green 1974). However, the 1974 estimates for the whiteschist were regarded as a minimum pressure estimate, and the current results were obtained from the garnet cores, with the peak conditions occurring at a higher temperature (see above). The results presented here from

garnet core isopleth thermobarometery for the metapelites from the Collingwood River are the first attempt at elucidating the early stages of metamorphism for these samples. These results show a slightly lower pressure and higher temperature than those obtained by Råheim (1976) for the early stages of the eclogite from this area but overlap with the early-stage eclogite results from this study (Appendix 2). The maximum P/T presented here for the metapelitic schists in this area is similar (if slightly higher T) to the previously published results for the nearby eclogites (Goscombe 1990; Kamperman 1984), and higher in temperature and lower in pressure than the peak eclogite results from this study (Appendix 2). Most of the data from both this study and the previously published results from the central portion of the state fall along the greenschist facies curve as calculated by Llana-Fúnez and Marcos (2007), though the results from Goscombe (1990) are above that curve, and the whiteschist results from this study plot solidly along the high pressure curve, while the Raglan Range and Collingwood River metapelite schist garnet cores from this study and the Strathgordon results (Råheim 1977) all fall between the HT amphibolite and amphibolite facies curves (Figure 6-6B).

The results from the Forth Metamorphic Complex for this study (Figure 6-7B) are higher in pressure and slightly lower in temperature than the previously published data for this region (Berry and Holm 2001; Lewis 1991). The previously published data from the Forth region falls along the greenschist and amphibolite facies curves, while the results from this study are in between the greenschist and high pressure curves (Figure 6-7B). Finally, the Port Davey Metamorphic Complex (Figure 6-8A) results from this study are slightly higher in temperature than the previously published data (McNeill 1985; Turner 1989). However, these results for maximum temperature and pressure, being just into the sillimanite field, are more consistent with the presence of fine-grained sillimanite in these samples. In addition, all of the

southwest coast results, from this study and previously published data, fall along the HT amphibolite facies curve (Figure 6-8). In contrast, the previously published data from Port Sorell plots on three different curves—the high pressure, amphibolite, and HT amphibolite facies curves (Figure 6-9A) while that from the Arthur metamorphic complex plots on the amphibolite, greenschist facies curves, and one just below the high pressure curve (Figure 6-9B).

6.2: TIMING OF METAMORPHISM

This study primarily used U-Th-Pb Chemical dating of monazite to constrain the timing of metamorphism. The results range in age from Mesoproterozoic to Devonian. However, the Cambrian-aged monazite analyses comprise the bulk of the data. In general, the grains of monazite which have Cambrian-aged analyses are located within the matrix or the rims of garnet, rather than the garnet cores. The Cambrian metamorphic event is interpreted to have not only resulted in monazite growth, but also to have been responsible for the growth of the garnet rims and matrix minerals and their above reported geothermobarometric results. Therefore, the results with younger and older ages will be discussed briefly first before addressing the main metamorphic event and the implications thereof. Note that the weighted mean errors reported below have been calculated by Isoplot (Ludwig 2003) based upon the individual analyses errors, which were estimated from the counting statistics. See the discussion in Berry et al. (2007—Appendix 1) on additional errors to be considered. They estimate the systematic error on the standards for our laboratory using this technique as < 0.5% by comparison with a range of standards.

6.2.1: Devonian

As discussed in Chapter 5, there are two samples which show Devonian monazite growth (347 ± 23 Ma) which may be linked to reactivation of a mylonite zone. This

age is younger than that which has been suggested for the Tabberabberan Orogeny (Black et al. 2005) but is close to the age of the Kanimblan Orogeny. North-south shortening has been recognized in the eastern Lachlan Fold Orogen, including Tasmania, at 330 Ma (Gray and Foster 2004) and this is consistent with the geometry of the Linda Zone which affects these rocks.

6.2.2: Neoproterozoic

The monazite results with Neoproterozoic ages (specifically those > 600 and < 950 Ma—see Chapter 5 for discussion on choice of range) from this study comprise < 4 % of the total analyses obtained (35 of 960). Of these, one analysis comes from the Forth Metamorphic Complex, 22 from the Franklin Metamorphic Complex, and 12 from the Port Davey Metamorphic Complex. Most (30 of 35) of these analyses come from samples which also have Cambrian age analyses (15 of these analyses are from samples wherein single grains show both ages). Likewise 24 of the 35 of these analyses come from samples which also show Mesoproterozoic ages (9 of these analyses are from samples wherein single grains show both ages, and two of the samples show instances of all three age ranges analysed on a single grain). Given the sparseness in the data from this age range and its association with the other generations, it is likely that these Mesoproterozoic age monazite analyses represent "mixed" ages with these individual analysis spots comprising material from both an older core and a younger overgrowth.

The U-Pb-Th monazite results from the Eastern Orthogneiss of the Western Tasmania terrane from off shore Tasmania records high-grade metamorphism at 920 ± 7 Ma, with a possible earlier event at 1015 ± 24 Ma recorded in a single sample (Berry et al. 2008). However, the on-shore Tasmanian data acquired for this project, which includes the data published in Berry et al. (2007), shows a low at ~ 910-950, with only three data points falling in that range (Figure 6-10). There are also known

events elsewhere in Tasmania during this time period, such as the intrusion of the granites on King Island at 750-780 Ma (Black et al. 1997; Turner et al. 1998), but insufficient monazite grains were found in this study which have ages in Neoproterozoic to determine if there is a correlation in this data with any or all of those events. However, the mafic igneous rock which was the protolith for the eclogite is thought to have formed at some time after 1,200 Ma due to the presence in the eclogite of xenocrystic zircons of that age (Turner et al. 1998).

6.2.3: Mesoproterozoic

The monazite results with Mesoproterozoic ages (> 950 Ma) from this study comprise 28% of the total analyses from this study (276 analyses of 960). Of these, five come from the Mersey River Metamorphic Complex, 195 are from the Franklin Metamorphic Complex, and 76 from the Port Davey Metamorphic Complex.

As shown in Figure 6-10, this data has a major peak at ~ 1,366 Ma which is likely to represent a discrete monazite growth event. There is sufficient spread in the data to the right of that peak to allow but not require a monazite growth episode to correlate with the wide-spread Tasmanian 1,450 Ma zircon component (Black et al. 2004). That zircon population is considered to be detrital, and it is possible that the few (15-20) monazite analyses in these samples which fall into that age range could be inherited from the same source(s).

The lesser Mesoproterozoic peaks in this data fall into the Grenville age range (Rivers 1997), and while the spread in the data is wide, it remains possible that one or more of these minor peaks (Figure 6-10) represent discrete monazite growth phases. One potential correlation is the minor peak which corresponds to the off-shore (Berry et al. 2008) minor peak at ~ 1015 Ma (Figure 6-10), with 14 analysis points falling into that range. In addition there are similar age events to this data which are recorded in the Musgrave Block of Central Australia, Antarctica, and, of

course, the Grenville province of eastern North America (Fitzsimons 2000; Rivers 1997; White et al. 1999). Burrett and Berry (2000) had concluded that there is no evidence of the Grenville orogeny in Tasmania; if one or more of these lesser Mesoproterozoic peaks represents discrete monazite growth events rather than mixed ages and/or detrital grains that would provide one potential line of evidence for Grenville aged deformation in Tasmania. The analysis of detrital zircons in this study for two Collingwood River schists (see section 5.3) found metamorphic zircon at 1,220 ± 36 Ma, which is compatible with the Elzevirian Orogeny, an early stage of deformation in the Grenville Province (Gower and Krogh 2002). These zircon crystals could have originated as detrital grains from such a source, or they could represent an episode of metamorphism for this rock which was later overprinted by the Cambrian metamorphism.

The detrital zircon record for Tasmania is dominated by a 1,800-1,650 Ma population, which may have originated in the Caborca-Hermosilla terrane in Mexico (Black et al. 2004). The Collingwood River zircons are no exception to this pattern (see Figure 5-123). However, the Tasmanian metamorphic rocks do not record an episode of monazite growth due to metamorphism in that age range; the oldest monazite grain analysed in this study is 1,549 ± 23 Ma. The lack of 1,800-1,650 Ma detrital monazite remains unexplained.

6.2.4: Cambrian

The primary peak metamorphism in Tasmania took place in the Cambrian at ~ 505 Ma. The regional data which is combined to yield this age includes data from the Settlers Schist (513 ±8 Ma) and Forth Metamorphics (509 ± 7 Ma) on the north coast, Mersey River Metamorphics (497 ± 3) in north central Tasmania, the north (512 ± 4 Ma) and south (504 ± 5 Ma) blocks of the Collingwood River in the Franklin Metamorphic Complex, the Strathgordon Metamorphic Complex (510 ± 11

Ma), and the Port Davey Metamorphic Complex (505 ± 2 Ma) on the southwest coast of Tasmania.

There are several possible ways to interpret this data. The first option, referred to here as the slab breakoff model, is to assume that the interpretation outlined in Berry et al. (2007) is correct and all metamorphism pre-dated the Mount Read Volcanics, which within the limits of the current data, started at 506 Ma, or perhaps as late as 504 Ma (Turner and Bottrill 2001). Most of the data gathered for this study are compatible with this interpretation. The exceptions are the 497 ± 3 Ma result for the 171 analyses on sample 7401 from the Mersey River Metamorphic Complex and a less significant sample from the southwest coast with an age of 494 ± 7 Ma for 18 analyses on sample 143147, both of which are otherwise indistinguishable from the other samples. In the slab breakoff model, the average age of 505 ± 1 Ma for all Tasmanian Cambrian analyses (or 507 ± 1 Ma if the above mentioned younger two samples are discarded) represents peak metamorphism associated with slab breakoff in a subduction collisional setting (Figure 6-11), and all rocks were returned to near-surface levels in less than 5 million years. This is equivalent to 4 km/m.y. (or, perhaps 10 km/m.y. for the high pressure units) which is typical for plate tectonic rates (Agard et al. 2009). Traditionally such rates had been considered too high for erosional unroofing, with the average for such rates being estimated at 0.5 km/m.y. (Duchêne et al. 1997). However, some recent estimates yield erosion rates that achieve or exceed the rates necessary to bring these sample back to the surface as rapidly as indicated by these results (Burbank 2002 and references therein). The Forth Metamorphic Complex cooled through the Ar/Ar muscovite closure temperature at 508 Ma (Foster et al. 2005) which is consistent with uplift at this rate from 510 to 506 Ma. In the slab breakoff model the chemical U-Th-Pb monazite ages of the above mentioned younger samples are anomalous. These younger ages

could represent an unknown interference problem with the EPM analyses, or a partial resetting to a later event which could not be identified despite extensive scrutiny of the analyses themselves. The Mount Read Volcanics are seen as post-collisional volcanics related to extensional collapse as asthenospheric mantle replaces old lithosphere carried away with the slab (Crawford and Berry 1992) as suggested for West Irian by Cloos et al. (2005), who argued that post-collisional volcanism started in West Irian 2 m.y. after crustal delamination. The West Irian model is a key analogue for this interpretation.

A second model, referred to here as the sequential metamorphism model, is that the younger (~ 497 Ma) metamorphic ages are real and that some of these metamorphic rocks were emplaced during and after the formation of the ~ 507 Ma metamorphic rocks. As discussed in the introduction to Chapter 5, the monazite ages may be considered to belong to three different sub categories of older (511 ± 3 Ma), intermediate (504 ± 2 Ma), and young (497 ± 3 Ma) Cambrian ages; these ages span the range that has long been accepted for the Tyennan Orogeny (Turner et al. 1998). Young mountain belts appear to preserve temporal relationships in metamorphic units despite thrusting and subsequent exhumation, permitting fossil subduction zones and the temperatures thereof to be traced along a profile (e.g. Gabalda et al. 2009). Such a study has not been attempted in Tasmania. The current estimate of spatial variation in temperature/pressure results (Figure 6-2, Figure 6-5) for various regions across the state would indicate that had such a fossil record of changes in temperature with depth along a subduction zone been preserved during the initial thrusting and exhumation, subsequent deformation has removed most traces of that pattern. However, despite the complexity in Tasmania's metamorphic history, there does appear to be some pattern. In the sequential metamorphism model there is an apparent range of ~ 10 Ma in the age of the monazite which grew during Cambrian

metamorphic events, with different regions showing different weighted mean ages (Figure 6-1). This apparent range in ages and the distribution thereof appears to be, at least in part, related to the temperature and pressure of formation.

The oldest apparent age for the Cambrian metamorphic event (~ 511 Ma) is obtained from the highest pressure areas, particularly the north block of the Collingwood River and the north coast (Figure 6-1). These samples first commenced their garnet growth at ~ 6,000 bars, and then continued to grow garnet as pressure increased an additional ~ 10,000 bars. The Cambrian age monazite in these samples tends to be located in the matrix or the rims of the garnet, and it may have required a higher initial starting pressure and/or temperature than did the garnet. The older apparent age of metamorphism for these samples is compatible with both the slab breakoff model and the sequential metamorphism model, and reflects collision before the Mount Read Volcanics. However, in the sequential metamorphism model, it is the oldest episode of metamorphism within a sequence of sub-events (Figure 6-12). These events could have different timings due to either latitude-based, or depth based affects.

The southwest coast samples combined have an intermediate (~ 505 Ma) Cambrian age recorded in the monazite (~ 506 if the above mentioned younger sample were to be discarded). As stated above, this region had a very different metamorphic history from the Franklin Metamorphic Complex—it was buried to similar initial depths (~ 6,000 Ma) as the north block Collingwood River samples for the garnet core growth, but, unlike the Collingwood River samples, did not then continue to higher pressures before returning to the surface (Figure 6-12). The Cambrian monazites of the southwest coast tend to be located in the garnet rims or in the matrix suggesting they formed near peak metamorphism.

The other sample showing the ~ 505 Ma age is the whiteschist, which did not commence its garnet growth until achieving high pressure (Figure 6-12). The monazite in this sample, as with the other regions, is most commonly associated with the garnet rims and matrix, and it appears to have been growing both garnet and monazite at ~ 505 Ma. The south block of the Collingwood River, where the whiteschist is located, is separated by a major fault boundary (see Chapter 2) from the north block, and it is not unreasonable for the units on either side to have achieved their peak metamorphic conditions at different times before being juxtaposed. The variation is compatible with the latitude-based variation of the sequential metamorphism model, which could be due to a migration of the deformation towards the south with time, but the errors on the age are too large to prove this relationship. More accurate dating such as Ar/Ar muscovite may solve this problem but the southern samples were strongly reheated in the Devonian making this method uncertain. The apparent age of the whiteschist in relation to the other samples is also compatible with the depth-based variation of the sequential metamorphism model (Figure 6-12), the difference being due to the timing of initial subduction and the point at which that package begun its exhumation process. In this variant the individual faults responsible for movement within the entire exhuming block could be active at different times, with the result of the eventually exposure at the surface of units in close proximity to one another which had achieved differing levels of depth at different times. The review of Hynes (2002) addresses several possibilities that could account for the whiteschist's return to the surface in less time than was available for the other high pressure units, as different paths require differing lengths of time; for instance unroofing along the subduction path is thought to require less time than the corner-flow or wedge spreading due to underplating models.

The sequential metamorphism models fail to explain the eruption of the Mount Read Volcanics in an extensional setting and with post-collisional chemistry at the same time as the collision is taking place. Some of the metamorphic rocks were on surface and shedding metamorphic detritus in to the basin at 505 Ma. This has been used by Hall (1998) to argue for a core complex model for the metamorphism. However, the compressed range of metamorphic ages, and the very steep compressional paths in P/T space are difficult to fit into that model.

A north-south migration of metamorphism with time cannot explain the young age of the Mersey Valley sample 7401, located as it is between the Forth and Franklin Metamorphic Complexes, both of which appear to be ~ 10 Ma older. This sample shows the youngest Cambrian metamorphism found in this study (~ 497 Ma). Rocks from this area never exceeded greenschist facies conditions but no specific P/T estimate is available. This sample is of a lower grade than the schists analysed from the other regions, with the largest (~ 2 mm) mineral present being the late-stage albite porphyroblasts. Therefore it may not have buried as deeply as the other samples, and may have been late down the subduction zone, achieving its maximum metamorphic grade more recently than the others and returning promptly back to the surface. However, the apparent age is significantly younger than the post-orogenic volcanism so the exhumation cannot be a result of slab breakoff. The Mersey Valley sample is from a domain of strong D3 deformation and south directed transport. This D3 folding affects Middle Cambrian rocks (Baillie et al. 1986; Berry and Bull 2004; Seymour 1981) exhumed by a late N-S shortening event within the Tyennan Orogeny after the Mount Read Volcanics were complete.

The Tasmanian metapelites studied have little to no record of decompression—the zoning patterns in the garnet from high P metamorphic rocks require a very rapid compression followed by an even more rapid decompression so that no diffusive

resetting of garnet rims can occur. The eclogites, on the other had, do record a decompression path. The evidence for that decompression was recorded by the presence of the retrograde symplectites (see Appendix 2), and it is likely to have been very rapid. The mylonitic textures in those samples are texturally correlated with the late, decompressional stages of mineral growth/breakdown. As discussed in Chapter 2, the sense of shear recorded in the oriented mylonite samples collected for this study is top to the east, which is indicative of normal fault movement if the subduction direction is towards the east (e.g. Berry and Crawford 1988; Crawford and Berry 1992; Meffre et al. 2000). This pattern is similar to that observed in the Alps, where extension dominated during decompression and brought medium grade metamorphic units into contact with lower grade metamorphic units (Ganne et al. 2005; Ganne et al. 2006).

The results from this study, which indicate nearly isothermal loading followed by rapid isothermal decompression for the Franklin Metamorphic complex are unusual. There are other areas that show rapid decompression; the results from the Franklin Metamorphic Complex record an isothermal decompression path similar to Type II of Agard et al. (Figure 10 of Agard et al. 2009), which includes results from the Alps and the Himalayas (Figure 6-13). However, isothermal decompression is more typically associated with a clockwise path, with a marked temperature increase as the pressure goes up, and cooling in response to a decrease in pressure. Modelling of such systems shows (Yamato et al. 2008) that rapid decompression is likely in situations where continental material encounters a subduction zone.

The fact that the high-pressure rocks of the Tyennan Orogeny show an abrupt increase in pressure, followed by an abrupt decrease in pressure, with very little accompanying change in temperature implies very fast transitional periods. The possible variation from one unit to another in terms of the rate of that transition is of

interest. It appears that all of the units accomplished these transitions faster than is recorded in areas which show a typical clockwise path. There are multiple possibilities to account for faster than normal return to medium pressures, or for variations in the rate from one unit to another. One of these involves non-lithostatic pressure. The concept of "tectonic overpressure" has been dismissed as a "failed concept" (Green 2005). However, Raimbourg and Kimura (2008) discuss variations in pressure achieved in different portions of a subduction channel based on variations in the width of the channel. The geometry of the channel itself can account for specific regions within the channel achieving higher than expected pressure with respect to its depth. Such a situation could explain an isothermal increase in pressure followed by decompression since a transient over-pressure affect does not require the rock to move at all. The very steep compressional path recorded from the Collingwood River from 6,000 bars to 15,000 bars with little or no increase in temperature and an almost exact retrace to 6,000 bars seen in the eclogites makes a non-lithostatic pressure origin for the Tasmanian high-pressure rocks very attractive In this model the rock does not have to travel from 20 km to 60 km deep and back in less than two million years and without changing temperature.

6.3:CONCLUSIONS

The Cambrian regional metamorphic rocks of Tasmania are closely associated with ophiolite emplacement. Most of the rocks were metamorphosed at medium pressure and greenschist to low amphibolite facies. A few fault slices of marginal blueschist facies have been reported. Almost all of the medium-grade rocks included in this study were first metamorphosed at medium P/T metamorphism (e.g. ~ 600° C, 6,000 bars). At two localities this metamorphism is overprinted by a high pressure event (~ 15,000 bars). The pelitic schists record a near isothermal compression event with no evidence of the retrograde path. The eclogites have both a near isothermal

compression and a retrace to the original P/T condition. The medium grade metamorphism occurred at ~ 507 Ma and detritus from these metamorphic rocks is found in Middle Cambrian sedimentary rocks which unconformably overly them. This requires exhumation at plate tectonic rates. A schist sample from the Mersey Valley Metamorphic Complex has a metamorphic age of ~ 497 Ma, which is inconsistent with most of the other dating evidence and the geological constraints. This data may indicate a later tectonic event, at least locally.

REFERENCES

Adams, C. J., Black, L. P., Corbett, K. D. and Green, G. R. (1985). "Reconnaissance isotopic studies bearing on the tectonothermal history of Early Palaeozoic and Late Proterozoic sequences in western Tasmania." Australian Journal of Earth Sciences **32**: 7-36.

Agard, P., Yamato, P., Jolivet, L. and Burov, E. (2009). "Exhumation of oceanic blueschists and eclogites in subduction zones: Timing and mechanism." Earth Science Reviews **92**(1-2): 53-79.

Baillie, P. W., Williams, P. R., Seymour, D. B., Lennox, P. G. and Green, G. R. (1986) Geological Atlas 1:50 000 Series. Sheet 36 (8015N). St Valentines. Department of Mines Tasmania,

Berry, R. F. and Bull, S. (2004). A Geological Excursion to Northwestern Tasmania. A2 26 pp.

Berry, R. F., Chmielowski, R. M., Steele, D. A. and Meffre, S. (2007). "Chemical U-Th-Pb monazite dating of the Cambrian Tyennan Orogeny." Australian Journal of Earth Sciences **54**(5): 757-771.

Berry, R. F. and Crawford, A. J. (1988). "The tectonic significance of Cambrian allochthonous mafic-ultramafic complexes in Tasmania." Australian Journal of Earth Sciences **35**(4): 523-533.

Berry, R. F., Elliott, C. G. and Gray, D. R. (1990). Structure and Tectonics of Western and Northern Tasmania Excursion Guide E3. Hobart, 10th Australian Geological Convention.

Berry, R. F. and Holm, O. H. (2001). The Structure of Northwestern Tasmania. Specialist Group in Tectonics and Structural Geology Field Guide 11, Ulverstoe, Tasmania, University of Tasmania.

Berry, R. F., Steele, D. A. and Meffre, S. (2008). "Proterozoic metamorphism in Tasmania: Implications for tectonic reconstructions." Precambrian Research **166**: 387-396.

Black, L. P., Calver, C. R., Seymour, D. B. and Reed, A. (2004). "SHRIMP U-Pb detrital zircon ages from Proterozoic and Early Palaeozoic sandstones and their bearing on the early geological evolution of Tasmania." Australian Journal of Earth Sciences **51**(6): 885-900.

Black, L. P., McClenaghan, M. P., Korsch, R. J., Everard, J. L. and Foudoulis, C. (2005). "Significance of Devonian-Carboniferous igneous activity in Tasmania as derived from U-Pb SHRIMP dating of zircon." Australian Journal of Earth Sciences **52**(6): 807-829.

Black, L. P., Seymour, D. B., Corbett, K. D., Cox, S. E., Streit, J. E., Bottrill, R. S., Calver, C. R., Everard, J. L., Green, G. R., McClenaghan, M. P., Pemberton, J., Taheri, J. and Turner, N. J. (1997). Dating Tasmania's Oldest Geological Events. Mineral Resources Tasmania, Australian Geological Survey Organisation. 1997/15 57 pp

Boulter, C. A. (1972). "Structural Sequence in the Metamorphosed Precambrian Rocks of the Franklin and Wilmont Ranges, Southwestern Tasmania." The Papers and Proceedings of the Royal Society of Tasmania **107**.

Boulter, C. A. (1978). The Structural and Metamorphic History of the Wilmot and Frankland Ranges, South-West Tasmania. *Unpub. PhD Thesis, University of Tasmania, Hobart.*

Boulter, C. A. (1989). Wilmont and Frankland Ranges. *in* Geology and mineral resources of Tasmania. C. F. Burrett and E. L. Martin *eds.*, Geological Society of Australia.

Brown, A. V. (1972). Petrology and Structure of the Adamsfield Ultramafic Mass. *Unpub. B.SC. Honours Thesis, University of Tasmania, Hobart.*

Brown, A. V. (1986). Geology of the Dundas-Mt Lindsay-Mt Youngbuck region. 62 221 pp.

Brown, A. V., Calver, C. R., Corbett, K. D., Forsyth, S. M., Goscombe, B. A., Green, G. R., Mclenaghan, M. P., Pemberton, J., Seymour, D. B. and Vicary, M. J. (2005) 2005, 1. Geological Atlas 1:250 000 Digital Series. Mineral Resources Tasmania, Hobart.

Burbank, D. W. (2002). "Rates of erosion and their implications for exhumation." Mineralogical Magazine **66**(1): 25-52.

Burns, K. L. (1964) One mile geological map series K/55-6-29 Devonport. Tasmania Department of Mines,

Burrett, C. and Berry, R. (2000). "Proterozoic Australia-Western United States (AUSWUS) fit between Laurentia and Australia." Geology **28**(2): 103-106.

Calver, C. R., Everard, J. L., Seymour, D. B., Williams, P. R., Forsyth, S. M., Turner, N. J. and Williams, E. (1987) Lyell Geological Atlas 1:50,000 series. Tasmania Geological Survey, Department of Mines, Hobart.

Calver, C. R., Turner, N. J., McClenaghan, M. P. and McClenaghan, J. (1990). Geological Survey Explanatory Report, Pedder, *Geological Atlas 1 Mile Series* Report: **80**, 105 pp., 1 sheet. Government Printer, Hobart, Tasmania, Australia (AUS).

Campana, B. and King, D. (1963). "Palaeozoic tectonism, sedimentation and mineralization in West Tasmania." Australian Journal of Earth Sciences **10**(1): 1 - 53.

Cayley, R. A., Taylor, D. H., VandenBerg, A. H. M. and Moore, D. H. (2002). "Proterozoic - Early palaeozoic rocks and the Tyennan Orogeny in central Victoria: The Selwyn Block and its tectonic implications." Australian Journal of Earth Sciences **49**(2): 225-254.

Chester, A. D. (2007). Petroleum source rocks, maturation and thermal history, onshore Tasmania. CODES- ARC Centre of Excellence & School of Earth Sciences. Hobart, University of Tasmania. **PhD**.

Cloos, M., Sapiie, B., van Ufford, A. Q., Weiland, R. J., Warren, P. Q. and McMahon, T. P. (2005). "Collisional delamination in New Guinea: The geotectonics of subducting slab breakoff." Geological Society of America Special Publications **400**: 1-51.

Connolly, J. A. D. (2005). "Computation of phase equilibria by linear programming: A tool for geodynamic modeling and its application to subduction zone decarbonation." Earth and Planetary Science Letters **236**(1-2): 524-541.

Connolly, J. A. D. and Petrini, K. (2002). "An automated strategy for calculation of phase diagram sections and retrieval of rock properties as a function of physical conditions." Journal of Metamorphic Geology **20**(7): 697-708.

Corbett, K. D. and Lees, T. C. (1987). "Stratigraphic and structural relationships and evidence for Cambrian deformation at the western margin of the Mt Read Volcanics, Tasmania." Australian Journal of Earth Sciences **34**(1): 45 - 67.

Crawford, A. J. and Berry, R. F. (1992). "Tectonic implications of late Proterozoic-early Palaeozoic igneous rock associations in western Tasmania." Tectonophysics **214**(1-4): 37-56.

Crook, K. A. W. (1980). "Fore-arc evolution in the Tasman Geosyncline: The origin of the southeast Australian continental crust." Australian Journal of Earth Sciences **27**(1): 215 - 232.

Davies, J. H. and Von Blanckenburg, F. (1995). "Slab breakoff: a model for syncollisional magmatism and tectonics in the Alps." Tectonics **14**(1): 120-131.

Duchêne, S., Lardeaux, J. M. and Albarède, F. (1997). "Exhumation of eclogites: Insights from depth-time path analysis." Tectonophysics **280**(1-2): 125-140.

Duncan, D. M. (1972). "Reconnaissance Geology of the Frenchmans Cap National Park." The Papers and Proceedings of the Royal Society of Tasmania **107**.

Everard, J. L. (1999). A blue amphibole occurrence from the Flowerdale River, northern Arthur Lineament. Mineral Resources Tasmania. Geological Survey Record 1999/05 1-17

Faryad, S. W. and Chakraborty, S. (2005). "Duration of Eo-Alpine metamorphic events obtained from multicomponent diffusion modeling of garnet: A case study from the Eastern Alps." Contributions to Mineralogy and Petrology **150**(3): 306-318.

Finger, F. and Krenn, E. (2007). "Three metamorphic monazite generations in a high-pressure rock from the Bohemian Massif and the potentially important role of apatite in stimulating polyphase monazite growth along a PT loop." Lithos **95**(1-2): 103-115.

Fitzsimons, I. C. W. (2000). "Grenville-age basement provinces in East Antarctica: Evidence for three separate collisional orogens." Geology **28**(10): 879-882.

Foster, D. A., Gray, D. R. and Spaggiari, C. (2005). "Timing of subduction and exhumation along the Cambrian East Gondwana margin, and the formation of Paleozoic backarc basins." Geological Society of America Bulletin **117**(1): 105-116.

Gabalda, S., Beyssac, O., Jolivet, L., Agard, P. and Chopin, C. (2009). "Thermal structure of a fossil subduction wedge in the Western Alps." Terra Nova **21**(1): 28-34.

Gaidies, F., Abart, R., De Capitani, C., Schuster, R., Connolly, J. A. D. and Reusser, E. (2006). "Characterization of polymetamorphism in the Austroalpine basement east of the Tauern Window using garnet isopleth thermobarometry." Journal of Metamorphic Geology **24**(6): 451-475.

Gaidies, F., de Capitani, C., Abart, R. and Schuster, R. (2008). "Prograde garnet growth along complex P-T-t paths: results from numerical experiments on polyphase garnet from the Wölz Complex (Austroalpine basement)." Contributions to Mineralogy and Petrology **155**(6): 673-688.

Ganne, J., Jertrand, J.-M. and Fudral, S. (2005). "Fold interference pattern at the top of basement domes and apparent vertical extrusion of HP rocks (Ambin and South Vanoise massifs, Western Alps)." Journal of Structural Geology **27**: 553-570.

Ganne, J., Marquer, D., Rosenbaum, G., Bertrand, J.-M. and Fudral, S. (2006). "Partitioning of deformation within a subduction channel during exhumation of high-pressure rocks: a case study from the Western Alps." Journal of Structural Geology **28**: 1193-1207.

Gee, D. (1962). Structure and Petrology of the Raglan Range. *Unpub. B. SC. Honours Thesis, University of Tasmania, Hobart.*

Gee, R. D. and Legge, P. J. (1979) Beaconsfield, Geological Atlas 1 Mile Series. Sheet 30. Beaconsfield. Department of Mines Explanatory Report, Hobart.

Gibson, H. D., Carr, S. D., Brown, R. L. and Hamilton, M. A. (2004). "Correlations between chemical and age domains in monazite, and metamorphic reactions involving major pelitic phases: An integration of ID-TIMS and SHRIMP geochronology with Y-Th-U X-ray mapping." Chemical Geology **211**(3-4): 237-260.

Goscombe, B. D. (1990). Equlibrium thermodynamics of the Lyell Highway ecologites. Tasmania Department of Resources and Energy Division of Mines and Mineral Rrsources. 19 1-10

Gower, C. F. and Krogh, T. E. (2002). "A U-Pb geochronological review of the Proterozoic history of the eastern Grenville Province." Canadian Journal of Earth Sciences **39**(5): 795-829.

Gray, D. R. and Foster, D. A. (2004). "Tectonic evolution of the Lachlan Orogen, southeast Australia: Historical review, data synthesis and modern perspectives." Australian Journal of Earth Sciences **51**(6): 773-817.

Green, D. H. (1959). Geology of the Beaconsfield District, including the Andersons Creek Ultrabasic Complex. Records of the Queen Victoria Museum10.

Green, G. R. (1983). The geological setting and formation of the Rosebery volcanic-hosted massive sulphide orebody, Tasmania. Hobart, University of Tasmania.

Green, H. W., II, 2005. Psychology of a changing paradigm: 40+ years of high-pressure metamorphism. International Geology Review, 47(5), 439-456.

Hall, M. (1998). The Structural History of northern Tasmania and the Bass Strait connection. AGCRC Symposium--Mineral Systems and the Crust-Upper Mantle of SE Australia.

Harley, S. L., Kelly, N. M. and Möller, A. (2007). "Zircon behaviour and the thermal histories of moutain chains." Elements **3**(1): 25-30.

Henson, P. (2002). Geology of the Port Sorell Formation. Earth Sciences. Hobart, University of Tasmania.

Holdaway, M. J. (2000). "Application of new experimental and garnet Margules data to the garnet-biotite geothermometer." American Mineralogist **85**(7-8): 881-892.

Holdaway, M. J. (2001). "Recalibration of the GASP geobarometer in light of recent garnet and plagioclase activity models and versions of the garnet-biotite geothermometer." American Mineralogist **86**(10): 1117-1129.

Holland, T. and Powell, R. (2000). AX-Activity-Composition Software, Department of Earth Sciences, University of Cambridge.

Holland, T. J. B. and Powell, R. (1998). "An internally consistent thermodynamic data set for phases of petrological interest." Journal of Metamorphic Geology **16**(3): 309-343.

Holm, O. H. (2002). Structural and Metamorphic Evolution of the Arthur Lineament, Northwestern Tasmania, Australia. *Unpub. PhD Thesis, University of Tasmania, Hobart.*

Holm, O. H. and Berry, R. F. (2002). "Structural history of the Arthur Lineament, northwest Tasmania: an analysis of critical outcrops." Australian Journal of Earth Sciences **49**(2): 167-185.

Holm, O. H., Crawford, A. J. and Berry, R. F. (2003). "Geochemistry and tectonic settings of meta-igneous rocks in the Arthur Lineament and surrounding area, northwest Tasmania." Australian Journal of Earth Sciences **50**(6): 903-918.

Holm, O. H., Berry, R. F. and Steele, D. (accepted). Chemical dating of metamorphic monazites in the Arthur Lineament, NW Tasmania. GA Bulletin.

Hoschek, G. (2004). "Comparison of calculated P-T pseudosections for a kyanite eclogite from the Tauern Window, Eastern Alps, Austria." European Journal of Mineralogy **16**(1): 59-72.

Hynes, A. (2002). "Encouraging the extrusion of deep-crustal rocks in collisional zones." Mineralogical Magazine **66**(1): 5-24.

Kamperman, M. (1984). The Precambrian Metamorphic Geology of the Lyell Highway - Collingwood River Area. *Unpub. B. Sc. Honours Thesis, University of Tasmania, Hobart.*

Kohn, M. J. (2004). "Geochemical Zoning in Metamorphic Minerals." Treatise on Geochemistry **3**: 229-261.

Krenn, E., Ustaszewski, K. and Finger, F. (2008). "Detrital and newly formed metamorphic monazite in amphibolite-facies metapelites from the Motajica Massif, Bosnia." Chemical Geology **254**(3-4): 164-174.

Lewis, R. (1991). Structure and Metamorphic Petrology of the Forth Metamorphic Complex. *Unpub. B. Sc. Honours Thesis, University of Tasmania, Hobart.*

Llana-Fúnez, S. and Marcos, A. (2007). "Convergence in a thermally softened thick crust: Variscan intracontinental tectonics in Iberian plate rocks." Terra Nova **19**(0): 1-8.

Ludwig, K. R. (2003). Isoplot 3.00: a geochronological toolkit for Microsoft Excel. 4 70 pp

McDougall, I. and Leggo, P. J. (1965). "Isotopic age determinations on granitic rocks from Tasmania." Journal of the Geological Society of Australia **12**: 295-332.

McIntyre, E. B. (1964). The Structure and Petrology of the Collingwood Area. *Unpub. B. Sc. Honours Thesis, University of Tasmania, Hobart.*

McNeill, A. W. (1985). The Structure and Petrology of the Nye Bay Area, South West Tasmania. *Unpub. B. Sc. Honours Thesis, University of Tasmania, Hobart.*

Meffre, S., Berry, R. F. and Hall, M. (2000). "Cambrian metamorphic complexes in Tasmania: tectonic implications." Australian Journal of Earth Sciences **47**(6): 971-985.

Meffre, S., Large, R. R., Scott, R., Woodhead, J., Chang, Z., Gilbert, S. E., Danyushevsky, L. V., Maslennikov, V. and Hergt, J. M. (2008). "Age and pyrite Pb-isotopic composition of the giant Sukhoi Log sediment-hosted gold deposit, Russia." Geochimica et Cosmochimica Acta **72**(9): 2377-2391.

Münker, C. and Crawford, A. J. (2000). "Cambrian arc evolution along the se gondwana active margin: A synthesis from Tasmania-New Zealand-Australia-Antarctica correlations." Tectonics **19**(3): 415-432.

Noll, C. A. and Hall, M. (2005). "Great Lyell Fault, western Tasmania: A collage of Middle and Late Cambrian growth faults reactivated during Devonian orogenesis." Australian Journal of Earth Sciences **52**(3): 427-442.

Palmeri, R., Chmielowski, R. M., Sandroni, S., Talarico, F. and Ricci, C. A. (2009). "Petrology of the eclogites from western Tasmania: Insights to the Cambro-Ordovician evolution of the paleo-Pacific margin of Gondwana." Lithos **109**(3-4): 223-239.

Patison, N. L., Berry, R. F., Davidson, G. J., Taylor, B. P., Bottrill, R. S., Manzi, B., Ryba, J. and Shepherd, R. E. (2001). "Regional metamorphism of the Mathinna group, northeast Tasmania." Australian Journal of Earth Sciences **48**(2): 281-292.

Paxton, G. C. (1965). Chemistry of Tasmanian Eclogites. *Unpub. B. Sc. Honours Thesis, University of Tasmania, Hobart*.

Powell, R., Holland, T. and Worley, B. (1998). "Calculating phase diagrams involving solid solutions via non-linear equations, with examples using THERMOCALC." Journal of Metamorphic Geology **16**(4): 577-588.

Pyle, J. M. and Spear, F. S. (2003). "Yttrium zoning in garnet: Coupling of major and accessory phases during metamorphic reactions." American Mineralogist **88**(4): 708.

Råheim, A. (1976). "Petrology of Eclogites and Surrounding Schists from the Lyell Highway--Collingwood River Area." Journal of the Geological Society of Australia **23**: 313-327.

Råheim, A. (1977). "Petrology of the Strathgordon Area, Western Tasmania: Si^{4+}-Content of Fengite Mica as Monitor of Metamorphic Grade." Journal of the Geological Society of Australia **25**: 329-338.

Råheim, A. and Compston, W. (1977). "Correlations between metamorphic events and Rb-Sr ages in metasediments and eclogite from western Tasmania." Lithos **10**: 271-289.

Råheim, A. and Green, D. H. (1974). "Talc-Garnet-Kyanite-Quartz Schist from and Eclogite-Bearing Terrane, Western Tasmania." Contributions to mineralogy and petrology **43**: 223-231.

Raimbourg, H. & Kimura, G., 2008. Non-lithostatic pressure in subduction zones. Earth and Planetary Science Letters, 274, 414-422.

Reed, A. R. (2001). Structure and setting of Proterozoic and Palaeozoic rocks in the Tamar region, northern Tasmania. Specialist Group in Tectonics and Structural Geology Field Guide No. 9, Geologicial Society of Australia.

Reed, A. R., Calver, C. and Bottrill, R. S. (2002). "Palaeozoic suturing of eastern and western Tasmania in the west Tamar region: implications for the tectonic evolution of southeast Australia." Australian Journal of Earth Sciences **49**(5): 809-830.

Reed, A. R., Zengerer, M. and Roach, M. (2001). Andersons Creek Ultramafic Complex and Simmonds Hill Metamorphics. *in* Structure and tectonics of Proterozoic and Palaeozoic rocks in the Tamar region, northern Tasmania SGTSG Field Guide no. **9**. A. R. Reed *eds.***:** 43-55.

Rivers, T. (1997). "Lithotectonic elements of the Grenville Province: Review and tectonic implications." Precambrian Research **86**(3-4): 117-154.

Robinson, P. (2003). XRF analysis of flux-fused discs. Geoanalysis 2003, The 5th International Conference on the Analysis of Geological and Environmental Materials, Finland.

Seymour, D. B. (1981). The Tabberabberan Orogeny in Northwest Tasmania. Hobart, University of Tasmania.

Shau, Y. H., Feather, M. E., Essene, E. J. and Peacor, D. R. (1991). "Genesis and solvus relations of submicroscopically intergrown paragonite and phengite in a blueschist from northern California." Contributions to Mineralogy and Petrology **106**(3): 367-378.

Shaw, D. M. (1956). "Major elements and general geochemistry, Part 3 of Geochemistry of pelitic rocks." Geological Society of America Bulletin **67**(7): 919-934.

Solomon, M. and Griffiths, J. R. (1972). "Tectonic Evolution of the Tasman Orogenic Zone, Eastern Australia." Nature Physical Science **237**(70): 3-6.

Solomon, M. and Griffiths, J. R. (1974). Aspects of the early history of the southern Tasman orogenic zone. The Tasman Geosyncline--a symposium in honour of Prof. D. Hill., Brisbane, Geological Society of Australia.

Spear, F. S. (1993). Metamorphic phase equilibria and pressure-temperature-time paths. Washington, D.C., Mineralogical Society of America.

Spry, A. H. (1957). "Precambrian Rocks of Tasmania, Part II, Mount Mary Area." The Papers and Proceedings of the Royal Society of Tasmania **91**(Publication 51): 95 - 108.

Spry, A. H. (1962). Some Aspects of the Stratigraphy, Structure and Petrology of the Precambrian Rocks of Tasmania. *Unpub. PhD Thesis, University of Tasmania, Hobart.*

Spry, A. H. (1963a). "The Occurrence of Ecloglite on the Lyell Highway, Tasmania." Mineralogical Magazine **33**(262): 589-593.

Spry, A. H. (1963b). "Precambrian Rocks of Tasmania, Part V, Petrology and Structure of the Frenchman's Cap Area." The Papers and Proceedings of the Royal Society of Tasmania **97**.

Spry, A. H. (1964). "Precambrian Rocks of Tasmania, Part VI, the Zeehan-Corinna Area." The Papers and Proceedings of the Royal Society of Tasmania **98**.

Spry, A. H. and Ford, R. J. (1957). "A Reconnaissance of the Corinna-Pieman Heads Area--Geology." The Papers and Proceedings of the Royal Society of Tasmania **91**.

Spry, A. H. and Gee, D. (1964). "Some Effects of Paleozoic Folding on the Precambrian Rocks of the Frenchman's Cap Area, Tasmania." Geological Magazine **101**(5): 385-396.

Spry, A. H. and Zimmerman, D. (1959). "The Precambrian Rocks of Tasmania, Part IV.--The Mt. Mullens Area." The Papers and Proceedings of the Royal Society of Tasmania **93**.

Symmes, G. H. and Ferry, J. M. (1992). "The effect of whole-rock MnO content on the stability of garnet in pelitic schists during metamorphism." Journal of Metamorphic Geology **10**(2): 221-237.

Tinkham, D. K. and Ghent, E. D. (2005). "Estimating P-T conditions of garnet growth with isochemical phase-diagram sections and the problem of effective bulk-composition." Canadian Mineralogist **43**(1): 35-50.

Todd, C. S. (1998). "Limits on the precision of geobarometry at low grossular and anorthite content." American Mineralogist **83**(11-12 PART 1): 1161-1167.

Tracy, R. J. (1982). Compositional zoning and inclusions in metamorphic minerals. *in* Characterization of Metamorphism through Mineral Equilibria. J. M. Ferry *eds.*, Mineralogical Society of America. **10:** 355-397.

Turner, N. J. (1971). Mt. Madge - Mt. Mary Area. *Unpub. B. Sc. Honours Thesis, University of Tasmania, Hobart.*

Turner, N. J. (1989). Precambrian. *in* Geology and Mineral Resources of Tasmania -- Special Publication 15. C. F. Burrett and E. L. Markin *eds.*, Geological Society of Australia.

Turner, N. J. (1993). K-Ar geochronology in the Arthur Metamorphic Complex, Tasmania. Mineral Resourses Tasmania. 1993/27

Turner, N. J., Black, L. P. and Kamperman, M. (1995). Pre-Middle Cambrian stratigraphy, orogenesis and geochronology in western Tasmania. Geological Society of Australia Abstracts. 51-56

Turner, N. J., Black, L. P. and Kamperman, M. (1998). "Dating of Neoproterozoic and Cambrian orogenies in Tasmania." Australian Journal of Earth Sciences **45**: 789-806.

Turner, N. J. and Bottrill, R. S. (2001). "Blue amphibole, Arthur Metamorphic Complex, Tasmania: composition and regional tectonic setting." Australian Journal of Earth Sciences **48**(1): 167-181.

Van Hinsberg, V. J. and Schumacher, J. C. (2007). "Using estimated thermodynamic properties to model accessory phases: The case of tourmaline." Journal of Metamorphic Geology **25**(7): 769-779.

Vance, D. and Mahar, E. (1998). "Pressure-temperature paths from P-T pseudosections and zoned garnets: Potential, limitations and examples from the Zanskar Himalaya, NW India." Contributions to Mineralogy and Petrology **132**(3): 225-245.

Varne, R. and Foden, J. (1987). "Tectonic setting of Cambrian rifting, volcanism and ophiolite formation in western Tasmania." Tectonophysics **140**(2-4): 275-295.

White, R. W., Powell, R. and Holland, M. (2007). "Progress relating to calculation of partial melting equilibria for metapelites." Journal of Metamorphic Geology **25**: 511-527.

White, W., Clarke, G. L. and Nelson, D. R. (1999). "SHRIMP U–Pb zircon dating of Grenvilleage events in the western part of the Musgrave Block, central Australia." Journal of Metamorphic Geology **17**: 465-481.

Williams, E. (1978). "Tasman Fold Belt System in Tasmania." Tectonophysics **48**: 159-205.

Williams, P. R. (1971). The Petrology and Structure of the Mt. McCall Area. *Unpub. B. Sc. Honours Thesis, University of Tasmania, Hobart.*

Williams, P. R. (1979). Basin Development, Environment of Deposition and Deformation of a Precambrian (?) Conglomeratic Flysch Sequence at Bathhurst Harbour, SW Tasmania. *Unpub. PhD Thesis, University of Tasmania, Hobart.*

Williams, P. R. (1982). Geological Survey Explanatory Report Geological Atlas 1:50 000 series Zone 7 Sheet 91 (8011S) Davey. Department of Mines.

Williams, S. J. (1976). "Structure and Metamorphism of the McPartlan Pass--Sentinels Area." The Papers and Proceedings of the Royal Society of Tasmania **110**.

Wing, B. A., Ferry, J. M. and Harrison, T. M. (2003). "Prograde destruction and formation of monazite and allanite during contact and regional metamorphism of pelites: Petrology and geochronology." Contributions to Mineralogy and Petrology **145**(2): 228-250.

Wu, C.-M., Zhang, J. and Ren, L.-D. (2004). "Empirical Garnet–Biotite–Plagioclase–Quartz (GBPQ) Geobarometry in Medium- to High-Grade Metapelites*." Journal of Petrology **48**(9): 1907-1921.

Wu, C.-M. and Zhao, G. C. (2007). "The metapelitic garnet-biotite-muscovite-aluminosilicate-quartz (GBMAQ) geobarometer." Lithos **97**(3-4): 365-372.

Yamato, P., Burov, E., Agard, P., Le Pourhiet, L. and Jolivet, L. (2008). "HP-UHP exhumation during slow continental subduction: Self-consistent thermodynamically and thermomechanically coupled model with application to the Western Alps." Earth and Planetary Science Letters **271**: 63-74.

Zeh, A. and Millar, I. L. (2001). "Metamorphic evolution of garnet-epidote-biotite gneiss from the Moine supergroup, Scotland, and geotectonic implications." Journal of Petrology **42**(3): 529-554.

Zhu, X. K. and O'Nions, R. K. (1999). "Monazite chemical composition: Some implications for monazite geochronology." Contributions to Mineralogy and Petrology **137**(4): 351-363.

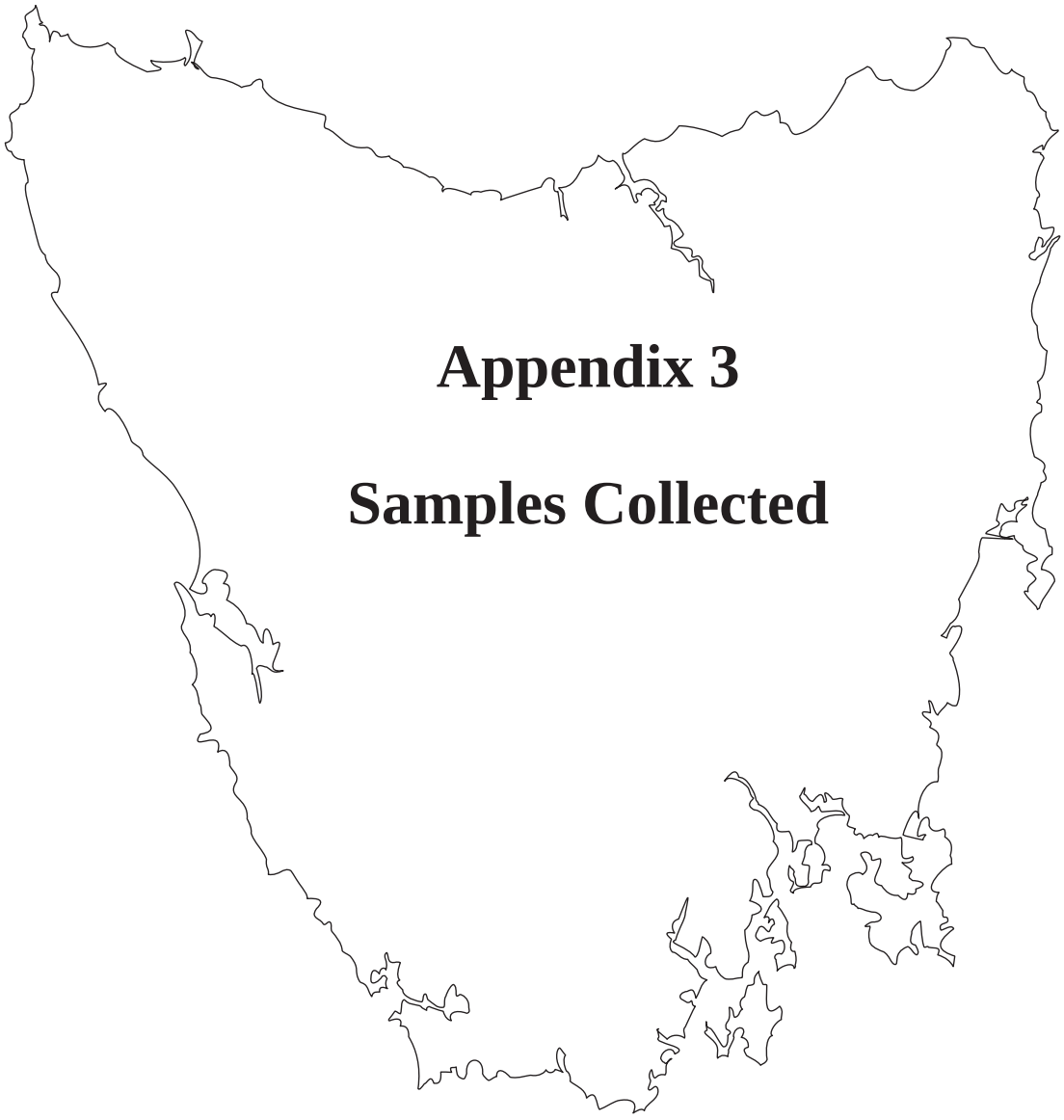

Appendix 3

Samples Collected

Appendix 3: Samples Collected

Utas#	Field Number	Class	Composition	Rock Name	major minerals	minor minerals	Map grid (N)	Map grid (E)	Hand sample	Powder	Coarse Crush	Thin Section	Polished block
160694	RC0601	met.	pelitic	Schist	white mica, quartz	garnet (tourmaline, little albite)	5335789	405390	R	PD		TS	PB
160695	RC0602	met.	pelitic	Schist	white mica, quartz	garnet, albite (biotite)	5335790	405434	R			TS	
160696	RC0603	met.	pelitic	Schist	quartz, white mica	garnet (kyanite, albite, biotite)	5335790	405436	R	PD		TS	
160697	RC0604	met.	pelitic	Schist	quartz, white mica	garnet	5335705	405538	R			TS	
160698	RC0605	met.	pelitic	Schist	quartz, white mica	albite, garnet (biotite, tourmaline)	5335705	405538	R	PD		TS	
160699	RC0606	met.	pelitic	Schist	quartz, white mica	biotite, albite (garnet)	5335671	405567	R			TS	
160700	RC0607	met.	pelitic	Schist	white mica, quartz	garnet, albite (biotite)	5335671	405567	R			TS	
160701	RC0608	met.	pelitic	Schist	quartz (white mica)	albite, biotite (garnet)	5335671	405567	R			TS	
160702	RC0609	met.	pelitic	Schist	white mica, quartz	garnet, albite (biotite)	5335642	405780	R	PD	CR	TS	
160703	RC0610	met.	mafic	Eclogite			5335642	405780	R			TS	
160704	RC0611	met.	mafic	Eclogite			5335654	405911	R			TS	
160705	RC0612	met.	pelitic	Schist	white mica, quartz	garnet, sercitized feldspar	5335654	405911	R			TS	
160706	RC0613	met.	pelitic	Schist	quartz, white mica	(garnet, kyanite, albite, tourmaline)	5335700	405325	R			TS	
160707	RC0614	met.	pelitic	Schist	white mica, quartz	garnet (albite, biotite)	5335679	405324	R	PD	CR	TS	PB
160708	RC0615	met.	pelitic	Schist	white mica, quartz	albite, garnet, biotite	5335635	405549	R	PD	CR	TS	
160709	RC0616	met.	pelitic	quartzite	quartz	(biotite, garnet)	5335658	405808	R			TS	
160710	RC0617	met.	pelitic	Schist	quartz, white mica	albite (biotite, garnet)	5335639	405895	R			TS	
160711	RC0618	met.	pelitic	Schist	white mica, quartz	albite, garnet, biotite	5335661	405952	R			TS	
160712	RC0619	met.	pelitic	Schist	white mica, quartz	albite, garnet	5335658	405986	R			TS	
160713	RC0620	met.	pelitic	Schist	quartz, white mica	albite, garnet (biotite, chlorite)	5335667	406013	R			TS	
160714	RC0621	met.	pelitic	Schist	white mica, quartz	albite, garnet (biotite)	5335669	406036	R			TS	
160715	RC0622	met.	mafic	Eclogite			5335716	406086	R			TS	

Grid locataions based on AGD_1966_ISG_55_1 (minerals in parentheses are less common than those not)

Appendix 3: Samples Collected

Utas#	Field Number	Class	Composition	Rock Name	major minerals	minor minerals	Map grid (N)	Map grid (E)	Hand sample	Powder	Coarse Crush	Thin Section	Polished block
160716	RC0623	met.	pelitic	Schist	quartz, white mica	garnet, albite (biotite)	5335728	406119	R			TS	
160717	RC0624	met.	pelitic	Schist	quartz, white mica	garnet (albite, biotite)	5335750	406129	R			TS	
160718	RC0625	met.	pelitic	Schist	quartz, white mica	garnet, biotite (albite)	5335770	406168	R			TS	
160719	RC0626	met.	pelitic	Schist	quartz, white mica	green-low bf	5335792	406199	R			TS	
160720	RC0627	met.	pelitic	Schist	quartz, white mica	albite (garnet)	5335800	406248	R			TS	
160721	RC0628	met.	mafic	Eclogite			5335801	406250	R			TS	
160722	RC0629	met.	pelitic	Schist	quartz, white mica	albite (biotite, chlorite, garnet)	5335851	406338	R			TS	
160723	RC0630	met.	pelitic	Schist	quartz, white mica	albite (garnet)	5335852	406384	R			TS	
160724	RC0631	met.	pelitic	Phyllite			5335693	407237	R				
160725	RC0632	met.	pelitic	Quartzite	quartz	chlorite replacing garnet	5335900	406550	R			TS	
160726	RC0633	met.	pelitic	Quartzite	quartz, white mica	green-low bf (garnet)	5335895	406536	R			TS	
160727	RC0701	met.	mafic	Eclogite			5332992	409929	R			TS	
160728	RC0702	met.	mafic	Eclogite			5332992	409929	R				
160729	RC0703	met.	mafic	Eclogite			5332993	409934	R			TS	
160730	RC0704	met.		whiteschist	garnet, kyanite	talc, sericite (quartz)	5333001	409967	R	PD?		TS	
160731	RC0705	met.	pelitic		quartz	(biotite)	5332931	410099	R			TS	
160732	RC0706	ig.	mafic	mafic, fine grained dyke, undeformed, cuts between layers of defor			5332971	410103	R				
160733	RC0707	met.	pelitic	Schist			5332990	409927	R				
160734	RC0708	met.	pelitic		quartz, white mica	garnet, biotite, albite	5332938	409857	R			TS	
160735	RC0709	met.	pelitic		quartz, white mica	(garnet)	5335737	405298	R			TS	
160736	RC0710	met.	pelitic		white mica, quartz	(garnet)	5335714	405338	R			TS	
160737	RC0711	met.	pelitic		quartz	sericite, altered garnets	5328570	412335	R			TS	

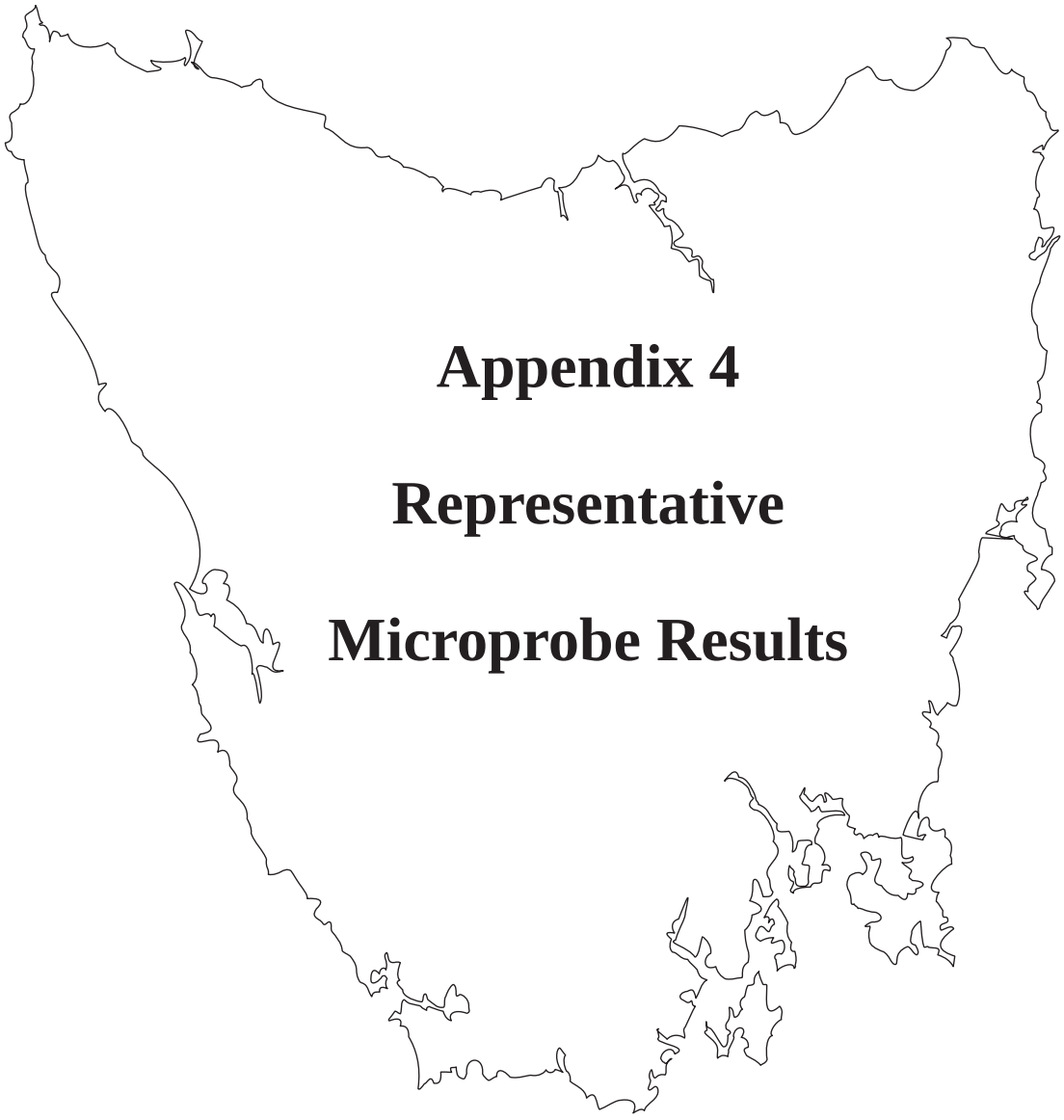

Appendix 4

Representative

Microprobe Results

Appendix 4: Representative Microprobe Results

Na2O	SiO2	Al2O3	MgO	K2O	CaO	Cr2O3	MnO	Fe2O3	FeO	TiO2
bi	68319-b3-2									
0.1055	33.4738	19.4257	7.7352	9.1834	0.0173	-0.0053	0.0314	0.001	22.8623	2.3369
mu	68319-m2-1									
0.0926	40.8858	29.3655	4.3401	7.1059	-0.0053	0.0275	0.0401	0.001	10.143	0.428
fsp	68319-fsp-2b-1									
9.6277	65.0966	21.6504	-0.0006	0.1459	2.0759	-0.0115	0.0322	0.001	0.0133	0.052
g	68319-g3-1									
0.0248	36.436	21.8921	2.9968	-0.0008	0.642	0.0516	0.5292	0.001	38.7626	-0.0116
*										

Na2O	SiO2	Al2O3	MgO	K2O	CaO	NiO	Fe2O3	FeO	MnO	TiO2
bi	68335-b2-3									
0.085	34.3547	19.6439	6.395	9.477	-0.0087	0.049	0.001	21.5325	0.177	3.2773
g	68335-g1-1									
0.0145	36.7653	21.0726	2.8192	0.0068	3.9734	0.0599	0.001	34.3965	0.8344	0.0449
mu	68335-m2-1									
0.2418	45.2679	35.9878	0.4211	10.8894	0.0508	0.0386	0.001	0.8517	-0.0199	0.0446
*										

Na2O	SiO2	Al2O3	MgO	K2O	CaO	Cr2O3	MnO	Fe2O3	FeO	TiO2
mu	143072-m1-3									
0.7321	45.3536	33.2927	1.1574	10.1578	0.007	-0.0109	-0.002	0.001	1.6071	0.6149
bi	143072-b1-2									
0.3235	34.8085	18.3958	8.6471	8.9201	0.0489	0.0604	0.1214	0.001	21.2419	1.3762
g	143072-g1-20									
0.0283	36.9826	21.376	5.4399	-0.0104	1.5189	-0.0125	0.3896	0.001	34.8621	0.0261
*										

Appendix 4: Representative Microprobe Results

Na2O	SiO2	Al2O3	MgO	K2O	CaO	Cr2O3	MnO	Fe2O3	FeO	TiO2
bi	30145-b3-1									
0.0883	36.5325	18.4404	12.0408	9.1466	-0.0106	0.0573	0.2956	0.001	16.4653	2.0462
fsp	30145-f1-3									
7.6047	59.2253	26.0308	-0.0121	0.2197	6.9346	-0.0116	0.0392	0.001	0.0399	0.0209
g	30145-g-2-1									
0.0128	37.9688	22.438	5.1722	0.0211	7.9346	0.0505	0.7331	0.001	27.1918	0.1211
mu	30145-m3-2									
0.7942	48.3159	30.7712	2.9428	10.2969	-0.0036	-0.0201	0.036	0.001	1.7232	0.4914
*										

Na2O	SiO2	Al2O3	MgO	K2O	CaO	Fe2O3	FeO	MnO	TiO2	Cr2O3
bi	39463-b1-1-1									
0.003	33.5299	18.8798	5.9648	8.0207	0.0142	0.001	26.1948	0.22	1.3394	-0.008
fsp	39463-f2-4-31									
10.4243	66.5986	20.703	0	0.1324	1.1317	0.001	0	0.0017	0.0011	0.0204
g	39463-g2-3-24									
0.0371	36.8737	21.3452	0.7839	0.0038	5.6542	0.001	34.338	1.829	0.0677	-0.0013
mu	39463-m2-2-26									
0.5064	48.1635	32.0887	1.6366	10.2959	-0.029	0.001	2.0584	0.0361	0.375	0
*										

Na2O	SiO2	Al2O3	MgO	K2O	Fe2O3	FeO	MnO	CaO	TiO2	Cr2O3
bi	39456-b2-2									
0.0473	34.4721	18.3	6.0312	8.861	0.001	25.4683	0.0635	-0.019	1.1568	0.0442
fsp	39456-f1-6									
9.8255	64.572	21.551	0.0023	0.0982	0.001	0.031	0.0297	3.1645	-0.0052	0
g	39456-g1-1									
0.0132	37.1369	21.0454	2.6605	-0.0082	0.001	33.9997	0.5028	5.5415	0.0835	0.0181
mu	39456-m2-1									
0.5296	46.5639	30.7044	1.5938	10.3939	0.001	2.1487	0.0325	-0.0271	0.5722	0.0028
*										

Na2O	SiO2	Al2O3	MgO	K2O	CaO	Cr2O3	MnO	Fe2O3	FeO	TiO2

Appendix 4: Representative Microprobe Results

fsp 75637-f1-1
11.6057 67.3472 19.7332 0.0053 0.0461 0.3424 -0.0283 0.0103 0.001 0.0455 0
mu 75637-m2-2
1.3582 47.3782 31.5194 2.0161 9.1848 0.0198 0.0308 0.0181 0.001 1.9581 0.6952
bi 75637-m3-1
0.2004 37.7021 16.4666 12.0566 8.4502 0.063 0.0027 0.0202 0.001 17.2147 1.6434
g 75637-g1-1
0.0414 37.1931 21.4475 4.7953 0.011 2.2193 0.0074 0.2288 0.001 34.7786 0.0928
*

Na2O	SiO2	Al2O3	MgO	K2O	CaO	Cr2O3	MnO	Fe2O3	FeO	TiO2
ctd	75596-ctd-A-1									
0.0251	24.583	41.9788	4.4811	-0.0285	-0.0052	-0.0053	-0.0031	0.001	21.9187	-0.015
chl	75596-x-3									
0.0326	25.9398	21.6908	16.1899	-0.0016	0.0275	-0.0104	0.0825	0.001	24.0097	0.0473
g	75596-g-A-1									
0.0231	37.9942	21.9592	5.9794	-0.0026	0.963	0.0384	0.1553	0.001	34.5299	0.0424
mu	75596-m1-3									
1.2107	47.3771	33.4717	1.4571	9.5995	0.0036	-0.0345	0.0348	0.001	1.5432	0.3028
*										

Na2O	SiO2	Al2O3	MgO	K2O	CaO	Cr2O3	MnO	Fe2O3	FeO	TiO2
bi	RC0624-mb4-1									
0.1047	34.7876	19.0134	8.2905	8.5767	0.0488	-0.0291	0.0943	0.001	22.0913	1.6085
fsp	RC0624-f-a-2									
9.8876	63.7654	22.6384	0.0053	0.0977	3.1773	-0.0345	-0.0158	0.001	0.0266	0.0029
g	RC0624-g-2-2									
0.0416	36.9285	21.9729	2.9946	0.0004	6.4606	0.0064	0.4745	0.001	32.467	0.1486
mu	RC0624-m3-1									
0.6566	47.1329	30.7044	2.0888	9.4319	-0.0235	-0.0425	0.0171	0.001	2.5501	1.2489
*										

Na2O	SiO2	Al2O3	MgO	K2O	CaO	Cr2O3	MnO	Fe2O3	FeO	TiO2
g	RC0620g3-1									

Appendix 4: Representative Microprobe Results

-0.01	37.12	21.33628	4.72	0	1.89	0	0.65	0.001	35.31	0.01
bi	RC0620b3-3									
0.167	35.6952	18.39595	10.9767	8.6782	0.0381	0.0107	0.0418	0.001	20.3347	1.6348
fsp	RC0620f3-2									
9.5838	65.0166	22.55872	-0.0096	0.0486	2.7211	0.0094	-0.0043	0.001	0.0402	-0.001
mu	RC0620m1-1-55									
0.8781	47.9604	30.95048	2.5657	9.5043	-0.009	0.0601	-0.0017	0.001	2.0839	0.8233
*										
Na2O	**SiO2**	**Al2O3**	**MgO**	**K2O**	**CaO**	**Cr2O3**	**MnO**	**Fe2O3**	**FeO**	**TiO2**
bi	67659c1b3-1									
0.4048	35.4336	17.9841	8.6866	8.3747	0.0951	0.044	0.0932	0.001	20.6777	2.4312
fsp	67659c1f1-1									
10.2299	66.505	21.437	-0.0091	0.0716	2.009	0	-0.0029	0.001	0.2911	-0.0475
g	67659c1g2-8									
0.1278	37.3925	21.1479	2.8728	-0.0185	5.4075	-0.0149	0.4419	0.001	32.4972	0.0089
mu	67659c1m1-1									
0.7215	49.1777	31.4417	2.3781	5.9328	0.0597	0.0304	0.0265	0.001	2.6408	1.0044
*										
Na2O	**SiO2**	**Al2O3**	**MgO**	**K2O**	**CaO**	**Cr2O3**	**MnO**	**Fe2O3**	**FeO**	**TiO2**
bi	RC0615c2b2-1									
0.21	35.85	17.47	8.38	8.06	0.13	0.04	0.04	0.001	21.51	2.3
fsp	RC0615c2f2-2									
10.91	66.24	20.4	0	0.06	1.43	0.02	-0.04	0.001	0.04	-0.02
mu	RC0615c2m2-1									
0.74	48.06	29.9	2.14	9.41	-0.02	0.04	-0.03	0.001	2.39	0.96
g	RC0615c2g1-2									
0.06	37.26	21.12	3.26	0	5.73	0.03	0.46	0.001	32.68	0.8
*										
Na2O	**SiO2**	**Al2O3**	**MgO**	**K2O**	**CaO**	**Cr2O3**	**MnO**	**Fe203**	**FeO**	**TiO2**
bi	RC0609c2b3-1									
0.12	35.25	18.03	7.88	9.04	-0.01	-0.01	0.06	0.001	21.55	2.11

Appendix 4: Representative Microprobe Results

fsp	RC0609c2f4-1										
	10.67	66.88	20.36	0.01	0.03	1.26	-0.01	0.01	0.001	-0.02	0
g	avg tiny RC0609										
	0.02	37	21.25	3.47	0	4.23	0.01	0.28	0	34.26	0.09
mu	RC0609c2m1-1										
	0.93	47.28	30.81	1.96	9.36	-0.02	0	-0.05	0.001	2.18	1.03

*

	Na2O	**SiO2**	**MgO**	**Al2O3**	**K2O**	**CaO**	**Cr2O3**	**Fe2O3**	**MnO**	**FeO**	**TiO2**
bi	RC0605b3-2										
	0.0953	36.1767	8.775	19.05594	8.4668	0.0519	0.0194	0.001	0.0984	21.3573	2.2724
fsp	RC0605f3-2										
	10.6558	67.0931	-0.0019	21.4235	0.0648	1.0997	0.0014	0.001	0.0001	0.0119	0.0154
g	RC0605g2-1										
	0.04	37.58	4.64	21.00634	-0.01	2.53	0	0.26	0.001	34.12	0.03
mu	RC0605m2-2										
	0.7788	47.3665	2.2788	31.27228	9.4919	-0.0099	0.0328	0.001	-0.0092	2.1914	1.264

*

	Na2O	**SiO2**	**Al2O3**	**MgO**	**K2O**	**CaO**	**MnO**	**Fe2O3**	**FeO**	**TiO2**	**Cr2O3**
bi	67661c1b1-1										
	0.3493	34.7246	17.5703	8.0061	8.0402	0.3336	0.0072	0.001	21.5259	2.3596	0.0258
fsp	67661c1f2-2										
	10.6143	66.8599	20.7811	0.0057	0.0448	1.0581	0.0151	0.001	0.0183	-0.0095	0.0462
g	67661c1g1-1										
	0.1526	36.8789	20.9382	3.5288	0.0017	3.3085	0.6179	0.001	34.4762	0.0264	0.0221
mu	67661c1m3-3										
	0.8343	49.3619	32.0414	2.1446	5.9364	-0.0175	0.0018	0.001	2.4153	1.3572	0.0221

*

	Na2O	**SiO2**	**Al2O3**	**MgO**	**K2O**	**Fe2O3**	**FeO**	**MnO**	**CaO**	**TiO2**	**Cr2O3**
g	RC0614-g2-37										
	0.038	37.4168	21.3577	5.0572	0.0198	0.001	34.892	0.4405	1.8376	0.0258	0.0215
bi	RC0614-b1-1-9										

Appendix 4: Representative Microprobe Results

0.2961	35.5926	18.1122	9.3539	8.5543	0.001	20.72	0.0065	-0.0038	1.8418	-0.0292
mu	RC0614-m1-2-13									
0.9898	47.9542	30.2093	2.1167	9.2192	0.001	1.7082	-0.008	-0.0127	0.7835	0
fsp	RC0614-f1-1-15									
11.1831	66.2389	19.6023	0.0116	0.1105	0.001	-0.0111	0.0368	0.9991	-0.0052	-0.0143
*										
Na2O	**SiO2**	**Al2O3**	**MgO**	**K2O**	**CaO**	**Cr2O3**	**MnO**	**Fe2O3**	**FeO**	**TiO2**
bi	RC0618b1-2									
0.1967	35.3477	18.61437	7.4533	8.1441	0.0095	0.0139	0.0658	0.001	24.2052	1.6386
fsp	RC0618f2-1									
10.8713	67.2255	21.22256	-0.0148	0.0823	0.6978	-0.0297	-0.0203	0.001	-0.0011	-0.0019
mu	RC0618m1-2									
0.5561	48.1568	30.07712	2.2891	9.6658	-0.009	0.0394	0.0029	0.001	2.9278	1.2383
g	RC0618g1-1									
0.02	36.69	21.8202	2.86	0	3.21	0.03	0.39	0.001	35.92	0.06
*										
SiO2	**TiO2**	**Al2O3**	**FeO**	**MnO**	**MgO**	**CaO**	**Na2O**	**K2O**	**Cr2O3**	**Fe2O3**
bi	RC0603-b1-2									
35.0453	1.4576	19.6054	20.8297	0.0421	8.7375	0.014	0.3507	8.5379	0.0163	0.001
fsp	RC0603-f2-1									
66.885	-0.002	20.1283	0.0985	0.0019	-0.0129	0.6546	10.9701	0.0742	0.0088	0.001
g	RC0603-g3-1									
37.163	0.0186	21.3508	36.3044	0.3348	4.4322	1.0184	-0.0046	0.003	-0.0163	0.001
mu	RC0603-m1-3									
47.3299	0.9308	31.9174	1.629	0.0413	1.6986	-0.0217	0.8347	9.7196	0.0363	0.001
*										

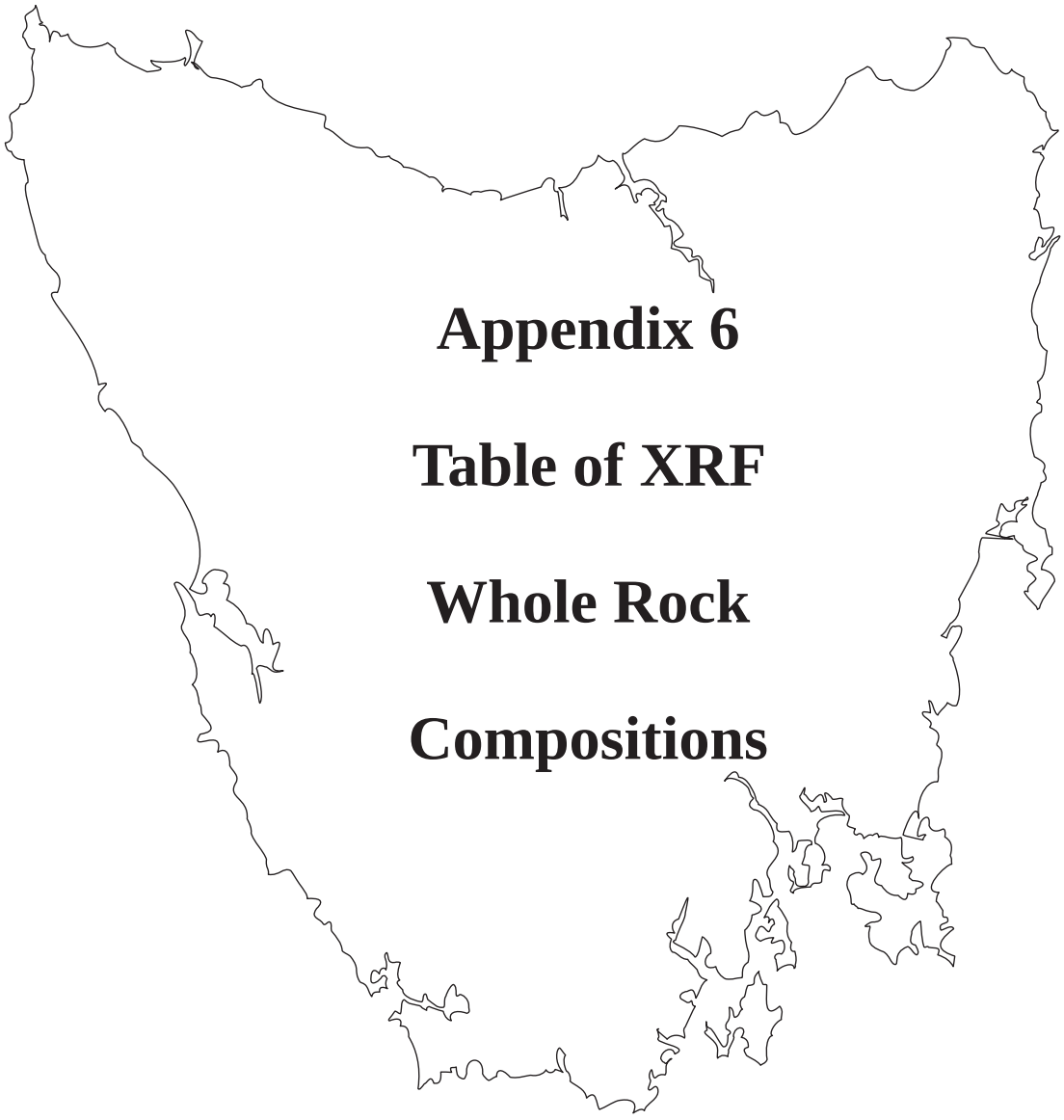

Appendix 6

Table of XRF Whole Rock Compositions

Appendix 6: Table of XRF Whole Rock compositions

Sample	SiO2	TiO2	Al2O3	FeO*	MnO	MgO	CaO*	Na2O	K2O	P2O5	Loss inc. S	Total
67659	66.15	0.73	17.29	4.33	0.07	1.23	0.66	2.50	3.28	0.06	2.41	98.80
67662	63.83	0.68	18.98	5.55	0.04	1.63	0.41	0.90	3.89	0.08	2.51	99.79
67665	64.96	0.65	18.44	4.79	0.04	1.71	0.33	0.60	4.48	0.14	2.44	98.68
68318	68.62	0.67	11.10	9.23	0.05	2.92	0.18	0.76	2.45	0.04	1.28	99.47
68319	68.98	0.66	11.79	8.46	0.05	2.62	0.25	0.84	2.58	0.07	1.46	99.74
68320	61.38	0.87	12.32	12.59	0.08	4.95	0.35	0.26	1.83	0.05	2.12	99.76
68788	63.35	0.69	19.49	4.94	0.03	1.53	0.38	0.76	4.20	0.08	3.10	98.66
143072	70.51	0.40	13.09	6.93	0.09	2.11	0.21	0.19	2.68	0.10	2.04	99.96
143076	66.72	0.53	12.98	9.96	0.11	3.00	0.23	0.10	2.55	0.14	1.15	99.81
143097	65.01	0.65	17.27	5.84	0.06	2.63	0.43	0.50	4.19	0.15	1.98	100.08
143145	74.28	0.28	8.08	10.62	0.05	2.21	0.14	0.03	0.40	0.06	1.25	99.89
143147	72.77	0.35	10.43	5.63	0.04	2.63	0.14	1.38	3.05	0.04	2.02	99.80
160694	64.17	0.68	18.92	5.39	0.03	1.68	0.14	0.63	4.48	0.06	2.34	98.62
160696	64.98	0.66	18.75	4.53	0.02	1.38	0.06	0.61	4.75	0.09	3.03	98.96
160698	66.65	0.72	17.62	4.64	0.06	1.46	0.26	1.62	3.78	0.06	2.14	99.11
160702	66.74	0.73	17.71	4.72	0.06	1.44	0.59	2.24	3.41	0.09	1.56	99.39
160707	63.51	0.63	19.30	5.65	0.07	1.88	0.24	1.01	4.17	0.10	2.28	98.94
160708	69.24	0.71	16.26	3.60	0.06	1.17	0.48	2.15	3.46	0.07	1.95	99.25
160730	59.96	0.40	12.77	8.63	0.10	12.71	0.55	0.13	0.42	0.05	2.44	100.19

FeO* = (reported Fe_2O_3) x ((2 X 71.85)/159.69)

CaO* = (reported CaO) - ((((P_2O_5)/(55/42)) x 0.95)

note: for sample 160696 the CaO listed is that reported for the analysis; the correction for apatite results in a negative CaO for this sample (see Chapter 2).

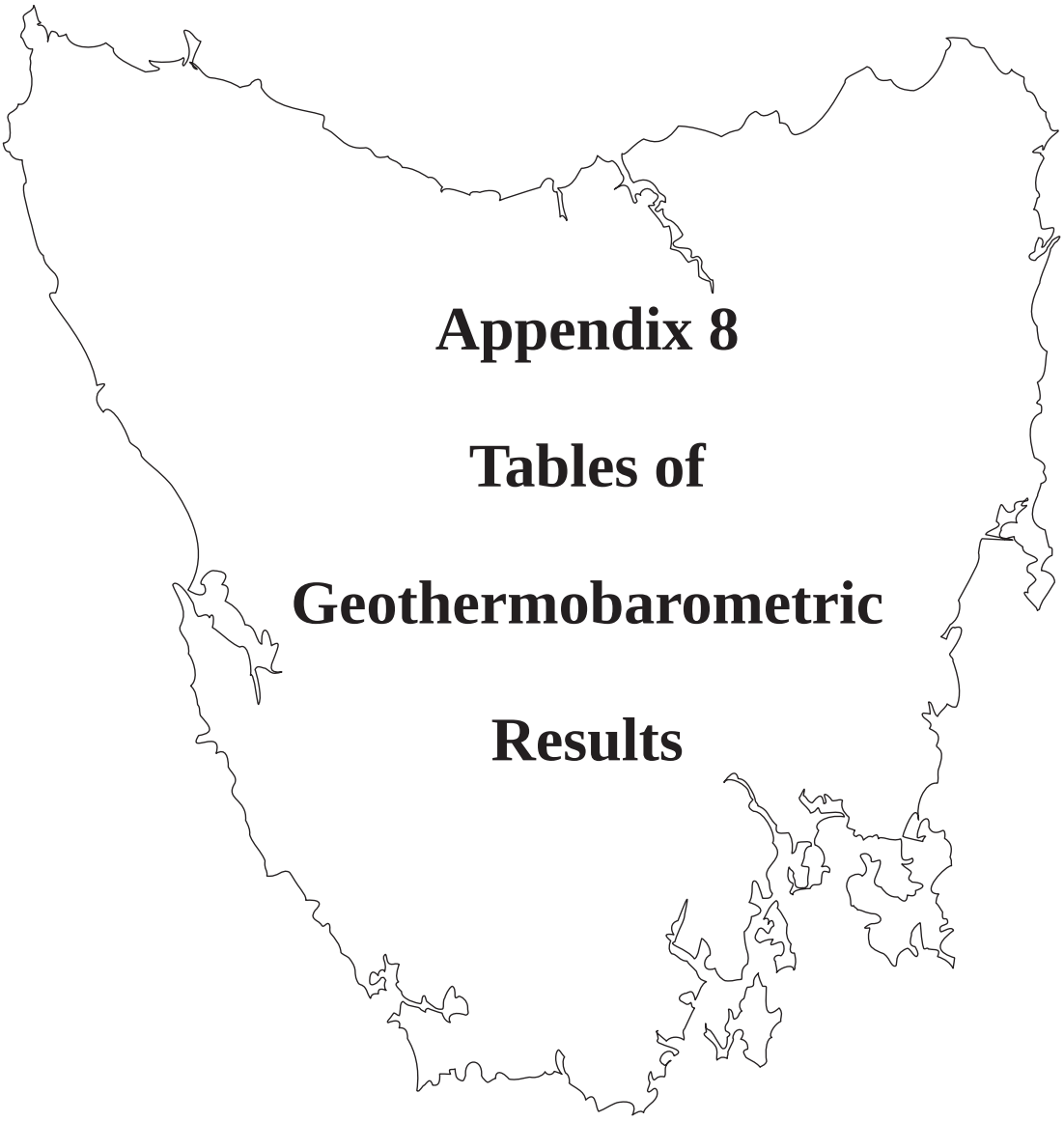

Appendix 8

Tables of Geothermobarometric Results

Appendix 8.1 Table of final P/T selected as representative for each region

region	type	what	T (C)	error	P (bars)	error	cor.
Forth	thermocalc max P/T	weighte mean average	672	59	16900	1500	0.7
C River metapelite	GB-GBPQ max P/T	sample 160717	715	30	13968	1200	0.7
C River metapelite	Perple_X garnet core	weighte mean average	578	31	5966	650	0.7
C River whiteschist	Perple_X garnet core	sample 160730	545	30	19600	1000	0.7
C. River eclogite	stage I/II	see Appendix 2	550	50	6250	750	0.7
C. River eclogite	stage III	see Appendix 2	623	28	16000	3000	0.7
C. River eclogite	stage IV	see Appendix 2	581	29	8500	1500	0.7
C. River eclogite	stage V	see Appendix 2	551	24	5000	1000	0.7
C. River eclogite	stage VI	see Appendix 2	639	21	6000	1000	0.7
Mt. Mary	thermocalc max P/T	39456 (d456)	567	83	8600	1400	0.8
Raglan Range	GB-GBPQ max P/T	Sample 30145	723	30	11402	1000	0.8
SW coast	core perple x	weighte mean average	562	20	5750	1700	0.7
SW coast	point of overlap of all techniques		650	30	6000	1000	0.7

Appendix 8.2 Thermocalc Results

sample	T (C)	sd	P (kb)	sd	cor	sigfit	additional end members used	T used in Ax	kb used in Ax	Reactions used		
67659	642	82	12300	1500	0.766	1.09	q, dry	600	12	3east + 6q = phl + py + 2mu gr + alm + mu = ann + 3an	phl + east + 6q = py + 2cel east + py + gr + cel = 2phl + 3an	2ann + mu + 6q = alm + 3fcel
~~67661~~	~~639~~	~~101~~	~~12600~~	~~1800~~	~~0.751~~	~~1.26~~	~~q, dry~~	~~600~~	~~12~~	~~3east + 6q = phl + py + 2mu~~ ~~gr + alm + mu = ann + 3an~~	~~phl + east + 6q = py + 2cel~~ ~~east + py + gr + cel = 2phl + 3an~~	~~2ann + mu + 6q = alm + 3fcel~~
~~160696~~	~~709~~	~~165~~	~~14300~~	~~2900~~	~~0.716~~	~~2.04~~	~~q, ky, dry~~	~~725~~	~~14.5~~	~~gr + q + 2ky = 3an~~ ~~2phl + mu + 2ky = 3east + 5q~~	~~3east + 6q = phl + py + 2mu~~ ~~2ann + mu + 6q = alm + 3fcel~~	~~phl + east + 6q = py + 2cel~~ ~~3ann + 7q + 2ky = 2alm + 3fcel~~
160698	772	128	14600	2100	0.714	1.39	q, dry	750	14.5	3east + 6q = phl + py + 2mu gr + alm + mu = ann + 3an	phl + east + 6q = py + 2cel east + py + gr + cel = 2phl + 3an	2ann + mu + 6q = alm + 3fcel
160702	687	120	13200	2100	0.742	1.5	q, dry	750	12.5	3east + 6q = phl + py + 2mu gr + alm + mu = ann + 3an	phl + east + 6q = py + 2cel east + py + gr + cel = 2phl + 3an	2ann + mu + 6q = alm + 3fcel
~~160707~~	~~842~~	~~175~~	~~16000~~	~~2900~~	~~0.708~~	~~1.77~~	~~q, dry~~	~~700~~	~~14~~	~~3east + 6q = phl + py + 2mu~~ ~~ann + 3an = gr + alm + mu~~	~~phl + east + 6q = py + 2cel~~ ~~phl + 3an = py + gr + mu~~	~~2ann + mu + 6q = alm + 3fcel~~
160708	736	121	15200	2200	0.757	1.48	q, dry	700	14	3east + 6q = phl + py + 2mu mu + gr + alm = ann + 3an	phl + east + 6q = py + 2cel mu + py + gr = phl + 3an	2ann + mu + 6q = alm + 3fcel
~~160711~~	~~676~~	~~118~~	~~14200~~	~~2100~~	~~0.717~~	~~1.55~~	~~q, dry~~	~~700~~	~~14~~	~~3east + 6q = phl + py + 2mu~~ ~~mu + gr + alm = ann + 3an~~	~~phl + east + 6q = py + 2cel~~ ~~mu + py + gr = phl + 3an~~	~~2ann + mu + 6q = alm + 3fcel~~
160713	883	195	13600	2800	0.695	1.79	q, dry	800	14	3east + 6q = phl + py + 2mu gr + alm + mu = ann + 3an	phl + east + 6q = py + 2cel py + gr + east + cel = 2phl + 3an	2ann + mu + 6q = alm + 3fcel
160717	742	108	13100	1800	0.757	1.35	q, dry	700	12.5	3east + 6q = phl + py + 2mu gr + alm + mu = ann + 3an	phl + east + 6q = py + 2cel east + py + gr + cel = 2phl + 3an	2ann + mu + 6q = alm + 3fcel

Appendix 8.2 Thermocalc Results

sample	file name	biotite	Mg/M+Fe	feldspar	xAn	garnet	xAlm	xPrp	xGrs	xSps	muscovite	Na/Na+K
67659	659a	67659c1b3-1	**0.43**	67659c1f1-1	**0.10**	67659c1g2-8	**0.72**	**0.11**	**0.15**	**0.010**	67659c1m1-1	**0.16**
~~**67661**~~	~~661ah~~	~~67661c1b1-1~~	~~**0.40**~~	~~67661c1f2-2~~	~~**0.05**~~	~~67661c1g1-11~~	~~**0.78**~~	~~**0.12**~~	~~**0.08**~~	~~**0.013**~~	~~67661c1m3-3~~	~~**0.18**~~
~~**RC0603**~~	~~03y~~	~~RC0603-b1-2~~	~~**0.43**~~	~~RC0603-f2-1~~	~~**0.03**~~	~~RC0603-g3-1~~	~~**0.79**~~	~~**0.17**~~	~~**0.03**~~	~~**0.008**~~	~~RC0603-m1-3~~	~~**0.12**~~
RC0605	05d	RC0605b3-2	**0.42**	RC0605f3-2	**0.05**	RC0605g2-1	**0.74**	**0.18**	**0.07**	**0.006**	RC0605m2-2	**0.11**
RC0609	09w	RC0609c2b3-1	**0.39**	RC0609c2f4-1	**0.06**	avg tiny	**0.74**	**0.13**	**0.12**	**0.006**	RC0609c2m1-1	**0.13**
~~**RC0614**~~	~~14k~~	~~RC0614-b1-1-9~~	~~**0.45**~~	~~RC0614-f1-1-15~~	~~**0.05**~~	~~RC0614-g2-37~~	~~**0.75**~~	~~**0.19**~~	~~**0.05**~~	~~**0.010**~~	~~RC0614-m1-2-13~~	~~**0.14**~~
RC0615	15n	RC0615c2b2-1	**0.41**	RC0615c2f2-2	**0.07**	RC0615c2g1-2	**0.71**	**0.13**	**0.16**	**0.010**	RC0615c2m2-1	**0.11**
~~**RC0618**~~	~~18j~~	~~RC0618b1-2~~	~~**0.35**~~	~~RC0618f2-1~~	~~**0.03**~~	~~RC0618g1-1~~	~~**0.79**~~	~~**0.11**~~	~~**0.09**~~	~~**0.009**~~	~~RC0618m1-2~~	~~**0.08**~~
RC0620	20g	RC0620b3-3	**0.49**	RC0620f3-2	**0.14**	RC0620g3-1	**0.75**	**0.18**	**0.05**	**0.014**	RC0620m1-1-55	**0.12**
RC0624	24b	RC0624-mb4-1	**0.40**	RC0624-f-a-2	**0.15**	RC0624-g-2-2	**0.70**	**0.11**	**0.18**	**0.010**	RC0624-m3-1	**0.10**

Appendix 8.3 GB_GBPQ Results*

Sample	Tgb(calc)	P(1, 2) ave	P(1)	P(2)	Si(bio)	Ti bio	Al(tot) bio	Fe(tot) bio	Mg bio	Al (IV) bio	Al(VI) bio	Ca pl	Na Pl	K Pl	Fe grt	Mn grt	Mg grt	Ca grt
67659	671	15065	14875	15254	2.734	0.141	1.636	1.335	0.999	1.266	0.37	0.094	0.866	0.004	2.175	0.03	0.343	0.464
67661	725	17182	16976	17388	2.731	0.14	1.629	1.416	0.938	1.269	0.36	0.05	0.905	0.003	2.32	0.042	0.423	0.285
160696	717	15165	14989	15342	2.691	0.084	1.775	1.338	1	1.309	0.466	0.031	0.941	0.004	2.422	0.023	0.527	0.087
160698	759	17343	17149	17536	2.724	0.129	1.692	1.345	0.985	1.276	0.416	0.051	0.9	0.004	2.271	0.018	0.55	0.216
160702	745	16937	16800	17075	2.645	0.119	1.595	1.352	0.881	1.355	0.24	0.06	0.912	0.002	2.287	0.019	0.413	0.361
160707	757	16434	16307	16562	2.738	0.107	1.642	1.333	1.072	1.262	0.38	0.048	0.968	0.006	2.307	0.03	0.596	0.156
160708	723	18046	17837	18256	2.775	0.134	1.594	1.393	0.967	1.225	0.369	0.068	0.936	0.003	2.159	0.031	0.384	0.485
160711	717	18400	18140	18659	2.721	0.095	1.689	1.558	0.855	1.279	0.41	0.033	0.92	0.005	2.40	0.026	0.341	0.275
160713	684	9773	9706	9840	2.698	0.093	1.639	1.285	1.236	1.302	0.337	0.128	0.816	0.003	2.345	0.044	0.559	0.161
160717	707	13948	13767	14128	2.692	0.094	1.734	1.43	0.956	1.308	0.426	0.151	0.849	0.006	2.145	0.032	0.353	0.547

* Summary only; for full data see Excel Spreadsheet on CD

Appendix 8.4 GASP results

			P (bars)					
68319		**700**	**ºC**	**6186**	**bars**			
spot #	Si(bio)	Ti bio	Al(tot) bio	Fe(tot) bio		Mg bio	Al (IV) bio	Al(VI) bio
68319-b3-2	**2.603**	**0.137**	**1.781**	**1.487**	**0.002**	**0.896**	**1.397**	**0.384**
spot #	Ca pl	Na Pl	K Pl					
68319-fsp-2b-1	**0.099**	**0.829**	**0.008**					
spot #	Fe grt	Mn grt	Mg grt	Ca grt				
68319-g3-1	**2.599**	**0.036**	**0.358**	**0.055**				

Appendix 8.5 GBMAQ results

143072	**Al-phase**	Ky		**792 °C**		**11868 bars**			
spot #	**SiO2 mus**	**TiO2 mus**	**Al2O3 mus**	**FeO mus**	**MnO mus**	**MgO mus**	**CaO mus**	**Na2O mus**	**K2O mus**
143072-m1-3	45.35	0.61	33.29	1.61	0.00	1.16	0.01	0.73	10.16
spot #	**SiO2 bio**	**TiO2 bio**	**Al2O3 bio**	**FeO bio**	**MnO bio**	**MgO bio**	**CaO bio**	**Na2O bio**	**K2O bio**
143072-b1-2	34.81	1.38	18.40	21.24	0.12	8.65	0.05	0.32	8.92
spot #	**SiO2 grt**	**TiO2 grt**	**Al2O3 grt**	**FeO grt**	**MnO grt**	**MgO grt**	**CaO grt**	**Na2O grt**	**K2O grt**
143072-g1-20	36.98	0.03	21.38	34.86	0.39	5.44	1.52	0.03	-0.01
160696	**Al-phase**	Ky		**697 °C**		**9432 bars**			
spot #	**SiO2 mus**	**TiO2 mus**	**Al2O3 mus**	**FeO mus**	**MnO mus**	**MgO mus**	**CaO mus**	**Na2O mus**	**K2O mus**
RC0603-m2-1	47.31	0.75	31.80	1.57	0.00	1.73	0.02	0.83	9.54
spot #	**SiO2 bio**	**TiO2 bio**	**Al2O3 bio**	**FeO bio**	**MnO bio**	**MgO bio**	**CaO bio**	**Na2O bio**	**K2O bio**
RC0603-b1-2	35.05	1.46	19.61	20.83	0.04	8.74	0.01	0.35	8.54
spot #	**SiO2 grt**	**TiO2 grt**	**Al2O3 grt**	**FeO grt**	**MnO grt**	**MgO grt**	**CaO grt**	**Na2O grt**	**K2O grt**
RC0603-g3-1	37.16	0.02	21.35	36.30	0.33	4.43	1.02	0.00	0.00
68319	**Al-phase**	**Ky**		**636 °C**		**6998 bars**			
spot #	**SiO2 mus**	**TiO2 mus**	**Al2O3 mus**	**FeO mus**	**MnO mus**	**MgO mus**	**CaO mus**	**Na2O mus**	**K2O mus**
68319-m2-1	40.8858	0.428	29.3655	10.143	0.0401	4.3401	-0.0053	0.0926	7.1059
spot #	**SiO2 bio**	**TiO2 bio**	**Al2O3 bio**	**FeO bio**	**MnO bio**	**MgO bio**	**CaO bio**	**Na2O bio**	**K2O bio**
68319-b3-2	33.4738	2.3369	19.4257	22.8623	0.0314	7.7352	0.0173	0.1055	9.1834
spot #	**SiO2 grt**	**TiO2 grt**	**Al2O3 grt**	**FeO grt**	**MnO grt**	**MgO grt**	**CaO grt**	**Na2O grt**	**K2O grt**
68319-g3-1 22	36.436	-0.0116	21.8921	38.7626	0.5292	2.9968	0.642	0.0248	-0.0008

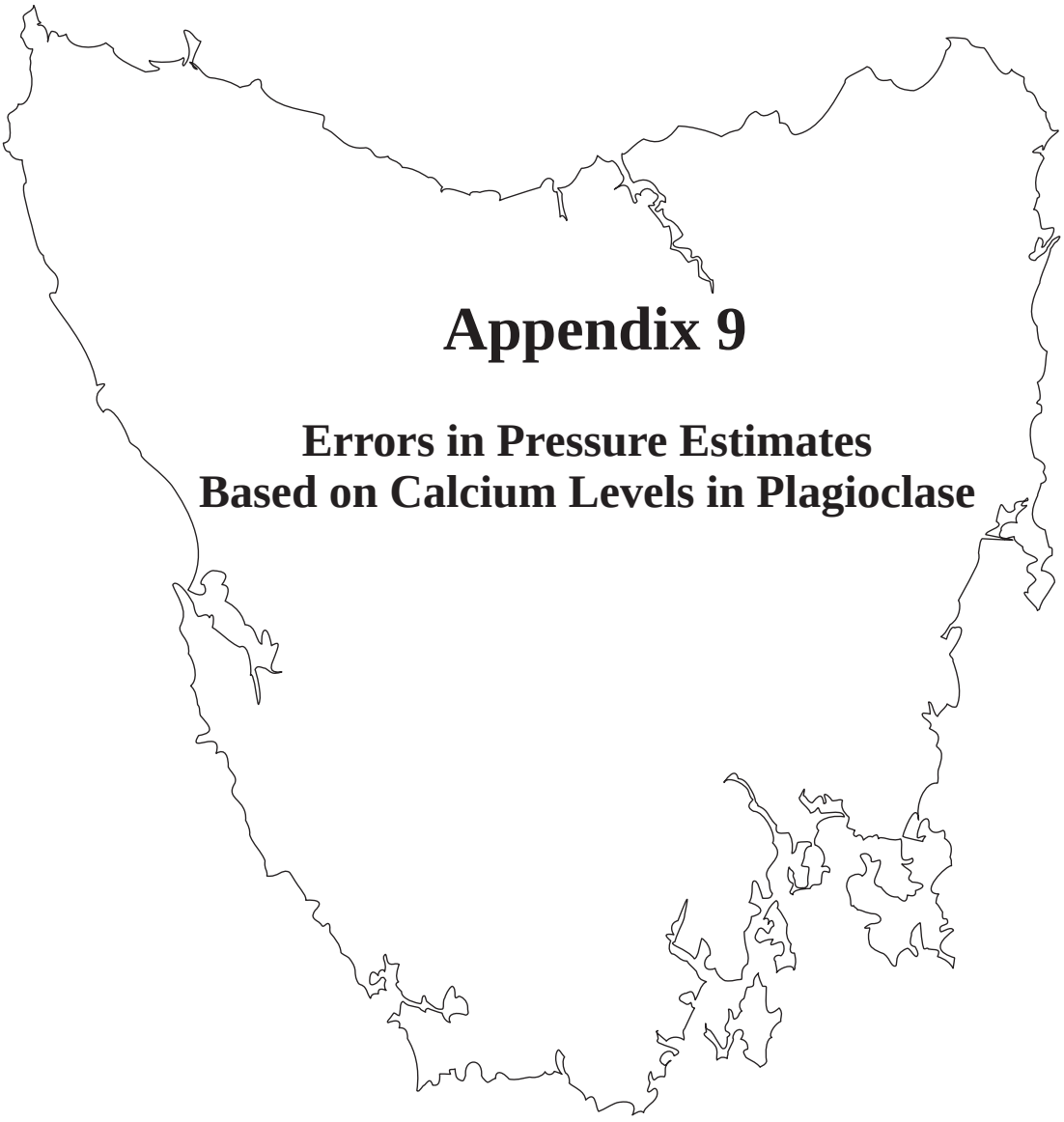

Appendix 9

Errors in Pressure Estimates Based on Calcium Levels in Plagioclase

APPENDIX 9: APPLICATIONS OF GASP AND GBPQ GEOBAROMETERS TO ALBITE AND OLIGOCLASE BEARING PELITIC ROCKS.

In general, there has been a recognition that plagioclase linked geobarometers become less reliable as the An content of the plagioclase decreases. Most authors (e.g. Holdaway 2001) argue that plagioclase with $X_{An} > 0.17$ can be reliably used in geobarometry. However Todd (1998) argued that if $X_{An} < 0.3$ then the errors associated with geobarometers based on reactions between anorthite and grossular are substantially increased. If this limit were to be applied more than 60% of all published analysis would not acceptable for application of the GASP and related geobarometers.

This discussion reviews the discussion of Todd (1998) to consider exactly how much the error is increased in low Ca samples. Rather than assuming that a result should be rejected, the aim here is to calculate the error bars for compositions with $X_{An}<0.3$. (In this discussion X_{An} is the cation ratio Ca/(Ca+Na+K) in plagioclase and X_{Grs} is the cation ration Ca/(Fe+Mg+Mn+Ca) in garnet.) The discussion follows that of Todd (1988) and then looks at the application to the Holdaway (2001) calibration of the GASP geobarometer and the Wu et al (2004) calibration of the GBPQ geobarometer.

The primary limits to accuracy of any GASP geobarometer are the analytical limits on small components in plagioclase. The accuracy of X_{An} in plagioclase can be calculated from the counting statistics of the EPMA analysis. For the conditions used in this study the relative error due to counting statistics is shown on Fig. 1. The relative error dramatically increases below X_{An} of 0.06.

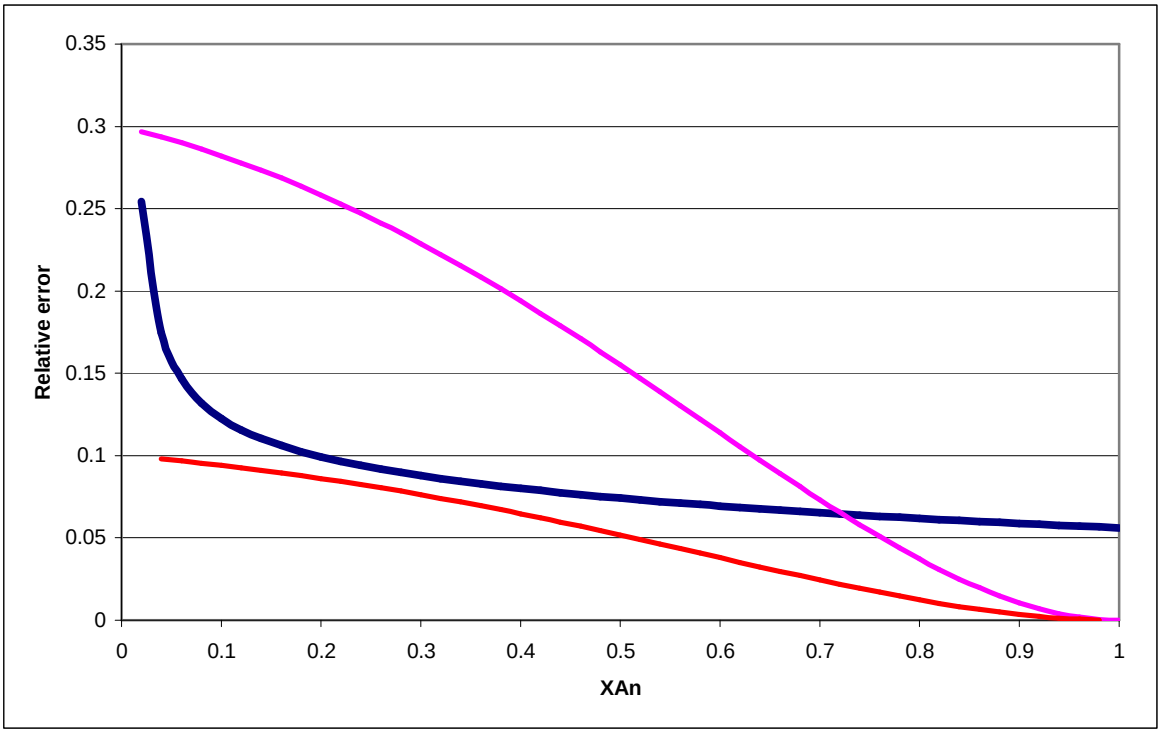

Fig. 1. Relative error for X_{An} based on the standard error in analyses reported by the Cameca SX100 at the conditions used in this project (Blue line). Errors propagated using the rules for normally distributed errors. For comparison, errors calculated from formula of Powell & Holland (1988) for absolute values (Pink) and comparison values (Red) of the activity model. Where the activity model is part of the calibration the comparison value is more appropriate.

These errors can be propagated through the GASP equation to identify how this error affects the calculated pressure (Fig. 2). Holdaway (2001) claimed a total relative error on 640 bars for his calculated GASP equation for $X_{An} > 0.17$. Apparently half this uncertainty comes from the plagioclase analyses. For An values down to X_{An} 0.05 the analytical uncertainty increases this error to about 1,000 bars.

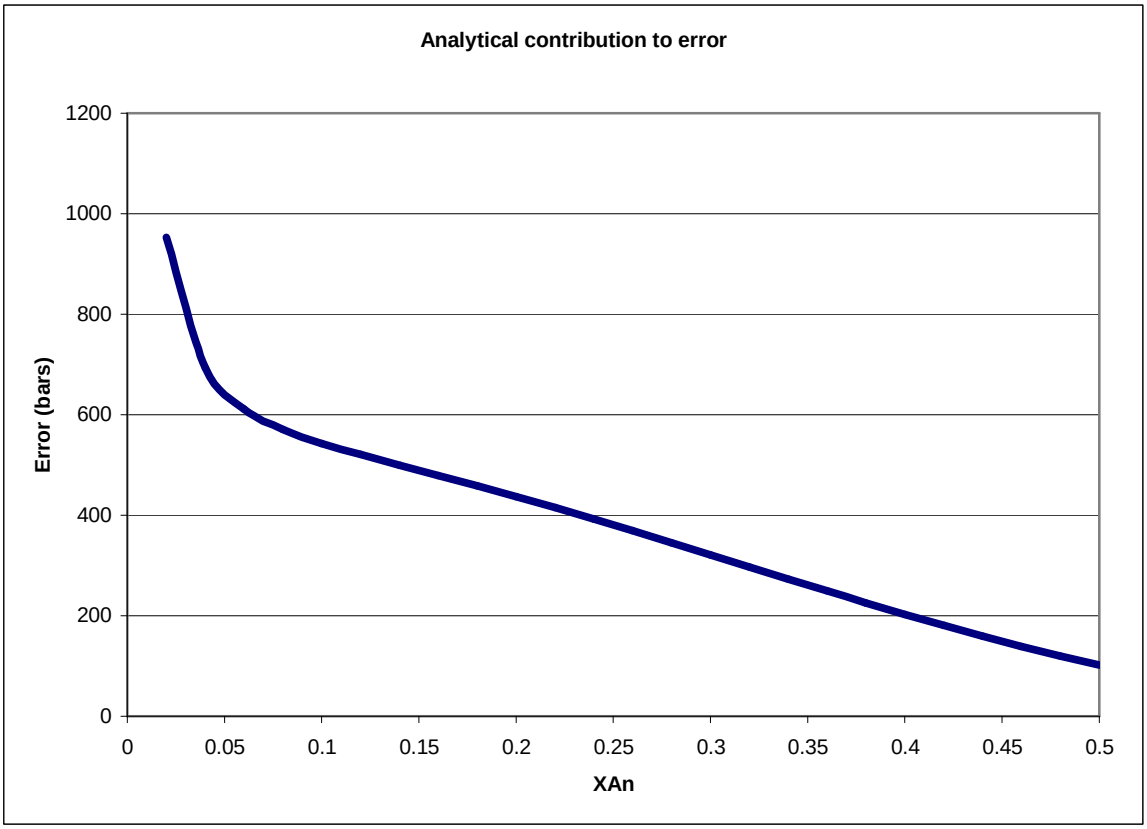

Fig. 2. Error in GASP (Holdaway (2001) pressure (one standard deviation) arising from analytical errors in the plagioclase composition. Errors calculated at 600ºC and 8000 bars.

Todd (1988) used the approximation suggested by Powell and Holland (1988) to estimate uncertainty in the activity model for plagioclase and grossular. He recommended a very high level of uncertainty (absolute values on Fig. 1). These values are not appropriate for the formulation of a geobarometer where absolute errors are absorbed into the calibration of the geobarometers and only relative errors are significant. The uncertainty model for relative activities suggested by Powell & Holland 1988) is much smaller. On this basis the errors suggested in Fig. 4 of Todd (1988) are unrealistically high. The analytical uncertainty in pressure estimates increases smoothly down to X_{An} 0.06. The relative pressure uncertainty calculated by Todd (1988) using the lower relative error curve for the activity models varies from 250 bars at high Ca to 1000 bars at a X_{An} of 0.1.

The peristerite “solvus” occupies the region X_{An} 0.02 to X_{An} 0.16 at low T with a peak at X_{An} 0.06. Powell & Holland (1998) have argued against using activities calculated from the wrong side of a solvus since these are usually very inaccurate. This implies analyses below X_{An} 0.06 should be excluded. The plagioclase activity

model used in the GASP and GBPQ calibrations discussed here are from Fuhrman & Lindsay (1988). This model is optimised for T above 700ºC. Holland & Powell (1992) produced an activity model for application in metamorphic rocks. The model recommended by Holland & Powell (1998) is the model 1 from this paper. Comparison of anorthite activity calculated from Fuhrman & Lindsay (1988) with the value calculated from Holland & Powell (1992) (Fig. 3) shows a dramatic deviation in calculated activity below X_{An} of 0.2 (a_{An}=0.3 in Fig 3). This difference may be important in limiting the application of GASP calibrations which largely use the Fuhrman & Lindsay (1988) feldspar model. The Holland & Powell (1992) model gives significantly lower pressures for GASP calibrations below X_{An} of 0.15. At X_{An} of 0.1 this difference is 350 bars (Fig.4).

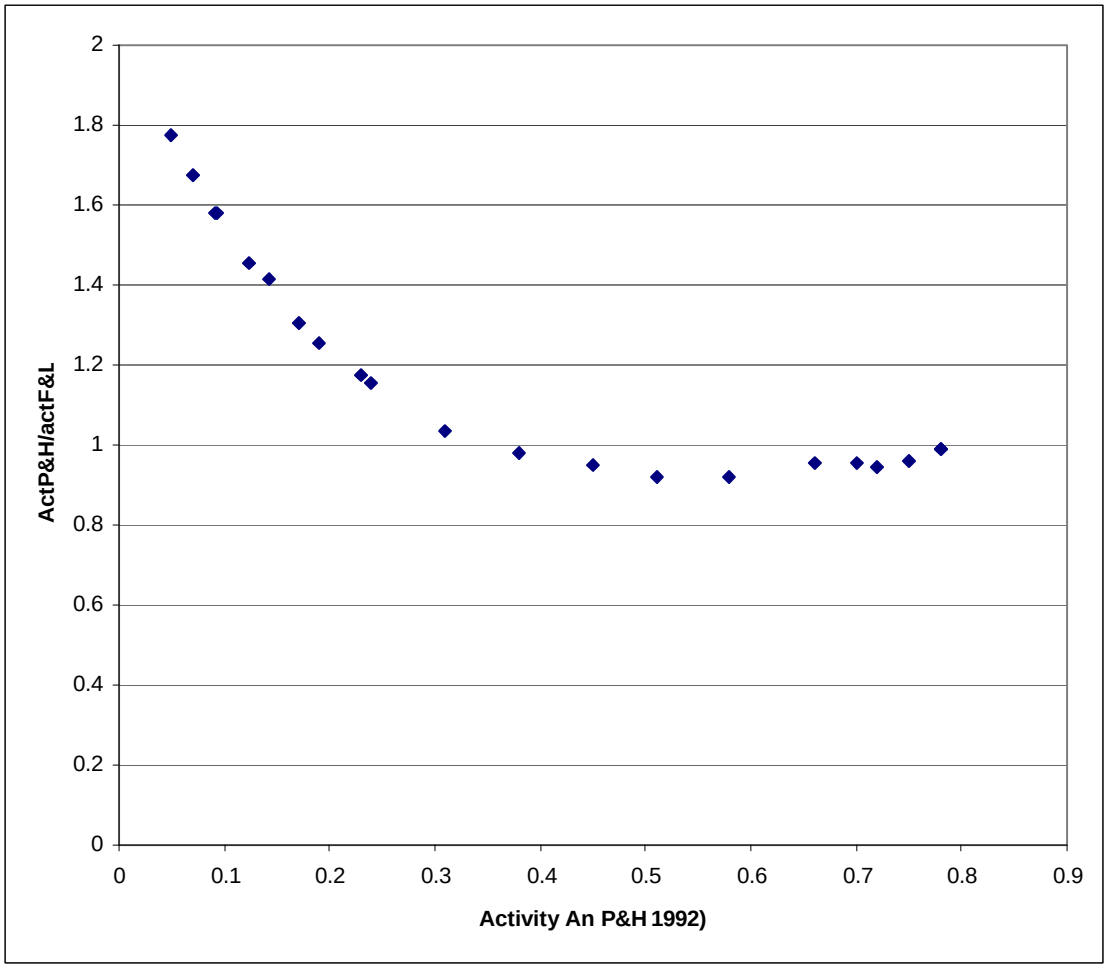

Fig. 3. Ratio of An activity calculated from method of Fuhrman & Lindsay (1988) to activity calculated from Holland & Powell (1992). Activities calculated at 600ºC and 6000 bars.

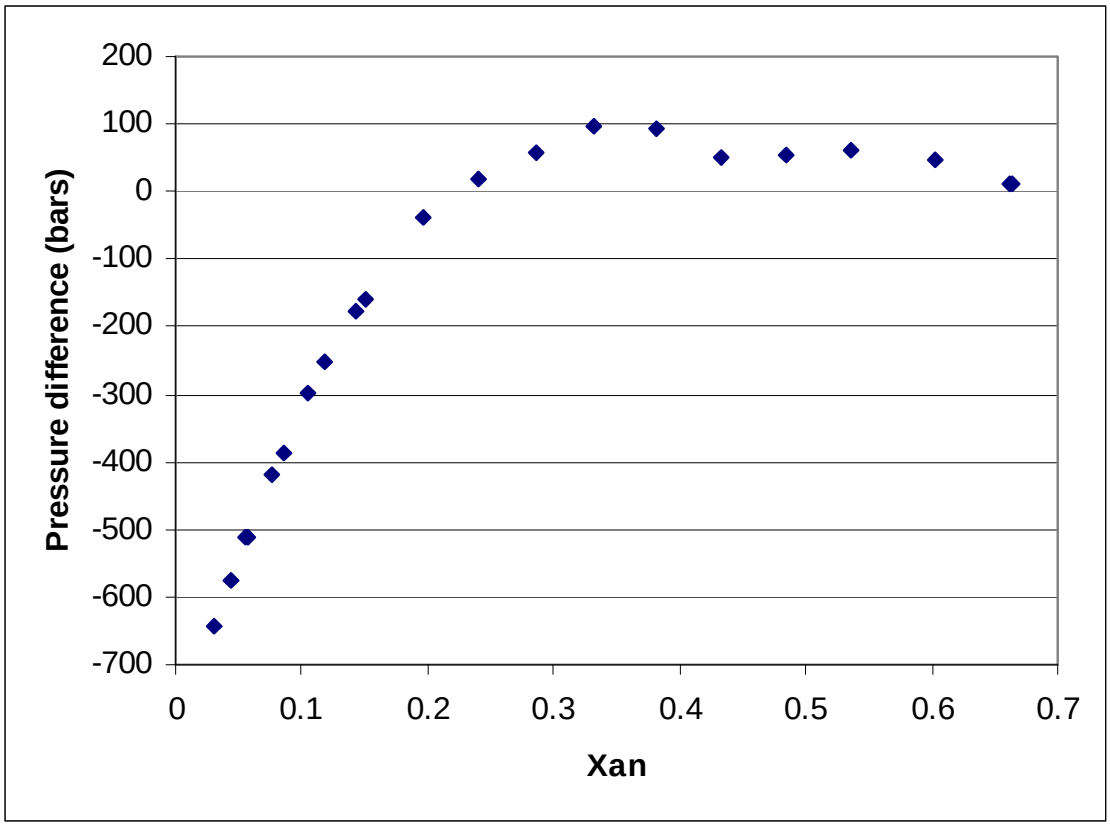

Figure 4. The change in calculated pressure using the GASP calibration of Holdaway (2001) if the Fuhrman & Lindsay (1988) plagioclase activity model is relaced by that of Holland & Powell (1992). Activities calculated at 600ºC and 6000 bars.

In this project, the Ca in garnet was analysed at twice the beam current and three times the counting time that were used for feldspar. Thus the analytical errors for garnet are very small down to 0.5% Ca or X_{Grs} of 0.02. No problems were detected with the activity model of grossular at this level.

Todd (1998) used a set of 42 samples to test the affect of decreasing Ca activity on the accuracy of pressure estimates by comparing pressure estimates using reactions between Ca bearing phases against calculated pressure where Ca bearing phases were excluded. The calculations were carried out using the program PTA (Berman 1988) and a range of activity models including the Fuhrman & Lindsey (1988) feldspar model. He showed these relationships in his Figure 5 and Table 1. He claimed that these data indicated a dramatic increase in errors when $X_{Grs} \cdot X_{An}$ is less than 0.05. The data (from Table 1 of Todd 1998) have been compiled into three compositional ranges and summarised in Table 1. Most of the samples reported have a $X_{Grs} \cdot X_{An}$ below 0.02; 70% of the results have $X_{Grs} \cdot X_{An}$ less than 0.05. In fact, the data

suggest only a very small increase in the associated error in low Ca samples. The standard deviation of the low Ca samples is 1.2 Kbars, while the high Ca samples have a standard deviation of 0.8 Kbars. The difference is even less if the single anomalous value in this dataset is excluded. On this analysis there is no evidence for increasing uncertainty within the sample set as Ca is decreased.

Todd (1988) also recommended that only sample with $X_{Grs} > 0.1$ should be used. However on his sample set the low Ca samples with X_{Grs} below 0.05 show less variability than high Ca samples. There is no evidence in this dataset that low Ca samples should be excluded on the basis of a low X_{Grs}. The situation with X_{An} is similar. Todd (1988) recommended X_{An} should exceed 0.3. The pressure estimates from samples with low X_{An} (below 0.2) show no more variability than samples above 0.3. There is a systematic increase in the average pressure difference. This can be a sampling problem, since samples where a non-representative low X_{An} plagioclase is analysed will have a positive pressure differential. It is assumed here that this effect is the cause of the negative shift in average pressure differential for low X_{Grs} samples. An alternative for the plagioclase is that the use of the Fuhrman & Lindsay (1988) plagioclase model may be causing the pressure estimate to be high. In the range of these samples the affect should be 0.2 to 0.3 kbars. The actual shift is twice this size suggesting there is also a problem with the selection of equilibrium plagioclase compositions.

	Range	Number of samples	Pressure difference standard deviation	Average P difference
xan	<0.2*	11	1.1	1.1
	<0.2	12	1.3	1.4
	0.2-0.3	19	1.2	0.5
	>0.3	11	1.1	0.1
xgr	<0.05	12	0.7	-0.1
	0.05-0.1*	16	1.2	0.9
	0.05-0.1	17	1.4	1.1
	>0.1	13	1.4	0.8
Xgrs.Xan	<0.02*	29	1.1	0.6
	<0.02	30	1.2	0.7
	0.02-0.05	4	2.4	0.5
	>0.05	8	0.8	0.3

Table 1. Summary of the relationship between differences of pressure estimated with and without Ca bearing phases for a range of compositions of plagioclase, garnet and the product of X_{An} and X_{Grs}. Based on data from Todd (1998)

* excludes single sample that is an outlier more than 2 standard deviations from the mean.

In conclusion, the natural samples reported by Todd (1988) fail to show any evidence of increasing errors in pressure estimates at low Ca contents. These samples have plagioclase compositions down to X_{An} 0.1 and garnet compositions with X_{Grs} down to 0.03.

A better test of the limits to the application of GASP and GBPQ to low Ca samples can be made using the suite of samples from the Hunt Valley Mall, Maryland, USA (Lang 1991). These samples were collected from a small area (within 500m) in a regional metamorphic area and should all have experience the same metamorphic conditions. There are thirteen samples with a suitable composition to apply the GASP or GBPQ geobarometers. The average garnet biotite temperature (Holdaway 2000) is 590ºC and all pressures are calculated at that temperature. Six samples contain the assemblage Gnt-plag-qtz-ky-bi and have $X_{An} > 0.17$ as suggested by Holdaway (2001) for the GASP geobarometer. These samples have an average GASP pressure of 5750 bars.

There are four samples with low Ca in this dataset. However none of these contain kyanite. Therefore the pressure estimates of the thirteen samples were calculated using the GBPQ equation of Wu et al (2004). With this sample set (Fig. 5), most samples with X_{An} above 0.1 have pressure estimates within error of the average GASP pressure for moderate Ca samples. Two samples with X_{An} of 0.08 have a calculated pressure 1000 bars high and the samples with X_{An} of 0.03 and 0.05 are seriously in error.

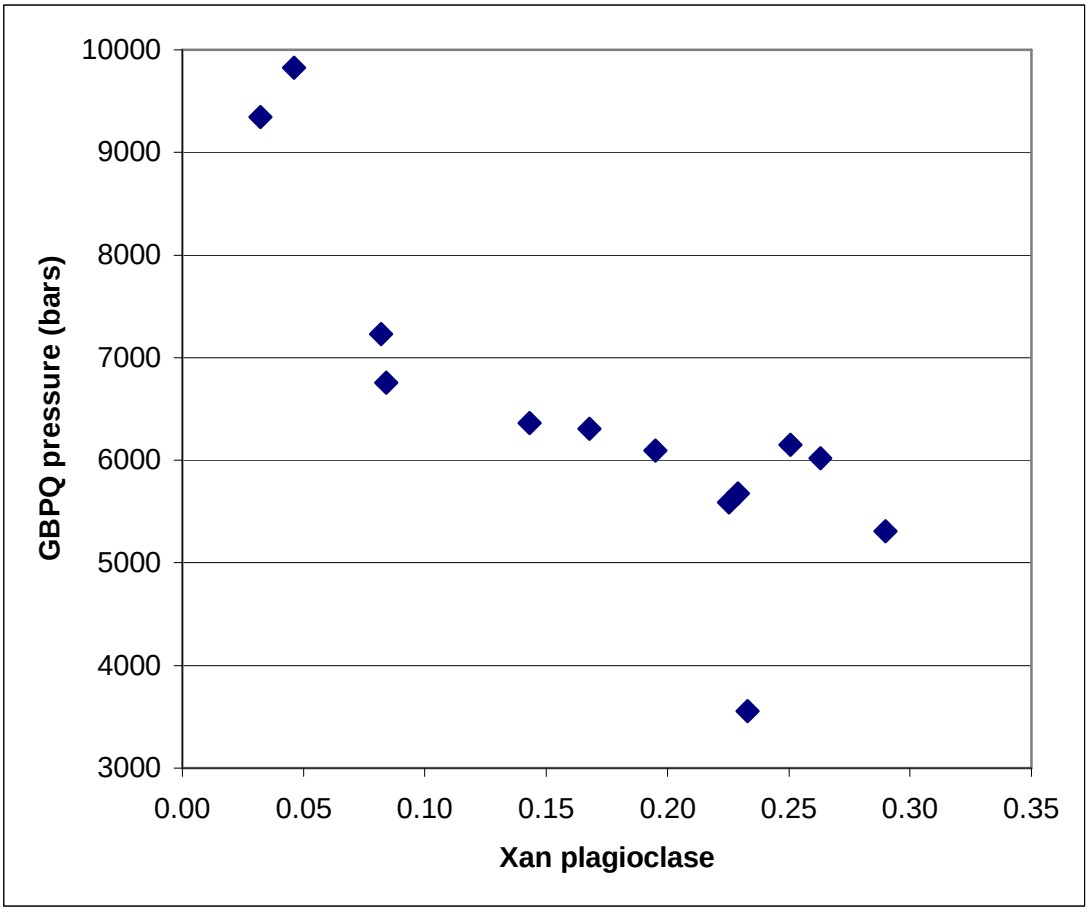

Figure 5. GBPQ pressure estimates for a range of samples from Hunt Valley Mall, Maryland (Lang 1991) showing the range in pressure estimated (at 590ºC) for a range of Xan plagioclase.

In conclusion there is very little increase in the error for pressure estimates from Ca phases where the X_{An} of plagioclase is above 0.1. The pressure is significantly over-estimated by GBPQ and probably GASP for samples with X_{An} below 0.1. Under the analytical conditions in this project. Analytical errors and activity model errors add 500 bars extra error to pressure estimates at X_{An} 0.1 compared to more typical values near X_{An} = 0.3. The activity model errors are systematically toward higher pressure estimates at very low X_{An}. This systematic error becomes significant below X_{An} of 0.1.

REFERENCES

Berman RG 1988.Internally consistent thermodynamic data for minerals in the system Na_2O-K_2O-CaO-MgO-FeO-Fe_2O_3-Al_2O_3-SiO_2-TiO_2-H_2O-CO_2. Journal of Petrology 29, 445-522.

Fuhrman, M.L. and Lindsley, D.H. (1988) Ternary-feldspar modeling and thermometry. American Mineralogist, 73, 201–215.

Holdaway MJ 2000. Application of new experimental and garnet Margules data to the garnet-biotite geothermometer. American Mineralogist 85, 881-892.

Holland, T. J. B. & Powell, R., 1992. Plagioclase feldspars activity composition relations based upon Darken's Quadratic Formalism and Landau theory. American Mineralogist, 77, 53–61.

Holdaway MJ 2001. Recalibration of the GASP geobarometer in the light of recent garnet and plagioclase activity models and versions of the garnet-biotite geothermometer. American Mineralogist, 86, 1117-1129.

Holland TJB & Powell R. 1998. An internally consistent thermodynamic data set for phases of petrological interest. Journal metamorphic geology 16, 309-343.

Lang HM 1991. Quantitative interpretation of within-outcop variation in metamorphic assemblage in staurolite-kyanite-grade metapelites, Baltimore, Maryland. Canadian Mineralogist 29, 655-671.

Powell, R. and Holland, T.J.B. (1988) An internally consistent thermodynamic dataset with uncertainties and correlations: 3. Applications to geobarometry, worked examples and a computer program. Journal of Metamorphic Geology, 6, 173–204.

Todd CS 1998. Limits to the precision of geobarometry at low grossular and anorthite content. American Mineralogist. 83, 1161-1167.

Wu C-M, Zhang J & Ren L-D 2004. Empirical garnet–biotite–plagioclase–quartz (GBPQ) geobarometry in medium- to high-grade metapelites. Journal of Petrology, 45, 1907-1921.

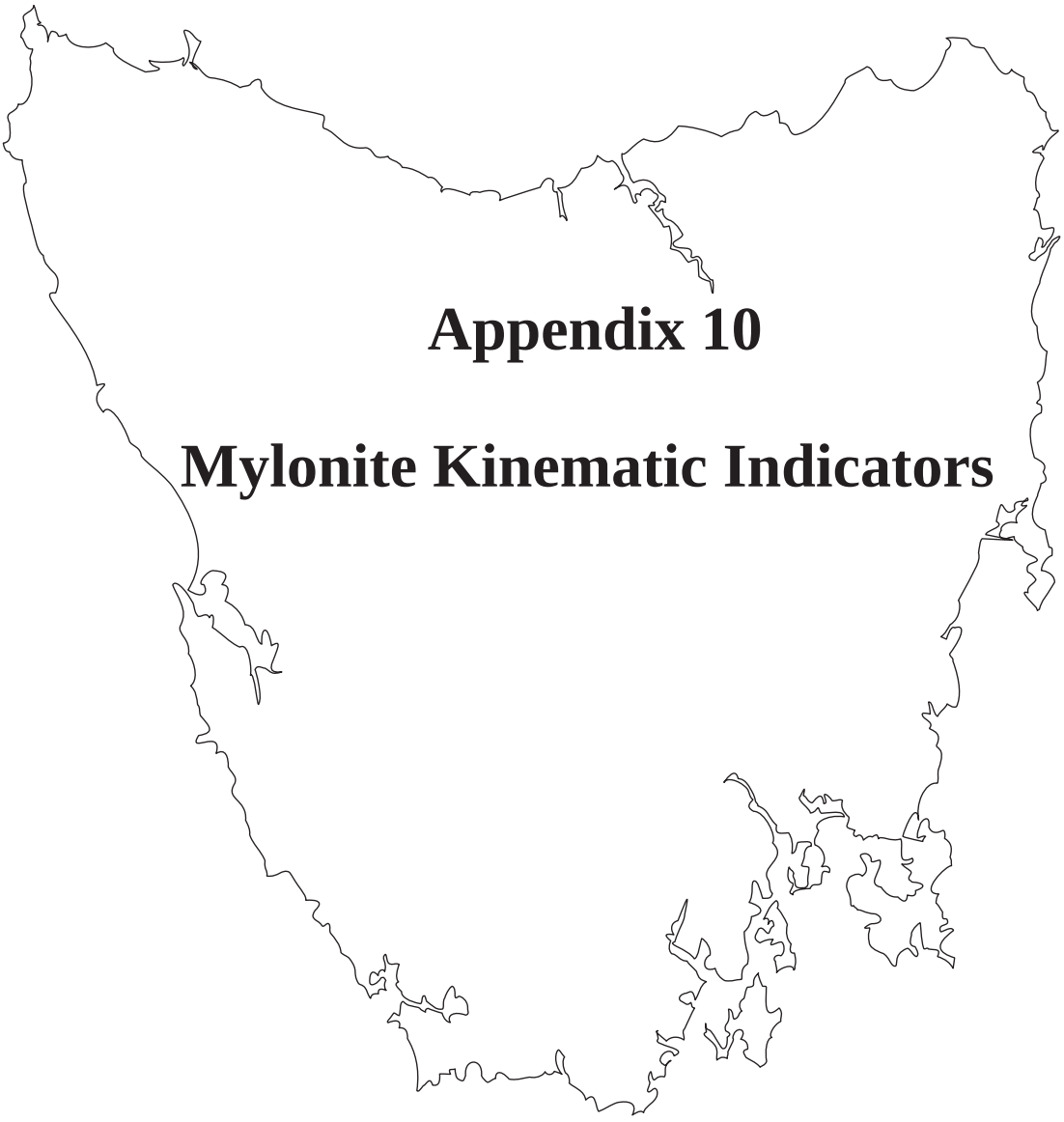

Appendix 10

Mylonite Kinematic Indicators

Appendix 10 Mylonite Kinematic Indicators

Sample		East	North	in slide	in world	foliation dip	foliation dip direction	lineation dip	lineation dip direction	face direction of face dip	face direction of face dip dip
160706	north block C. River	405325	5335700	dextral	top to the east	40	258	39	268	(n/a)	
Same sort of bands as in 160735 and 160736, with thin brown lines between--some are mostly qtz, others actually mica flakes, others are fine grained (sercite?) and there is a decent sized kyanite grain (which was analysed).											
160731	south block C. River	410099	5332931	sinstral	top to the east	61	204	59	241	73	209
Shows sense of shear well, but not intensity of temp/deformation. moslty quartz, thin brown lines between layers, very fine grained mica much smaller than quartz (which is finer grained than the northern sampels)											
160734	south block C. River	409857	5332938	dextral	top to the north	63	206	59	151	(n/a)	
Shows intensity of temp/deformation well, but not so good at sense of shear. Much larger grained than 160731. Mica flakes, large qtz grains. Alas, the section is quite thick, so the quartz is largely yellow in x-polars. Possible feldspar, difficult to tell in such a thick section, but that looks like cleavage & twinning. Garnets all appear to be surrounded by "dirty" coating											
160735	north block C. River	405298	5335737	sinstral	top to the east	32	258	32	258	(n/a)	
vith muscovite, very thin brown lines between layers											
160736	north block C. River	405338	5335714	sinstral	top to the east	32	231	33	235	(n/a)	
The white band--sillmanite? Perhaps a second high relief mineral as well? (Section too thick!) More mica rich than 160735, but still bands of quartz and bands of mica, seperated by thin brown lines, occasisonal spray of small garnets parallel with layers, one line of ?kyanite (looks similar to that in 160706, which was analysed).											

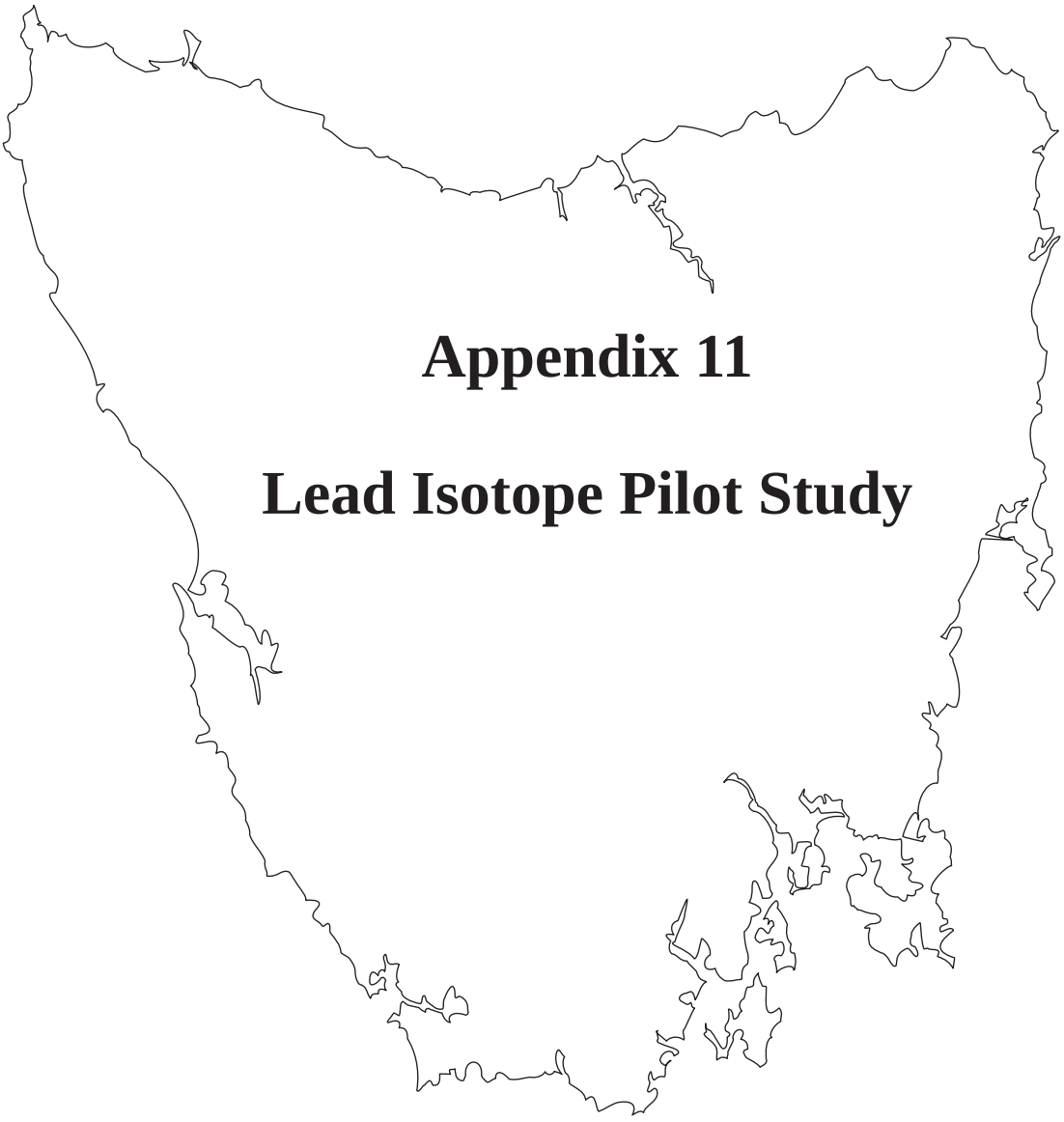

Appendix 11

Lead Isotope Pilot Study

APPENDIX 11: LEAD ISOTOPE PILOT STUDY

The Pb isotopic composition of minerals has been used to constrain tectonic reconstructions (e.g. Fioretti et al. 2005) (and for the dating of ore deposits in western Tasmania (e.g. Large et al. 1987). A preliminary investigation into the Pb isotopic composition of minerals in the pelitic metamorphic rocks in three regions of Tasmania was conducted in the hopes of differentiating Pb-rich minerals which formed early, at the same time as the older generation (1,100-1,300 Ma) monazite, which often occurs as inclusions in garnets, and the younger generation (505-515 Ma) of monazite, which is more likely to be located within the garnet rims, or in the matrix (see Chapter 5). Unfortunately, save for a single mica inclusion (in sample 68334), no Pb-bearing minerals were found as inclusions within the garnets, and the garnets themselves are very low in Pb. However, the Pb isotopic composition of micas in the matrix was found to be very different from that previously documented from the Mt Read Volcanics and other Cambrian rocks from Tasmania (Gulson et al. 1987; Gulson and Porritt 1987; Large et al. 1987). The full significance of these results is beyond the scope of this thesis; however the preliminary results are discussed briefly here so that the data will be available for any who might wish to undertake a more comprehensive study.

Six pelitic samples, three (RC0601, RC0614, and 68788; see Chapter 2 for sample descriptions) from the Collingwood River (Figure 2-1) area and three from the southwest coast (Figure 3-1) (143072 from Mulcahy Bay, 68334 and 68335 from Nye Bay; see Chapter Three for sample descriptions) were chosen for common-lead analysis using the Laser-ICPMS using the techniques outlined in Meffre et al. (2008). Each of the polished blocks to be analysed was prepared from other half of the block from which the thin section for that sample was cut, permitting a direct comparison of the mineral assemblage present in block and thin section, minus only

such material lost in the cutting and polishing process. The Pb isotopes were determined from the micas (muscovite in the Collingwood River, both muscovite and biotite in the southwest coast), which were the only minerals within the sample that contained sufficient Pb for Pb isotopic determinations by LAM ICP-MS. The lead signatures of the 3 areas are quite different. The Collingwood River samples show ages which plot along the bulk crustal growth curve of Stacey and Kramers (1975) between 600 and 800 Ma. The micas analysed from the single sample from Mulcahy Bay contain highly radiogenic Pb. The two samples from Nye Bay contain Pb that is transitional between Collingwood River and Mulcahy Bay. Applying a correction for the in situ decay of the U and Th measured in the samples makes very little differences to the Pb isotopic ratios so that the differences in between the samples can not have arisen from differences in U and Th contents of the micas but must reflect Pb sourced from different reservoirs.

The Pb isotopic composition of the micas from Collingwood River Complex are surprisingly non radiogenic given the 505-510 Ma age for the high pressure metamorphism experienced by these rocks. These results suggest that the Pb was separated from any additions from the decay of U and Th from at least 800 Ma. If it had remained with its parent U and Th it would have continued to evolve along the growth curve until crystallisation of the micas at 505 Ma and would record a 505 Ma Pb-Pb (growth curve) age.

The data from the monazite geochronology (see Chapter 5) suggest that at least part of the radiogenic Pb has remained locked within older generation of monazites (Genvillian, 1,000-1,200 Ma). The Pb isotopic results suggest that the micas, or their pre-cursors, have been chemically isolated for a long period of time receiving very little new Pb, U or Th since the Proterozoic. (Save for sample 143072 in Mulcahy Bay, which not only has micas with highly radiogenic Pb, it also lacks the older

generation of monazite.) A possible scenario to explain the Pb isotopic composition of the samples is that they initially formed within an igneous protolith to the pelitic sediment from which these samples crystallized, or in the course of an earlier medium to high grade metamorphic event at 1,100-1,200 Ma. Subsequent metamorphism at 505-510 Ma then partially reset the Pb isotopic composition of the micas with only small addition of new radiogenic Pb while the bulk of the radiogenic Pb remained locked within the older monazites. The common Pb from the micas (with high Pb and low U) would then record a much older Pb-Pb age than their crystallisation age.

At present the Pb isotopic composition of Grenvillian rocks in the area is known only from samples dredged from 300 km to the south of Tasmania (Fioretti et al. 2005). These samples have a similar $^{206}Pb/^{204}Pb$ ratio but lower $^{207}Pb/^{204}Pb$ ratio suggesting derivation from a mantle source rather than the upper crustal source of the Collingwood River micas.

Both the Nye Bay and Mulcahy Bay samples have more radiogenic Pb isotopic composition within their micas. These rocks are more chloritised and retrogressed than the Collingwood River samples and it is possible that their radiogenic composition is related to late stage processes and fluids rather than their original (Cambrian) composition. A full understanding of the Pb isotopic systematics of Tasmanian Cambrian and Proterozoic rocks would require a much more in-depth and focussed study on this topic.

REFERENCES

Fioretti, A. M., Black, L. P., Foden, J. and Visonà, D. (2005). "Grenville-age magmatism at the South Tasman Rise (Australia): A new piercing point for the reconstruction of Rodinia." Geology **33**(10): 769-772.

Gulson, B. L., Large, R. R. and Porritt, P. M. (1987). "Base metal exploration of the Mount Read Volcanics, western Tasmania: pt. III. Application of lead isotopes at Elliott Bay." Economic Geology **82**(2): 308-327.

Gulson, B. L. and Porritt, P. M. (1987). "Base metal exploration of the Mount Read Volcanics, western Tasmania: pt. II. Lead isotope signatures and genetic implications." Economic Geology **82**(2): 291-307.

Large, R. R., Herrmann, W. and Corbett, K. D. (1987). "Base metal exploration of the Mount Read Volcanics, western Tasmania: pt. I. Geology and exploration, Elliott Bay." Economic Geology **82**(2): 267-290.

Meffre, S., Large, R. R., Scott, R., Woodhead, J., Chang, Z., Gilbert, S. E., Danyushevsky, L. V., Maslennikov, V. and Hergt, J. M. (2008). "Age and pyrite Pb-isotopic composition of the giant Sukhoi Log sediment-hosted gold deposit, Russia." Geochimica et Cosmochimica Acta **72**(9): 2377-2391.

Stacey, J. S. and Kramers, J. D. (1975). "Approximation of terrestrial lead isotope evolution by a two-stage model." Earth and Planetary Science Letters **26**(2): 207-221.